POTENTIAL IMPACTS OF WHARF EXTENSIONS ON THE HYDRODYNAMICS OF STELLA PASSAGE AND UPSTREAM REGIONS OF TAURANGA HARBOUR, NEW ZEALAND

A thesis submitted in partial fulfilment

of the requirements for the degree

of

Masters of Science

in Earth and Ocean Sciences

at

The University of Waikato

by

Holly Margaret Watson

KO TE TANGATA

THE UNIVERSITY OF
WAIKATO
Te Whare Wānanga o Waikato

2016

ABSTRACT

The Port of Tauranga have proposed extending the berthage of both the Sulphur Point and Maunganui wharves southward to provide a combined length of 1,303 m. The dredged channel (Stella Passage) will also be extended south into Town Reach, with the dredged sediment used to reclaim 4.7 ha behind the wharf extensions and along the Sulphur Point shoreline. In this thesis a hydrodynamic model of the southern basin was developed and used to predict the potential impacts of the wharf extensions on the hydrodynamics in Stella Passage and the upper harbour.

Numerical modelling of the southern basin was undertaken with Deltares Delft3D FLOW modelling software, using a 2D model with a 20 x 20 m rectangular grid. Sensitivity analysis identified bottom roughness and bathymetry as having the largest influence on model outcomes. Successful calibration and verification of the southern basin model was carried out using field data collected from instruments deployed in Stella Passage and the upper harbour. Statistical analysis of the modelled water levels showed ‘excellent’ agreement with the field data. The modelled current velocities did not match quite as well, but the results were sufficiently good to provide confidence in the model predictions.

The modelled hydrodynamics in Stella Passage were similar to those predicted by previous studies. Compression of the tidal volume and acceleration over the steep boundary between the two areas meant current speeds within the shallower Town Reach were significantly higher than those in the dredged Stella Passage. A clockwise eddy of residual velocities indicated increased sediment transport on the ebb dominant western side of Town Reach. No previous models of the southern basin have modelled the hydrodynamics in the upper harbour beyond the Railway Bridge. Within the upper harbour the largest effects on the existing hydrodynamics were caused by the bridge causeways and the size and shape of the basins. Residual velocity eddies were created around the causeways from velocity gradients caused by shadow zones on the lee sides of the causeways. As the residual velocities and net sediment transport rates were low, the upper harbour was deemed to be in dynamic equilibrium

Modelled existing hydrodynamics within Stella Passage, Town Reach and the upper harbour were compared to three modelling scenarios simulating the 2015-2016 capital dredging, and proposed wharf extensions, dredging and reclamation. The modelled harbour developments had no significant impact on the hydrodynamics in the upper harbour; changes to water levels and current speeds were less than 0.025 m and 0.05 $m.s^{-1}$, which were smaller than model errors and the impacts of weather events. The largest impacts were localised within Stella Passage and Town Reach close to the proposed developments. The 2015-2016 dredging reinforced the existing patterns in residual velocity and potential sediment transport pathways. Differences in current speeds between models indicated that the largest impacts on the hydrodynamics within Stella Passage and Town Reach were from the extension of the dredged channel into Town Reach rather than the wharf extensions and reclamation. Current speeds decreased significantly within the newly dredged channel, but this effect was compensated for to a degree by the restrictions of the channel width when the wharves were constructed. In western Town Reach, current speeds increased due to the drop-off moving south and the asymmetrical shape of the dredging extension channelling the tidal flow. The potential for sediment transport and erosion increased in western Town Reach, however the actual sediment transport may be reduced following the formation of a shell lag facies which are common areas of high flow within the harbour.

ACKNOWLEDGEMENTS

Firstly, I would like to express my thanks to my supervisor, Dr Willem de Lange, for liaising with the Port of Tauranga to arrange the thesis topic and organise funding. In particular, the organisation of field work and providing input into manipulation of the datasets was much appreciated.

A sincere thank you to the Port of Tauranga for awarding me a research scholarship and for their continued support and enthusiasm for the project. Thank you to Lance Wood and Rowan Johnstone in particular for providing access to relevant documents, proposed construction plans, datasets, and for their support and guidance. Having access to the Port of Tauranga's onsite library to review the extensive number of technical reports was greatly appreciated.

To the staff and fellow students at the University of Waikato, thank you for your support and guidance. I would like to express my gratitude to the staff at the Coastal Marine Field Station for allowing me to be based at their offices. In particular Te Puea Dempsey who organised access to a computer with modelling software as well as sharing her knowledge of the masters process. Thank you to Dirk Immenga for help with the instrument deployment and collection of the field data. I would like to thank Bradley Monahan for providing a template of the Delft3D model as well as explanations into the models set-up and the datasets used. Thanks are expressed to Cheryl Ward for her limitless support and expertise in referencing and thesis presentation. I would also like to thank the University of Waikato for awarding me a scholarship to undertake this research.

Finally, a special thank you to my parents in New Zealand and my sister in the UK. Their continued support and enthusiasm was essential in the completion of this thesis.

TABLE OF CONTENTS

Chapter Eight

LIST OF FIGURES

CHAPTER ONE
INTRODUCTION

1.1 Background

Located within the southern basin of Tauranga Harbour, the Port of Tauranga is the largest export port in New Zealand and continues to undergo harbour development to provide access for the increasing number of vessels (Figure 1.1). Creating more berthage and deeper shipping channels is essential to accommodate the ever increasing ship sizes. The Port of Tauranga plans to increase the berthage of both the Sulphur Point and Maunganui wharves. The proposed works include a combined 1,303 m of wharf extensions, 4.7 ha of reclamation, and 2,000,000 m^3 of dredging. As with previous alterations to Tauranga Harbour, the Port of Tauranga requires a resource consent to carry out the proposed developments.

Under New Zealand's Resource Management Act (RMA) 1991, any activity that may alter or effect the environment requires a resource consent. Resource consents may be issued after thorough investigation is undertaken into any potential impacts the activity may have. The hydrodynamic conditions within a harbour system may be altered by the addition of any new man-made structures or changes to the morphology (de Lange, 2011). Numerical models are often used to simulate the real world conditions and predict any potential impacts that may occur. Calibrated and verified numerical models can predict the existing hydrodynamics and sediment transport pathways, as well as modelling any proposed harbour developments. Having accurate predictions of the future hydrodynamics after harbour developments such as dredging and wharf extensions can mitigate any potential adverse effects (Krüger & Healy, 2006).

Numerical models of past wharf extensions and dredging works at the Port of Tauranga have been carried out by various consultancies and as postgraduate studies through the University of Waikato. The University of Waikato was approached by the Port of Tauranga to develop a numerical model to predict the potential impacts of the wharf extensions on the hydrodynamics in Stella Passage and the upper harbour. Sections of the wharf extension works have been modelled by Bell (1994) and McKenzie (2014) but the impacts of the current wharf extension plans have yet to be modelled (Bell, 1991; McKenzie, 2014). Previous hydrodynamic models of the southern basin of Tauranga Harbour have been calibrated and verified with field data collected within the lower harbour and Stella Passage. However there are no hydrodynamic models that simulate the hydrodynamic conditions beyond Stella Passage into the upper harbour, and there is limited field data. As a result, little is known about the existing hydrodynamic conditions within the upper harbour.

Figure 1.1: A north facing aerial photograph of the Port of Tauranga located within the southern basin of Tauranga Harbour, New Zealand. Stella Passage is the main channel in the foreground and the proposed wharf extensions are to extend south from the existing wharves at Sulphur Point and Maunganui wharves (western and eastern Stella Passage respectively). Source: The Port of Tauranga (2015). Personal Communication (email).

1.2 Thesis Objectives

The primary aim of this thesis was to predict the potential impacts of the Port of Tauranga's proposed wharf extensions on the hydrodynamic conditions within Stella Passage and the upper harbour. To achieve this aim a Delft3D hydrodynamic model was produced and three key objectives addressed:

1) Develop a hydrodynamic model of the southern basin of Tauranga harbour. Calibrate and verify the model with field data recorded by oceanographic instruments deployed over a spring and neap tide.

2) Simulate and discuss the existing hydrodynamic conditions and inferred sediment transport pathways within Stella Passage and the upper harbour.

3) Predict the impacts of the Port of Tauranga's 2015-2016 capital dredging and the proposed wharf extension works on the existing hydrodynamic conditions and the inferred sediment transport pathways within Stella Passage and the upper harbour.

1.3 Thesis Structure

Within this thesis, subsequent chapters were structured as follows:

Chapter Two introduces and describes the field site and gives descriptions of the physical environment of Tauranga Harbour and the development of the Port of Tauranga.

Chapter Three reviews previous studies in the southern basin of Tauranga Harbour and the findings from reports on the Port of Tauranga's previous wharf extensions.

Chapter Four describes the field data used in the set-up, calibration and verification of the hydrodynamic model. The Delft3D FLOW software is introduced as well as a description of the modelling approach and basic set-up of the southern basin model.

Chapter Five describes the model parameters used in the sensitivity analysis of the southern basin model and the subsequent calibration and verification of the model by means of statistical analysis.

Chapter Six describes the results from the southern basin model to characterise the hydrodynamic conditions with the southern basin, Stella Passage, Town Reach, and the upper harbour. Discussion is focused on the patterns in water levels, current speeds and residual velocity in the overall study area as well as localised areas. Model results are used to infer sediment transport pathways and the potential patterns of erosion and accretion in Stella Passage, Town Reach and the upper harbour.

Chapter Seven describes the set-up of four modelling scenarios used to simulate pre-works conditions, the Port of Tauranga's 2015-2016 capital dredging, and the two main stages of wharf extension works (dredging into Town Reach and the wharf extensions and reclamation). Model results were used to describe and discuss the potential impacts of the dredging and wharf extensions on the existing hydrodynamic conditions, the inferred sediment transport pathways, and the potential patterns of erosion and accretion in Stella Passage, Town Reach and the upper harbour.

Chapter Eight summarises the significant results and addresses the three key objectives and primary aim of the thesis. Final recommendations are given with areas for future research identified.

CHAPTER TWO

FIELD SITE DESCRIPTION

2.1 Overview of Tauranga Harbour

There are 443 estuaries around New Zealand's 10,000 km length of coastline (Hume et al., 2007). Being some 40 km long and one of the largest estuaries in New Zealand, Tauranga Harbour is a barrier enclosed estuarine lagoon that is located in Western Bay of Plenty on the northeast coast of the North Island (Tay et al., 2013). Hume et al. (2007) developed a classification system for New Zealand estuaries based on broad scale physical components and hydrodynamic processes. Level 2 of the system identifies eight common estuary types based on hydrodynamic processes. Tauranga Harbour falls into Category F, the barrier enclosed lagoon, which is the most common type of estuary on the northeast coast of New Zealand. Barrier enclosed lagoons are generally shallow with extensive tidal flats and are well mixed (Hume et al., 2007).

An aerial view of Tauranga Harbour in Figure 2.1 shows the two basins and inlets, both which are tidally dominated. The Port of Tauranga is New Zealand's largest export port and is located in the southern basin (Tay et al., 2013). There is little to no exchange between the two basins, and past studies have assumed that the basins can be treated as separate systems (Tay et al., 2013). This study looks at the southern basin of Tauranga Harbour, particularly Stella Passage and the upper harbour estuaries. An overview of the geology, hydrology and wind and wave processes in Tauranga Harbour are given in this chapter along with a more detailed description of the southern basin.

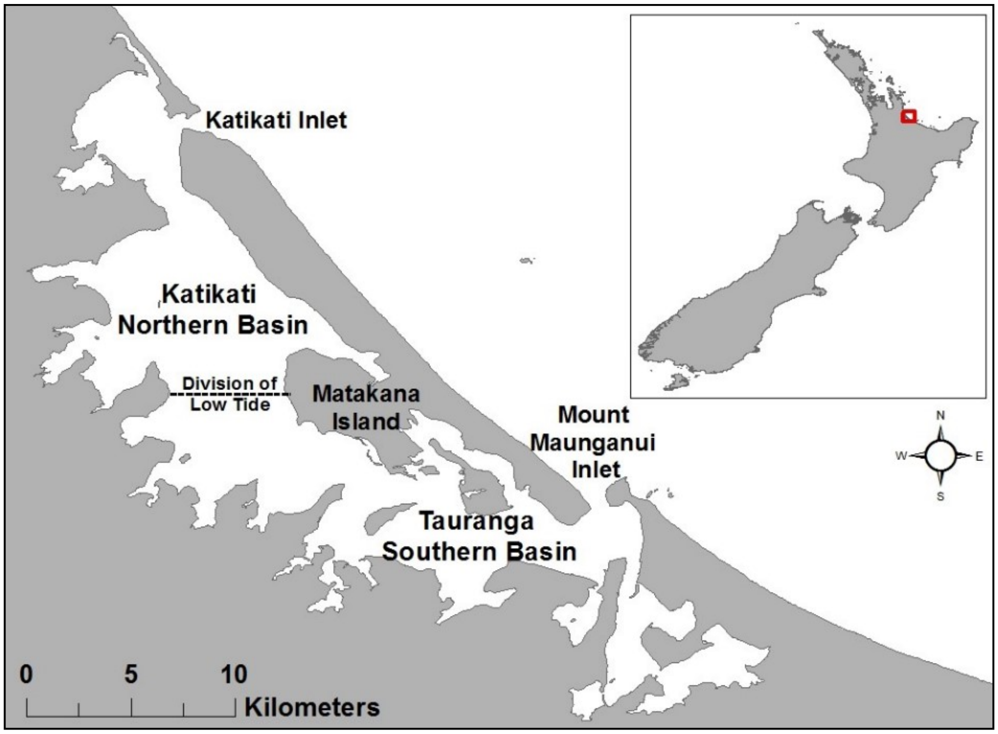

Figure 2.1: Tauranga Harbour in Western Bay of Plenty, New Zealand.

2.2 Geology of Tauranga Harbour

The Tauranga Harbour sandy barrier system is 851 km^2 long and was formed from impounded Holocene beach ridges with a smaller Pleistocene barrier in the inner harbour (Healy et al., 1996). The sand barrier extends 24 km and is known as Matakana Island (Spiers et al., 2009). The harbour's two tidal inlets are located at each end of Matakana Island which is bordered by two rhyolite tombolos, Bowentown at the Katikati entrance and Mount Maunganui at the Tauranga entrance (de Lange et al., 2015).

Five lithofacies have been identified in Tauranga Harbour (Table 2.1) which are part of the wider Tauranga Group.

Table 2.1: Descriptions of the five lithofacies identified in Tauranga Harbour's southern basin from over 70 core records and the origin of the three main facies in the lower southern basin (Healy et al., 2009).

Lithofacies	Description and Origin
Pumiceous facies	The basal member of the cores contains intercalated muds and pumice gravel. Within the core logs the facies was measured as 2-8 m thick, but the base of the layer was not penetrated.

Undifferentiated mud	Ranging up to 8 m thick in some of the core records, the mud layer only appeared in cores that were drilled before 1970. The mud was assumed to be volcanic as no shells are mentioned in the descriptions.
Undifferentiated sand	Underlying the shelly facies are medium sands. The sand was a thin facies, ranging from only 2-4 m thick.
Shelly mud	A shelly mud facies of around 8-14 m thick was identified in some core records. The silt and clay content of the shelly mud layer was high.
Shelly sand	Overlying modern Holocene marine sand was the upper most member of the cores and the layer thickened seaward. The thickness ranges from 5-25 m.

The three major lithofacies were the basal pumiceous, shelly mud and shelly sand (Healy et al., 2009). Origins of the pumiceous facies were thought to be from fluvial and fan deposits due to the bedding and rounded pumice clasts. Eroded volcanic material was deposited in river valleys as a Quaternary alluvial fan deposit during the Pleistocene low sea levels. Post-glacial sea level rise flooded valleys and muddy estuarine sediments were then deposited as the shelly mud facies. The upper most lithofacies was deposited after the post-glacial transgression had stabilised. Marine sands were transported off the continental shelf and moved back onshore to form the barrier system (Healy et al., 2009).

In New Zealand it has been found that when compared to estuaries on stable continental margins, estuaries that are on a tectonic plate margin infill at a higher rate (Healy et al., 1996). Like most New Zealand estuaries, Tauranga Harbour is gradually infilled with fine sediments from both terrestrial, fluvial and marine origins (Krüger & Healy, 2006). Outside the harbour, the littoral drift regime runs from northwest to southeast, and the drift rate determined in 1980's was 80,000 m^3 per year. The two tombolos act as partial barriers to the littoral system (Krüger & Healy, 2006).

2.3 The Southern Basin

The southern basin of Tauranga Harbour has a total area of 95 x 10^6 m^2 and a volume of 174 x 10^6 m^2 at mean sea level (MSL) (Tay et al., 2013). The division of low tide in Figure 2.1 is opposite Kauri Point and the southern basin extends from this point to Mount Maunganui. Typical of a barrier enclosed lagoon, the bathymetry in the southern basin is shallow (Tay et al., 2013). Intertidal flat regions cover 41 km^2 of the basin area, and 70 % of the harbour floor is exposed at low tide (de Lange & Healy, 1990; Tay et al., 2013). Wairoa River is the main fresh water input in the southern basin with a mean inflow of 17.6 $m.s^{-3}$ (Tay et al., 2013). The Mount Maunganui entrance to Tauranga Harbour and inside the tidal inlet have been modified by capital dredging by the Port of Tauranga (de Lange et al., 2015). The main components of Tauranga Harbour's tidal inlet system and the Port of Tauranga are indicated in Figure 2.2.

Figure 2.2: The main components of the tidal inlet system in the southern basin of Tauranga Harbour. The inset map shows the model domain in blue and the black box outlines the pictured area. ETD and FTD are the ebb tidal delta and flood tidal delta respectively. Source: Google Earth.

A large ebb tidal delta extends out from the Entrance Channel, formed by sediment laden currents which were jetted out from the southern basin (Davies-Colley & Healy, 1978). The Entrance Channel through the Tauranga Inlet is 34 m deep and 500 m wide (Spiers et al., 2009). Inside the harbour the majority of the tidal volume flows through either the Western Channel or Maunganui Roads

(Davies-Colley & Healy, 1978). Artificial Cutter Channel was first dredged in 1966 for port access. The majority of the inner harbour is dominated by the Centre Bank which is a large shoal that makes up the flood tidal delta (Davies-Colley & Healy, 1978). The narrow deep entrance and the ebb and flood deltas of the lower southern basin are all part of the tidal inlet system (Hume et al., 1992). The area of interest for this study is Stella Passage and the upper limits of the harbour, which are not considered to be part of the tidal inlet system (de Lange, 2011).

Stella Passage and the estuaries and bays in the upper harbour are identified in Figure 2.3. Stella Passage and Town Reach are the two main channel systems in the southern arm of the southern basin. Dredging has taken place in Stella Passage and the area has also been modified by the Port of Tauranga wharves, a boat mooring marina and two harbour bridges. Beyond and to the east of the Railway Bridge there are extensive tidal flats, continuing on into the upper reaches which include Waipu Bay, Waimapu Estuary, Rangataua Bay and Welcome Bay and the Maungatapu and Hairini Bridges (Tay et al., 2013). From historical photos, the morphology of the upper harbour is seen to be relatively stable (ASR, 2007). The main fresh water input in the upper harbour is the Waimapu Stream.

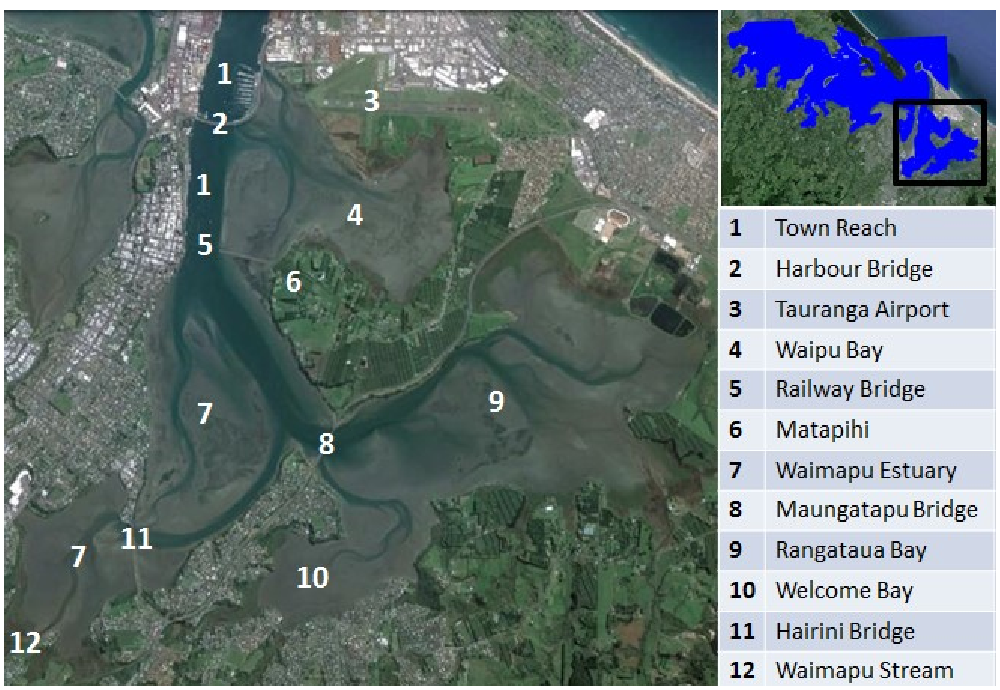

Figure 2.3: The main components of Stella Passage and the upper harbour in the southern basin of Tauranga Harbour. The inset map shows the model domain in blue and the black box outlines the pictured area. Source: Google Earth.

2.4 Sediments

Inside the harbour the sediments consist of mostly sand-sized material with some coarser sediments comprised mostly of biogenic carbonate material (shells) (Davies-Colley, 1976). The sediment composition in the channels where the strongest tidal currents occur are bimodal, with coarser sediments and sand-sized material (Davies-Colley, 1976). In the presence of fast current velocities the finer sands are removed and the shell fraction is left as it is less-easily transported (ASR, 2007). In some channels in the harbour a lag surface (shell lag) could develop where the sea bed is armoured. Armoured shell lag areas have a lower rate of net sediment transport (ASR, 2007). Studies have found that the stronger the currents, the denser the shell coverage (Boulay, 2012).

Stella Passage is dominated by fine sand-sized sediments with some areas of very fine sand next to the container terminals, and a shelly sand region in the northern Stella Passage (Boulay, 2012). In Town Reach between dredged Stella Passage and the Harbour Bridge, shell lag facies have armoured the shallow shelf. On the western side of Town Reach is an area of smaller very shelly medium sand (Boulay, 2012). Finer sediments are found on the extensive tidal flats and in the upper harbour. It is common for bedforms to change and deform on the harbour floor as, apart from shell lag sections, the sediments are generally unconsolidated (Davies-Colley, 1976).

2.5 Hydrodynamics

The greatest influence on circulation and hydrodynamics in an estuary are the tidal range, wind and wave action and fresh water inputs (Healy et al., 1996; Tay et al., 2013). A brief overview of the tides and waves in Tauranga Harbour is given in this section and are discussed in greater detail in Chapter Four. Tauranga Harbour has a weak salinity gradient that varies with the tide and has limited effect on estuarine circulation (Tay et al., 2013). The large ebb tidal deltas at both entrances to Tauranga Harbour indicate that the inlets are strongly tidally dominated (de Lange & Healy, 1990).

2.5.1 Tidal Currents

Tidal range is the main driver of circulation in the southern basin (Healy et al., 1996). In New Zealand the M2 and S2 tidal constituents have the most influence on the tidal signal. Tides around New Zealand are semi-diurnal and usually have a tidal range of 2 m on the east coast and 3-4 m on the west coast (Healy et al., 1996). Tauranga Harbour is a mesotidal estuary that has a spring tidal range of around 2 m (Tay et al., 2013). The main tidal constituents are used to set the boundary conditions and force numerical models, and are also used in calibration (Hume et al., 1992). Most areas of the southern basin have a dominant tidal phase, either ebb or flood (Davies-Colley & Healy, 1978).

Tidal wave surge is the phenomena that is responsible for the delayed high water and peak currents behind the tide as a wave moves into the lagoon (de Lange & Healy, 1990). Lagging of the sea level between outside the Tauranga Harbour inlet and the upper reaches is evident (ASR, 2007). The lagging sea levels drive currents within the harbour by way of a gradient, pulling and pushing the water through the Entrance Channel (ASR, 2007). In the harbour the largest phase change is through the Entrance Channel, but the tidal wave is also attenuated through the constricted entrances to sub-estuaries (Tay et al., 2013). Attenuation of the tide changes the tidal amplitude measured in the harbour (Tay et al., 2013). Shallow-water over-tide amplitudes like M4 and S4 also change throughout the harbour (Hume et al., 1992; Tay et al., 2013). The phase of the over-tides is determined by differences in the geometry and frictional effects in tidal flats to those in deep channels (Tay et al., 2013). Currents vary within the harbour, with velocities greater than 2 $m.s^{-1}$ at the Entrance Channel, and around 1 $m.s^{-1}$ throughout the rest of the harbour (ASR, 2007).

2.5.2 Waves

Hydrodynamics in the main channels of the harbour are dominated by tidal currents, but on intertidal flats, shallow areas and shorelines waves are also important; especially wind waves (Davies-Colley & Healy, 1978). The harbour has two dominant wave frequency bands, one high and the other low frequency (de Lange & Healy, 1990). In the high frequency wave spectra, 70 % of the high frequency waves at 3.5 seconds are due to waves passing through the Entrance Channel. Another peak at 1.2 seconds accounts for 10 % of the high frequency wave energy and represents wind waves generated within the harbour (de Lange & Healy, 1990). The most frequent prevailing winds are westerly which are also the strongest winds (Davies-Colley & Healy, 1978). The longest fetch is from the east to west, and coupled with the prevailing westerlies, gives the largest wind waves in the southern basin in front of the Port of Tauranga (No. 6 in Figure 2.2) (Davies-Colley & Healy, 1978). Long period low frequency waves from seiches and edge waves (>14 seconds excluding tidal waves) account for 5 % of the wave spectra and are caused by external forcing from tsunamis, high wind speeds over 9.5 $m.s^{-1}$, large swell waves and storm surges (de Lange & Healy, 1990). Although tidal currents and wind generated waves are the two major hydrodynamic drivers, minor water movements such as seiching or harbour resonance and transient estuarine circulation also contribute to the hydrodynamics of the area (Davies-Colley & Healy, 1978).

2.6 History of the Port of Tauranga

The Port of Tauranga, formerly known as the Bay of Plenty Harbour Board, was established in 1873 but the first berths and pier at Mount Maunganui were not constructed until 1919 (de Lange et al., 2015). Since construction, major harbour development works have been undertaken by the Port of Tauranga (Krüger & Healy, 2006; Tay et al., 2013). Figure 2.4 identifies the wharves that have been constructed by the Port of Tauranga and other major engineering structures that have influenced Stella Passage and Town Reach.

1	Tug and pilot boat wharves outside main office, constructed 1986
2	Maunganui Wharves, constructed 1953 - 1996
3	Sulphur Point, reclamation 1968
4	Sulphur Point Wharves, constructed 1988-2014
5	Butters Tanker Berth, constructed 1996
6	Tauranga Bridge Marina, opened 1996
7	Aerodrome Bridge, opened 1988
8	Tauranga Harbour Bridges, opened 1988 and 2009

Figure 2.4: Wharves and other engineering structures constructed by the Port of Tauranga and other major structures in the southern basin of Tauranga Harbour. Source: Google Earth.

The main stages of the Port of Tauranga's development are summarised below:

1927 The Port constructed a railway wharf and upgraded facilities in 1927, ready for the opening of the railway between Hamilton and Tauranga in 1928 (Hansen, 1997).

1950 By the 1950's port trade had increased with the addition of timber, pulp and paper exports (de Lange et al., 2015).

1953-65 Need for new wharf facilities lead to the construction of the first wharves on the Mount Maunganui side in 1953, with 372 m of concrete wharf which by 1965 had been extended to 1,067 m (Fletcher Construction, 1986).

1965-68	Dredging regimes have worked since 1965 to increase the channel and ship approach depths to allow larger ships access to the port (de Lange et al., 2015). In 1968 the first major dredging works deepened the existing channels and also the harbour approach, cutting through the ebb tidal delta and eventually the flood tidal delta to create Cutter Channel. The dredged sediment was used to reclaim 85 ha of land in the Sulphur Point area which was originally a large intertidal sandflat; 58 ha of the reclaimed land was used by the Port of Tauranga (Port of Tauranga Ltd, 1990).
1986	In 1986 a tug and pilot boat wharf was built at Pilot Bay outside the Port of Tauranga offices (Fletcher Construction, 1986).
1988-92	With the continued increase in trade and storage constraints on the Mount Maunganui side of the port, construction began on the first Sulphur Point wharf in 1988 (Port of Tauranga Ltd, 1990). The 340 m pile and deck wharf had a dredged depth of 11.6 m alongside it, and in 1990 the consent was extended to approve an extra 260 m (known as extension No.1) to give 600 m of wharf and a revised depth of 14.5 m. The 600 m of wharf was completed in 1992 (Port of Tauranga Ltd, 1990).
1991-92	A second phase of capital dredging in 1991-92 deepened shipping channels inside the harbour and in the Entrance Channel and approach to 12.9 m and 14.1 m below chart datum (CD) respectively (Healy et al., 2009). The Port of Tauranga carried out maintenance dredging works between capital dredging schemes, with the initial dredged volume of 70,000 m^3 per year increasing to 110,000-130,000 m^3 per year after the 1991-92 works (Healy et al., 2009).
1996	The 1,067 m Maunganui wharf was extended to 2,055 m in 1996 (Hansen, 1997). South of the concrete wharf extension, an 80 m long concrete dolphin type berth for tankers and carriers (known as Butters) was also constructed (de Lange, 2011).
2014	The most recently completed wharf extension (extension No.2) was at the northern end of Sulphur Point in March 2014 (Winthrop, 2014). The pile and deck wharf added 170 m to the 600 m of berthage already at Sulphur Point (Winthrop, 2014). 50,000 m^3 of sand and silt were dredged and used in the reclamation of the 0.4 ha behind the wharf

(Thompson, 2001; Winthrop, 2014).

2015-16 Capital dredging works for a deepening and widening project commenced in October 2015 and continued until August 2016. Channels inside the harbour were deepened to 14.5 m and to 15.8 m below CD in the Entrance Channel and approach to allow for 13.2 m draught container vessels. The extent of the dredged area for the 2015 deepening and widening works is shown in Figure 2.5 (de Lange et al., 2015).

Future The Port of Tauranga plans to extend both the Sulphur Point and Maunganui wharves south to increase berthage by another 385 m at Sulphur Point and 918 m on the Mount Maunganui side. Plans also include an increase in depth in front of the wharf extensions to 12.9 m and 16 m below CD extending the dredged area south. The plans for the wharf extensions and associated dredging is shown in Figure 2.6; the dredged sediments will be used in the reclamation behind the wharves. This thesis aims to model the impacts that the proposed wharf extension works may have on the hydrodynamics of Stella Passage and the upper harbour.

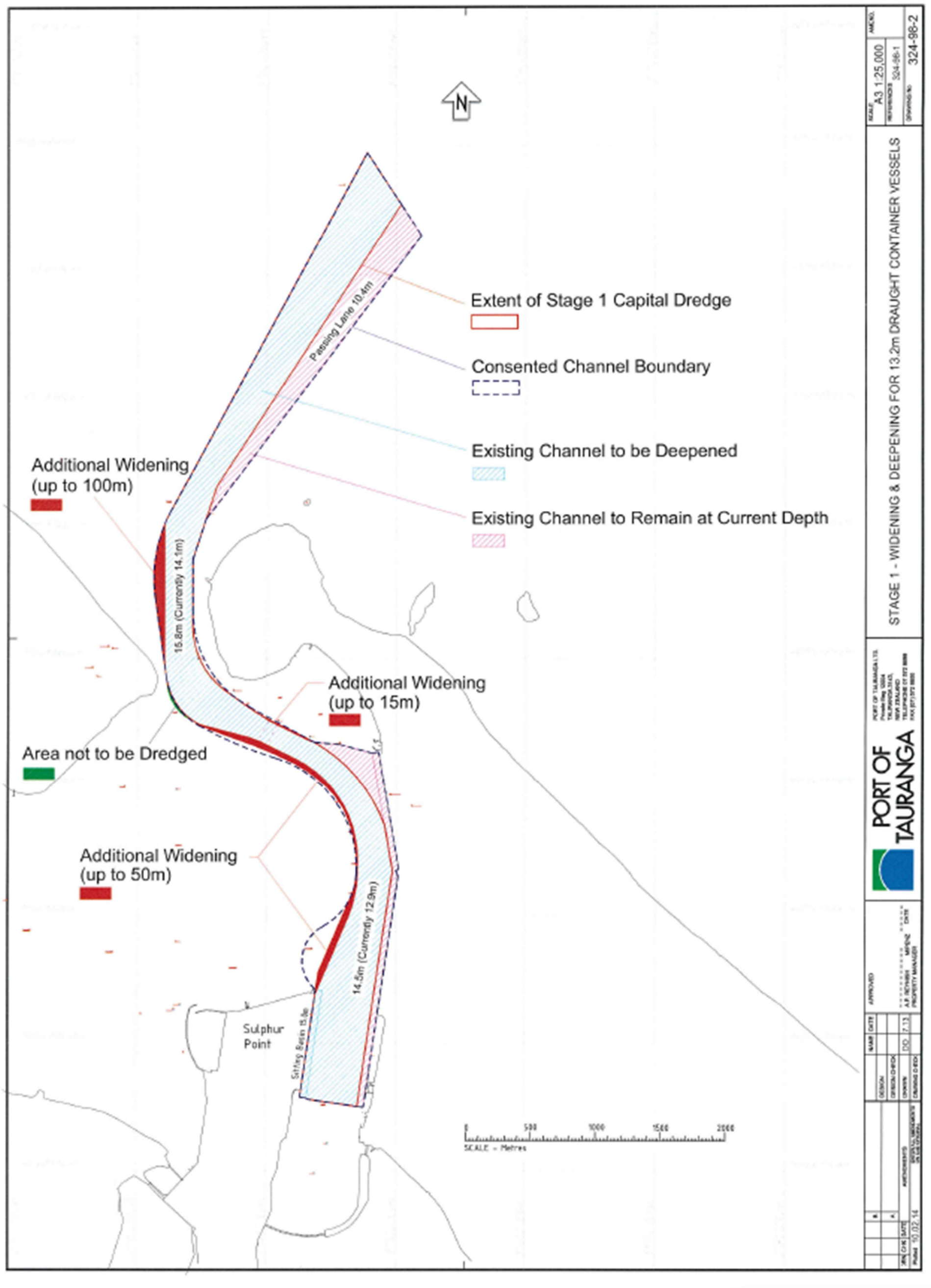

Figure 2.5: Port of Tauranga plans for the 2015-2016 capital dredging works in the southern basin of Tauranga Harbour. Source: The Port of Tauranga (2015). Personal Communication (email).

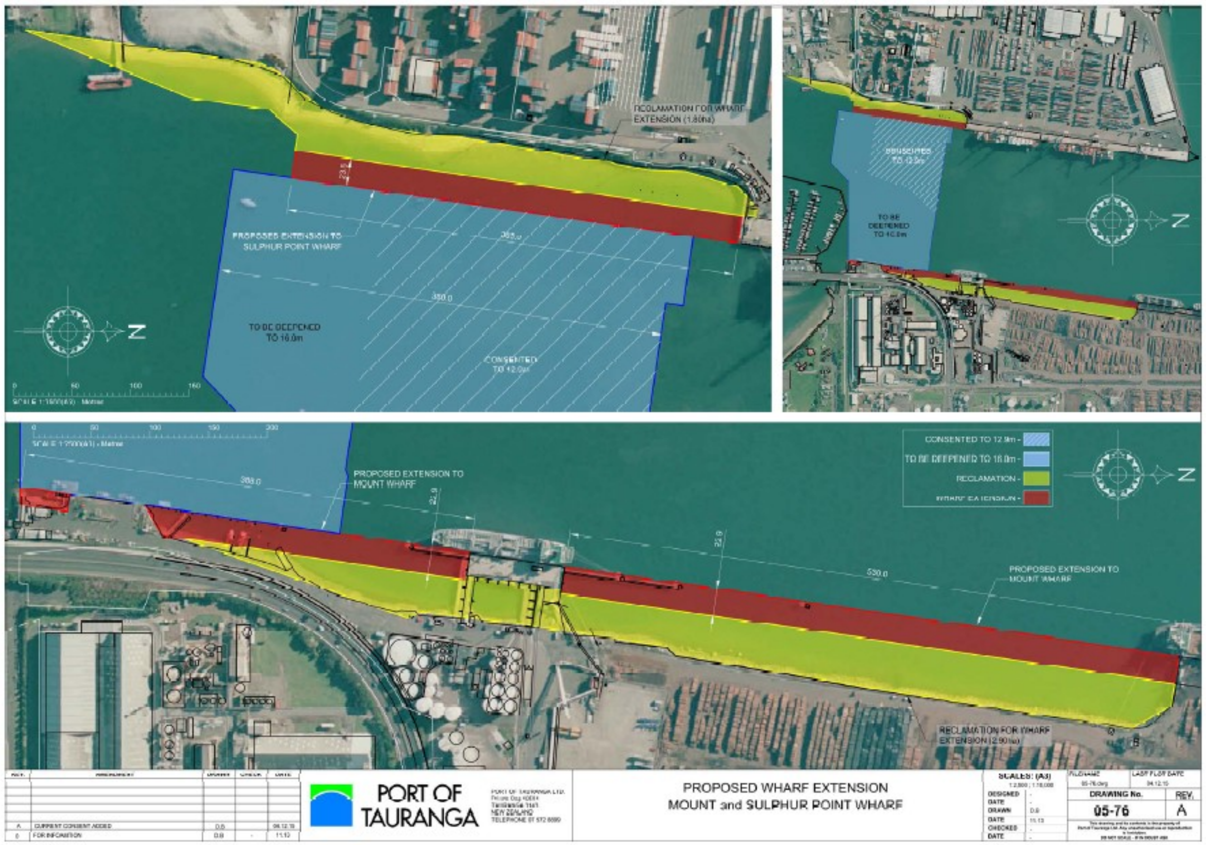

Figure 2.6: Port of Tauranga plans for the proposed wharf extensions to the existing Sulphur Point and Maunganui wharves south towards Town Reach and the associated dredging and reclamation in the southern basin of Tauranga Harbour. Source: The Port of Tauranga (2015). Personal Communication (email).

CHAPTER THREE

PREVIOUS STUDIES AND WHARF CONSTRUCTION IN TAURANGA HARBOUR

3.1 Introduction

Larger studies of the Tauranga Harbour area are reviewed in this chapter to characterise the physical environment, concentrating on works that described the hydrodynamics and sediment transport in Stella Passage and the upper harbour, discussed changes to the environment from engineering structures, and those using numerical models. This overview of studies in Tauranga Harbour is followed by reports on the potential and observed impacts of the wharf and wharf extensions at Sulphur Point. Many of the reports were required to ensure no new man-made structures would change the dynamic equilibrium of Tauranga Harbour (ASR, 2007). In general, structures that narrow channels create flow constriction and increase current velocity, whereas dredging increases the cross-sectional area and decreases current velocity (ASR, 2007). Patterns of erosion and accretion were also thoroughly studied as sediment transport loops are often interrupted by engineering structures (ASR, 2007). The aim of this chapter is to form a background knowledge of all the relevant information so accurate predictions can be made on the potential impacts of the wharf extension on Stella Passage and the upper harbour.

3.2 Previous Studies of Tauranga Harbour

3.2.1 Tauranga Harbour Physical Model 1959

In May 1959, during the early stages of harbour development, the Tauranga Harbour Board commissioned the Hydraulics Research Station, Wallingford, England to develop a physical model of Tauranga Harbour (Hydraulics Research Station, 1968). Two scale models, one with a fixed bed and the other a partially mobile bed, were constructed to examine the benefits of many possible developments and schemes. The fixed bed model was used to provide boundary conditions for the second model, to eliminate any schemes that were unsuitable and to reduce the number of simulations run on the second model (ASR, 2007). The second model with the partially mobile bed is shown in Figure 3.1.

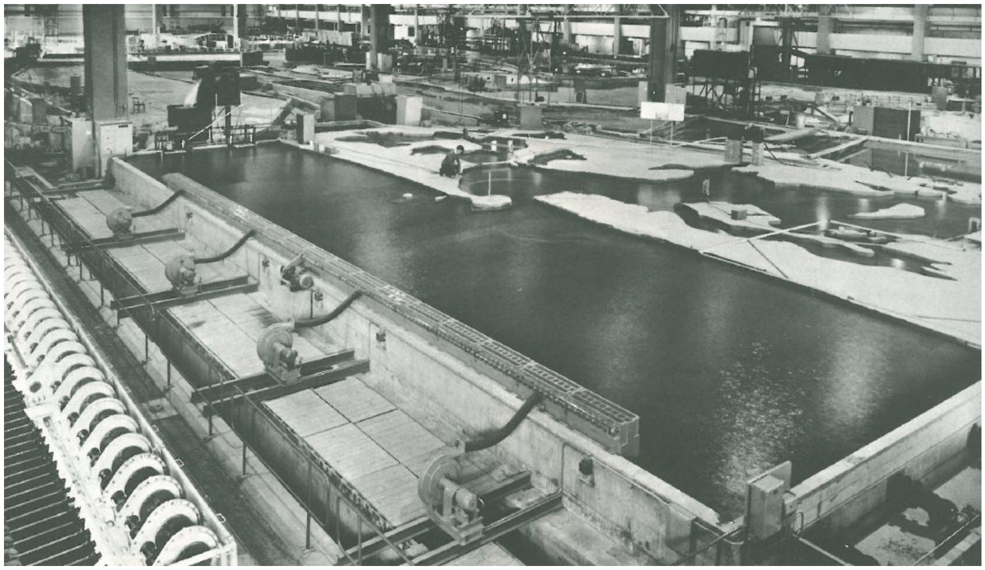

Figure 3.1: View of the Tauranga Harbour physical model with a partially mobile bed. Source: (Hydraulics Research Station, 1968).

Hydraulic Research Station (1968) used historical charts, field measurements and the two physical models to increase the depths within the harbour and to identify locations suitable for additional wharfage. Simulations on the second model with the partially mobile bed were run using a number of conditions and different ordering of development stages to identify the ideal scheme. The runs were over a period that simulated six years of sediment movement (Hydraulics Research Station, 1968). Hydraulics Research Station (1968) recommended the dredging of Cutter Channel through the flood tidal delta rather than using training walls or groynes.

3.2.2 Tauranga Harbour Study 1983

The potential for harmful effects from the development of Tauranga Harbour saw the first major numerical model developed in the 1980's (Barnett, 1985). The Tauranga Harbour Study was the first large scope study to be undertaken by a New Zealand consultant. The aim was to produce a long term management strategy for Tauranga Harbour. The Ministry of Works Development (MWD) arranged the project into five parts; Part I overview, Part II field data collection programme, Part III hydrodynamics, Part IV sediment transport and Part V morphological study (Barnett, 1985). Barnett (1983) was the project leader and presented parts I and III. Parts II and V were coordinated by Healy (1983). Black (1983) generated a sediment transport model for Part IV of the Tauranga Harbour Study.

3.2.2.1 Field Data Collection

Collected over three months between June and September 1983, the field data included an extensive array of water level, current, sediment and sonar recordings (Healy, 1985). Braystoke current meters gauged current speed profiles, and continuous current recordings were taken by six Aanderaa meters. Three permanent and four temporary tide gauges recorded water levels. The field data was used to calibrate the hydrological models developed by Barnett (1983). Sediment and suspended sediment sampling, underwater photography, sediment size analysis, side-scan sonar and seismic sediment profiling were used in the calibration of the sediment transport model in Part IV. When compared to historic surveys from 1962, the new recordings and aerial photography showed that little change had occurred in the harbour beyond the immediate vicinity of shipping channels and reclamations (Healy, 1985).

3.2.2.2 Hydrodynamics

A 2D numerical model of the hydrodynamics in Tauranga Harbour was developed on the Danish Hydraulic Institute (DHI) System 21 software (Barnett, 1985). The hydrodynamic model simulated the tidal flow patterns in the harbour and was used to predict the effects of the proposed Harbour Bridge, Sulphur Point Marina and dredging on tidal currents. A coarse 300 x 300 m grid gave the tidal signal that was then used for the boundary conditions in the smaller PORT model with a 75 x 75 m grid. With Stella Passage being less than 75 m wide, the PORT model was not accurate enough to model the proposed Harbour Bridge. A BRIDGE model was used for the Harbour Bridge predictions based on a 25 x 25 m grid. As with many of the applications that were run on the hydrodynamic model, different alternatives and iterations of the Harbour Bridge were examined before deciding on a final design (Barnett, 1985).

The strongest ebb and flood currents were predicted in the Entrance Channel, Western Channel and Cutter Channel (Barnett, 1985). After flowing through the Entrance Channel the peak flood currents did not form a single flood jet, but rather divided into the Western and Cutter Channels. The flood currents through Pilot Bay and across the shallow Centre Bank were weak. During the ebb tide a pronounced ebb jet developed to the west of the dredged channel outside the harbour (Barnett, 1985).

3.2.2.3 Morphodynamics

In Part V, Healy (1983) assessed the compatibility of the hydrodynamic and sediment transport modelled results against the harbour morphology and identified nine major facies. The nine facies were shell lag, very shelly sand, clean sand, shelly sand, silty sands, rock outcrops, gravel and boulders, sandwaves and megaripples, and undefined megaripples (Healy, 1985). Figure 3.2 displays the location of the sediment facies that were found in Stella Passage and Town Reach.

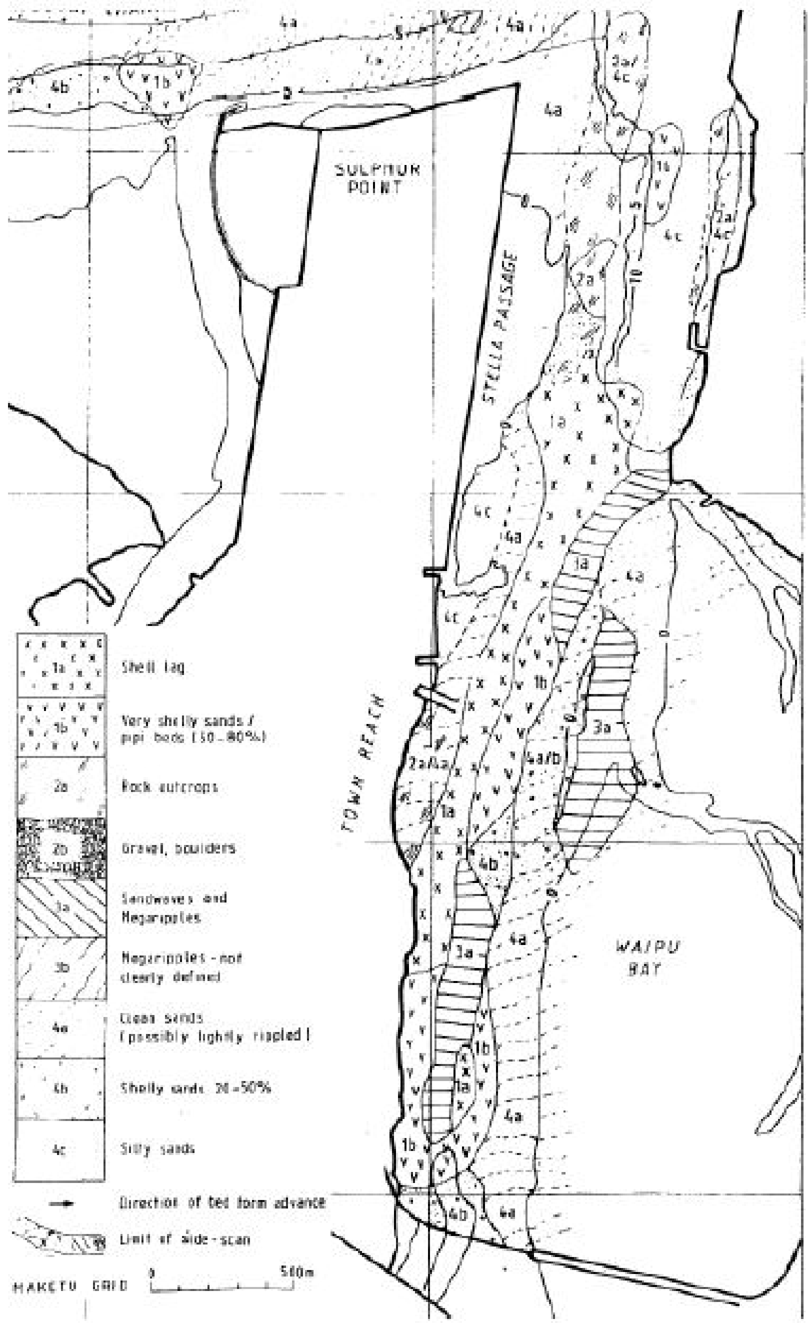

Figure 3.2: Map of the sediment facies on the seabed of Stella Passage and Town Reach in Tauranga Harbour in 1983. Source: (Healy, 1985).

Comparisons showed that the active sediment pathways could be defined by the strongly bedformed zones (Healy, 1985). Strong correlations were found between shell lag areas and strong current speeds. Stella Passage was found to be comprised of marine sand and shell to a depth of 20-30 m, with silt and fluvial deposits underneath. Near the surface of Town Reach however were weakly consolidated ignimbrite beds. Found within the northern part of Town Reach near the unconstructed Harbour Bridge, "bright spots" were indicative of organic silts and clays (Healy, 1985).

3.2.2.4 Sediment Transport

Black (1984) generated a sediment transport model for Tauranga Harbour using his previously developed 2SS model. When calibrating the model with the field data collected in Part II of the study calibration was found to be good in the high energy areas but less so in the lower energy areas. The largest sediment transport rates within the harbour were through the Western Channel. Sediment transport via the Western Channel was found to be part of one of the two major recirculating loops in the harbour which characterised the larger sediment transport pattern. Both loops originated from Panepane Point, with the Western Channel being the final stage of the clockwise loop. Figure 3.3 identifies the pathway of the clockwise loop along with the second smaller anticlockwise loop which was ebb dominant and flowed along Pilot Bay (Black, 1984).

Only light dredging was needed to maintain the channel depths in Cutter Channel and Maunganui Roads as the anticlockwise sediment transport loop had lower sediment transport rates (Black, 1984). The southern end of Cutter Channel which is part of the Port of Tauranga's shipping basin was identified as an area of concern, as accretion at the rate of 10,000-20,000 m^3 per year was predicted. The flow patterns throughout the rest of the harbour were determined by the balance between the two major loops. Dredging of the Cutter Channel and Maunganui Roads altered the flow rates through the anticlockwise system and in turn the larger clockwise loop. It was found that there was a decrease in flow and accretion through the Western Channel which was judged to be naturally occurring but intensified by the dredging (Black, 1984).

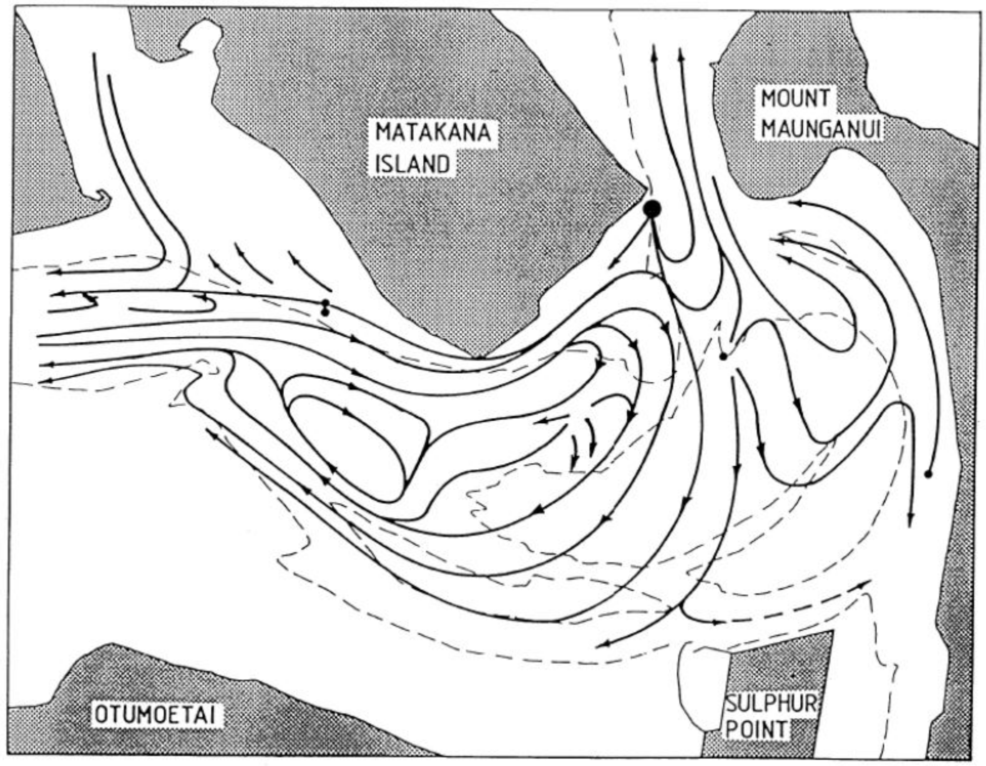

Figure 3.3: The major sediment circulation patterns within the lower southern basin of Tauranga Harbour. Source: (Black, 1984).

3.2.3 Tauranga Harbour Crossing 1985

Under the request of Fletcher Construction, Black and Barnett (1986) developed a smaller Tauranga Harbour Study model covering the local area around the bridge crossing on a 25 x 25 m grid to predict the potential effects of various bridge and causeway designs (Fletcher Construction, 1986). Model runs simulated any effects on current velocities and patterns, as well as accretion and scour (Fletcher Construction, 1986). The causeway between the Aerodrome and Harbour Bridges was predicted to cause restrictions to tidal flow (Fletcher Construction, 1986). From model runs it was determined that impacts from the Harbour Bridge and causeway would be minor and the structure was constructed (Fletcher Construction, 1985). Scour and undercutting of the seabed in front of the rock bund would occur during construction, but rock spillage formed a blanket and some protection after construction (Fletcher Construction, 1985).

3.2.4 Port of Tauranga Model Study 1991: Dredging Works 1991-92

Over the first six months of 1992, another round of capital dredging was carried out which would increase the waterway cross-sectional area within the shipping channels by 400 % (Port of Tauranga Ltd, 1990; Healy, 1996). As part of the consent process for the engineering works, the Port of Tauranga commissioned Bell (1991) to model the proposed dredging. A calibrated hydrodynamic model was used to determine the effects of the dredging on the current patterns and velocities in the area. The proposal was for the shipping channels to have a depth of at least 11.7 m during all tides (Bell, 1991).

Bell (1991) used both the calibrated 300 x 300 m coarse grid and 75 x 75 m PORT hydrodynamic models developed in the Tauranga Harbour Study. Since 1985 harbour works such as dredging for the new Sulphur Point wharves, construction of the Harbour Bridge and maintenance dredging had taken place, so both of the models were updated to have 1990 bathymetry. The model bathymetry was then lowered to give the depths below CD after dredging which were 12.9 m inside the harbour and 14.1 m in the Entrance Channel and approach. The boundary conditions of the coarse grid were kept the same as the 1985 model to preserve the calibration. To ensure that any change in current was due solely to the change in bathymetry used, the eddy viscosity and bed resistance were kept the same as the Tauranga Harbour Study model. Bell (1991) simulated model runs at both mean and spring tides with tidal ranges of 1.4 m and 2 m respectively.

From plots of mean and spring tide simulations, the increased cross-sectional area in the dredged model caused changes in the currents and water level (Bell, 1991). The tides between the Entrance Channel and Town Reach after dredging were predicted to have the same amplitude but a slight change in phase. The tidal curve was predicted to advance in time on both high and low water by 6 minutes (Bell, 1991).

Throughout the harbour the current velocities both increased and decreased after the dredging of the model (Bell, 1991). In dredged channels current velocities were expected to reduce to conserve mass continuity through the increased cross-sectional area. However the modelled velocities were not as low as expected. Changes to current velocity were determined by looking at the differences in ebb and flood tide flow volumes (Figure 3.4). Only small changes in the flood volumes and currents velocities were predicted in Stella Passage and Town Reach, with -5 % difference on the ebb tide and +1 % on the flood tide. Overall, Bell (1991) found that increasing the area of the channels by dredging would increase the flow from the Entrance Channel through the dredged channels, but that the additional flow onwards to Stella Passage and through to the upper harbour would be small.

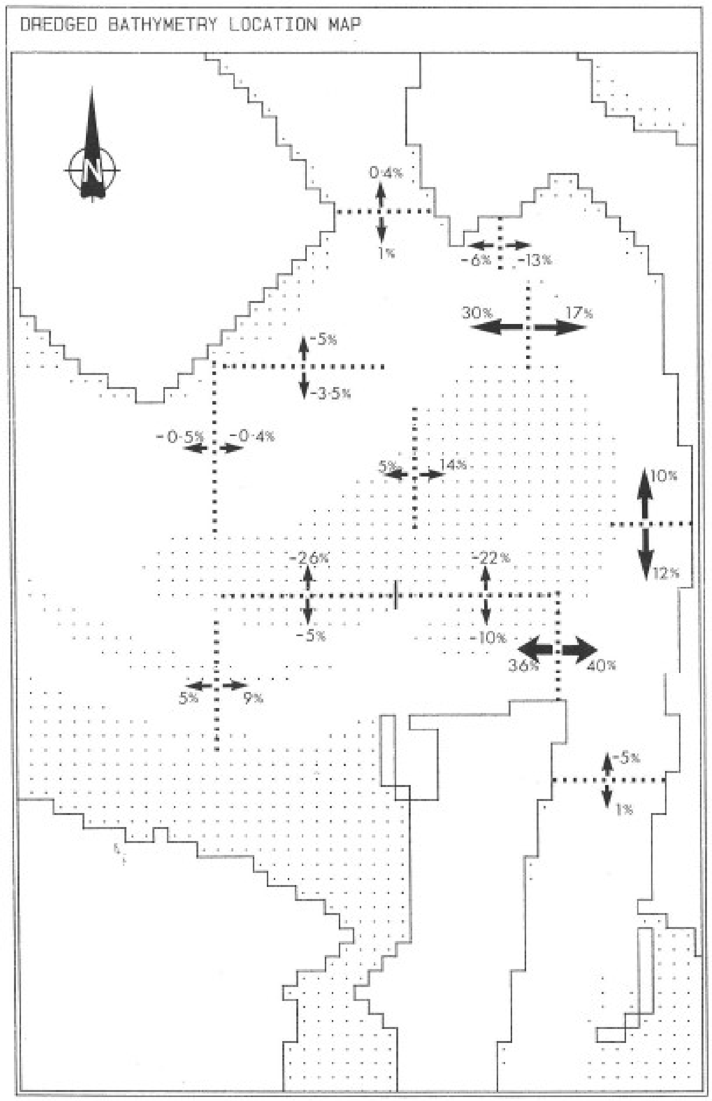

Figure 3.4: The difference in ebb and flood tide flow volumes between the 1990 and the dredged bathymetry for a mean tide (a –ve % change is a reduction in flow volume). Source: (Bell, 1991).

Residual velocity plots showed the non-linear changes in currents, which also indicate sediment transport pathways and areas that may be susceptible to scour or accretion (Bell, 1991). It was found that there would be only small differences in the overall current patterns due to the proposed dredging. The greatest difference in the residual velocity plots of the mean tide throughout the harbour were in Stella Passage and Town Reach area. A clockwise residual eddy overlaid an existing weak eddy, enhancing the clockwise circulation within Stella Passage and Town Reach (Bell, 1991).

A velocity above 0.3 $m.s^{-1}$ was chosen as a threshold for the sediment residual, which isolated the currents that have the potential for transporting sediment (Bell, 1991). Sediment residuals during a spring tide were then compared between the dredged and non-dredged simulations in Figure 3.5. Changes were due solely to the proposed dredging works, and the greatest changes were in Stella Passage and Town Reach. The difference plot showed a decrease in sediment residual velocity (and current speed) on the eastern side, and an increase on the western side, creating a clockwise circulation pattern (Bell, 1991).

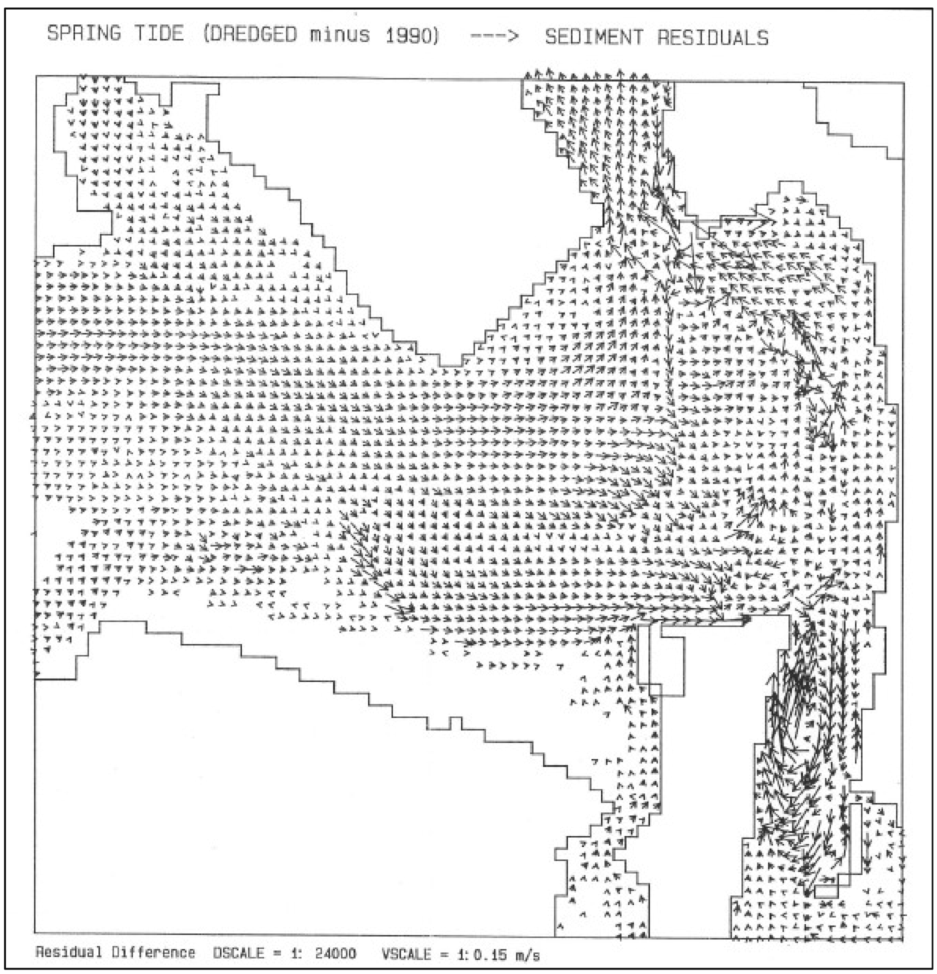

Figure 3.5: The difference in sediment residual velocity patterns during a spring tide between 1990 bathymetry and bathymetry that had been altered by the proposed 1991-92 dredging works in Tauranga Harbour. Visual scale is 1:0.15 $m.s^{-1}$. Source: (Bell, 1991).

3.2.5 Harbour Shoreline Erosion Fronting Whareroa Marae 1994

An investigation into the receding shoreline in front of the Whareroa Marae examined any potential causes and extent of the erosion on the shoreline (Healy, 1994). Healy (1994) conducted field investigations which included a volumetric analysis of beach profiles between 1986 and 1993 and concluded that the shoreline was eroding. The processes that were causing the erosion were deemed to be naturally induced. Diabathic transport of beach sand was attributable to natural cut and fill processes from wind forced wave action. Healy (1994) noted that since mid-1991 New Zealand had experienced a negative phase of the El-Niño Southern Oscillation (ENSO), in which eastern margins of the Tauranga Harbour experience strong westerly winds, increasing erosion in front of the Whareroa Marae. The theory that erosion was caused by cut and fill processes was supported by the expansion of the flood tidal delta near the causeway which is where the sand from the beach had been taken out over the intertidal flats. The estimated volume of sand transported was small and in the order of 113 m^3 per year (Healy, 1994).

Dredging works and the Harbour Bridge and causeway were found to have minor effects on the state of the shoreline (Healy, 1994). Changes to the hydrodynamics were interpreted from the Tauranga Harbour Study model for the Harbour Bridge design and Bell's (1991) model. Constriction of the tidal flow under Aerodrome Bridge increased current speeds on an ebb tide. Faster ebb tides would not have induced erosion, but Healy (1994) noted that if wind chop suspended beach sediments, sand may be removed from the beach system by the stronger ebb tides and not be transported back onshore. South of Aerodrome Bridge, stronger flood tidal currents were attributed to the 1991-92 capital dredging, resulting in an increase in deposition on the flood tidal delta offshore of the Whareroa Marae. Overall the engineering works that had taken place in Tauranga Harbour were deemed to have had no significant influence on the erosion in front of the Whareroa Marae (Healy, 1994).

3.2.6 Review of 1991-92 Capital Dredging Impacts 1996

Consents were given for the port area to be dredged to 12.9 m and the Entrance Channel and approach to 14.1 m (Healy, 1996). 5.5 million m^3 of material was dredged from the channels and was comprised of largely non-cohesive sand and gravelly broken shell. Although it was included in the consented works, Otumoetai Channel was not dredged. The sediment dredged under the capital dredging scheme, and the 340,000 m^3 dredged annually for maintenance was dumped off Mount Maunganui at a dump ground. All aspects of the dredging programme were monitored under the consent conditions. To adhere to the monitoring conditions, Healy (1996) compiled a review of the dredging programme and monitoring results which included MSc and PhD theses on turbidity, biodiversity and impacts from the dump ground. The key points of the summary were (Healy, 1996):

- There had been no substantial change to the ebb tidal delta.
- The flood tidal delta was more sensitive and the sediment pathways over the Centre Bank changed to have a greater west-to-east flow; leading to minor shoaling (50 cm) on the shallow sections of Centre Bank.
- The greatest impact was immediately after dredging; from then on the pattern stabilised.
- The long term average maintenance dredging amounts increased.

3.2.7 Southern Pipeline 2007

URS New Zealand Ltd engaged ASR Marine Consulting and Research (ASR) to determine the effects of a pipeline that would carry wastewater alongside the Matapihi Railway Bridge in Tauranga Harbour (ASR, 2007). Funded by Tauranga City Council (TCC), the Southern Pipeline was designed to transport wastewater from southern Tauranga to the Te Maunga Wastewater Treatment Plant by crossing the upper harbour alongside the Railway Bridge. ASR (2007) investigated any environmental effects that might arise from the construction of the Southern Pipeline. USR put forward various options for the possible design of the wastewater pipeline. Designs included building a second bridge alongside the Railway Bridge and submarine options where the pipeline was located on the seabed. The study involved using numerical models to simulate the effects of the pipeline on the hydrodynamics, sediment transport and waves in the area (ASR, 2007).

Historical analyses of the area involved using previous surveys and aerial photos to give an idea on the general conditions and development of the area (ASR, 2007). The harbour bed was found to be in dynamic equilibrium, whereby the morphology did move but the general locations of the bars, channels and conditions remained. Comparing aerial photos also found that the dynamic equilibrium was disrupted by dredging and the construction of the Railway Bridge and causeway in the 1920's, but the effects were not far reaching. Dredging especially has modified the dynamics of the area, stabilising of the main channel left only the smaller sub-tidal channels and sand bars to move around. Rapid scour around the bridge piers occurred after construction with a mean maximum scour hole depth of 2.15 m. Once shell lags developed a dynamic equilibrium was reached in the 1970's. The key historical changes in the larger bed morphology were the northwest movement of the large sand bar south of the Railway Bridge and erosion on the western shoreline (ASR, 2007).

Modelling suite 3-Dimensional Dynamics (3DD) was used to construct four models to examine the effects on the hydrodynamics, sediment transport, long term sediment transport and wave conditions (ASR, 2007). Four different grid sizes (75 x 75, 15 x 15, 2 x 2 and 1 x 1 m) were used in each of the models. Model simulations that were carried out without the addition of any Southern Pipeline option gave the baseline for comparisons. The highest modelled current velocities were under the Railway Bridge and exceeded 0.9 $m.s^{-1}$. The high current velocities were created by flow restriction from the causeway and bridge piers. In the lee of the Railway Bridge a current shadow zone was identified; where the current velocities were lower on the south and north of the bridge on the flood and ebb tides respectively. The current shadow zones caused a large gradient in current velocities in the vicinity of the Railway Bridge at all stages of the tide. ASR (2007) had difficulty calibrating the currents around the Railway Bridge causeway.

Sediment transport models were compared to surficial sediment samples taken during the study (ASR, 2007). During the study 64 sediment samples were collected and the median sediment grain size of each sample used to create the distribution map in Figure 3.6 (ASR, 2007).

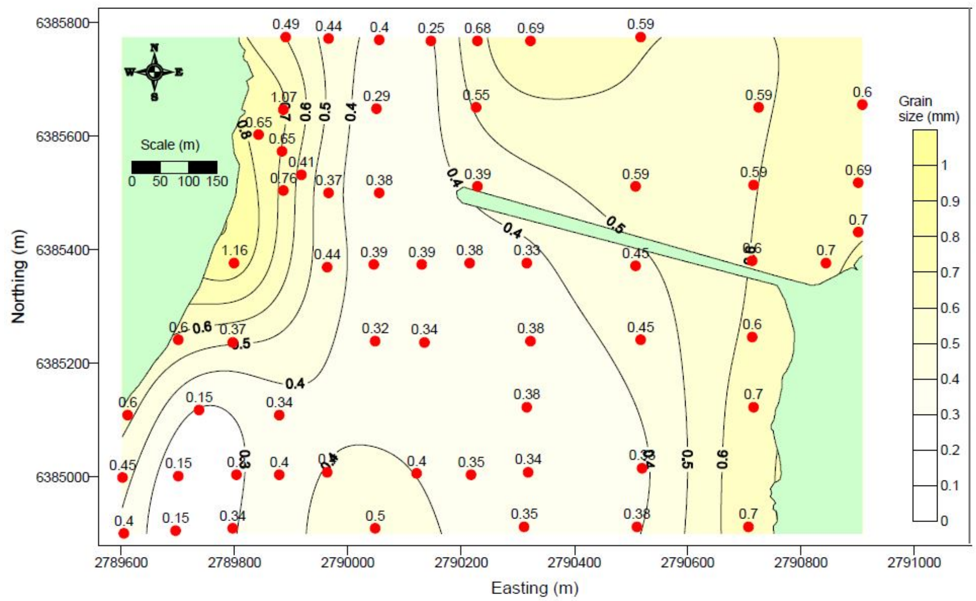

Figure 3.6: Median sediment grain size distribution map from 64 surficial sediment sample sites (each site location is indicted by a red point with the mean sediment grain size of each sample) at the site of the Southern Pipeline and Railway Bridge in Tauranga Harbour. Source: (ASR, 2007).

The seabed was found to vary from east to west with coarse sand on the eastern intertidal area, medium sand in the channel and coarse to very coarse sand on the western shoreline; consistent with the stronger velocities on the western side of the channel (ASR, 2007). Model results also confirmed that the site was near dynamic equilibrium due to low net sediment transport rates; 20,000 m^3 per year. Areas that were especially stable were shell lag areas around the bridge piers, where scour and high current velocities had removed fine sediments and shell lags protected the seabed (ASR, 2007).

Various options for the Southern Pipeline were then simulated in the numerical models (ASR, 2007). Concerns were raised over the above water pipeline options involving new bridges with new piers. As the largest scour and change in the seabed occurs around bridge piers, the pipeline could not be placed alongside the exiting bridge but would need to be at least 25 m away to avoid interaction between pier scour sites. Simulations with the submarine pipeline option showed potential for muds to build up which would negatively affect the biota. However the effects on current velocities were significantly less with the submarine pipeline than in bridge pipeline options. The final recommendation was to construct a submarine pipeline either on top of the seafloor or buried. In both options, building the Southern Pipeline was expected to influence the area 40-50 m both upstream and downstream of the Railway Bridge (ASR, 2007).

3.2.8 Tauranga Harbour Sediment Study 2009

Environment Bay of Plenty (EBOP) commissioned NIWA (National Institute of Water and Atmosphere) to investigate the sediment characteristics and sediment accumulation in Tauranga Harbour (Hancock et al., 2009). The purpose of the sediment study was to understand the impacts of harbour development on sediments and for the calibration and verification of sediment models. Hancock et al. (2009) complied 26 past studies which contained information on sediment grain size, sediment composition and sediment accumulation rates and combined the data in ArcGIS. The intertidal areas in the southern basin of Tauranga Harbour were divided into 26 subestuaries with common depths, sediment characteristics and hydrodynamic processes and then divided into 11 categories (Figure 3.7) (Hancock et al., 2009).

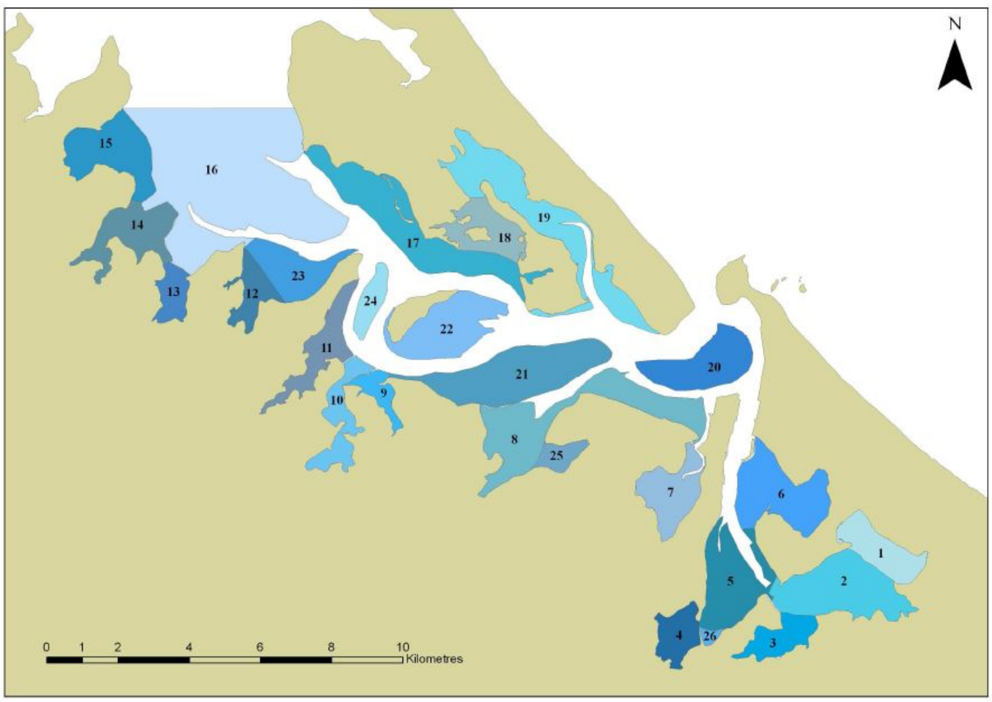

Figure 3.7: Intertidal areas of the southern basin of Tauranga Harbour divided into 26 subestuaries. Source: (Hancock et al., 2009).

Of the subestuaries, 1-6 and 26 are the upper estuaries beyond Stella Passage. The complied results of the previous studies in the 7 subestuaries are presented in Table 3.1. Subestuaries that were sheltered and further removed from the main channels like 1, 3, 4 and 26 had the highest percentage of mud (Hancock et al., 2009). Subestuaries 2 and 5 had the highest sand and gravel content respectively, and subestuary 6 Waipu Bay was categorised as a silty embayment. Hancock et al. (2009) determined that all of the subestuaries listed in Table 3.1 had simplified sorting parameters of 'poor'. 90 years of sediment accumulation rates were used to verify sediment models. It was found that compared to other harbours and estuaries on the east coast, Tauranga Harbour had a low rate of sediment accumulation (Hancock et al., 2009).

Table 3.1: Sediment grain size, mean grain size and category of the subestuaries in the upper harbour beyond Stella Passage based on the Tauranga Harbour Sediment Study. The size range for sediment grain size was mud < 63 µm, sand 63 µm – 2 mm, gravel > 2 mm. Source: (Hancock et al., 2009).

No.	Name of Area	% Mud	% Sand	% Gravel	Mean Grain Size (mm)	Category
1	Rangataua Bay	13.95	85.36	0.69	0.273	Sheltered muddy embayment east
2	Rangataua Bay	6.89	92.04	1.07	0.324	Southern harbour - open
3	Welcome Bay	31.14	68.25	0.61	0.270	Sheltered muddy embayment west
4	Waimapu Estuary	30.32	68.22	1.46	0.335	Sheltered muddy embayment west
5	Waimapu Estuary	9.80	87.56	2.69	0.403	Southern harbour - transition
6	Waipu Bay	8.13	91.16	0.71	0.321	Open silty embayment east
26	Waimapu Estuary	14.29	83.80	1.91	0.287	Sheltered muddy embayment west

3.2.9 Channel Deepening and Widening 2009-2015

The planning for the Channel Deepening and Widening project (2015-2016 capital dredging) started in 2009 and dredging commenced in October 2015 (Healy et al., 2009). The proposed dredging would lower the channels to 16 m inside the harbour and 17.4 m outside the harbour. An estimated 15 million m^3 of material was to be dredged; 5.9 million m^3 from the Entrance Channel, 0.4 million m^3 from the ebb tidal delta, 7.4 million m^3 from Cutter Channel, Maunganui Roads and to enlarge the turning basin, and 1.3 million m^3 from Stella Passage (Healy et al., 2009).

3.2.9.1 Assessment of Environmental Effects 2009

The Port of Tauranga commissioned an Assessment of Environmental Effects (AEE) report on the effects that the dredging programme may have on the environment as part of the application for a coastal permit under the RMA 1991 (Healy et al., 2009). As well as assessing changes to the hydrodynamics and sediment transport in Tauranga Harbour, the AEE also included sections on the type of sediments that would be dredged. The AEE noted that of the 5.9 million m^3 to be dredged, the material was mainly Holocene marine sands with some shells, some boulders and 1.5-2.1 million m^3 of muddy silt and clay. Estimates were made based on the records of over 70 sediment cores and seismic survey data, which were used to determine the composition of the dredged sediments over the harbour (Healy et al., 2009).

In 2009 the Port of Tauranga commissioned Perry Drilling Ltd to drill cores in the dredged area down to 18 m deep, four of the cores were in Stella Passage (Healy et al., 2009). Three of the cores for Stella Passage showed the upper portion of the sediments to be light pink to orange weathered ignimbrite that had a high clay and silt content. The weathered ignimbrite was identified as part of the pumiceous facies which is listed as the basal member of the Tauranga Group in Table 2.1. The high clay content would cause turbidity in the water column due to suspension of the clay; a back-hoe digger was recommended to reduce turbidity. There was also a possibility that the area to be dredged in Stella Passage would contain ancient buried trees (Healy et al., 2009).

A 3DD numerical model was used to develop a 2D simulation of tidal flow and determine the hydrodynamics before and after the Channel Deepening and Widening project (Healy et al., 2009). Both spring and neap tides were modelled, but the spring tidal simulation was used to determine any potential effects as spring tides have a larger potential for inducing change. The model bathymetry ran on a 25 x 25 m grid and was compiled from channel surveys, multibeam data, soundings, digitised charts and those used in previous model grids (Healy et al., 2009).

Model calibration was undertaken using measurements of tidal elevation and velocity from five current meters (Healy et al., 2009). Eddy viscosity and bed roughness which were both constant across the entire model were adjusted to obtain the most accurate predictions. The best fit was achieved using a Chezy Coefficient of 58 $m^{1/2}.s^{-1}$ to define the bed roughness, and an eddy viscosity of 1.2 $m^2.s^{-1}$. Calibration was against the five current meters to give the mean absolute error (MAE). There was an overall MAE for elevation of 1.8 ± 0.8 cm, speed of 6.3 ± 1.8 $cm.s^{-1}$ and a direction error of 17.6 ± 7.8 °. One of the instruments was positioned on the channel wall and the velocities were the worst represented within the model as currents converged and shearing occurred. The largest errors in current direction occurred at slack tides. Automated Doppler Current Profiler (ADCP) survey data from the Port of Tauranga were used to verify the model (Healy et al., 2009). Table 3.2 summarises the MAE obtained during verification.

Table 3.2: Summary of the mean absolute errors (MAE) during verification of the 3DD model of Tauranga Harbour. Source: (Healy et al., 2009).

Location	**Speed ($cm.s^{-1}$)**	**Direction (°)**
Stella Passage	3.3 ± 0.9	15.2 ± 3.1
Overall MAE	5.6 ± 2.0	10.2 ± 5.7
Spring tide	5.6 ± 2.1	10.9 ± 5.7
Neap tide	5.7 ± 2.0	9.6 ± 5.6

Overall the effect of the dredging on the hydrodynamics of the harbour were an increase in tidal volume from the deepening of the channels (Healy et al., 2009). In turn causing minor changes to the phase and amplitude of the tide in the lower harbour. There were some changes to the areas where scour and deposition occur, but overall there was no residual change and the dredging was predicted to reinforce pre-dredging sediment transport patterns. For Stella Passage the increase in depth was predicted to bring about the changes to the tidal curve which are listed below (Healy et al., 2009):

- The tidal phase would advance by 5 minutes during spring tides and 4 minutes on a neap tide.
- At high tide, tidal elevation may be increased by 0.013 m and < 0.01 m during a spring and neap tide respectively.
- Velocities would reduce by a maximum of 12.5 % at peak flood and 40 % at peak ebb during spring tides.
- Along Town Reach an increase in ebb velocity was predicted as the flow volume is sucked into the dredged Stella Passage.

- The widening of the cross-section would increase flow volume and reduced velocity, especially during ebb tides.

Sediment residual velocities were identified as current speeds > 0.3 ms^{-1} and indicated areas of deposition (where vectors decelerate or converge) and scour (where vectors accelerate). Sediment residuals predicted an increase in the potential for sediment transport and deposition of fine sediments and seston especially at the southern end near Town Reach (Healy et al., 2009).

3.2.9.2 Statement of Evidence Dr Willem Pieter de Lange 2011

A statement of evidence was given by Dr Willem Pieter de Lange in 2011 to identify any environmental issues that may be caused by the Channel Deepening and Widening project (de Lange, 2011). The evidence presented the issues in chapters 6-12 of the 2009 AEE as well as assessing the potential for erosion up harbour of the dredging, and the benefits of staging the dredging. Dredging was found to have the most impact on the immediate area but minor impacts on surrounding areas. As Stella Passage was not considered part of the tidal inlet system and has a smaller portion of the tidal prism passing through it, the dredging would have had less of an impact in Stella Passage (de Lange, 2011).

When comparing the benefits of completing the dredging in one short period and staged dredging, there was no change in the overall impact in most areas. Stella Passage however may have benefited from staged dredging (de Lange, 2011). The increased sediment transport predicted in Stella Passage would increase the potential for a shell lag to develop. A staged dredging programme would have allowed time for the shell lag formation, protecting the seabed and reducing the impact to the area (de Lange, 2011).

3.2.10 Analysis of Multibeam Sonar Data 2012

In his MSc thesis, Boulay (2012) analysed the impacts of the developments in the Port of Tauranga on the sedimentology in Stella Passage and Town Reach using multibeam sonar data. A Starfish 452F sidescan sonar and a multibeam echosounder were used in July and August 2011 to create a bathymetry map and a 3D side view of the study area (Figure 3.8). Maps of surficial sediment types (Figure 3.9) and shell coverage (Figure 3.10) were derived from grab sediment sampling and underwater videos taken at 42 sites within the study area in September 2011 (Boulay, 2012).

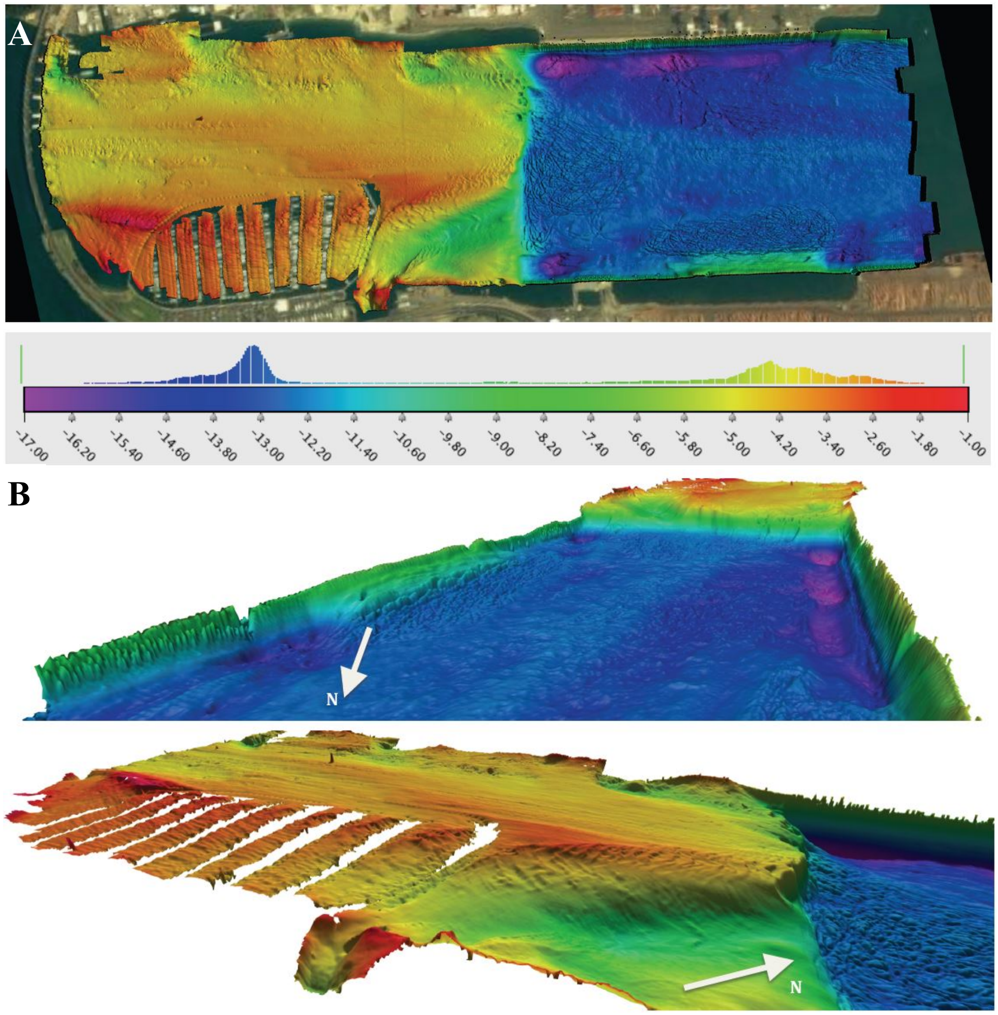

Figure 3.8: Bathymetry (A) and 3D side views of the bathymetry (B) in Stella Passage, Town Reach and Tauranga Bridge Marina in August 2011 derived from a multibeam echosounder survey. Water depths are based on the Moturiki CD and a 6 times vertical exaggeration is used in the 3D side views. Source: (Boulay, 2012).

Stella Passage was dominated by fine sand sized sediments (Boulay, 2012). The only area where silty very fine sands were located in Figure 3.9 was beside the Sulphur Point container wharf. As the areas of silty fine sand coincided with deeper areas in the acoustic mapping seen in Figure 3.8, Boulay (2012) hypothesized that the finer sediments were scour holes caused by propeller wash from the large boats docking alongside the wharves. When comparing past studies with the 2011 surveys, it was found that harbour development had removed layers and features identified previously by either the removal of material through dredging or through the increased water depth and reduced velocity. Boulay (2012) developed a final benthic habitat map, compiling all of the data in Figure 3.11.

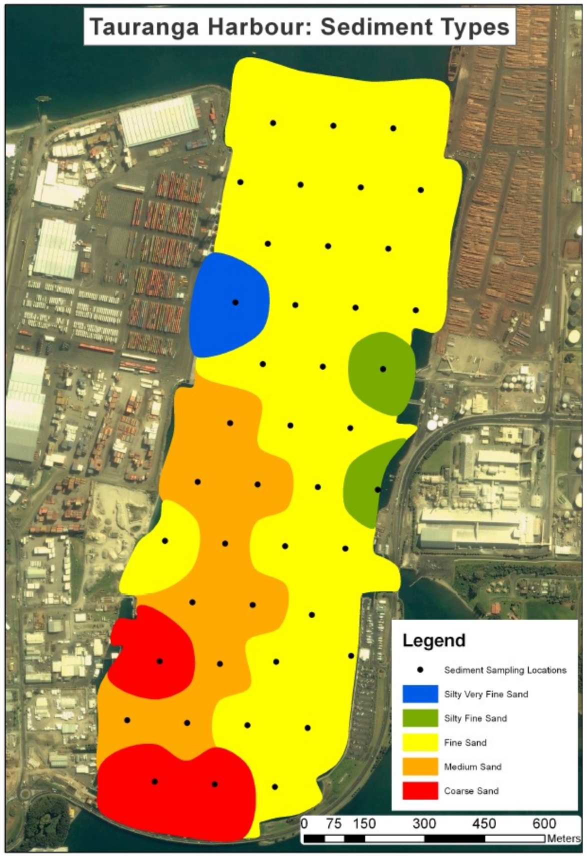

Figure 3.9: Map of the general boundary areas of surficial sediment types derived from grab samples in Stella Passage and Town Reach in September 2011. Source: (Boulay, 2012).

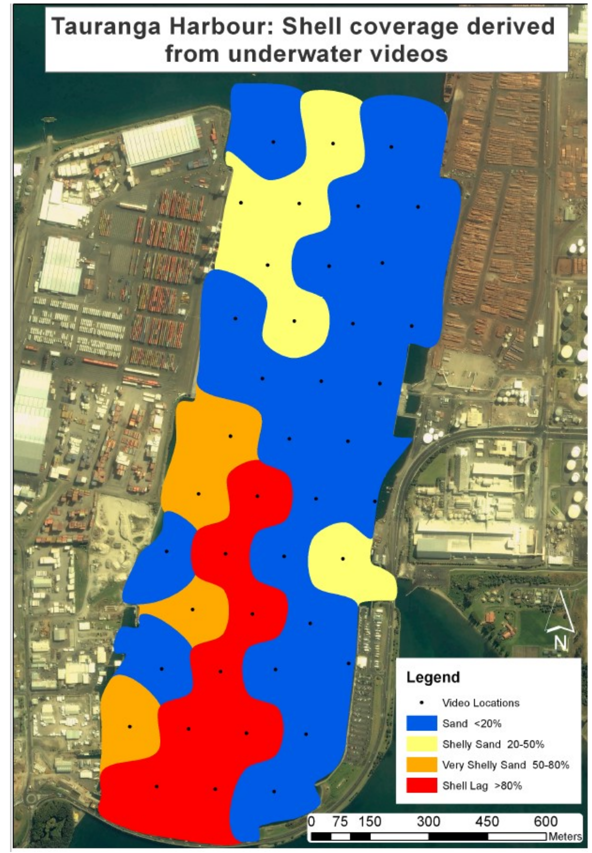

Figure 3.10: Map of the general boundary areas of surficial shell coverage taken from underwater video analysis of Stella Passage and Town Reach in September 2011. Source: (Boulay, 2012).

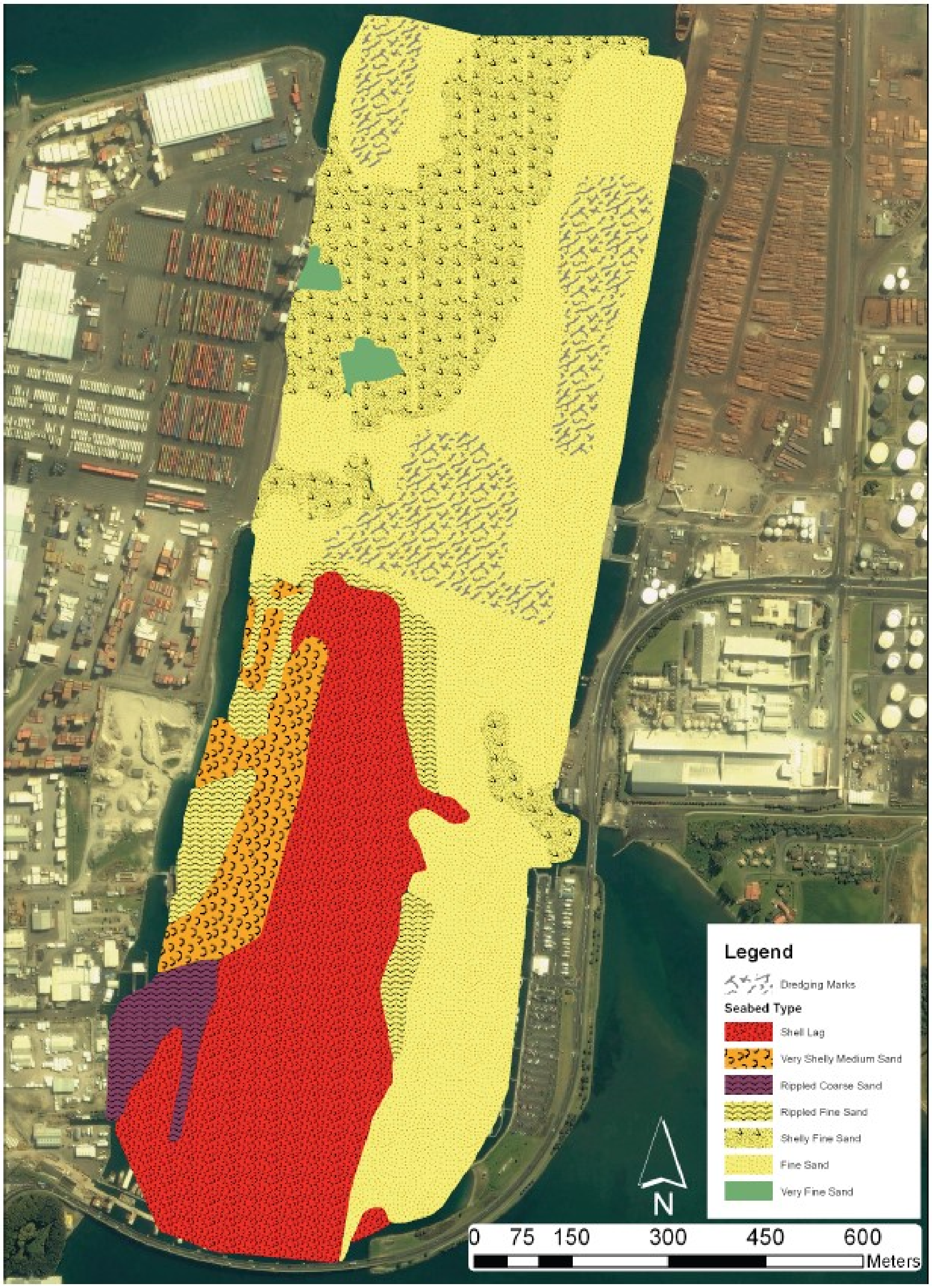

Figure 3.11: Final benthic habitat map of Stella Passage and Town Reach for July 2011. Source: (Boulay, 2012).

Figure 3.10 and Figure 3.11 showed the northern Stella Passage to be dominated by shelly sands and shell lag regions (Boulay, 2012). Prior to the 1991-92 dredging, northern Stella Passage consisted of shelly sand and silt. Other comparisons between historic sediment surveys found that an increase in grain size and shell density in Town Reach may have been caused by the increased current velocities on the flat shelf from the development of the Harbour Bridge and causeway. Since construction, the bridge causeway channelled ebb currents under Aerodrome Bridge, increasing the current velocities in the area and leading to the development of a shelly fine sand area north of Aerodrome Bridge. Boulay (2012) found that when current velocities were increased through harbour development works there was a direct association with shell coverage and shell lag areas; with stronger currents increasing the density of shell coverage.

3.2.11 Hydrodynamics of the Southern Basin 2013

Spatial and temporal patterns in circulation over a five year period in the southern basin were simulated using a 3D model developed by Tay et al. (2013). The ELCOM (Estuary, Lake and Coastal Ocean Model) hydrodynamic model was forced with a tidal signal taken from the NIWA tidal model and offshore wave conditions from a Bay of Plenty Regional Council (BOPRC) wave buoy. Bathymetry in the model was developed from a combination of singlebeam and multibeam echo sounder surveys, hydrographic soundings from the Port of Tauranga and digitized navy fairsheets. A grid resolution of 75 x 75 m with 12 vertical layers of varying thickness was used; vertical layer thickness increased with depth (6). Chézy-Manning numbers were used to define the Bottom Drag Coefficient (BDC) and simulate bottom stresses that cause dissipation over the water column. Values of BDC were varied over the grid as the optimal value was different throughout the harbour model. The best result was obtained by allocating a higher coefficient (lower friction) in the channel areas of 0.01 and a lower coefficient (higher friction) of 0.005 in intertidal areas < 1 m. Data collected in 1999 using S4 current meters and CTD casts, and older CTD and ADCP data were used to calibrate and verify the model (Tay et al., 2013).

Results were analysed with T_TIDE, a free tidal harmonic analysis script that extracts the tidal signal out of a time series (Tay et al., 2013). Attenuation in the amplitude and phase of the tidal signal occurred at different rates over the southern basin. Differences in amplitude and phase of the M2 tide through the southern basin are stated in A and B respectively in Figure 3.12. Over the short distance of 500 m the amplitude of the M2 tide changed from 0.73 m to 0.7 m through the Entrance Channel. M2 tidal amplitude increased towards Omokoroa but decreased through Stella Passage into the upper harbour to be 0.59 m in Waimapu Estuary and 0.64 m in Rangataua Bay. The largest differences in phase occurred through narrow channels like the Entrance Channel, and under Hairini and Maungatapu Bridges as the tidal wave was constricted (Tay et al., 2013).

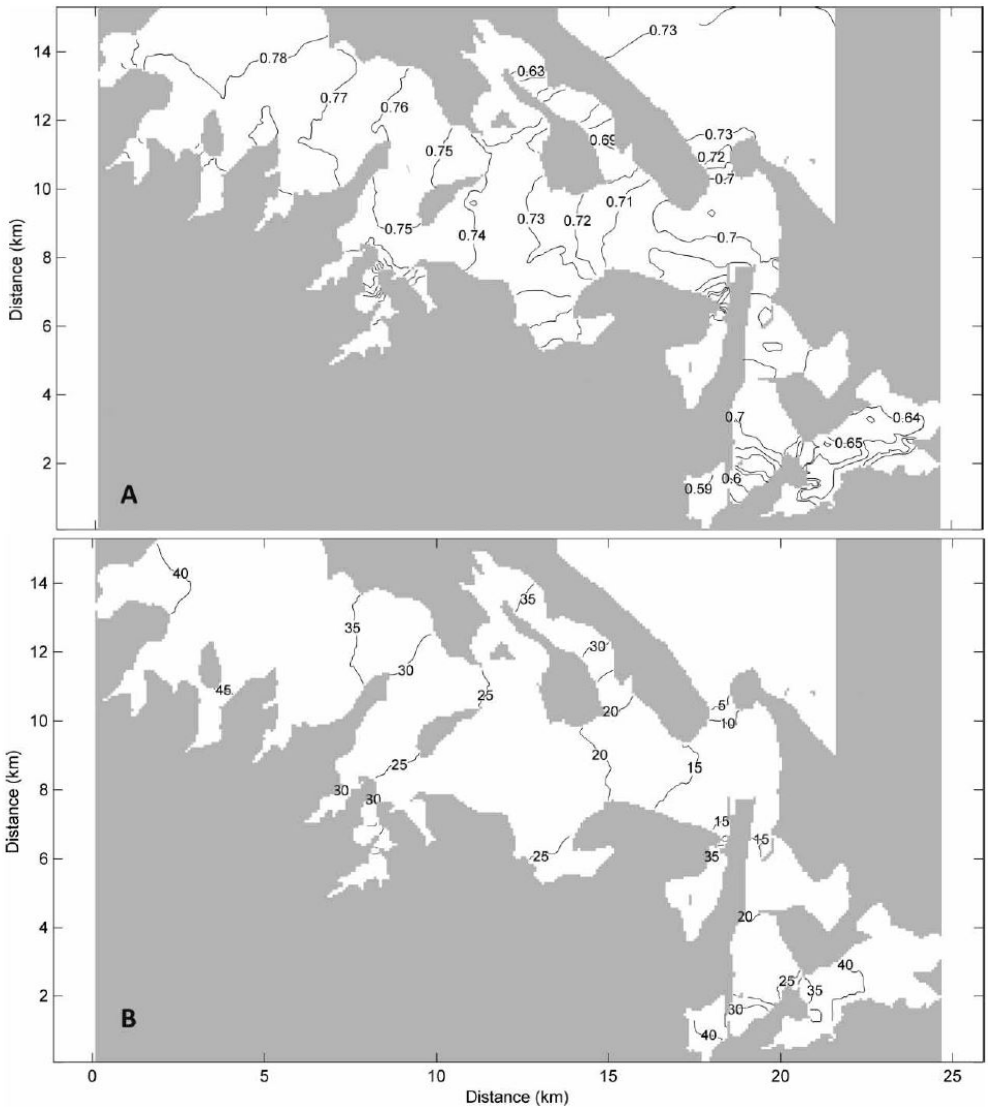

Figure 3.12: Differences in the M2 tidal (A) amplitude in m and (B) phase in degrees extracted from the 5 year model of the southern basin of Tauranga Harbour. Source: (Tay et al., 2013).

Attenuation of the tidal signal with distance from the Entrance Channel caused the water levels across the harbour to vary more at low tide than high tide (Tay et al., 2013). T_TIDE identified the M4 tidal signal which is also known as the overtide and has a phase that is 90 ° to the M2 tide. The M4 tide was seen to have an increase in amplitude from the Entrance Channel to the upper reaches of the harbour. Frictional effects and the bathymetry throughout the harbour controlled the phase of the M4 tide. Changes in the M4 tide resulted in the model predicting a time lag between the time of high and low tides over the harbour of 15 minutes (Tay et al., 2013).

Modelled residual currents in the harbour were more accurate when current speeds were stronger (Tay et al., 2013). Constricting morphology like that in the lower harbour increased the residual currents. The average time a body of water is retained before it moves on was the residence time. In the southern basin the residence time is shortest in the deep channels and longest in the bays that have restricted entrances and side embayments to curved channels (Tay et al., 2013). In Figure 3.13 the effect of wind on the salinity, temperature and residence times in the model are presented.

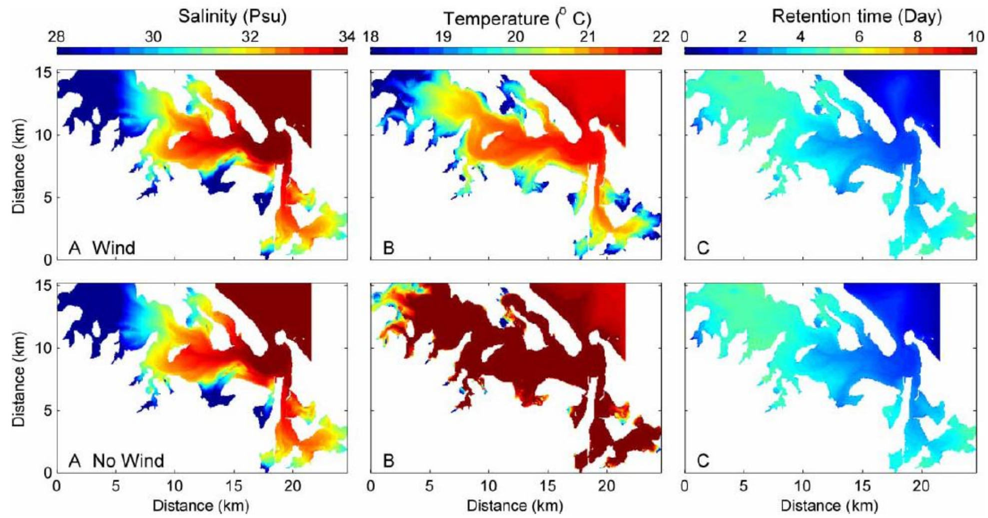

Figure 3.13: Depth averaged salinity, temperature and retention time with dominant winds (top) and without wind (bottom) during summer conditions from averaged results over a spring and neap tide (14 days) in the southern basin, Tauranga Harbour. Source: (Tay et al., 2013).

Weak salinity gradient within the harbour were controlled by the tide and the wind had no significant effect (Tay et al., 2013). Temperature varied diurnally and also when wind was added to the simulation, indicating that temperature was not affected by the tides. Tay et al. (2013) concluded that patterns in residence time were determined by the geometry of the harbour.

3.2.12 Predicted Hydrodynamic and Sediment Transport Impacts of Breakwater Construction 2014

A breakwater was planned to be constructed along the northern edge of the Tauranga Bridge Marina with the aim of providing better protection for the moorings from wave and storm surge (McKenzie, 2014). McKenzie (2014) submitted a MSc thesis with the University of Waikato on the potential impacts on the hydrodynamic and sediment transport from the breakwater. 2D numerical modelling was carried out on the Danish Hydraulic Institute (DHI) software MIKE 21. Two hydrodynamic models were generated, a larger regional model of the Tauranga Harbour on a 25 x 25 m grid and a local model of Stella Passage, Town Reach and Waipu Bay on a 4 x 4 m grid. A nearshore wave model and sediment transport model were also developed (McKenzie, 2014).

3.2.12.1 Regional Model: Setup, Calibration and Verification

The purpose of the regional model was to provide the boundary conditions for the smaller local model (McKenzie, 2014). Model runs were over 72 hours with 6 hours added for a warm up period and both spring and neap tides being simulated. Bathymetry was compiled from LINZ (Land Institute of New Zealand) data and charts obtained from the Port of Tauranga. During calibration, model input parameters were adjusted to obtain the best fit between the model predictions and tide gauge measurements of the M2 tide. The M2 tidal signal was extracted from the datasets with T_TIDE (McKenzie, 2014). The constant values of bed resistance, eddy viscosity and drying and flooding depths that were trialled throughout the sensitivity analysis are in Table 3.3, along with the input parameter values that gave the closest agreement.

Table 3.3: Values of model input parameters used in the sensitivity analysis of a MIKE 21 regional model of Tauranga Harbour and the values selected for calibration. Source: (McKenzie, 2014).

Model Parameter	**Trialled Constant Values**	**Selected Values**
Bed resistance (Manning M)	Upper limit 40 $m^{1/3}.s^{-1}$ Lower limit 20 $m^{1/3}.s^{-1}$ Default value 32 $m^{1/3}.s^{-1}$	Map of spatially varying bed resistance created.
Eddy viscosity (Smagorinsky factor)	Upper limit 1.0 Lower limit 0.25 Middle range 0.625	0.625
Drying and flooding depths	Drying-flooding 0.1-0.2 m Drying-flooding 0.2-0.3 m	Drying-flooding 0.1-0.2 m

Bed resistance values had the largest influence on the phase of the M2 tide and current speeds (McKenzie, 2014). Increasing the bed resistance (reducing the Manning number) was found to significantly reduce the tidal amplitude and delay the tidal propagation in the upper harbour, whereas decreasing the bed resistance (increasing the Manning number) slightly increased the tidal amplitude and advance the tidal phase. As the Manning number is determined by grain size and sediment characteristics, the value of bed resistance used had a greater impact in shallower intertidal areas and the upper reaches of the harbour. McKenzie (2014) determined that using a varied bed resistance over the model domain would give the closest agreement between the model predictions and tide gauge data. The final Manning numbers were specified by the seabed elevation and the bed resistance map used in the regional model is summarized in Figure 3.14.

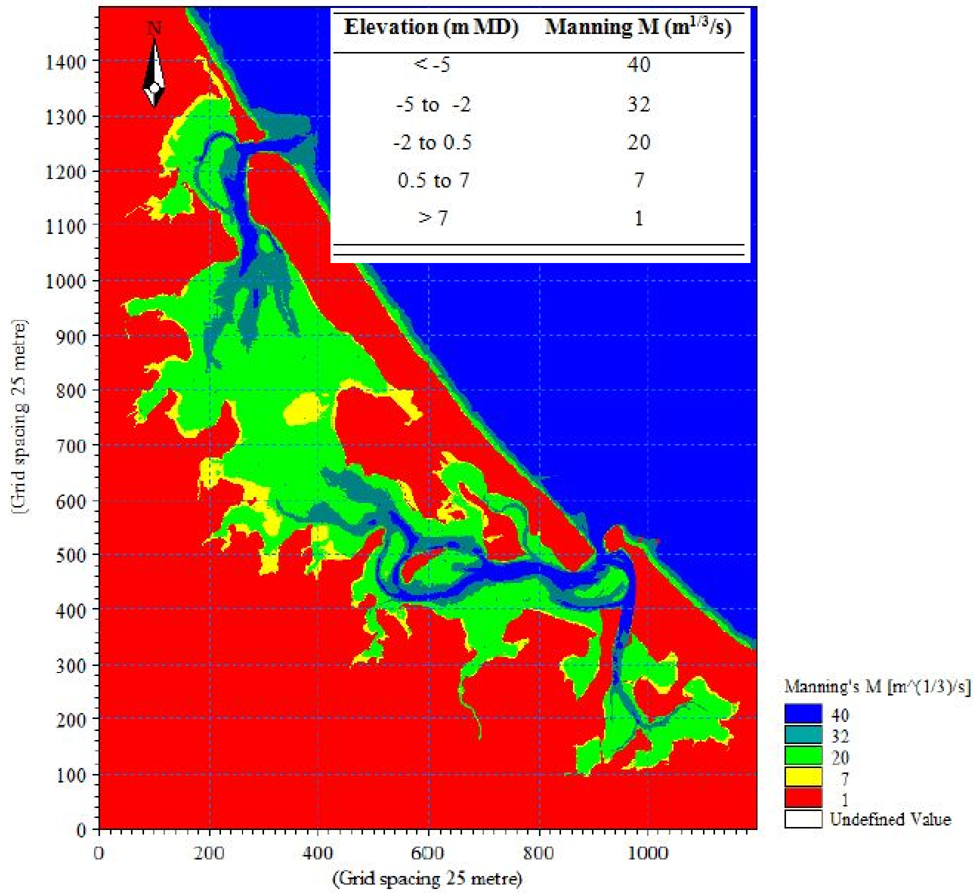

Figure 3.14: Bed resistance map used in the regional model of Tauranga Harbour with spatially varying values based on the elevation of the bathymetry. Inset table lists the Manning numbers used for each elevation. Source: (McKenzie, 2014).

McKenzie (2014) carried out statistical analysis of the calibrated model by calculating the bias of the model using $Bias_a$, the accuracy using MAE, Mean Square Error (MSE) and Root Mean Square Error (RMSE), and the skill using the Brier Skill Score (BSS). Statistical analysis gave errors of 0.03 m for tidal amplitude and 2-3 ° in the tidal phase. Errors between the model and the measured datasets were attributed to bathymetry and harmonic analysis. Calibrated models of both spring and neap tides were then compared to a different dataset to be verified in their predictions of not only the M2 tide but other tidal constituents. The upper harbour had the lowest BSS scores due to shallow water tidal constituents not being accurately predicted (McKenzie, 2014).

3.2.12.2 Local Model: Setup, Calibration and Verification

The hydrodynamic model used for simulating the effects of the Tauranga Bridge Marina breakwater was forced at north and south boundaries with a surface elevation time series from the regional model and run on a 4 x 4 m grid (McKenzie, 2014). Multibeam echosounder survey data, LINZ and Port of Tauranga charts produced the bathymetry (McKenzie, 2014). As with the regional model, a spatially varying bed resistance was applied over the grid (Figure 3.15).

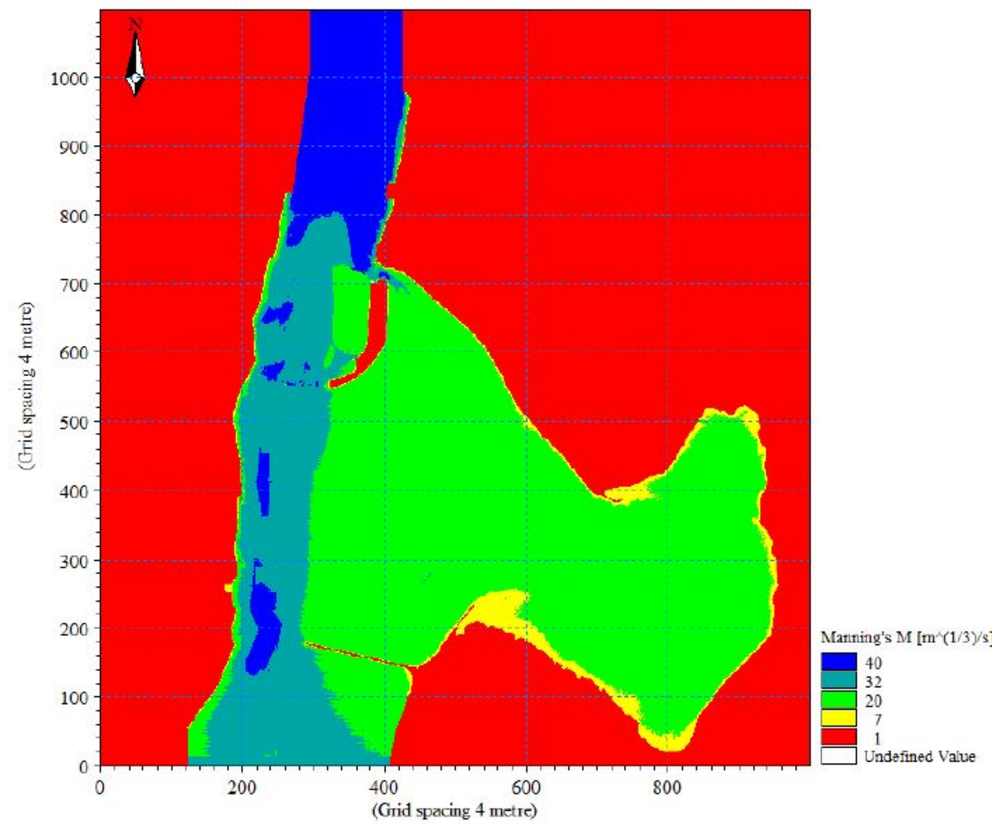

Figure 3.15: Spatially varying bed resistance map used in the local model of Tauranga Harbour. Source: (McKenzie, 2014).

Measurements from three Acoustic Doppler Velocimeter (ADV) instruments which were deployed in October and November 2011, and an ADCP which recorded current velocity over a full tidal cycle on the 1st of November 2011 were used to calibrate and verify the model (McKenzie, 2014). Measurements of a spring tide and neap tide were used in the calibration and verification respectively. Statistical analysis was carried out on tidal amplitude, current speed, current direction and U and V current velocities. The model was found to predict well through Stella Passage and Town Reach but under-predict the ebb currents under Aerodrome Bridge. Tidal elevation was over-predicted across the modelled area but only by an MAE of 0.1 m (McKenzie, 2014).

3.2.12.3 Local Model Hydrodynamics

Plots of depth averaged current velocities and velocity vectors over the local model during a spring tide in Figure 3.16 predicted eddy development in Stella Passage during both the flood and ebb tides (McKenzie, 2014). During the flood tide an anticlockwise eddy developed in the middle of Stella Passage which deflected currents to the east, then travelled south to Town Reach and faded before mid-tide. Current direction in Stella Passage and Town Reach throughout the flood tide was southwest, but as the width of the channel increased near the Railway Bridge the range in current direction widened to be southwest to southeast. During ebb tide, currents were also deflected to the east but by a clockwise eddy in the middle of Stella Passage (McKenzie, 2014).

Current velocity in Figure 3.16 accelerated when flow was constricted or channelled by narrowing bathymetry (McKenzie, 2014). Predictions of accelerated current velocity of 1 $m.s^{-1}$ on the western side of Town Reach occurred at mid-tides where the flow travelled from dredged Stella Passage to shallow Town Reach. McKenzie (2014) attributed the acceleration to vertical compression of flow, where current velocities increased to conserve mass. The maximum current velocities predicted were 1.1 $m.s^{-1}$ under the Tauranga Harbour Bridge and 1.0 $m.s^{-1}$ under the Railway Bridge and both occurred at mid-tide; which was consistent with the ASR (2007) Southern Pipeline study. Flow constriction from the bridge causeways caused the acceleration (McKenzie, 2014).

Residual velocity vector plots of the local model (Figure 3.17) showed that the predominant pattern in Stella Passage and south of the Railway Bridge was loops of residual velocity (McKenzie, 2014). Larger residual velocity vectors were predicted at the transition between dredged Stella Passage and shallow Town Reach. The deeper bathymetry in front of Sulphur Point wharves may have caused the current direction to be diverted northeast on an ebb tide. Other key patterns in Figure 3.17 were the currents that flowed northwest into Stella Passage under the Aerodrome Bridge, and the small velocities south of the Railway Bridge causeway that were sheltered on the flood tides. In the upper harbour of the model, higher order harmonics led to tidal asymmetry (McKenzie, 2014).

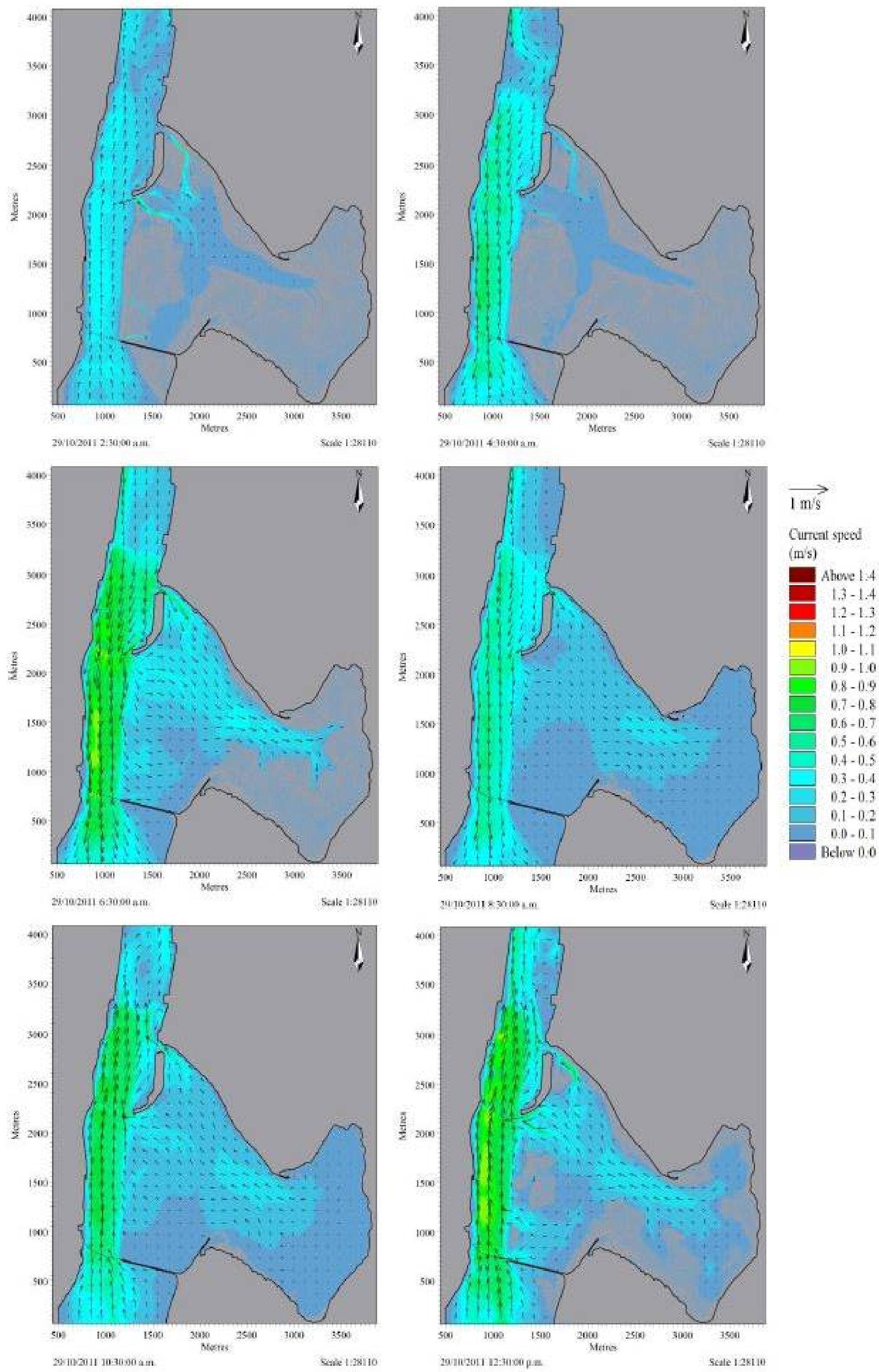

Figure 3.16: Depth averaged current speed and velocity vector plots over the local model during a spring tide. Source: (McKenzie, 2014).

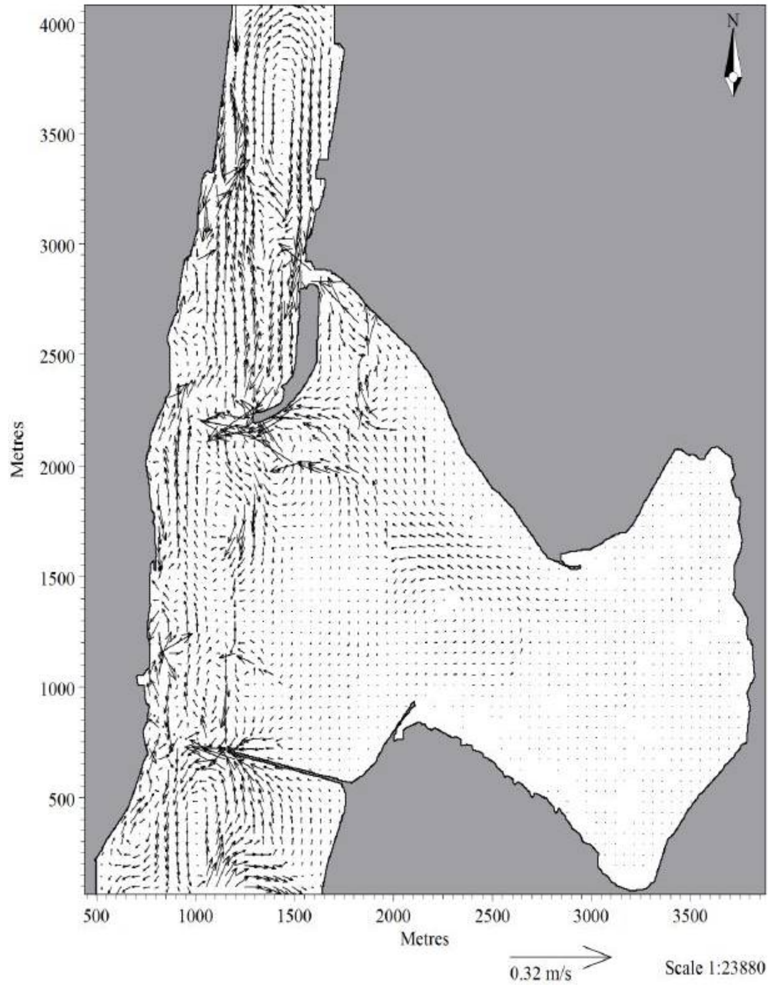

Figure 3.17: Residual velocity vector plot over the local model during a spring tide. Residuals calculated from predictions between the 28th October to the 31st November 2011 Source: (McKenzie, 2014).

3.2.12.4 Impacts of Breakwater Construction

Model runs before any harbour developments were added were compared to multiple simulations with varying breakwater designs (McKenzie, 2014). Breakwater construction was predicted to divert currents, causing a 10 % increase in the maximum current velocities near the transition between Stella Passage and Town Reach. Figure 3.18 was used to present the difference in current speeds caused by the breakwater construction. Off the western tip of the breakwater a flood jet developed, indicated by the red region in Figure 3.18; the blue region is inside the marina where the breakwater successfully reduced the current speeds. Construction of the breakwater constricted the channel and caused the ebb flow to converge into western Stella Passage, increasing current speeds (especially in front of the Sulphur Point wharves) (McKenzie, 2014).

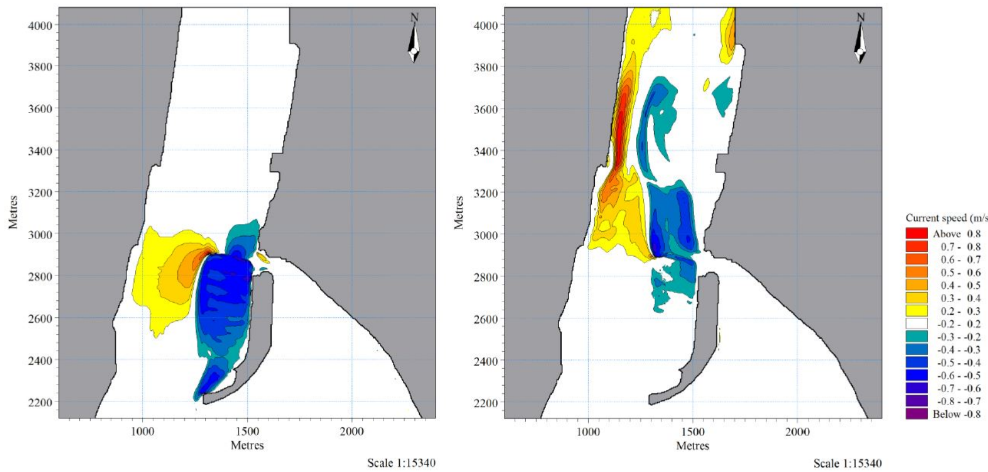

Figure 3.18: Differences in current speeds between the existing bathymetry and the bathymetry with the breakwater added at peak flood tide (left) and peak ebb tide (right) over the local model during a spring tide. Inset is the current speed scale where yellow to red indicated an increase and green to purple a decrease in current speed. Source: (McKenzie, 2014).

McKenzie (2014) also predicted an increase in sediment accretion in Stella Passage at the transition between the dredged and shallow bathymetry. Faster current speeds in western Town Reach increased erosion which changed the amount of coarse sediment and extended the shell lag area south (McKenzie, 2014).

3.2.12.5 Impacts of Dredging and Wharf Extensions

Two dredging scenarios were also modelled to predict the potential impacts of future developments (McKenzie, 2014). The first was the dredging of Stella Passage to 16 m below CD (2015-2016 capital dredging), and the second added an extension of the dredged area southward into Town Reach along with a 250 m extension of the Sulphur Point wharves south. The wharf extensions and reclamation were represented by increasing the bathymetry to above MSL in the construction area. Plans for the extension of the dredged area and the wharf extension and reclamation of Sulphur Point were the same as those modelled in this thesis. The combined impacts of the breakwater and dredging were also predicted. Modelled impacts of the Stella Passage dredging in scenario one were similar to those of just the breakwater (McKenzie, 2014).

McKenzie (2014) plotted the current speed and velocity vector plots of the peak flood and ebb tide (Figure 3.19) and the differences in current speed (Figure 3.20) from dredging scenario two.

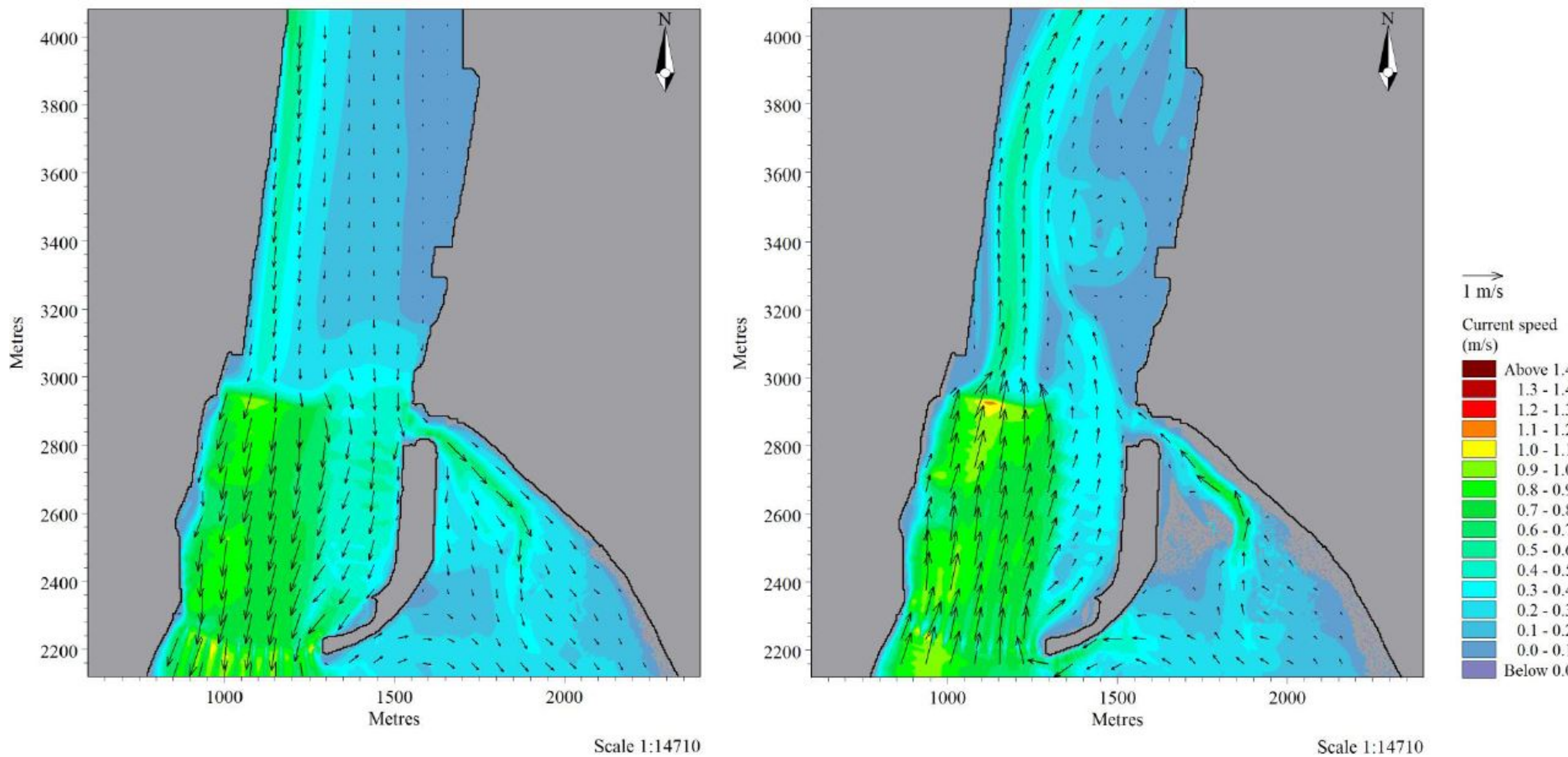

Figure 3.19: Depth averaged current speed and velocity vector plots of dredging scenario two over the local model during a spring tide. Source: (McKenzie, 2014).

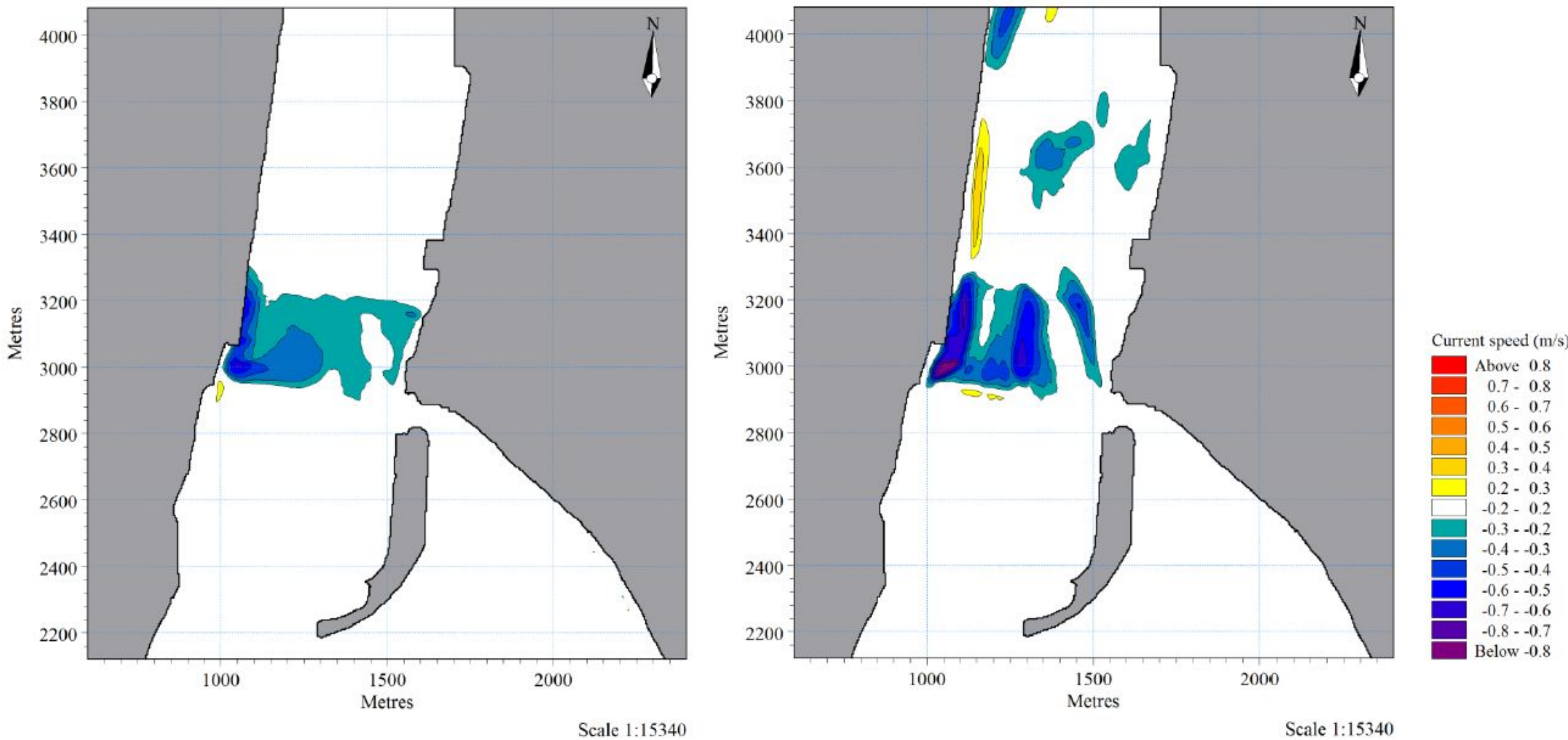

Figure 3.20: Differences in current speeds between the existing bathymetry and the bathymetry with dredging scenario two added at peak flood tide (left) and peak ebb tide (right) over the local model during a spring tide. Inset is the current speed scale where yellow to red indicated an increase and green to purple a decrease in current speed. Source: (McKenzie, 2014).

Simulations of dredging scenario two predicted several changes to the hydrodynamics in Stella Passage and Town Reach such as (McKenzie, 2014):

- Increased maximum flood velocity in western Stella Passage by 0.2 $m.s^{-1}$
- An increase in peak ebb velocity in front of the Sulphur Point wharves by 0.3 $m.s^{-1}$ which was indicated by the yellow region in Figure 3.20.
- A predicted decrease of 0.3 $m.s^{-1}$ in peak flood velocity for the area north of the marina.
- Movement of the area of flow acceleration 300 m southward into Town Reach (Figure 3.19); coinciding with the movement of the dredging boundary drop-off.

As both dredging scenario two and the breakwater worked to channel the flow through the western side of Stella Passage and Town Reach, combining the engineering works in the model predicted an increase in erosion at the edge of the dredged area. However as the dredging in scenario two decreased the peak flood velocity north of the marina the impact of the breakwater (which increased flood velocity) would be reduced. Dredging scenario two also reduced the influence of the breakwater on ebb velocity along the western side of the channel. Maximum ebb velocity increased by 29 % with the breakwater, and by 25 % and 20 % for the breakwater when modelled with dredging scenario one and two respectively (McKenzie, 2014).

3.3 Wharf Extensions

Wharf extensions are considered to be a Restricted Coastal Activities under section 117 of the RMA 1991. Prior to construction a coastal permit and resource consent must be granted which requires extensive assessments of any impacts the activity may have on the environment (Resource Management Act, 1991).

3.3.1 Sulphur Point Wharf and Extension No.1

Reclamation of Sulphur Point allowed the Port of Tauranga to expand its berthage by building wharves along the eastern side of the 85 ha reclamation. The first wharves at Sulphur Point that opened in 1992 were the original wharf and extension No.1 (Port of Tauranga Ltd, 1994).

3.3.1.1 Environmental Impact Assessments 1988-1991

Between 1988 and 1991, two Environmental Impact Assessment (EIA) reports for the 600 m of wharf at Sulphur Point were required under Sections 175 and 178 of the Harbours Act of 1950; one for the original 340 m wharf and another for the 260 m extension No.1 (Port of Tauranga Ltd, 1988, 1990). The EIA reports were completed by the Port of Tauranga. The authorisation for the reclamation of Sulphur Point had already been approved by the Empowering Act in 1967-68 (Port of Tauranga Ltd, 1990). A typical cross-section of the first 340 m of wharf in Figure 3.21 shows the pile design with rock placement under the wharf and backfilling that was constructed by pushing out over the water; both wharves had similar construction (Port of Tauranga Ltd, 1988).

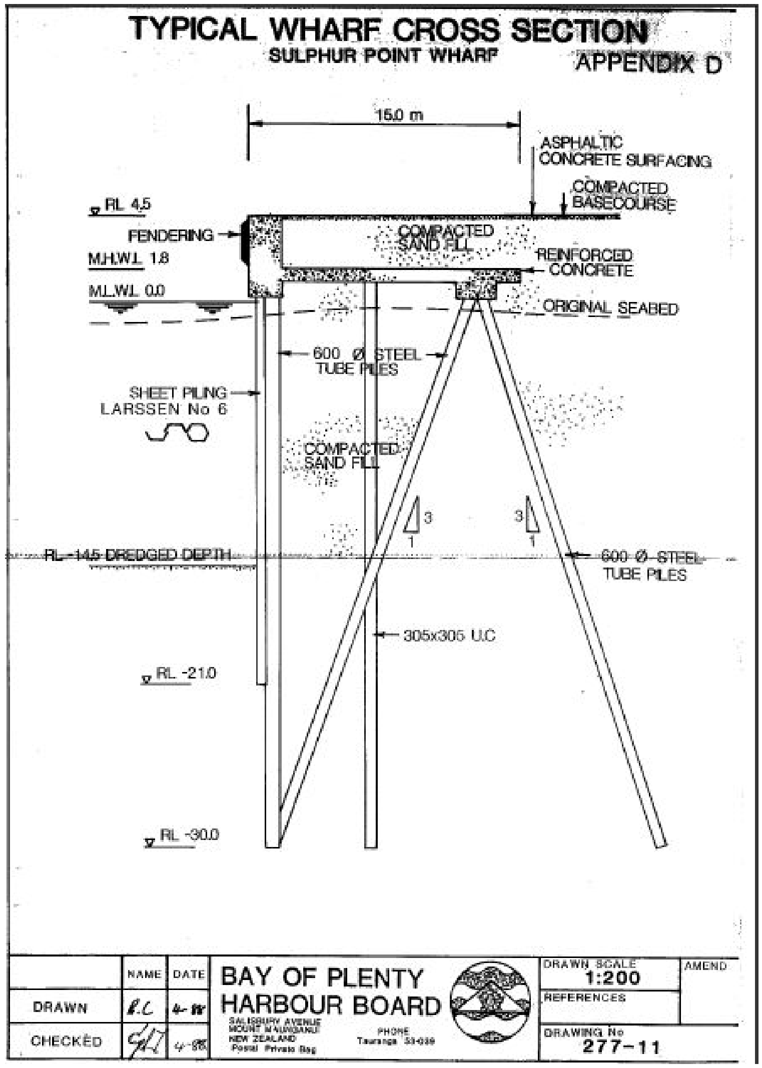

Figure 3.21: Typical cross-section of the original wharf built at Sulphur Point in Tauranga Harbour. Source: (Port of Tauranga Ltd, 1988).

The EIA reports used the model developed in the Tauranga Harbour Model Study in 1983 to make predictions on any impacts the wharf construction may have had on the hydrodynamics of the harbour (Port of Tauranga Ltd, 1990). In both reports the wharf construction and associated dredging caused a significant decrease in current speeds and changes to the sedimentation patterns in the area around the works. In the dredged area there was a switch to ebb dominance. However as the dredging also increased the cross-sectional area of Stella Passage, reducing the current speeds, the change in flow dominance was not deemed of concern to shipping. Hydraulically, the area was found to be highly suitable for a berth area. Modelled results predicted sediment to accumulate at the south-western corner of the shipping basin. It was concluded that apart from in the actual dredged area, any changes brought about by the wharf construction and dredging were negligible (Port of Tauranga Ltd, 1990).

3.3.2 Sulphur Point Wharf Extension No.2

Plans to extend the Sulphur Point wharves by 170 m north of the existing 600 m were in place since 1994, although not implemented until 2014 (Winthrop, 2014). The reclamation associated with the wharf was 0.4 ha and the dredging deepened the channel by a further 3.4 m. Development of the port area was due not only to the increased volumes of cargo and containers, making the Port of Tauranga the largest port in New Zealand by cargo, but also the increased average length of containerships (Winthrop, 2014). The location of wharf extension No.2 is displayed in Figure 3.22 with the first Sulphur Point wharf and wharf extension No.1 already constructed.

Figure 3.22: An outline of the area for the proposed wharf extension No.2 at Sulphur Point in Tauranga Harbour. Source: (Thompson, 2001).

3.3.2.1 Environmental Impact Assessment 1994

In 1994 the rate of cargo and containers passing through the port had increased 4.9 % over the previous 20 years, and 8.1 % over the preceding five years (Winthrop, 2014). Shortly after the completion of the first 600 m of wharf at Sulphur Point, the Port of Tauranga started the application process for coastal permits to build extension No.2 (Port of Tauranga Ltd, 1994). As with other major works in the Tauranga Harbour, the extension No.2 wharf was classified as a restricted coastal activity. An EIA was carried out by the Port of Tauranga on the construction effects of the 170 m wharf and was included in the application (Port of Tauranga Ltd, 1994). The application was submitted in 1995 and three coastal permits for the 50,000 m^3 dredging, 0.4 ha reclamation and wharf structure were granted in April 1996 (Thompson, 2001).

From MSc thesis studies on the site, the area was deemed to have little ecological value, and the addition of the piles and rock walls would only enhance the habitat and ecological value of the site (Port of Tauranga Ltd, 1994). Using results from numerical model simulations, no measurable changes in the current flows and sediment transport patterns due to the wharf extension could be seen within the harbour. Within Stella Passage the current speeds reduced when dredging on the point of Stella Passage and Otumoetai Channel was simulated. However as the wharf is an extension of the pre-existing wharf it would not have any significant impact on the current flows beyond what had already come about. Minor effects arising from the construction of the wharf were predicted to continue no longer than 12 months after completion. From sediment residuals the EIA indicated that on a spring tide there was a strong northward flux in front of the wharves on the western side of Stella Passage, which then reduced in front of the proposed wharf extension No.2. The north-eastern area of Stella Passage was identified as an area where there was a potential for sediment to accumulate; however annual sediment transport rates in the area are low so no adverse effects were expected (Port of Tauranga Ltd, 1994).

3.3.2.2 Assessment of Environmental Effects 2001

The coastal permits for the dredging and reclamation of extension No.2 that were granted in the 1995 application expired in 2000 (Thompson, 2001). An AEE was used in the application for new consents that would be held for a period of 14 years. The application included assessments of hydrodynamic, morphodynamic and ecological effects. Comparisons were made between the numerical models developed before the 1991-92 dredging works and simulations with wharf extension No.2. The AEE found, as did the 1994 EIA, that there would be no significant impacts on current flows as the 170 m wharf was an extension of the existing wharf (Thompson, 2001). The consents were granted for 50,000 m^3 of sand and silt to be dredged and used in the reclamation, as well as the wharf structure which had 353 piles and a batter slope comprised of 30,000 m^3 of rock (Winthrop, 2014). The design of wharf extension No.2 in Figure 3.23 was different to the wharves already constructed at Sulphur Point and was built over the water (Thompson, 2001). Wharf extension No.2 was completed in March 2014; Figure 3.24 shows the wharf under construction (Winthrop, 2014).

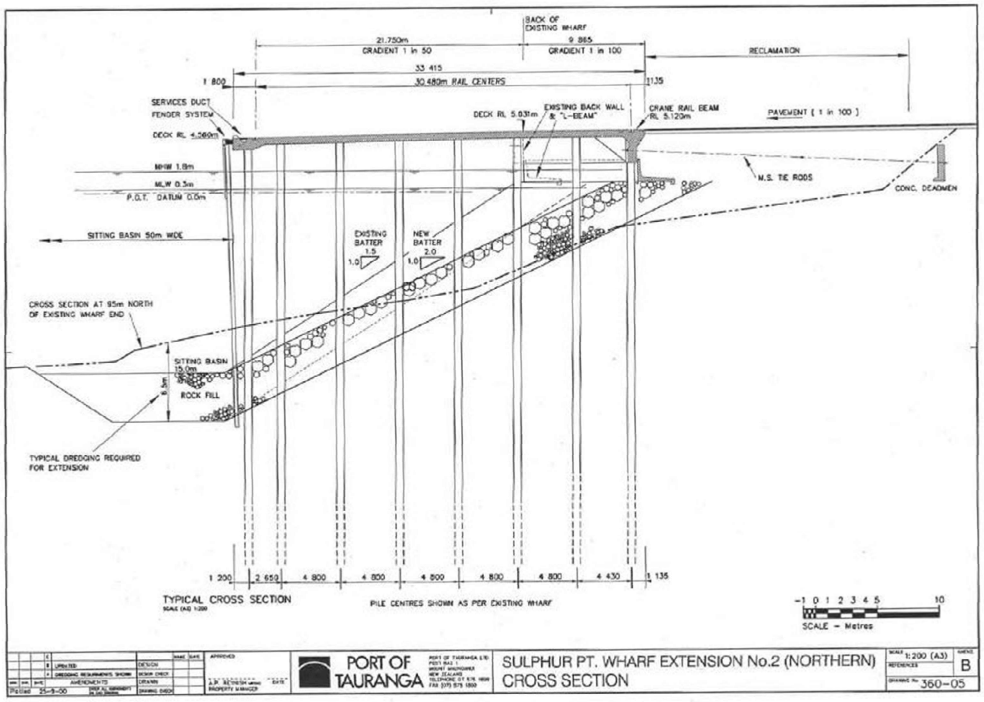

Figure 3.23: Cross-section of wharf extension No.2 at Sulphur Point in Tauranga Harbour. Source: (Thompson, 2001).

Figure 3.24: Construction of Sulphur Point wharf extension No.2 completed in March 2014. Source: (Winthrop, 2014).

3.3.3 Future Sulphur Point Wharf Extension

The wharf extension at Sulphur Point is one half of the Port of Tauranga's proposed wharf extensions in Stella Passage. Although no previous studies have been carried out on the Maunganui wharf extension, the Sulphur Point wharf extension and the dredging of southern Stella Passage into Town Reach have been modelled (Bell, 1994). Figure 3.25 shows the proposed plans for the Sulphur Point and Maunganui wharf extensions and dredging for the future works, some of which are the same as those modelled in a 1994 study and in the MSc thesis by McKenzie (2014) in Section 3.2.12.5 of this chapter.

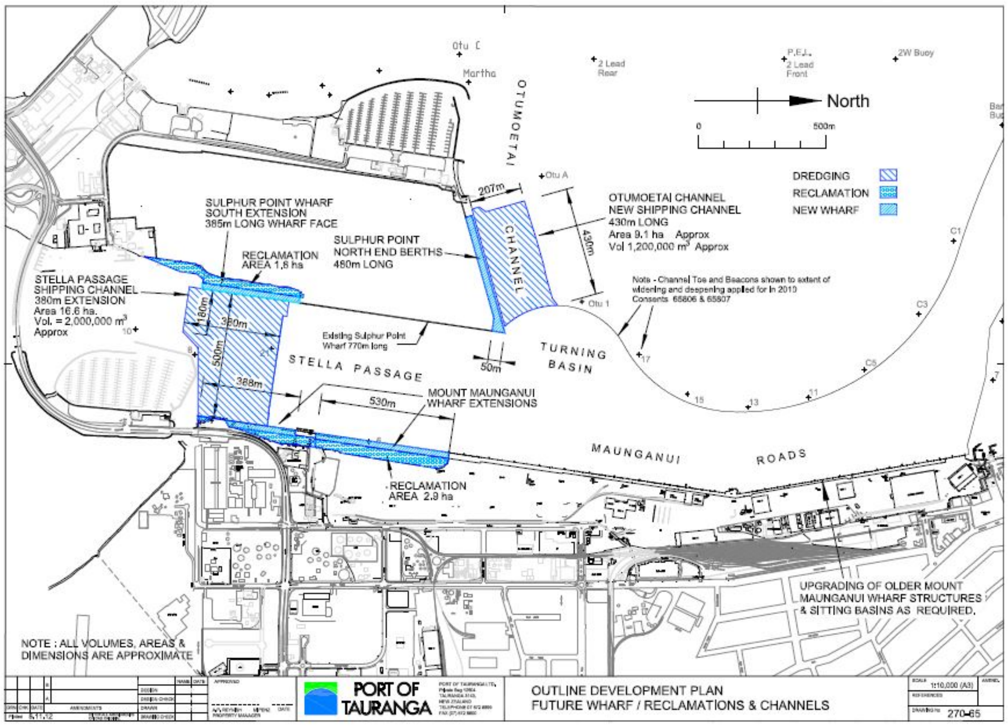

Figure 3.25: Proposed plans for the Port of Tauranga wharf extensions and associated dredging of Stella Passage in Tauranga Harbour. Note the North End wharf extension and dredging in Otumoetai Channel is not included in the works. Source: The Port of Tauranga (2015). Personal Communication (email).

3.3.3.1 Port of Tauranga Model Study 1994

As an extension of the Port of Tauranga Model Study used to determine the effects of the 1991-92 capital dredging works, the Port of Tauranga again commissioned Bell (1994) (now contracted through NIWA) to use the same calibrated hydrodynamic model to determine the effects of wharf extensions at Sulphur Point. The objective was to model the effects of the wharf extensions and associated dredging on the velocities and current patterns and from the predictions, infer sediment transport. Bell (1994) used the 300 x 300 m and

75 x 75 m grid models from the Tauranga Harbour Study but with updated 1994 bathymetry. The extensions modelled were the 170 m wharf extension No.2, and the 250 m extension south. The port specified a dredging area south of the drop-off of 5.9 ha, and a depth of 12.9 m that would extend the full 250 m alongside the wharf. The proposed southern extension to Sulphur Point wharf modelled by Bell (1994) was the same as the future wharf extension plans in Figure 3.25. The dredging area was the same as the future wharf plans, but Bell (1994) dredged to a depth of 12.9 m whereas the present plans have been updated to have a dredged depth of 16 m. Bell (1994) identified that the dredging of Stella Passage associated with the proposed 250 m wharf extension south was the main cause of any changes to currents and sediment pathways.

The overall effects of the dredging and wharf extension at the southern end of Stella Passage was that although there were no changes to the larger current patterns, the localised velocity patterns within Stella Passage were altered (Bell, 1994). The changes to local velocity patterns can be seen in Figure 3.26 where the differences in peak ebb tidal velocities between the model runs with 1994 bathymetry, and the wharf extension dredging bathymetry were the largest in the dredged area. The differences were due to the dredging of the ebb tidal shoal that is at the terminus of the dredging limits rather than the addition of the wharf extension (Bell, 1994).

During the ebb tide flow, the tidal volume was no longer deflected to the eastern side of Stella Passage (Bell, 1994). The change in flow direction caused current velocities alongside the Sulphur Point wharves to have a slight increase of around 2 %, and thus the eastern side had weaker current velocities. Larger (magnitude) peak ebb velocities on the western side of Stella Passage also increased the potential for sediment transport. Sediment transport residual velocities in Figure 3.27 showed the stronger currents in front of the Sulphur Point wharves, a decrease in velocity on the eastern side and indicated the sediment pathways (Bell, 1994).

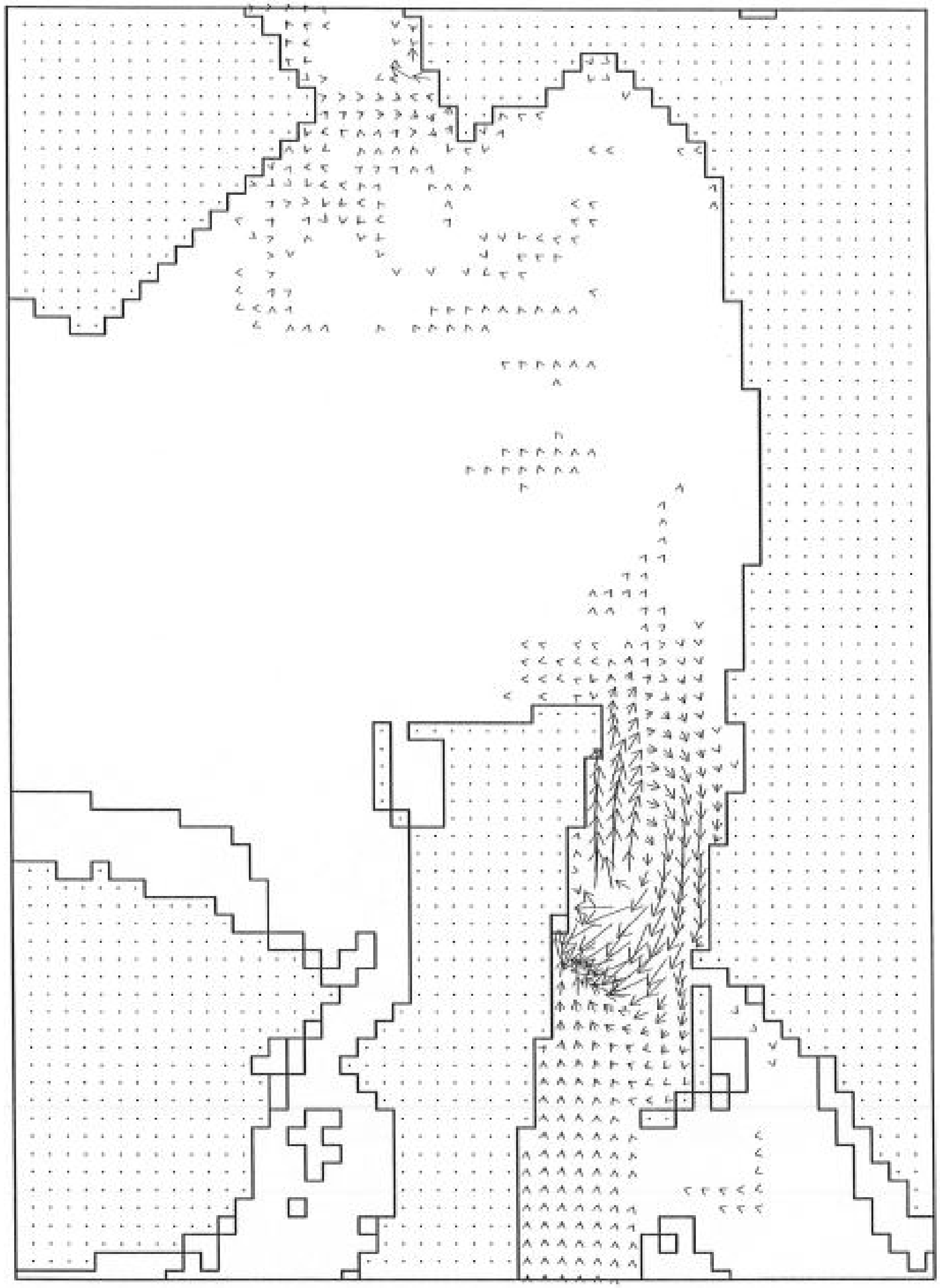

Figure 3.26: The difference in peak ebb tide velocities over 9.5 hours between the 1994 bathymetry, and bathymetry with the dredging extension into southern Stella Passage and Town Reach as part of the Sulphur Point wharf extension during a mean tide. The velocity vector scale is amplified where 1 mm:0.05 m.s^{-1}. Source: (Bell, 1994).

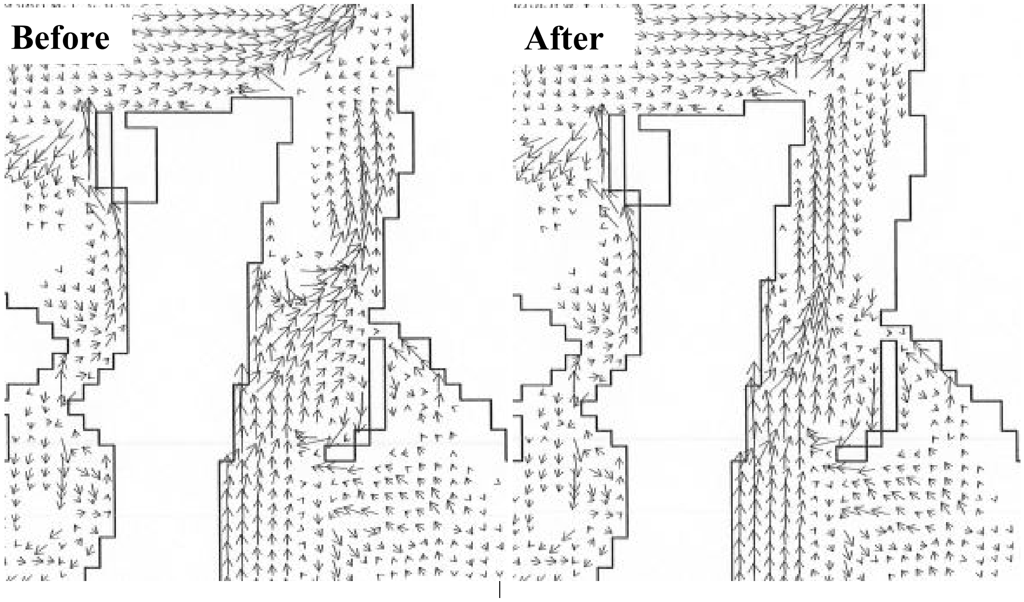

Figure 3.27: Residual velocities inferring sediment transport before and after the Sulphur Point wharf extension on a spring tide. The residual vector scale is 1 mm:0.02 $m.s^{-1}$. Source: (Bell, 1994).

Decreases in flow velocity on the eastern side lead to the development of a minor eddy in Town Reach near Aerodrome Bridge seen in Figure 3.27 (Bell, 1994). Either side of low water a tidal phase change of 2-4 minutes occurred, but the tidal range was unchanged. All changes were found to occur mainly during spring tides as any differences were amplified by the stronger tides occurring (Bell, 1994).

CHAPTER FOUR

FIELD DATA AND DELFT3D FLOW

4.1 Introduction

To predict the impacts of the proposed wharf extensions on the hydrodynamics of Stella Passage and the upper harbour, a numerical model was developed. The objective of this chapter is to summarise the field data collected and used in the development, calibration and verification of the hydrodynamic model as well as introducing the Delft3D FLOW hydrological modelling software and the modelling approach. The basic set-up of the hydrodynamic model including the bathymetry and grid, boundary conditions, observation points, discharges and the initial conditions that were used are justified. Model parameters used as the calibration parameters are described and typical values given. Justification of the model set-up is important as it impacted the validity of the hydrological modelling throughout the study.

4.2 Current Meters

A month of field data was collected in 2015 to be used in the calibration and verification of the Delft3D hydrodynamic model. Hydrodynamic data were measured with three SonTek Triton ADVs and an InterOcean Inc S4 ADW current meter, deployed from the 3rd September to the 2nd October 2015.

ADVs (Acoustic Doppler Velocimeter) measure the velocity of particles in the water column using the principle known as the Doppler shift (SonTek, 2011). Three acoustic receivers and an acoustic transmitter make up the ADV probe head displayed in Figure 4.1 A. Sound bursts are produced by the acoustic transmitter which are then intercepted by small particles passing through a remote sampling volume located 10 cm away from the transmitter (SonTek, 2011). The acoustic receivers record the echoes of the sound bursts that are reflected off the particles in the remote sampling volume (McKenzie, 2014). The change in frequency of the reflected sound bursts is known as the Doppler shift and gives measurements of instantaneous 3D velocity (McKenzie, 2014). The SonTek Triton ADV (Figure 4.1 B) measures pressure up to 30 m deep and has a velocity range of ± 0.1-4.8 $m.s^{-1}$ (SonTek, 2011).

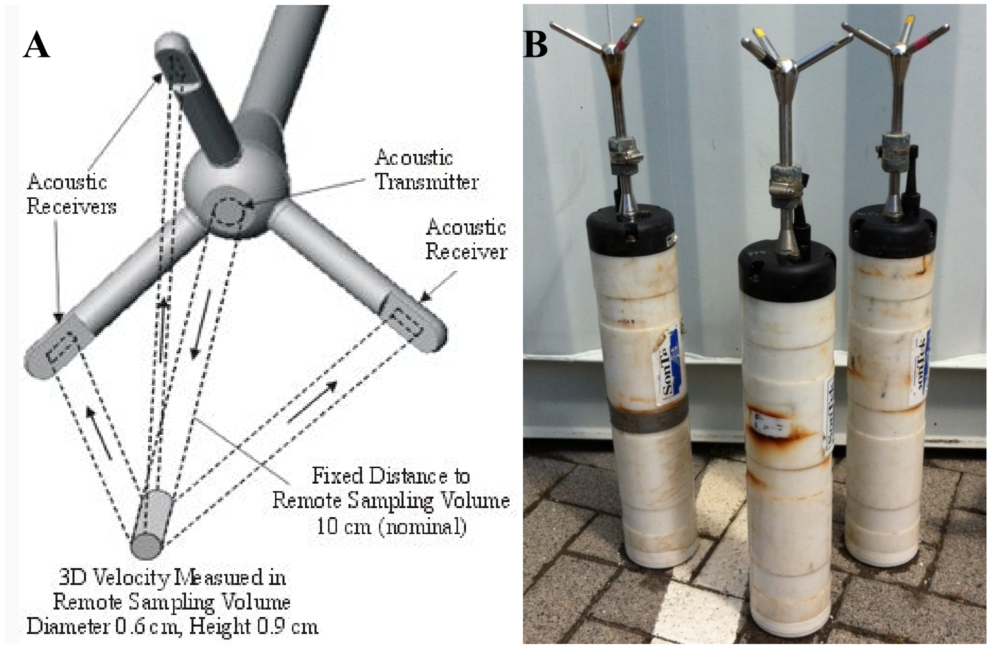

Figure 4.1: The probe head of a SonTek Triton ADV showing the position of the remote sampling volume (A) and the three SonTek Triton ADVs deployed in the field (B). Source (A): (SonTek, 2011).

S4 current meters use two pairs of titanium electrodes and an internal flux gate compass to provide direct measurements of the true current speed and direction (InterOcean Systems, 2016). Inside the S4 is a circular coil that acts as a magnetic field. As water is a conductor, the passing currents produce a voltage as they travel through the magnetic field. Faraday's law of electromagnetic induction determines the velocity of water, where the voltage produced is a product of the speed of the water multiplied by the magnitude of the magnetic field and the length of the conductor. The conductor length is the distance between each orthogonal pair of electrodes (Figure 4.2). As well as the magnitude and direction of the current, the InterOcean Systems Inc S4 ADW current meter (Figure 4.2) can precisely measure pressure, salinity, temperature, density, turbidity and chlorophyll. The S4 current meter can be deployed up to a depth of 70 m and can measure a velocity range of ± 0-3.5 $m.s^{-1}$ (InterOcean Systems, 2016).

Figure 4.2: InterOcean S4 ADW current meter with two orthogonal pairs of electrodes and sensors to measure salinity, pressure, temperature and density. Deployed in Tauranga Harbour by diver Dirk Immenga.

University of Waikato divers deployed the four instruments at the locations defined in Table 4.1, Figure 4.3 and Figure 4.4. The three ADVs were mounted on triangular frames weighted down with anchors and deployed at Hairini Bridge, Maungatapu Bridge and the Railway Bridge. Hairini and Maungatapu ADVs were secured to one of the bridge piles whereas the ADV at the Railway Bridge was tied to a boat mooring (Figure 4.4) to facilitate recovery. The S4 current meter was mounted on a large frame and weighted with anchors. The frame was secured to Marker 21 in Stella Passage (Figure 4.4); which is just up harbour of the dredging boundary (drop-off). GPS locations of each instrument were recorded on a handheld GPS device.

Table 4.1: Location of the instruments deployed in Tauranga Harbour from 9:00am 3rd September to 10:00am 2nd October 2015. GPS points were based on the WGS84 (World Geodetic Survey 1984) coordinate system. Note that the Chile tsunami occurred on the 17th September 2015 while the instruments were deployed.

Instrument	**Physical location**	**Site No.**	**GPS location**
ADV 252	Hirini Bridge	017	S37.71660 E176.16528
ADV 259	Mangatapu Bridge	018	S37.70778 E176.18894
ADV 228	Railway Bridge	019	S37.68633 E176.17226
S4 current meter	Stella Passage, Marker 21	020	S37.66606 E176.17663

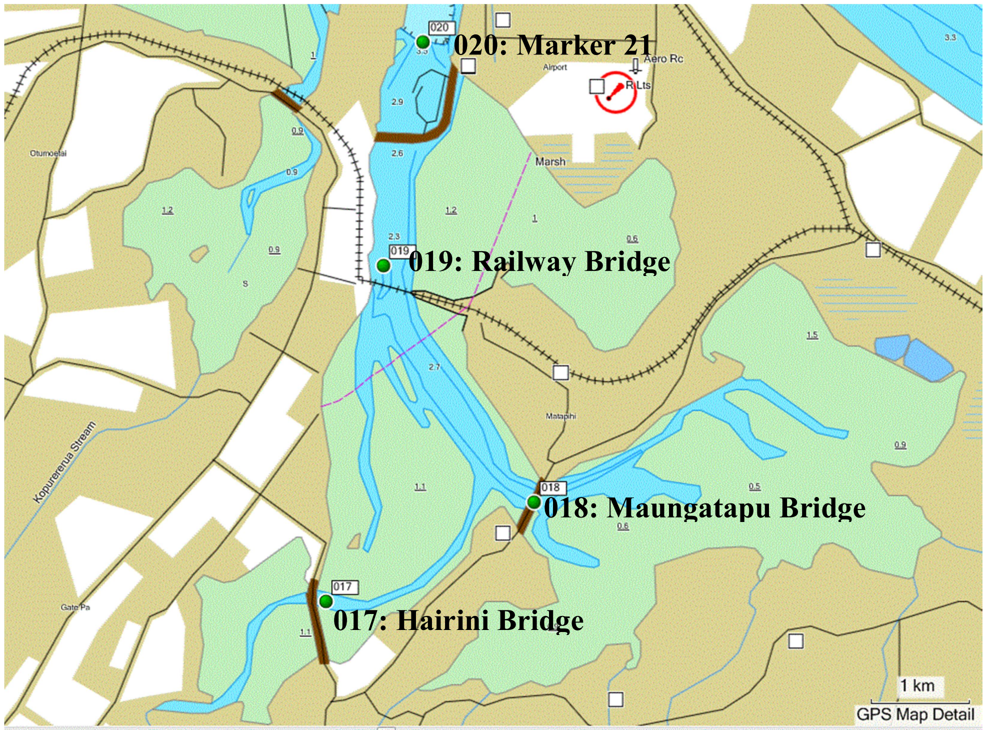

Figure 4.3: GPS location of the S4 current meter (point 020) and three ADVs (points 017, 018, 019) deployed from the 3rd September to 2nd October 2015. GPS points were based on the WGS84 (World Geodetic Survey 1984) coordinate system listed in Table 4.1.

Figure 4.4: Physical location of three ADVs (Hairini, Maungatapu and Railway) and an S4 current meter (Marker 21) deployed from the 3rd September to 2nd October 2015. The approximate location of each instrument is indicated by the white arrows. Orange buoys were used as a location device for divers during deployment and can be seen at the three ADV deployment sites.

The ADVs were programmed to sample every 5 minutes whereas the S4 sampled at a rate of 0.5 seconds over 1 minute every 10 minutes. New Zealand Daylight Saving started during the field data collection, but the instruments were set to continue recording on New Zealand Standard Time. On the 17th of September a tsunami warning was issued in New Zealand due to the 8.3 magnitude earthquake in Chile; the warning was later cancelled. Time series of pressure, U velocity and V velocity recorded by the instruments are presented in Figure 4.5 to Figure 4.8.

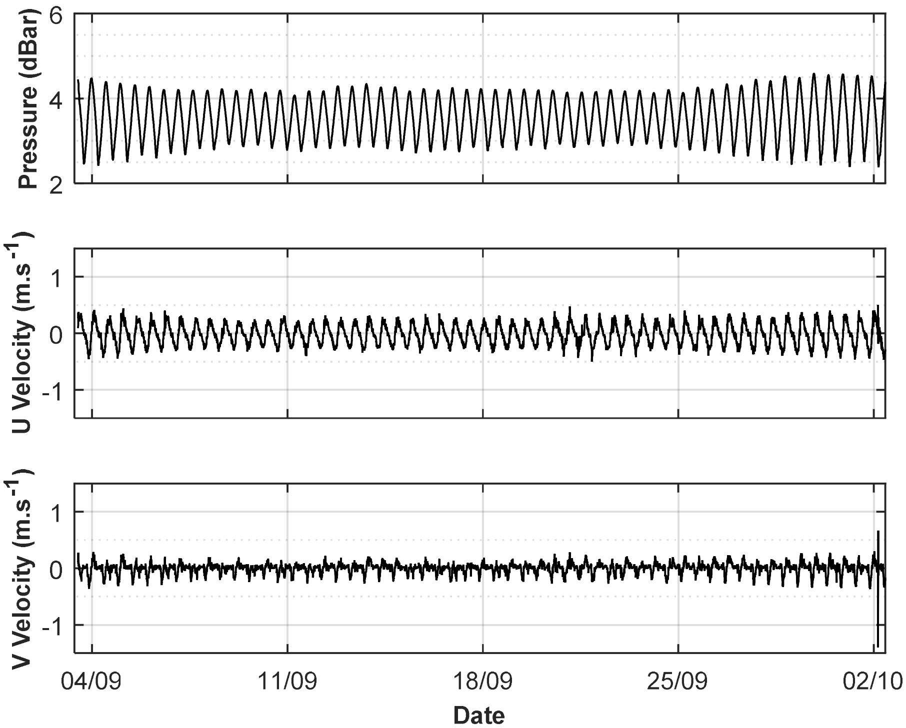

Figure 4.5: Time series of pressure, U velocity and V velocity recorded by the ADV at Hairini Bridge in Tauranga Harbour, deployed from the 3rd September to 2nd October 2015.

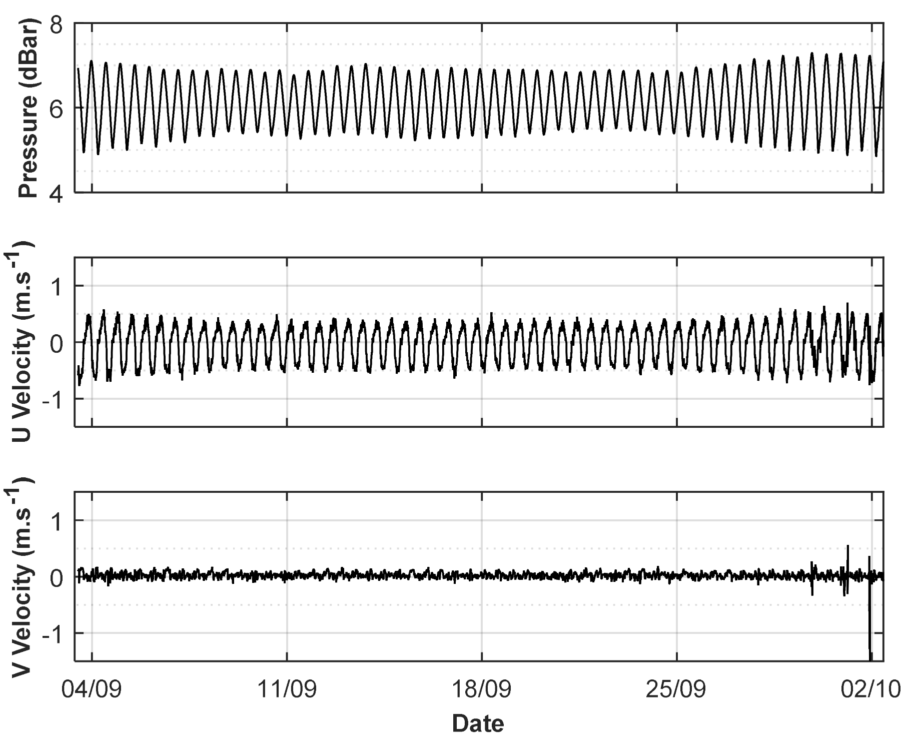

Figure 4.6: Time series of pressure, U velocity and V velocity recorded by the ADV at Maungatapu Bridge in Tauranga Harbour, deployed from the 3rd September to 2nd October 2015.

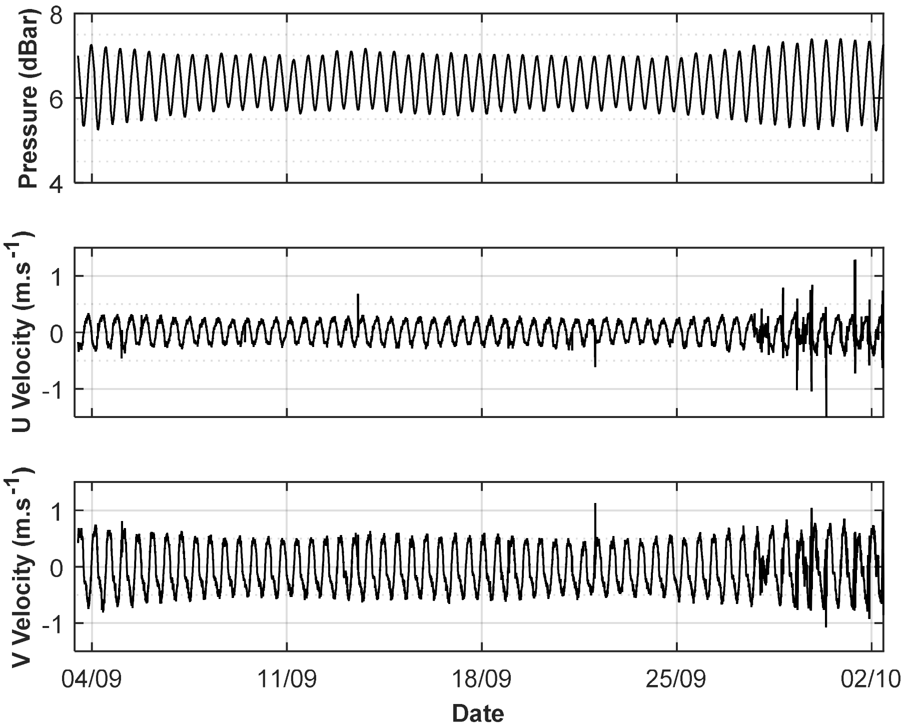

Figure 4.7: Time series of pressure, U velocity and V velocity recorded by the ADV at the Railway Bridge in Tauranga Harbour, deployed from the 3rd September to 2nd October 2015.

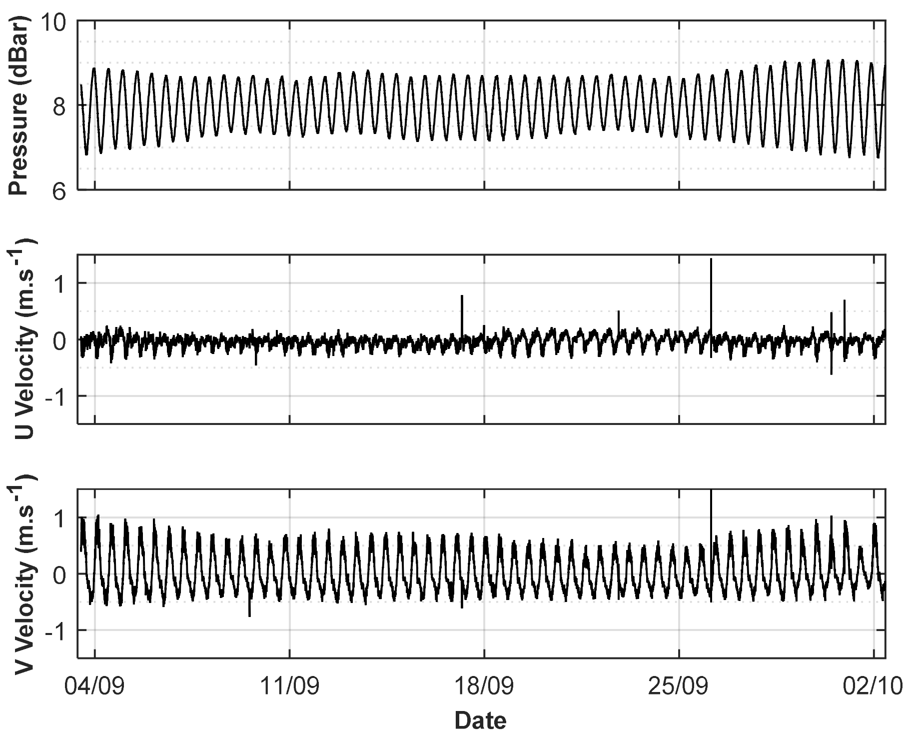

Figure 4.8: Time series of pressure, U velocity and V velocity recorded by the S4 current meter at Marker 21 in Stella Passage Tauranga Harbour, deployed from the 3rd September to 2nd October 2015.

U velocity represents the east-west or x component and V velocity the north-south or y component of velocity. From U and V velocities, measurements of current speed and current direction were calculated. Pressure was converted to water depth by assuming 1 dBar of pressure recorded by the ADVs and S4 is equal to 1 m of water depth and subtracting the change in atmospheric pressure around the average air pressure over the deployment period of 1015.02 hPa. The mean water depth was subtracted from the water depth time series to give the water elevations.

Time series of current velocity and current direction were also obtained from the Port of Tauranga's ADCP current meter. The ADCP is permanently deployed in the Entrance Channel of Tauranga Harbour for navigational and shipping purposes; the coordinates are given in Table 4.2 and Figure 4.10. Figure 4.9 shows the current measurements obtained from the Port of Tauranga during the field deployment period.

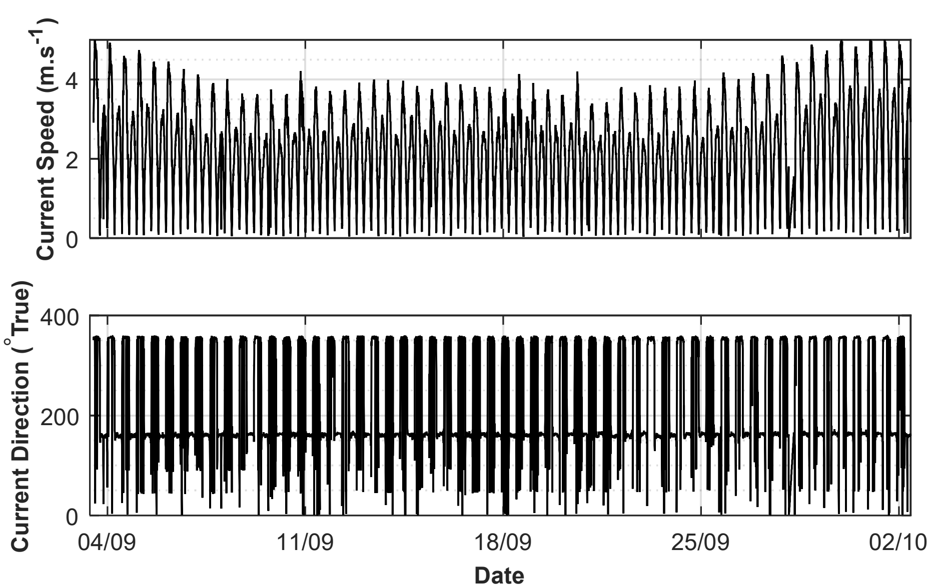

Figure 4.9: Time series of current speed and current direction recorded by the Port of Tauranga's ADCP current meter in the Entrance Channel to Tauranga Harbour from the 3rd September to 2nd October 2015.

4.3 Tide Gauges

Five tide gauges within the southern basin of Tauranga Harbour provided water depth or water level measurements every 5 minutes. The coordinates in New Zealand Transverse Mercator (NZTM) and physical location of the tide gauges along with the ADCP and the wave buoy at Moturiki Island are given in Table 4.2

and Figure 4.10. Two of the tide gauges, Sulphur Point and Tug Berth, are operated by the Port of Tauranga and measurements of water depth were taken by a VEGAPULS 61 sensor that uses radar technology. Water level data from the tide gauges at Hairini, Oruamatua and Omokoroa were collected and processed by the BOPRC on behalf of the TCC. Water levels from the five tide gauges over the course of the field deployment are displayed in Figure 4.11 and Figure 4.12.

Table 4.2: Coordinates of the Port of Tauranga ADCP current meter and two tide gauges and the three BOPRC tide gauges in Tauranga Harbour and the Moturiki Island wave buoy. Coordinates are based on the NZTM system.

Physical Location	**Instrument**	**Easting**	**Northing**
Entrance Channel	ADCP	1879319.9	5830039.3
Sulphur Point	Tide gauge	1880000.0	5826610.0
Tug Berth	Tide gauge	1880690.0	5829250.0
Hairini	Tide gauge	1879010.5	5820867.5
Oruamatua	Tide gauge	1882444.9	5822690.4
Omokoroa	Tide gauge	1868629.8	5827518.8
Moturiki Island	Wave buoy	1881060.1	5830280.4

Figure 4.10: Locations of the tide gauges (yellow markers), ADCP current meter (Red marker) and wave buoy (blue marker) in Tauranga Harbour. Source: Google Earth.

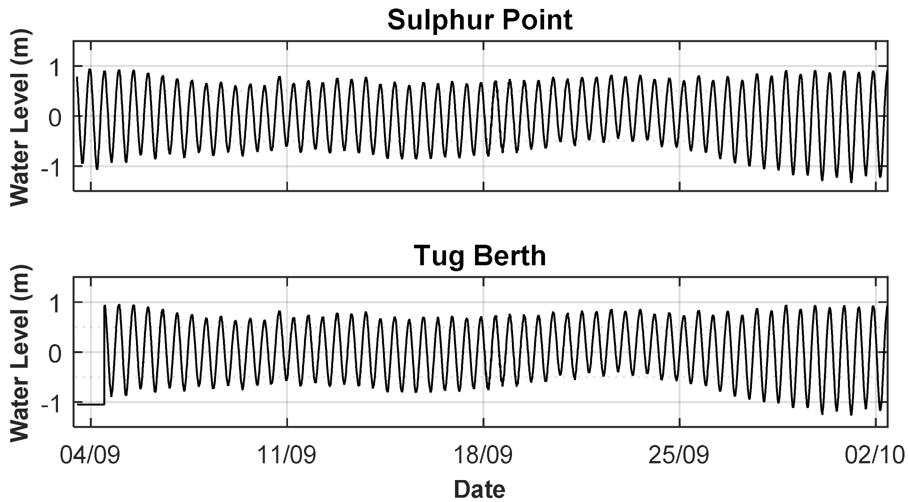

Figure 4.11: Time series of water levels recorded by the Port of Tauranga tide gauges at Sulphur Point and Tug Berth in Tauranga Harbour from the 3rd September to 2nd October 2015.

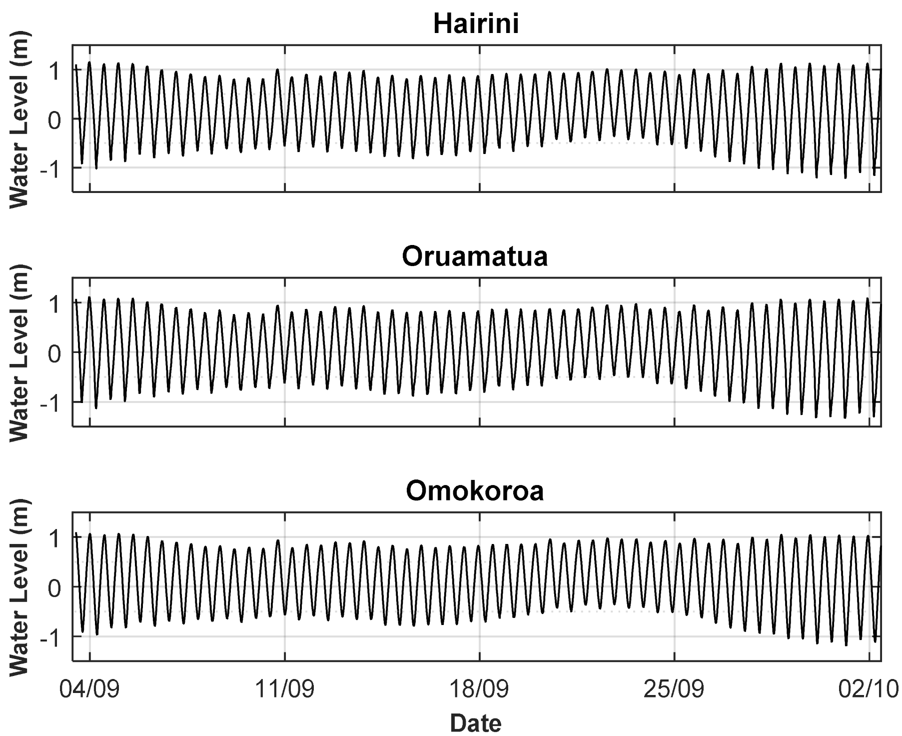

Figure 4.12: Time series of water levels recorded by the BOPRC tide gauges at Hairini, Oruamatua and Omokoroa in Tauranga Harbour from the 3rd September to 2nd October 2015.

4.4 Tides

Astronomical changes to water levels in the ocean are generated by the changing gravitational effects of the Sun and the Moon as they orbit around the Earth (Schwartz, 2005). The resulting long wave is the tide and the tidal currents are the horizontal movement of water. Movement of the tidal wave towards and away from the coastline are the flood and ebb tides respectively. Every two weeks the Sun, Moon and Earth align giving a full Moon or a new Moon, during which time a spring tide with the maximum tidal range occurs. The minimum tidal range occurs during a neap tide where the Sun and Moon are at 90° to the Earth, known as the first quarter and third quarter moons (Schwartz, 2005). Tides are commonly classified as diurnal or semi-diurnal where high water and low water occur once or twice a day respectively (Schwartz, 2005).

As the Sun and Moon orbits are not circular and vary with time there are many tidal frequencies that are produced. Each of the frequencies are a separate tidal constituent that combine to give the tidal signal. The two main tidal constituents are the M2 and S2 tides which are the principal lunar and solar semidiurnal tides that are forced by the Moon and Sun respectively (Schwartz, 2005). Other major tidal constituents are the N2 which is the larger lunar elliptic semidiurnal tide, and the O1 and K1 diurnal constituents which are the lunar declinational and the luni-solar declinational respectively (McKenzie, 2014).

When a long wave approaches a continental shelf or enters shallow water the tidal wave is also affected by hydrodynamics (Schwartz, 2005). The deep water tidal constituents are amplified or undergo resonance, producing additional tidal constituents. Within a harbour or estuary with a narrow entrance, astronomical forcing no longer has any effect on the tide which is then altered by the shape, width and bathymetry of the estuary. Shoaling through narrow tidal inlets may delay the propagation of the tide within the harbour and increase the amplitude of the tidal wave; as seen in Tauranga Harbour (Schwartz, 2005).

4.4.1 Tides in Tauranga Harbour

The LINZ database collates and makes predictions of tidal levels for Tauranga Harbour. Tidal levels were measured against the Port of Tauranga CD (LINZ, 2015). Table 4.3 presents the high and low water levels during a spring and neap cycle, tidal ranges, MSL and the highest and lowest predicted astronomical tide in Tauranga Harbour against CD and the Moturiki Vertical Datum 1953. The Moturiki Datum is located at the Port of Tauranga offices and is 0.96 m above CD (LINZ, 2015).

Table 4.3: Tidal levels for Tauranga Harbour. All levels were averaged from predictions of spring and neap cycles from the 1st July 2015 to the 30th June 2016, apart from the highest and lowest astronomical tides which are the levels predicted to occur under average meteorological conditions from the 1st January 2000 to 31st December 2018. Source: (LINZ, 2015).

Tidal Levels	Chart Datum (m)	Moturiki Datum (m)
Mean High Water Spring (MHWS)	1.93	0.97
Mean High Water Neap (MHWN)	1.67	0.71
Mean Low Water Spring (MLWS)	0.47	-0.49
Mean Low Water Neap (MLWN)	0.15	-0.81
Spring Range	1.78	0.82
Neap Range	1.20	0.24
Mean Sea Level (MSL)	1.08	0.12
Highest Astronomical Tide (HAT)	2.11	1.15
Lowest Astronomical Tide (LAT)	-0.07	-1.03

Timing of the spring and neap tidal cycles during the field deployment period were obtained from the NIWA tide forecaster (Figure 4.13) (NIWA, 2016). NIWA predicts the tide heights across all of New Zealand's Exclusive Economic Zone (EEZ) using a computer tidal model that is forced by 16 of the main tidal constituents (NIWA, 2016). During the field deployment there were 1.5 spring neap tidal cycles.

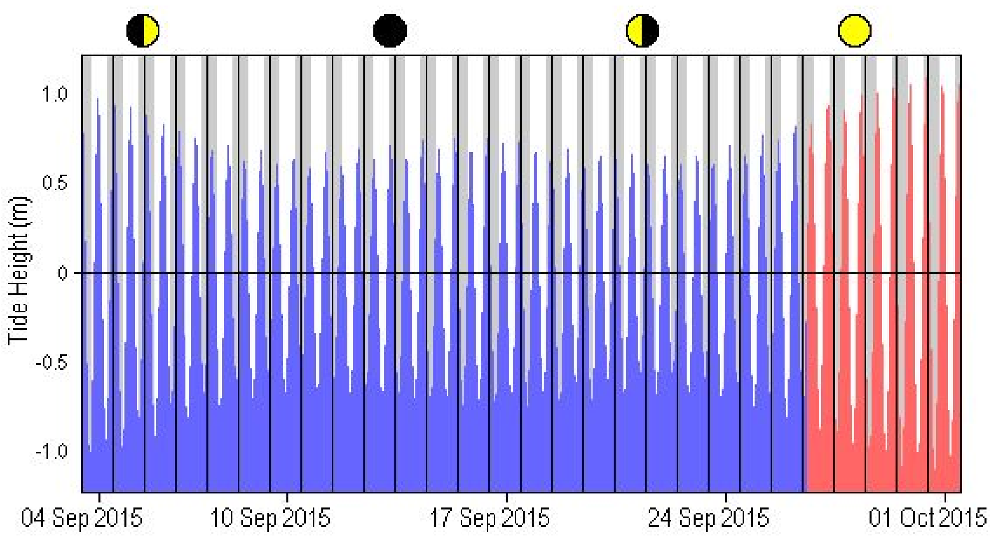

Figure 4.13: Tidal height and timing of the spring and neap tidal cycles at the Tauranga Harbour entrance from the 3rd September to 2nd October 2015. Moon symbols above the tide heights from left to right represent a first quarter (neap tide), new (spring tide), third quarter (neap tide) and full Moon (spring tide). Tidal heights are given in metres from MSL and those plotted in red indicate the start of New Zealand Daylight Saving. Source: (NIWA, 2016).

4.5 Tidal Harmonic Analysis

Developed by Rich Pawlowicz, Steve Lentz and Bob Beardsley in 2001 from the FORTRAN package by Mike Foreman, T_TIDE is a MATLAB function that is used to undertake tidal harmonic analysis by separating the tidal and non-tidal energy in a time series (Pawlowicz et al., 2002). The tidal harmonic analysis gives the frequency, period, amplitude and phase of up to 45 astronomical and 24 shallow water tidal constituents. The input time series can be either scalar for water levels or complex for U and V Velocities (Pawlowicz et al., 2002). Tidal harmonic analysis of the water levels at Tug Berth during the field deployment period gave an indication of the major tidal constituents in Tauranga Harbour and is displayed in Table 4.4. The major tidal constituents at Tug Berth were the M2, S2, N2 and K1. As found in previous literature, the dominant tidal constituent in Tauranga Harbour was the M2 tide which had the largest tidal amplitude of 0.7046 m. T_TIDE was also used to determine if the errors between the measured data and numerically modelled time series were due to environmental factors such as wind and waves by isolating and comparing the measured tidal energy.

Table 4.4: Tidal harmonic analysis showing the major tidal constituents at Tug Berth in Tauranga Harbour from water levels recorded by the Port of Tauranga's tide gauge at Tug Berth from the 3rd September to 2nd October 2015. Phase is in Greenwich Mean Time (GMT).

Tidal Constituent	Frequency	Amplitude (m)	Phase (° GMT)
M2	0.0805	0.7046	336.37
S2	0.0833	0.0943	284.31
N2	0.0790	0.1599	174.72
K1	0.0418	0.0365	281.54

4.6 Weather

A meteorological station at Tauranga Airport provided hourly wind, temperature and air pressure (also known as barometric or atmospheric pressure) data as well as yearly and monthly averages. The data is part of the National Climate Database and is available on NIWA's CliFlo database (CliFlo, 2016). The Tauranga Airport weather station is station number 1615 and is located 4 m above MSL (CliFlo, 2016). When comparing the averages of yearly mean and September mean wind speed and air pressure over 2000-2015 (Table 4.5), September means had lower minimum, and higher maximum and averages than the yearly means.

Table 4.5: Statistics of the wind speed and air pressure at MSL from yearly and monthly (September) means from 2000-2015 and hourly measurements from the 3rd September to 2nd October 2015 recorded by weather station number 1615 at Tauranga Airport located 4 m above MSL. Yearly and monthly means were obtained from the CliFlo database (CliFlo, 2016).

Meteorological Data	**Data Type**	**Min**	**Max**	**Average**
Air Pressure (hPa)	Yearly **mean**	1014.6	1017.5	1016.44
	September **mean**	1007.1	1023.8	1016.79
	Hourly (3/9-2/10 2015)	997.5	1033.6	1015.02
Wind Speed ($m.s^{-1}$)	Yearly **mean**	3.6	4.3	3.875
	September **mean**	3.0	5.1	4.013
	Hourly (3/9-2/10 2015)	0.0	11.8	3.364

Hourly measurements of air pressure, wind speed and wind direction in Figure 4.14 and Table 4.5 show that there was a higher maximum air pressure during the field deployment period than the yearly mean and September mean. During the field deployment period the average air pressure was below the New Zealand average of 1014 hPa. Variations in barometric pressure are important when measuring water levels, as a rise in pressure will cause a rise in water level; same holds for a drop in pressure (McKenzie, 2014). A change of 1 cm is caused by a 1 hPa difference in pressure (McKenzie, 2014). A 36 hPa difference in air pressure was measured over the field deployment period which would give a 36 cm variation in water levels.

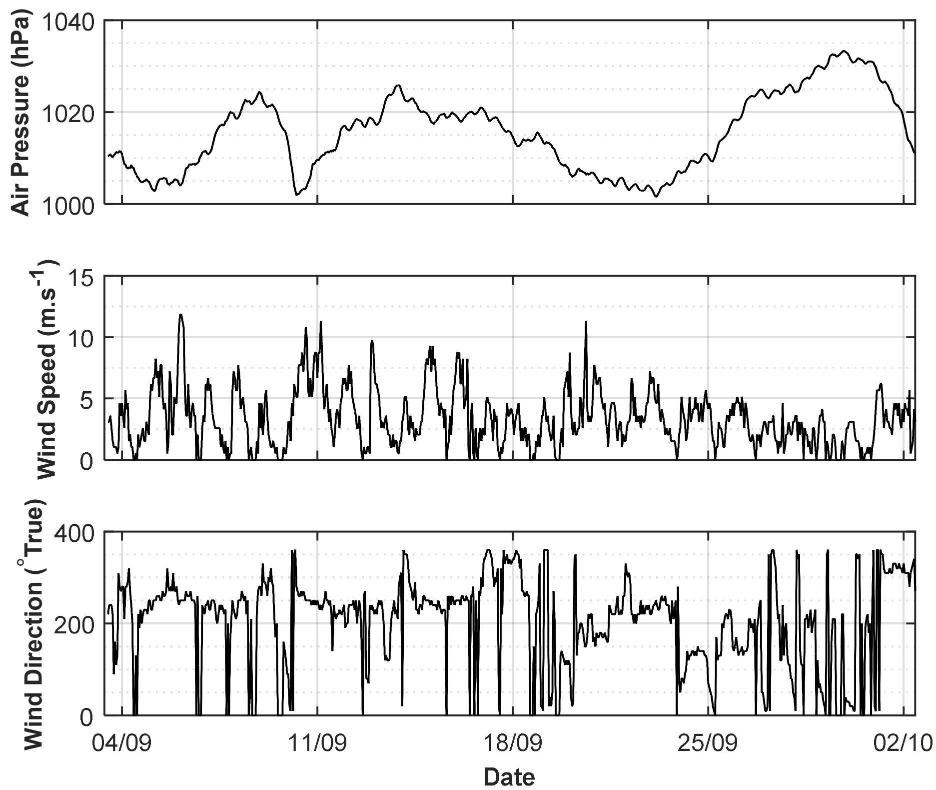

Figure 4.14: Time series of air pressure at MSL, wind speed and wind direction recorded by weather station number 1615 at Tauranga Airport located 4 m above MSL from the 3rd September to 2nd October 2015.

Analysis of the wind speed and wind direction data (Figure 4.14) collected at Tauranga Airport showed no obvious pattern in wind speed or direction over the month. The average wind speed over the field deployment period, displayed in Table 4.5, was 3.36 $m.s^{-1}$ which was lower than both the yearly mean and September mean averages obtained from the CliFlo database of 3.86 $m.s^{-1}$ and 4.01 $m.s^{-1}$ respectively. Figure 4.15 shows the predominant wind direction was from the southwest to south. South-southwest airflows were the most common as well as the strongest wind speeds, reaching up to 11.83 $m.s^{-1}$. Wind generated waves entrain and transport sediment on shallow intertidal flats and beaches within Tauranga Harbour (de Lange & Healy, 1990). Historically, westerly winds caused by fast eastward moving cold fronts are the most common in Tauranga Harbour and severe east to northeast storms occur episodically (de Lange & Healy, 1990). Within Tauranga Harbour, westerly winds pick up the waves giving higher water levels, whereas easterly winds flatten and decrease water levels.

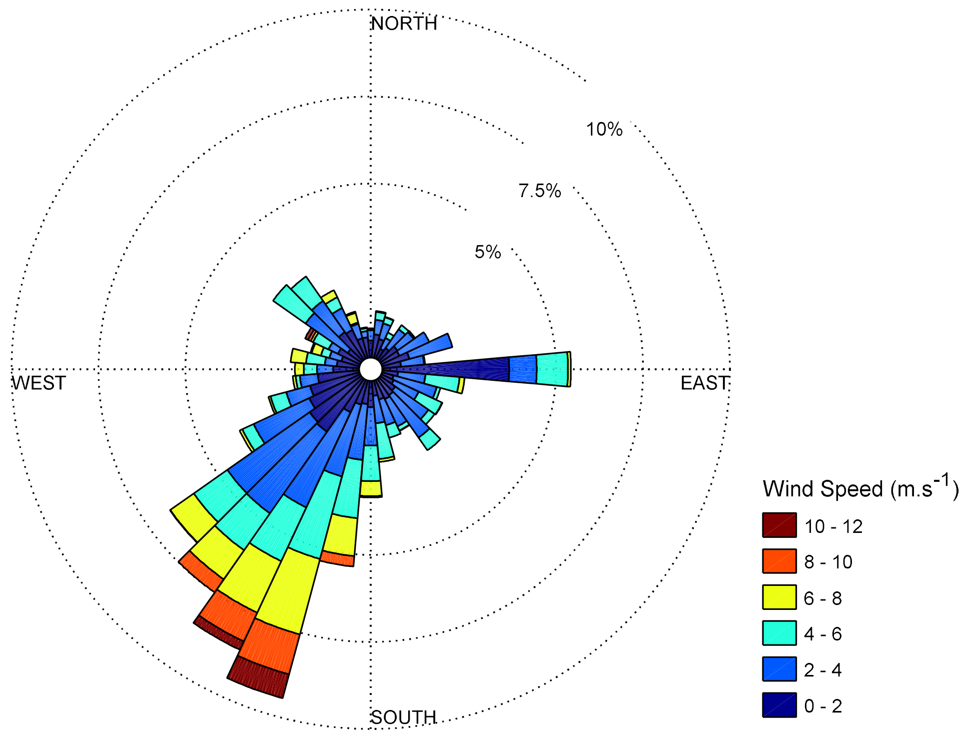

Figure 4.15: Wind rose of the percentage occurrence of wind speed and wind direction (°True) recorded by weather station number 1615 at Tauranga Airport located 4 m above MSL from the 3rd September to 2nd October 2015

4.7 Modelling Approach

Numerical modelling of the hydrodynamics in the southern basin of Tauranga Harbour was carried out in Delft3D, a numerical modelling software developed by Deltares (Deltares Systems, 2013). Delft3D FLOW is the flow module of the modelling suite which simulates complex 2D and 3D hydrodynamic systems. Typical applications of Delft3D FLOW are predicting the impacts of structures on hydrodynamics, dispersion of contaminants, stability of a hydrodynamic system and salt intrusion (Deltares Systems, 2013). Flow simulations were carried out in 2D (depth averaged) simulations as the harbour is shallow, well-mixed and vertically homogeneous.

A large 2D hydrodynamic model of the southern basin of Tauranga Harbour was developed and run on a 20 x 20 m grid; named the southern basin model. An uncalibrated Delft3D FLOW model of the southern basin was provided by Bradley Monahan and was developed as part of his PhD thesis with the University of Waikato. The uncalibrated model was used as a template for the southern basin model. The simulation period, bathymetry, numerical and physical parameters and observation points were altered and the southern basin model was calibrated and verified. Figure 4.16 shows the model domain of the southern basin model along with the location of other Delft3D FLOW parameters.

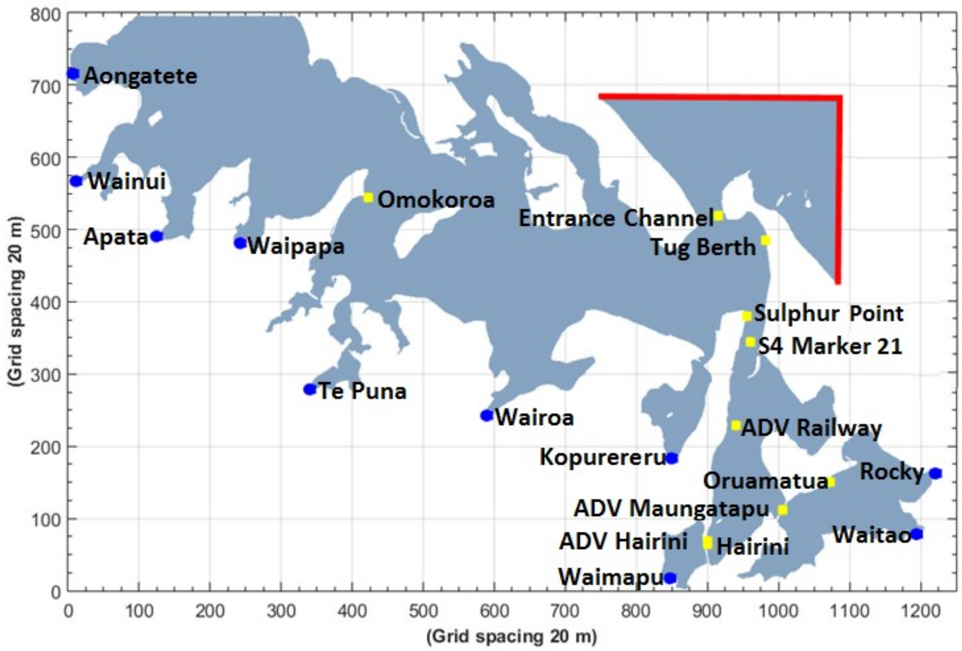

Figure 4.16: Placement of the southern basin model 20 x 20 m grid (grey), the open water boundaries (red), observation points (yellow), and river and stream discharge locations (blue) utilised in the Delft3D southern basin model.

4.8 Delft3D FLOW

Delft3D FLOW simulates hydrodynamic systems by solving the three dimensional Navier-Stokes equations using shallow water and Boussinesq assumptions (Deltares Systems, 2013). The final equations are known as the partial differential equations and consist of the horizontal equations of motion, the transport equation for conservative constituents and the continuity equation. The partial differential equations are solved by discretising over space and integrating over time on a finite difference grid which covers the entire model area. The grid is defined by a coordinate system, in this case a Cartesian coordinate system. The finite difference grid is in a staggered grid format, where water level and velocity components (descriptors of flow) are defined at different positions on the grid; water levels in the grid cell centres and velocities at the edge of the grid cells. Deltf3D FLOW models are forced at boundaries and initial conditions, physical parameters and numerical parameters are specified (Deltares Systems, 2013).

4.8.1 Bathymetry

The 20 x 20 m rectangular grid in the southern basin model was based on the Cartesian coordinate system and comprised of 1248 cells in the M direction and 796 cells in the N directions. Bathymetric data used in the 20 x 20 m southern basin model was comprised from a number of sources. Multibeam data from surveys undertaken by the Port of Tauranga as part of the dredging works provided the bathymetry for the dredged channels. The Port of Tauranga survey data had the finest resolution and was the most recent; the survey was undertaken before the 2015 dredging work commenced. Intertidal areas that were not included in the Port of Tauranga survey data were populated with LiDAR (Light Detection and Ranging) data from 2008 provided by the BOPRC. The entire model domain was covered by LINZ hydrological charts NZ 5411 and NZ 5412 which were obtained from the LINZ data service. Once digitised and geo-referenced, the LINZ charts provided the bathymetry in areas that were not covered by the multibeam or LiDAR survey data. LINZ charts are used to provide water depths for navigation within the harbour, and due to their conservative nature, may state shallower depths than the actual bathymetry. All of the bathymetric data were based on the NZTM2000 coordinate datum and the height datum of CD. The bathymetry was converted to MSL by adding 1.05 m to all of the data.

The original bathymetry that was provided was then updated for the purpose of this study, where the hydrodynamics of Stella Passage and the upper harbour were the key focus. Mean depths recorded by the ADVs and S4 during the simulation period were compared to the MSL heights in the original bathymetric data. It was found that the depth recorded at the three ADVs locations in the upper harbour were significantly deeper than those used in the original bathymetry. The bathymetry was lowered to as close to the ADV recorded mean depths as possible. The largest difference was at Hairini and Maungatapu Bridges which were both lowered by more than 2.5 m. Bathymetry at the Railway Bridge only had to be lowered by less than 1 m. Depths in the main channels between the bridges were also lowered and smoothed to give realistic depth changes and bathymetry. Differences between the bathymetric data and the actual mean depths recorded may have been due to the accuracy of the conservative LINZ hydrological charts that were used for the bathymetry in the upper harbour. Bathymetry in Stella

Passage was provided by the Port of Tauranga survey and had the same depth as that recorded on the S4 current meter.

Also notably absent in the original bathymetry is the causeway up to the Railway Bridge which spans half the channel. As the causeway drastically alters the hydrodynamics in the immediate area and in the upper harbour it was added into the bathymetry by increasing the elevation to above the highest water level. A set of thin dams were also added to block off the north-eastern most tip of Sulphur Point where the 2014 wharf extension No.2 was constructed; the wharf was not included in the original bathymetry file. The final bathymetry used in the southern basin model in displayed in Figure 4.17.

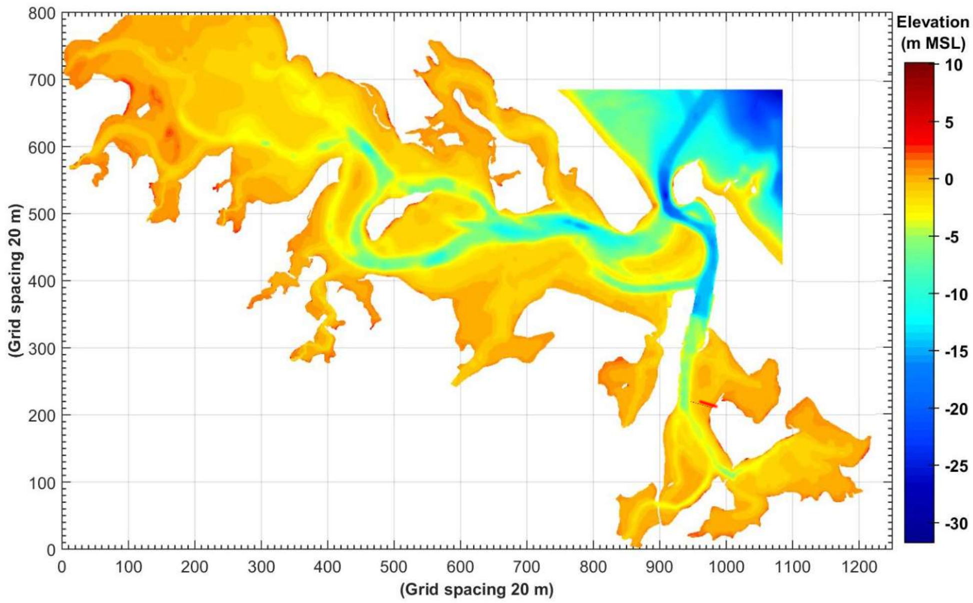

Figure 4.17: Final bathymetry used in the large Delft3D FLOW model of the southern basin of Tauranga Harbour. Note a negative elevation is below MSL.

4.8.2 Simulation Period

In this study the simulation period used in the southern basin model covered the same period as when the instruments were deployed. As the hydrodynamic model began with a cold start, 2.5 days was added to the start of the simulation period to serve as a spin-up time or initial period where the model could adjust and not be influenced by the boundary forcing conditions (Deltares Systems, 2013). The simulation period used in the southern basin model was from 00:00:00 on the 1st September to 00:00:00 on the 3rd October 2015.

The time step used in numerical simulations is restricted by the Courant-Friedrichs-Lewy (CFL) condition (Equation 4.1) which determines if the time step will give an accurate reproduction of the spatial length scales (Deltares Systems, 2013). The Courant number defines the CFL condition and takes into account the grid spacing and travel time, so a grid cell will not be skipped over in a time step.

$$CFL = \frac{\Delta t \sqrt{gH}}{\{\Delta x, \Delta y\}} \qquad 4.1$$

Where Δt is the time step in seconds, g is the value for acceleration of gravity, H is the water depth and Δx, Δy are the grid spacing. A smaller time step would reduce model instabilities but increase computation time, whereas a larger time step can significantly reduce computation time but at the expense of increased numerical errors. Courant numbers can also be calculated within Delft3D QUICKIN module (Deltares Systems, 2013). When calculated within Deft3D QUICKIN, the grid over the main channel of Stella Passage is capable of running with a Courant number of 15, but within the upper harbour Courant numbers were lower with 3 at Hairini Bridge and 6 at Maungatapu Bridge and the Railway Bridge. The Delft3D FLOW manual recommends that the Courant number denoting the time step not be beyond a value of 10 (Deltares Systems, 2013). A time step of 0.5 minutes was used in the hydrodynamic southern basin model so the shallow intertidal areas could be accurately simulated.

4.8.3 Boundary Conditions

The hydrodynamic forcing at the boundaries of Delft3D FLOW models are typically based on water levels or currents and can be described using astronomic components, harmonic components or as a time series (Deltares Systems, 2013). The Delft3D FLOW manual recommends forcing from water levels when modelling tidal flow in a basin or harbour (Deltares Systems, 2013). In this study, flow was forced by water levels at two open water boundaries shown in Figure 4.16. A year's worth (1999) of data from the Moturiki Island wave buoy (Figure 4.10) was run through T_TIDE and the tidal constituents were extracted. Tidal forcing conditions stating the amplitude and phase of the major tidal constituents (Table 4.6) were set at the beginning and end point of both boundaries, then linear interpolation between the points was carried out by the model (Deltares Systems, 2013). As the model boundaries were located in the open ocean, only the deep water primary tidal constituents were used.

Table 4.6: Amplitude and phase of the tidal constituents that were used as open boundary conditions in the southern basin model obtained from a year's worth (1999) of water levels from the Moturiki Island wave buoy and extracted with T_TIDE. Phase is in Greenwich Mean Time (GMT).

Tidal Constituent	Amplitude (m)	Phase (° GMT)
M2	0.7480	189.70
S2	0.0983	262.99
N2	0.1672	154.42
K2	0.0186	266.91
K1	0.0506	180.74
P1	0.0160	174.87
Q1	0.0017	50.19
O1	0.0107	126.71

4.8.4 Physical and Numerical Parameters

Delft3D FLOW simulations allow a number of physical and numerical parameters to be selected and applied across the model. Values of bottom roughness and eddy viscosity along with the drying and flooding threshold limit are the most common parameters that are altered during the calibration and verification stage of modelling and are so-called, calibration parameters. An overview of the three calibration parameters is given in this section and the specific values applied to the southern basin model are discussed in Chapter Five. Some physical and numerical parameters were less sensitive and were kept constant throughout the modelling process. The hydrodynamic constants that were used were a gravitational acceleration of 9.81 $m.s^{-2}$ and a water density of 1025 $kg.m^{-3}$.

4.8.4.1 Bottom Roughness

Roughness is a physical parameter and is the most common cause of error within a model (Deltares Systems, 2013; Tay et al., 2013; McKenzie, 2014). Bottom roughness is the hydraulic roughness or friction experienced by a fluid passing over a bed and is sometimes known as bed resistance (Tay et al., 2013; McKenzie, 2014). Increasing or decreasing the bottom roughness value can significantly alter the amplitude and phase of the tidal wave (Deltares Systems, 2013; McKenzie, 2014). Values of bottom roughness are required for every grid cell in the x and y directions and can be specified as either a uniform value or spatially varying (Deltares Systems, 2013). There are many formula that are used to denote bottom roughness such as the Manning formulation, the Manning coefficient, Chézy friction coefficient and the White-Colebrook formulation (Deltares Systems, 2013). In this study values of the Chézy friction coefficient ($m^{-1/2}.s$) were used.

A high Chézy value reduces the bottom friction and speeds up the current, where as a lower Chézy value increases the bottom friction experienced by the fluid and slows down the current (Deltares Systems, 2013; McKenzie, 2014). Typically, areas of greater water depths as well as fast flowing areas with low bed friction like main channels have higher Chézy values (Tay et al., 2013; McKenzie, 2014). Lower Chézy values are typical of shallow and intertidal areas and those with a high bed friction like rocky areas (Tay et al., 2013; McKenzie, 2014). Values of bottom roughness are often specified by either the water depth or the grain size distribution at each location (Deltares Systems, 2013). The default Chézy value in Delft3D FLOW is 65 $m^{-1/2}.s$. As the models were 2D and depth averaged, a first estimate of the Chézy friction coefficient could be calculated by (Deltares Systems, 2013):

$$C = 25 + H \qquad 4.2$$

Where H is the water depth (m). In this study both a constant value of bottom roughness and spatially varying values based on water depth were applied and the outcomes are discussed during sensitivity analysis.

4.8.4.2 Eddy Viscosity

Viscosity is a physical parameter in Delft3D FLOW where a constant or varying eddy viscosity may be specified. Eddy viscosity is the transfer of momentum or momentum fluxes caused by either turbulence, mixing or sub-grid scale effects (McKenzie, 2014). Often described through the Smagorinsky factor, in Delft3D FLOW values of eddy viscosity are given in $m^2.s$. Eddy viscosity is considered a calibration parameter as it can impact the details of the flow and is influenced by the grid size and flow type (Deltares Systems, 2013). For models with grid sizes below 100 m Delft3D FLOW suggests values of eddy viscosity ranging from 1-10 $m^2.s$. Values between 10-100 $m^2.s$ are recommended for models with grid sizes 100 m and above (Deltares Systems, 2013). A range of constant values of background horizontal eddy viscosity were applied during the calibration phase.

4.8.4.3 Drying and Flooding

The third calibration parameter specifies drying and flooding depths and is a numerical parameter within Delft3D FLOW. Drying and flooding depths are particularly important in models that include large areas of intertidal flats that are exposed during the low tide, as in the southern basin of Tauranga Harbour (McKenzie, 2014). If no depth was specified the current velocities over the intertidal area would increase due to mass conservation as the large dry area is instantly flooded on the incoming tide.

The threshold depth (m) states the depth of water needed for a cell to be deemed dry or flooded (Deltares Systems, 2013). The threshold parameter allows the tide to move more smoothly across the intertidal areas as the water depth does not become negative over a single time step. As Delft3D FLOW computation grids are staggered, drying and flooding checks are carried out at the grid cell faces (velocity points) and cell centres (water levels). For a grid cell to be dry and have temporary thin dams to be placed around the cell, the mean depth of all four cell faces must be below the threshold depth, otherwise the grid cell is flooded. Equation 4.3 is used to estimate the threshold depth and is a simplification of the equation recommended by Delft3D FLOW (Deltares Systems, 2013).

$$\delta \geq \frac{2\pi a}{N} \tag{4.3}$$

Where δ is the threshold depth, *a* is the characteristic tidal amplitude (m) and *N* is the number of time steps in a tidal period (Deltares Systems, 2013). The values used in the calculation of the threshold depths are presented in Chapter Five.

4.8.1 Freshwater Discharges

Discharge locations and volumes can be specified within Delft3D FLOW models. There were ten discharge points specified within the model which represented the main rivers and streams flowing into the southern basin of Tauranga Harbour. Figure 4.16 identifies the discharge locations on the model grid. Discharge events can be a one off discharge volumes specified during a specific time step within the simulation, or a continuous discharge with a constant or varying volume which are interpolated between time steps. Continuous constant discharge volumes for the ten freshwater input points were based on the average discharge of each river and stream (Table 4.7).

Table 4.7: Discharge volumes used for each of the freshwater inputs in the Delft3D FLOW model.

Freshwater input	**Discharge volume (m^3.s)**
Aongatete River	2.30
Wainui River	0.94
Apata Stream	0.21
Waipapa River	1.01
Te Puna Stream	0.69
Wairoa River	17.6
Kopurererua Stream	2.28
Waimapu River	3.34
Waitao Stream	1.03
Rocky Steam	1.09

4.8.2 Observation Points

Observation points are used in the Delft3D FLOW hydrodynamic model to monitor the water levels, velocities and other constituents over time at an exact location on the model grid (Deltares Systems, 2013). As the observation points record the flow at the same point over time, the points represent an Eulerian viewpoint (Deltares Systems, 2013). Ten observation points were specified in the model grid which are shown in Figure 4.16. To allow the southern basin model to be calibrated and verified against the measured data, the observation points represent the locations of the three ADVs, the S4 current meter, the Port of Tauranga ADCP and two tide gauges and the three BOPRC tide gauges.

CHAPTER FIVE

SOUTHERN BASIN MODEL: CALIBRATION AND VERIFICATION

5.1 Introduction

To have confidence in the predicted hydrodynamic impacts of the wharf extensions, the southern basin model needed to be calibrated and verified against measured field data. The first stage in improving the model outcomes was sensitivity analysis. Model parameters were adjusted to determine which had the greatest influence on the model outcomes and values were selected that produced hydrodynamic conditions closest to those measured. A spatially varying bed roughness map was developed as a result of the sensitivity analysis. Calibration and verification of the southern basin model was carried out using visual comparisons followed by statistical analysis of the model predictions against the measured field data. Statistical analysis provided confidence in the model outcomes and involved calculating the bias, accuracy and skill of the predictions.

5.2 Sensitivity Analysis

Sensitivity analysis was carried out before calibration and involves the assessment of modelling parameters to determine which variables had the greatest influence on the model (McKenzie, 2014). In previous studies involving the development of hydrodynamic models in Tauranga Harbour (Chapter Three), modelling parameters often selected for sensitivity analysis were bed roughness, eddy viscosity and drying and flooding depths. The same modelling parameters, also known as calibration parameters, were selected for sensitivity analysis of the southern basin model. Descriptions and recommended values of each calibration parameter were given in Section 4.8.4 Chapter Four

During sensitivity analysis of the southern basin model, multiple simulation runs were carried out with only one parameter being altered during each simulation. Four values for each calibration parameter were specified as constant values across the entire model grid in 12 separate simulation runs. The values used were either within the recommended range or calculated using the equations provided by Delft3D FLOW. Table 5.1 states the four constant values that were trialled for each calibration parameter. Values of bottom roughness and eddy viscosity are in the range recommended by Delft3D FLOW (McKenzie, 2014). Two threshold depths for the drying and flooding parameter were calculated from Equation 4.3 using two characteristic tidal amplitudes (*a*) for Tauranga Harbour, the spring tidal range of 1.78 m given in Table 4.3 and the tidal amplitude typically stated in literature of 2 m. The number of time steps in a tidal period (*N*) was 1470. The larger threshold depths were trialled as the depths calculated using Equation 4.3 from Delft3D FLOW gave depths that were significantly shallower than those used in previous models of Tauranga Harbour.

Table 5.1: Constant values specified for each calibration parameter during sensitivity analysis simulation runs.

Calibration Parameter	**Constant Value**
Bottom Roughness (Chézy $m^{-1/2}.s$)	65 (low friction) 55 45 35 (high friction)
Eddy Viscosity ($m^2.s$)	12 10 8 6
Drying and Flooding Threshold (m)	0.05 0.01 0.00855 (amplitude 2 m) 0.00760 (amplitude 1.78 m)

During sensitivity analysis it was found that eddy viscosity and the drying and flooding threshold depth both had limited influence on the modelling outcome. An eddy viscosity of 10 $m^2.s$ and a threshold depth of 0.05 m were the values selected for the southern basin model. However, the value of bottom roughness specified significantly influenced the model outcome, altering the modelled tidal phase and tidal amplitude at all of the observation points. The preferred bottom roughness value varied between each observation point. It was determined that to apply a constant Chézy value across the entire model domain would be inaccurate and considerably reduce the validity of the model outcomes.

5.2.1 Bottom Roughness Map

When applying a spatially varying bottom roughness map in a 2D depth averaged model, Delft3D FLOW recommends basing values on variations in elevation of the bathymetry. In the first application of a spatially varying bottom roughness map, initial estimates of Chézy values were based on Equation 4.2. Model outcomes were a poor fit and water levels and velocities were both over- and under-predicted. Four spatially varying bottom roughness maps were then created, with Chézy values similar to those used in previous hydrodynamic models of the southern basin and allocated to the different elevation ranges displayed in Table 5.2. From comparisons of both water levels and velocity at all observation points, option 3 was found to produce the best model outcomes over the majority of the sites. The final spatially varying bottom roughness map applied to the southern basin model is presented in Figure 5.1. The final model parameters used in the southern basin model are listed in Table 5.3.

Table 5.2: Spatially varying bottom roughness values based on the elevation of the bathymetry used to develop varying bottom roughness maps for model calibration. Note that a negative elevation is below MSL and an increase in water depth.

Chézy Value	**Elevation Range (m MSL)**			
($m^{-1/2}$.s)	**Option 1**	**Option 2**	**Option 3**	**Option 4**
65	-	-	< -5	< -7
55	< -5	< -2	-5 to -2	-7 to -3
45	-5 to -2	-2 to -1	-2 to -1	-3 to -1.5
35	-2 to 0.5	-1 to 1.5	-1 to 1.5	-1.5 to 1.5
7	0.5 to 5	1.5 to 7	1.5 to 7	1.5 to 7
1	> 7	> 7	> 7	> 7

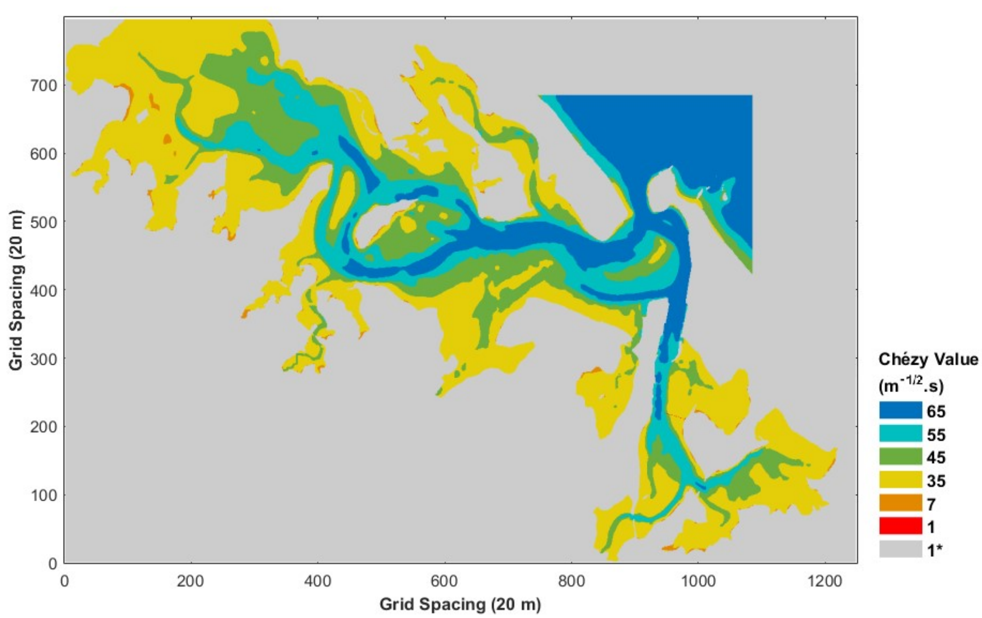

Figure 5.1: Spatially varying bottom roughness map based on elevation of the bathymetry and used in the southern basin model. In the key 1* indicates grid cells with no bathymetry which were given a Chézy value of 1.

Table 5.3: Final model parameters used in the Delft3D FLOW southern basin model.

Parameter	Value
Time Step Interval	0.5 min
Simulation Period	32 days (from 01/09/15 00:00:00)
Warm-up Period	3 days
Gravity	9.81 m.s^2
Water Density	1025 kg.m^3
Eddy Viscosity	10 m^2.s
Threshold Depth	0.05 m
Bottom Roughness Map	Option 3
Wind Conditions	No wind applied

5.3 Calibration

The calibration of a model provides confidence that the specified bathymetry, boundary forcing and initial conditions, will produce reliable predictions and represent the known hydrodynamic behaviour of the modelled area (Sutherland et al., 2004). During calibration, model predictions were compared against measured field data and statistical analyses were carried out to assess the bias, accuracy and skill between the datasets. Statistical analysis provides an objective assessment of the model and is essential for credibility when models are developed for an engineering application (Sutherland et al., 2004). Two four day periods were selected for calibration within the field deployment period. Figure 5.2 shows the two calibration periods, a neap and a spring tide, used to calibrate the southern basin model. The periods were selected to represent the minimum and maximum water levels within the southern basin.

Figure 5.3 and Figure 5.4 display the water level, current speed and U and V velocity plots between the model predictions and the measured field data at the three ADVs and S4 current meter during the neap and spring calibration periods respectively. Visual comparisons of the neap calibration plots indicate that the model was a good fit in terms of water levels at all four observation points, with the worst fit being at the ADV Hairini site.

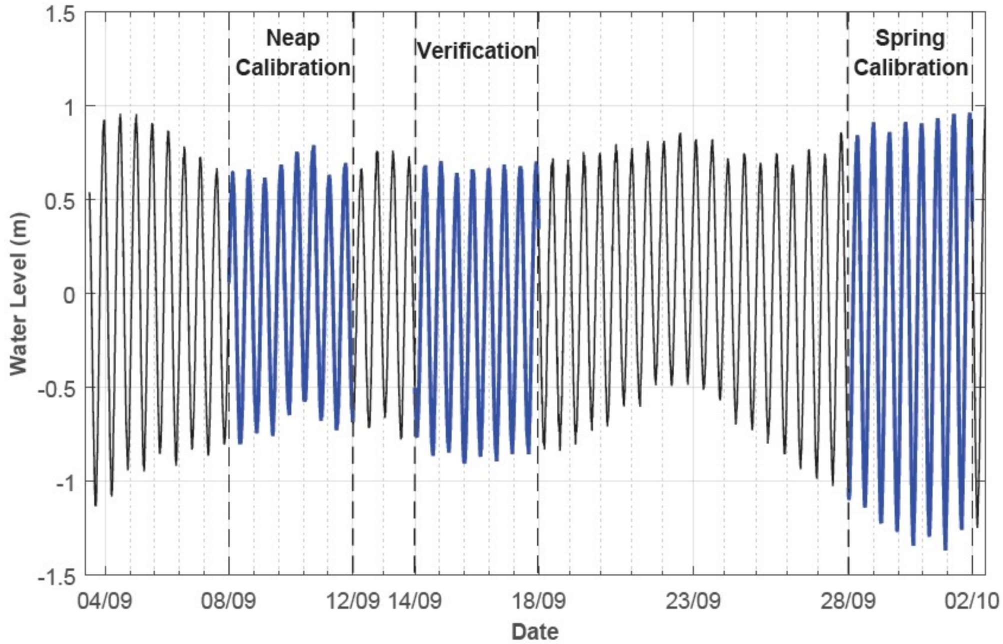

Figure 5.2: Four day periods selected for calibration of a neap and spring tide and verification of an average tide during the field deployment period from the 3rd September to 2nd October 2015. Water levels displayed are those recorded by the S4 current meter at Marker 21.

The predicted current speeds at ADV Hairini and S4 Marker 21 were similar to measured current speeds in both magnitude and timing, although the model failed to predict the higher current speeds on the ebb tide at Marker 21. At ADV Maungatapu the tidal asymmetry (ebb dominance) evident from measurements at the site was not modelled and current speeds were over-predicted on the flood tide by approximately 0.2 $m.s^{-1}$. The opposite occurred at ADV Railway where the model predicted well for the flood tide but over-predicted current speeds on the ebb tide; the measured ebb and flood current speeds were of the same magnitude. At all observation points either the U or V velocities were well predicted, the less dominant current direction was not predicted within the model.

Spring calibration plots in Figure 5.4 show similar patterns to those in the neap calibration plots, but the size of the error between the modelled and measured increased. During the spring calibration period, ADV Railway measured current speeds and velocities were erratic and followed no clear pattern. As the errors were only evident during one period of the dataset, the ADV measurements were most likely affected by seaweed or debris (that were in high abundance during the deployment period) that became tangled around the probe head.

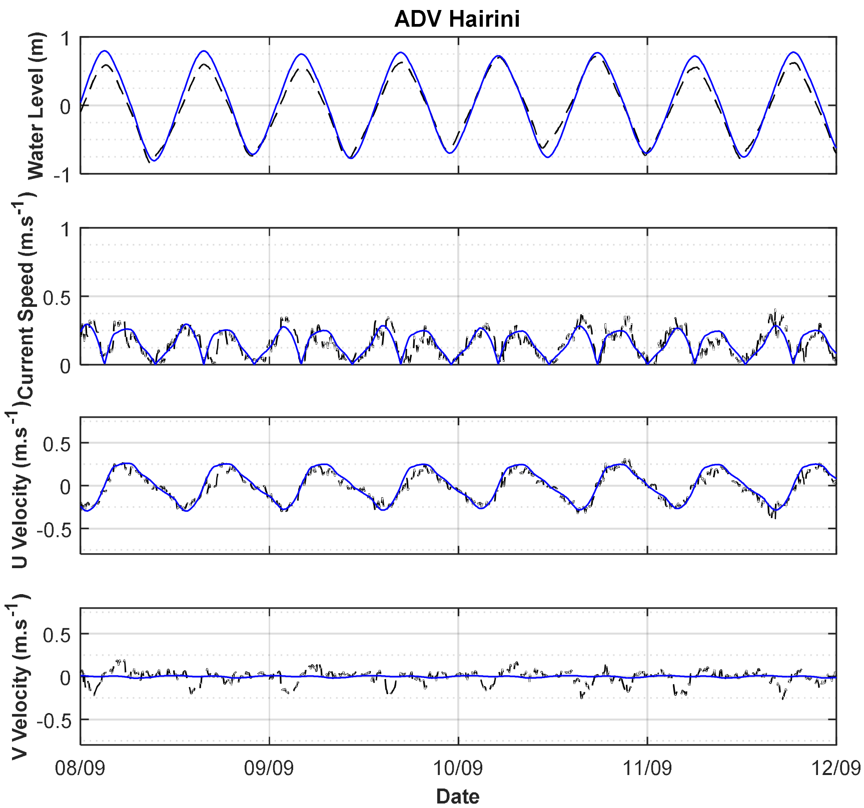
ADV Hairini
Water Level (m)
Current Speed (m.s^{-1})
U Velocity (m.s^{-1})
V Velocity (m.s^{-1})
08/09
09/09
10/09
11/09
12/09
Date

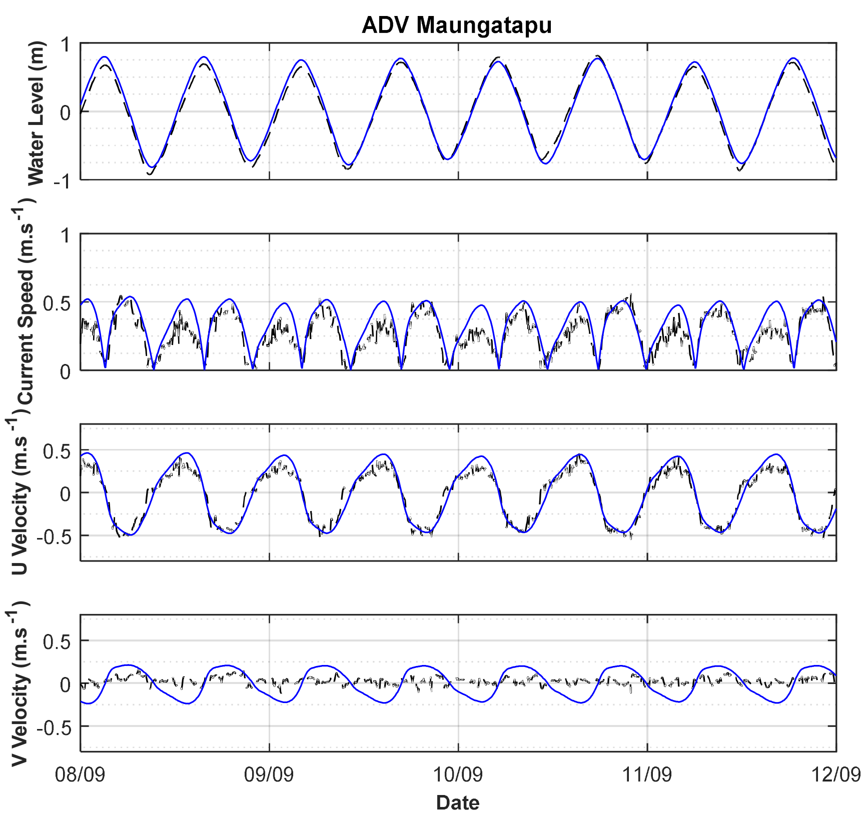
ADV Maungatapu
Water Level (m)
Current Speed (m.s^{-1})
U Velocity (m.s^{-1})
V Velocity (m.s^{-1})
08/09
09/09
10/09
11/09
12/09
Date

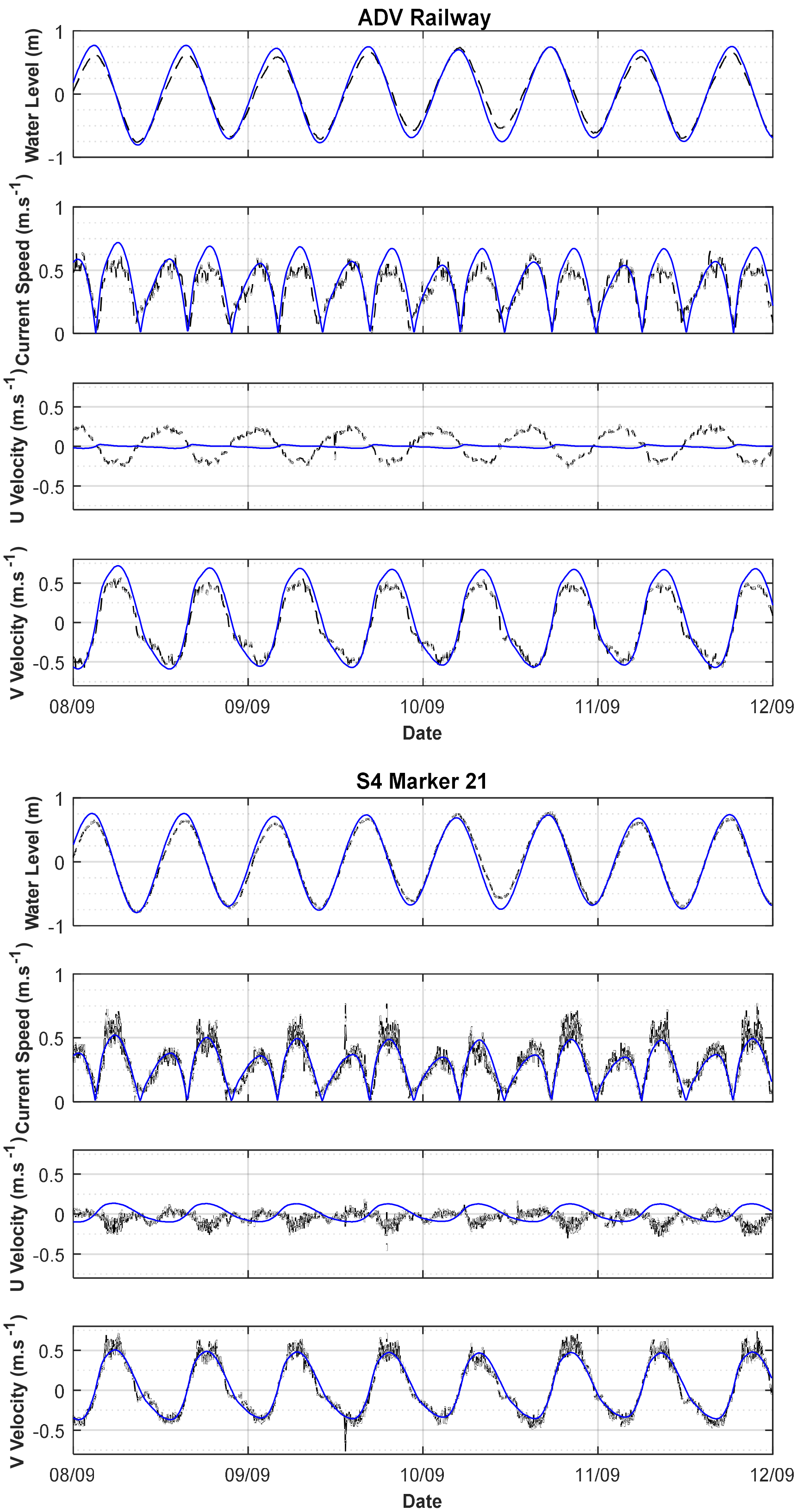

Figure 5.3: Neap calibration plots of measured (black dashed line) and modelled (solid blue line) water levels, current speeds, U velocities (east) and V velocities (north) from the 8th to the 12th September 2015 at ADV Hairini (A), ADV Maungatapu (B), ADV Railway (C) and the S4 at Marker 21 (D).

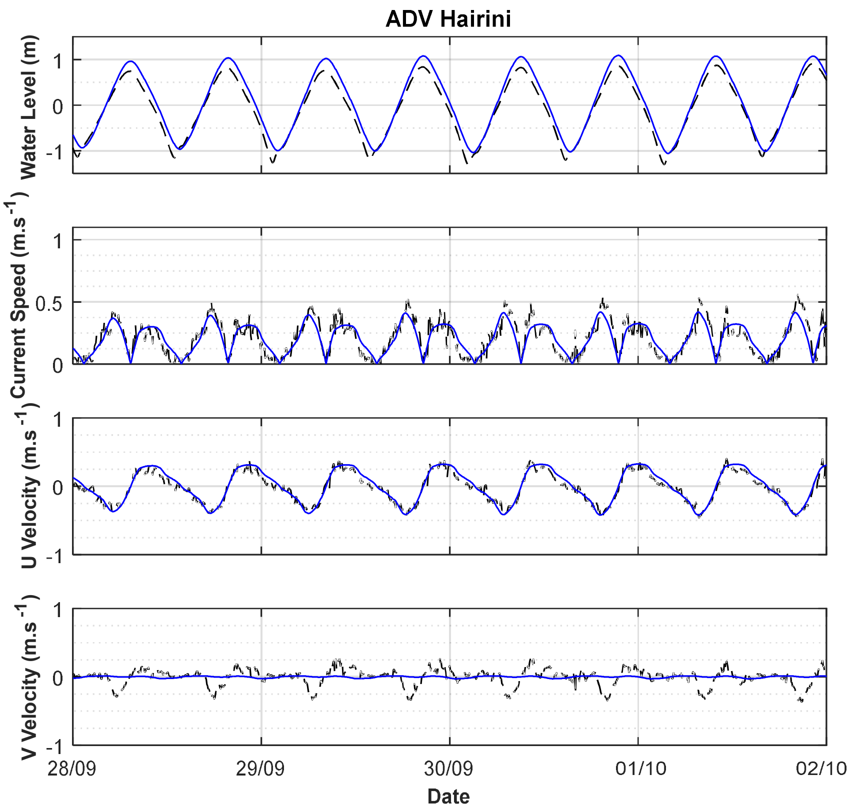
ADV Hairini
Water Level (m)
Current Speed (m.s-1)
U Velocity (m.s-1)
V Velocity (m.s-1)
28/09
29/09
30/09
01/10
02/10
Date

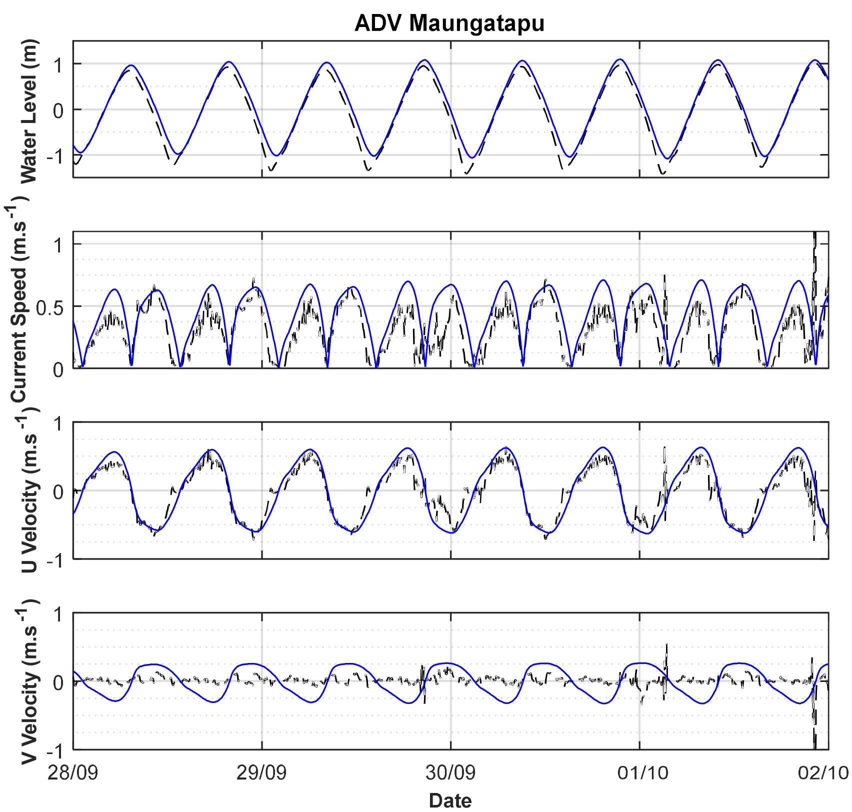
ADV Maungatapu
Water Level (m)
Current Speed (m.s-1)
U Velocity (m.s-1)
V Velocity (m.s-1)
28/09
29/09
30/09
01/10
02/10
Date

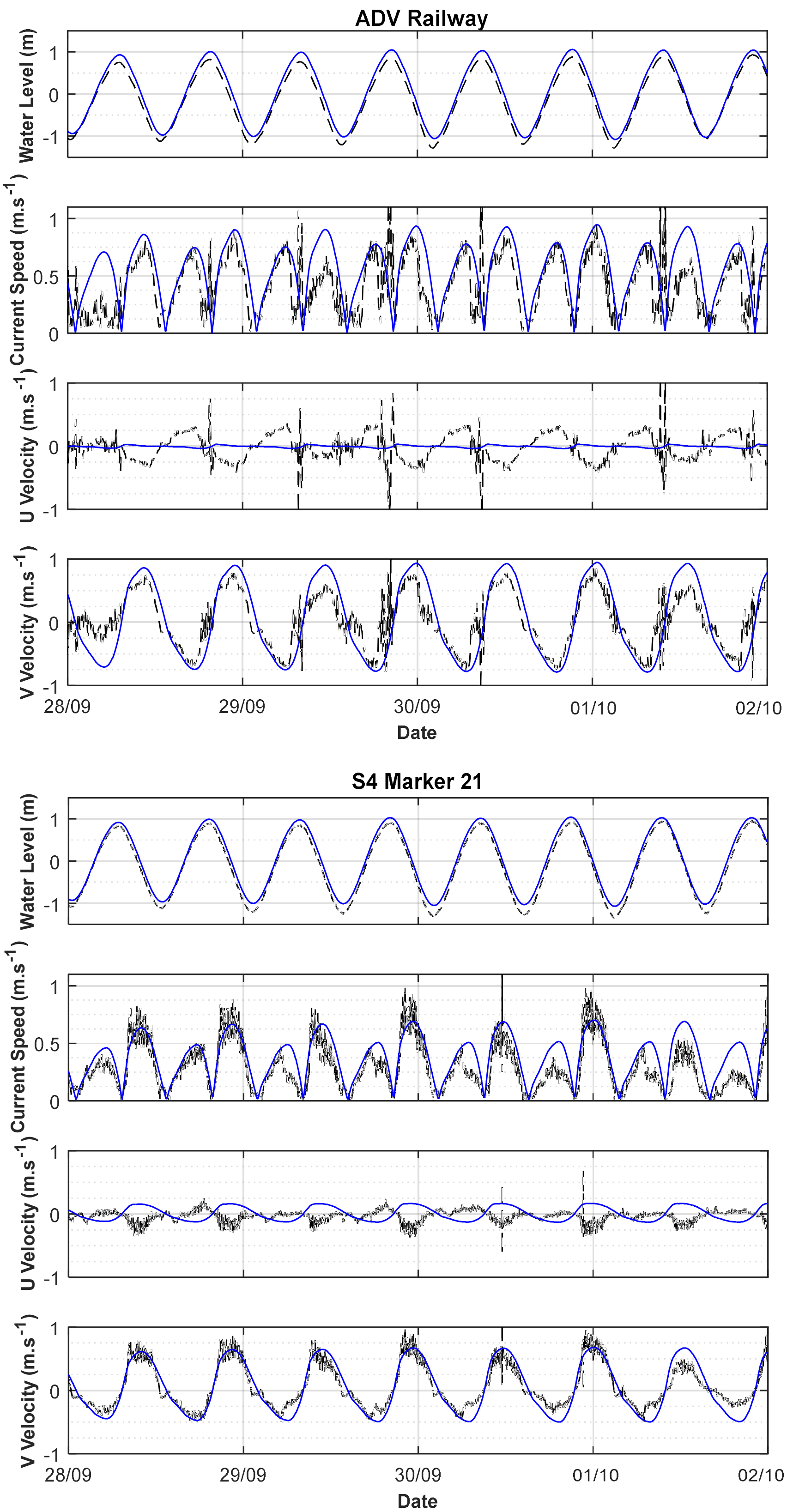

Figure 5.4: Spring calibration plots of measured (black dashed line) and modelled (solid blue line) water levels, current speeds, U velocities (east) and V velocities (north) from the 28th September to the 2nd October 2015 at ADV Hairini (A), ADV Maungatapu (B), ADV Railway (C) and the S4 at Marker 21 (D).

5.3.1 Statistical Analysis

Calculations of statistics for bias, accuracy and skill were used to objectively assess the southern basin model predictions. Differences in the central tendencies between the model predictions and measured field data is a measure of the bias or reliability of the model. Bias can be calculated using the central tendency of the mean or median. The bias in the mean was selected for this analysis, and bias_a of the model predictions calculated from Equation 5.1 (Sutherland et al., 2004).

$$Bias_a = \frac{1}{J}\sum_{j=1}^{J}(y_j - x_j) = \langle Y \rangle - \langle X \rangle \qquad 5.1$$

Where Y is a set of y_j model predictions and X is of a set of x_j observations (measured field data). The total number of values in the datasets is J. The angular brackets or chevrons specify that the mean of each dataset should be calculated.

Accuracy represents the average size of the average error by measuring the differences between the model predictions and measured field data (Sutherland et al., 2004). MAE and RMSE are two measures of accuracy that are commonly used to evaluate model performance (Equation 5.2 and Equation 5.3) (Sutherland et al., 2004).

$$MAE(Y, X) = \frac{1}{J}\sum_{j=1}^{J}(y_j - x_j) = \langle |Y - X| \rangle \qquad 5.2$$

$$RMSE(Y, X) = \sqrt{\frac{1}{J}\sum_{j-1}^{J}(y_j - x_j)^2} = \sqrt{\langle (Y - X)^2 \rangle} \qquad 5.3$$

MAE takes the absolute value of the errors before averaging, specified by the straight brackets. The main difference between the accuracy measures is that the RMSE squares the differences, increasing the influence of any outliers in the model datasets, making the RMSE the more conservative measure (Sutherland et al., 2004). MAE can be used on both vector and scalar datasets so is often used to assess the performance of hydrodynamic models. Both MAE and RMSE have the same scale and units as the model predictions and measured field data (Sutherland et al., 2004).

Skill is the final method for evaluating a models performance and compares a measure of accuracy of the model predictions against the accuracy of a baseline prediction (Sutherland et al., 2004). The baseline predictions (B) used in this study were the average values of the measured field datasets. The Brier Skill Score (BSS) is commonly used to evaluate the performance of hydrodynamic models (Equation 5.4) (Sutherland et al., 2004).

$$BSS = 1 - \frac{MSE(Y,X)}{MSE(B,X)} = 1 - \frac{\langle (Y-X)^2 \rangle}{\langle (B-X)^2 \rangle} \qquad 5.4$$

A BSS of 1 implies a perfect agreement between the model predictions and the field measurements in terms of the baseline predictions (Sutherland et al., 2004). Sutherland et al. (2004) proposed a classification scheme to interpret the BSS and assess the confidence of the model outcomes; the qualitative scale is presented in Table 5.4.

Table 5.4: Classification scheme for Brier Skill Score (BSS) proposed by Sutherland et al. (2004).

Classification	**BSS**
Excellent	1.0 - 0.5
Good	0.5 - 0.2
Reasonable/Fair	0.2 - 0.1
Poor	0.1 - 0.0
Bad	< 0.0

The BSS can be broken down to determine how much of the error was due to errors in the phase (α), amplitude (β) and average initial conditions (map mean, γ) (Sutherland et al., 2004). Equations 5.6 to 5.8 are used to identify which components have the largest contribution to the error in BSS and indicate areas where improvements can be made (Sutherland et al., 2004).

$$r_{Y'X'} = \frac{\langle Y'X' \rangle}{\sigma_{Y'}\sigma_{X'}} \qquad 5.5$$

$$\alpha = r^2{}_{Y'X'} \qquad 5.6$$

$$\beta = \left(r_{Y'X'} - \frac{\sigma_{Y'}}{\sigma_{X'}} \right)^2 \qquad 5.7$$

$$\gamma = \left(\frac{\langle Y' \rangle - \langle X' \rangle}{\sigma_{X'}}\right)^2 \qquad 5.8$$

Equation 5.5 ($r_{Y'X'}$) is the correlation coefficient between Y' and X', which are the anomalies in datasets Y and X, calculated by the dataset minus the baseline (in this case the mean of the same dataset) (Sutherland et al., 2004). $\sigma_{Y'}$ and $\sigma_{X'}$ are the standard deviations of the predicted and observed datasets respectively. Perfect modelling of the phase gives α of 1, while perfect modelling of the amplitude and map mean gives β and γ of 0 (Sutherland et al., 2004).

Table 5.5 presents the statistical analysis results of the water levels at the nine observation points during the neap calibration period. A slight bias was present at all observation points. Water levels were over-predicted at the three ADVs, the S4 current meter at Marker 21 and Sulphur Point, indicated by a positive bias. Tug Berth, Hairini, Oruamatua and Omokoroa tide gauges all under-predicted the water levels. MAE during the neap calibration period was < 0.1 m for all observation points except at Hairini tide gauge, which had an error of 0.13 m. As expected, the RMSE were higher than the MAE at all of the observation points due to the presence of outliers in the datasets. During the neap calibration period the BSS for the water levels at all of the observation points were above 0.9 which is deemed as 'excellent' by the Sutherland et al. (2004) classification scheme. From Table 5.6 the contribution of the errors in phase, amplitude and map mean to the BSS error in water levels at the four main observation points during the neap calibration period are given. The errors in phase and amplitude were all < 0.03. Map mean errors over the neap calibration period were small at all observation points. The largest contribution to the error was from differences in the phase.

Statistical analysis of the spring calibration period in Table 5.7 showed larger bias, MAE and RMSE during the spring calibration period than during the neap calibration period at all of the observation points except the Hairini and Omokoroa tide gauges which had smaller errors. All of the observation points except for Hairini over-predicted the water levels. The largest errors in accuracy were at ADV Hairini which had an MAE and RMSE of 0.16 m and 0.185 m respectively. The spring calibration period still displayed an 'excellent' BSS at all observation points.

Table 5.8 shows the largest source of error in the BSS was from errors in phase and map mean. As in the neap calibration period, the largest error in phase of 0.025 occurred at ADV Hairini. The error in phase increased with distance into the upper harbour.

Table 5.5: Neap tide calibration of water levels

Observation Point	**Bias$_a$ (m)**	**MAE (m)**	**RMSE (m)**	**BSS**
ADV Hairini	0.057	0.095	0.114	0.933
ADV Maungatapu	0.041	0.069	0.078	0.976
ADV Railway	0.004	0.079	0.096	0.954
S4 Marker 21	0.005	0.065	0.081	0.970
Sulphur Point	0.018	0.056	0.069	0.979
Tug Berth	-0.023	0.063	0.076	0.975
Hairini	-0.127	0.127	0.142	0.915
Oruamatua	-0.057	0.065	0.084	0.972
Omokoroa	-0.089	0.090	0.105	0.954

Table 5.6: Error in water levels from BSS during neap calibration

Observation Point	**Phase**	**Amplitude**	**Map Mean**
ADV Hairini	0.974	0.026	0.017
ADV Maungatapu	0.982	0.0006	0.007
ADV Railway	0.976	0.024	0.00008
S4 Marker 21	0.980	0.010	0.0001

Table 5.7: Spring tide calibration of water levels

Observation Point	**Bias$_a$ (m)**	**MAE (m)**	**RMSE (m)**	**BSS**
ADV Hairini	0.149	0.160	0.185	0.919
ADV Maungatapu	0.146	0.147	0.184	0.938
ADV Railway	0.156	0.156	0.169	0.942
S4 Marker 21	0.138	0.138	0.147	0.961
Sulphur Point	0.129	0.129	0.138	0.964
Tug Berth	0.091	0.093	0.101	0.980
Hairini	-0.045	0.083	0.110	0.975
Oruamatua	0.059	0.094	0.136	0.966
Omokoroa	0.003	0.037	0.050	0.995

Table 5.8: Error in water levels from BSS during spring calibration

Observation Point	Phase	Amplitude	Map Mean
ADV Hairini	0.975	0.006	0.053
ADV Maungatapu	0.976	0.001	0.039
ADV Railway	0.990	0.001	0.052
S4 Marker 21	0.996	0.0008	0.036

5.4 Verification

Verification of the calibrated model compares the model predictions against another dataset not used in the calibration to provide further confidence in the model predictions. A dataset containing a four day period over an average tide during the field deployment period was selected for verification (Figure 5.2). Comparisons of water levels, current speeds, U and V velocities during the verification period are shown in Figure 5.5. From a visual assessment, water levels at all of the observation points were accurately predicted. There was a slight phase lag with the measured field data at ADV Hairini and ADV Maungatapu, which were both in the upper harbour. There was minimal phase lag at the other two observation points, with the best agreement in water levels at ADV Railway.

As with the neap and spring calibration periods, the largest discrepancies are from differences in current speeds. Current speeds at ADV Hairini were in good agreement, but over-predicted on the ebb tide at ADV Railway and on the flood tide at ADV Maungatapu. The model predicted the ebb dominance at Marker 21 in Stella Passage but under-predicted the current speeds, especially during the dominant ebb tides. At all four observation points either the modelled U velocities or V velocities showed good agreement with the measured field data. Variations in the measured hydrodynamic conditions at the end of the verification period may have been due to the influence of the Chilean earthquake on the 17th of October when a tsunami warning was issued in New Zealand and a small tsunami was observed.

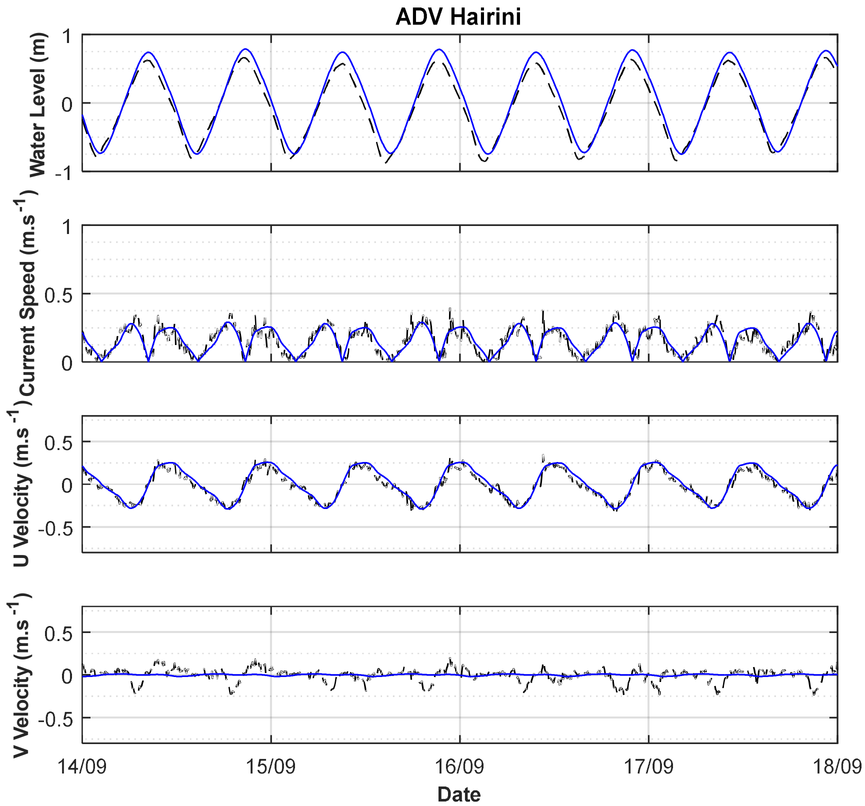
ADV Hairini
Water Level (m)
Current Speed (m.s-1)
U Velocity (m.s-1)
V Velocity (m.s-1)
14/09
15/09
16/09
17/09
18/09
Date

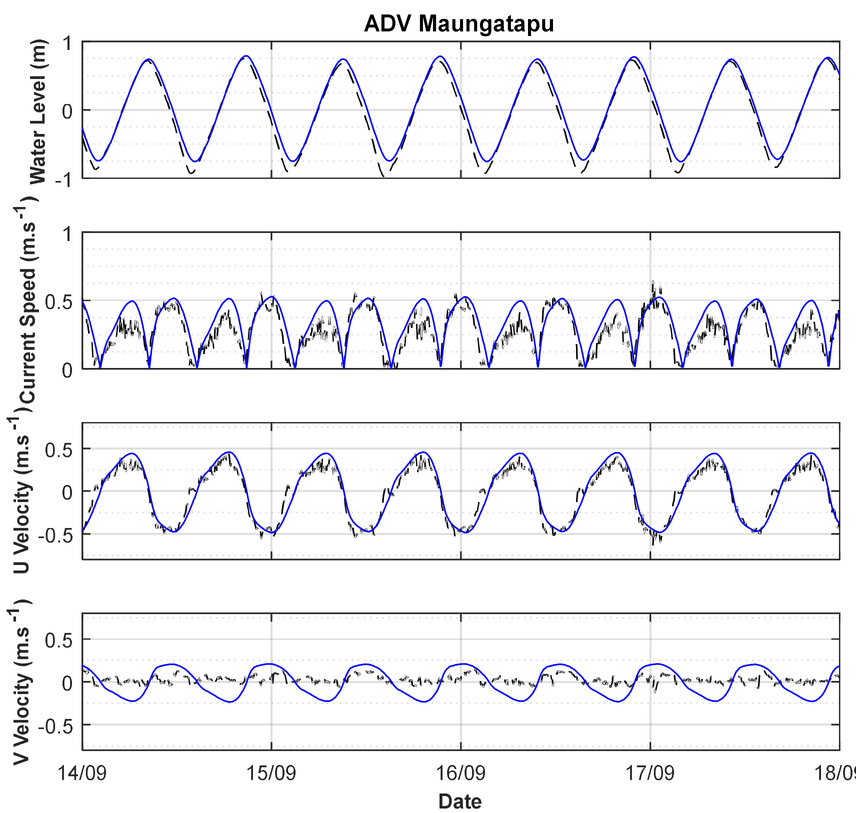
ADV Maungatapu
Water Level (m)
Current Speed (m.s-1)
U Velocity (m.s-1)
V Velocity (m.s-1)
14/09
15/09
16/09
17/09
18/09
Date

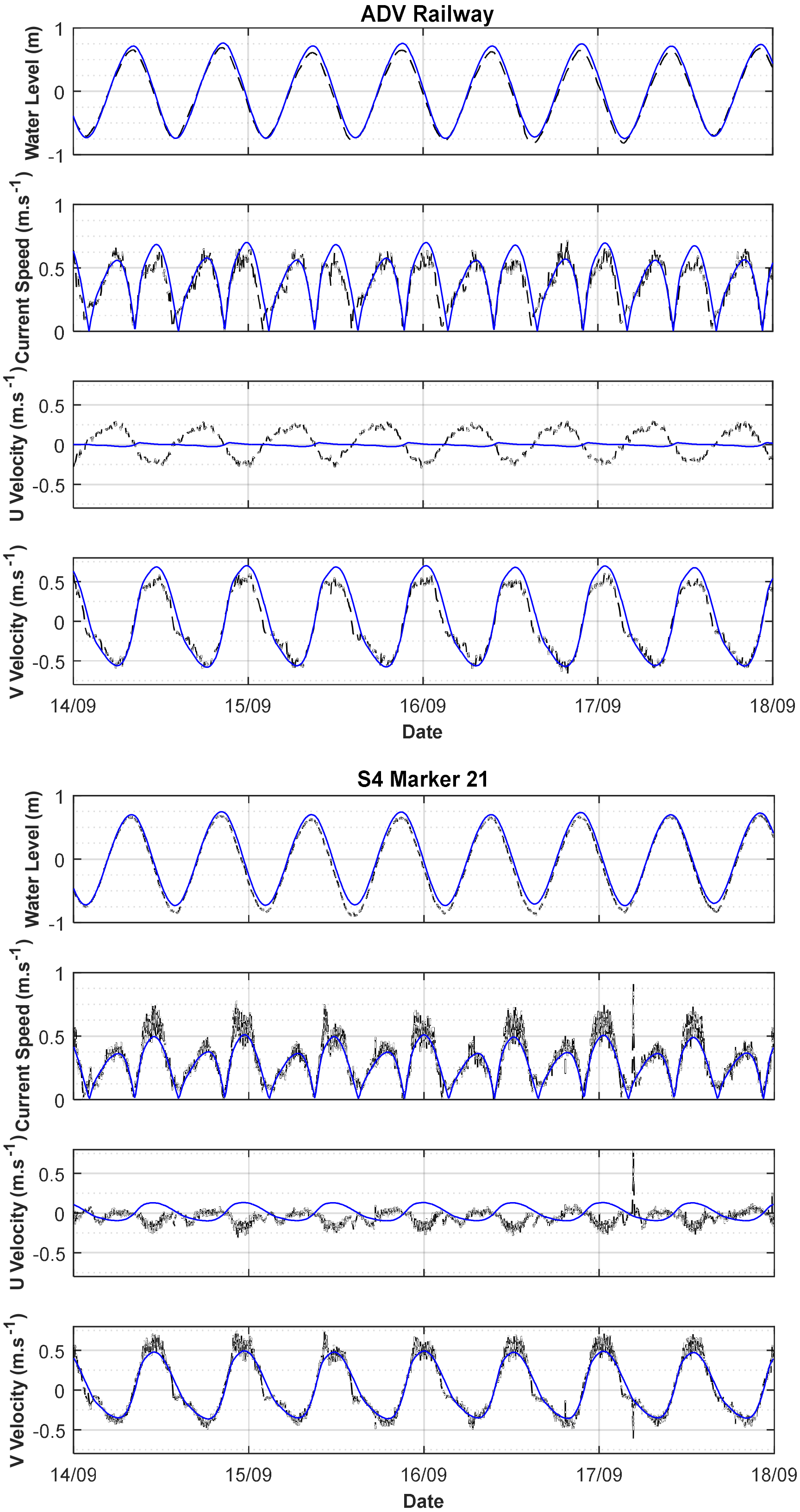

Figure 5.5: Verification plots of measured (black dashed line) and modelled (solid blue line) water levels, current speeds, U velocities (east) and V velocities (north) from the 14th to the 18th September 2015 at ADV Hairini (A), ADV Maungatapu (B), ADV Railway (C) and the S4 at Marker 21 (D).

5.4.1 Statistical Analysis

Verification by way of statistical analysis of water levels at the nine observation points in Table 5.9 shows the model displayed a high level of accuracy and skill. MAE was below 0.095 m at all observation points, apart from ADV Hairini which was over-predicted, but only by an MAE of 0.1 m. Modelled water levels at the three BOPRC tide gauges were under-predicted. An ‘excellent’ skill score was given to all of the observation sites according to Table 5.4. Phase and map mean were again identified as the main sources of error within the BSS in Table 5.10 rather than amplitude. With perfect modelling of phase having a value of 1, the phase of the water level at ADV Hairini had an error of 0.025. The southern basin model displayed ‘excellent’ skill levels and therefore, there is confidence in the predictions of the hydrodynamic conditions in Stella Passage and the upper harbour.

Table 5.9: Verification of water levels

Observation Point	$Bias_a$ (m)	MAE (m)	RMSE (m)	BSS
ADV Hairini	0.088	0.104	0.120	0.936
ADV Maungatapu	0.082	0.085	0.112	0.958
ADV Railway	0.053	0.062	0.072	0.978
S4 Marker 21	0.075	0.075	0.086	0.974
Sulphur Point	0.073	0.073	0.080	0.977
Tug Berth	0.034	0.036	0.044	0.993
Hairini	-0.081	0.095	0.108	0.958
Oruamatua	-0.016	0.063	0.073	0.982
Omokoroa	-0.044	0.050	0.056	0.989

Table 5.10: Error in water levels from BSS during verification period

Observation Point	Phase	Amplitude	Map Mean
ADV Hairini	0.976	0.008	0.034
ADV Maungatapu	0.981	0.002	0.023
ADV Railway	0.992	0.004	0.012
S4 Marker 21	0.994	0.0005	0.021

5.5 Sources of Error

Hydrodynamic systems are complex and there are a number of factors that may be contributing to error in a model. Overall the southern basin model was able to predict the hydrodynamic conditions during a neap tide with greater accuracy and skill than during a spring tide. Larger errors, especially in the upper harbour, during the spring calibration period may have been due to the shallow water tidal constituents not being accurately predicted as the constituents were not included in the boundary forcing. Although shallow water constituents only have a small contribution to the overall water level, when combined the constituents may account for the difference in error between the spring and neap calibration periods. Inclusion of shallow water constituents in the initial harmonic analysis and boundary forcing would increase the accuracy of predictions during a spring tide. McKenzie (2014) attributed errors in his calibrated hydrodynamic model to errors in harmonic analysis and bathymetry.

The initial bathymetry can significantly contribute to error within the model. Predictions within the upper harbour at ADV Hairini, ADV Maungatapu, ADV Railway and Hairini observation points had some of the largest errors in both the verification and calibration periods. Bathymetry in the upper harbour was heavily modified as the LINZ hydrological charts used for the initial bathymetry of the area were too conservative. The bathymetry in the upper harbour was lowered to better represent the measured depths at the observation points. Channels under the Hairini and Maungatapu Bridges were lowered as well as the channel approaches, changing the storage in the upper harbour estuaries and bays. A change in storage in the upper harbour would modify the current speeds, tidal asymmetry and phase of the tidal wave. However the modelled outcomes using the modified bathymetry gave more realistic predictions than those using the LINZ chart bathymetry. Another modification to the bathymetry was the addition of the causeway approach to the Railway Bridge which may also have contributed to errors at ADV Railway due to the reduced number of grid points across the channel.

During calibration, bottom roughness was identified as an influencing factor on model outcomes. Cea & French (2012) compared the importance of errors due to bathymetry and errors caused by bed friction during the calibration of a hydrodynamic model. It was determined that in shallow estuarine models with extensive intertidal areas, bathymetry had a stronger influence than changes to bed friction. Cea & French (2012) determined that bed friction, while being an important parameter for calibrating water levels, did not significantly affect current velocities. Whereas only small changes in initial bathymetry, especially in low intertidal zones, significantly altered the modelled current velocity (Cea & French, 2012).

In Section 4.6 Chapter Four the variations in air pressure and wind over the field deployment period were considered. Differences in air pressure shown in Figure 4.14 indicated a potential 36 cm variation in water levels across the simulation period. The largest difference in air pressure was over the neap calibration period shown in Figure 5.6. Air pressures were above average during the entire spring calibration period, with a maximum of almost 1034 hPa which may have contributed to the higher measured water levels during the spring calibration period.

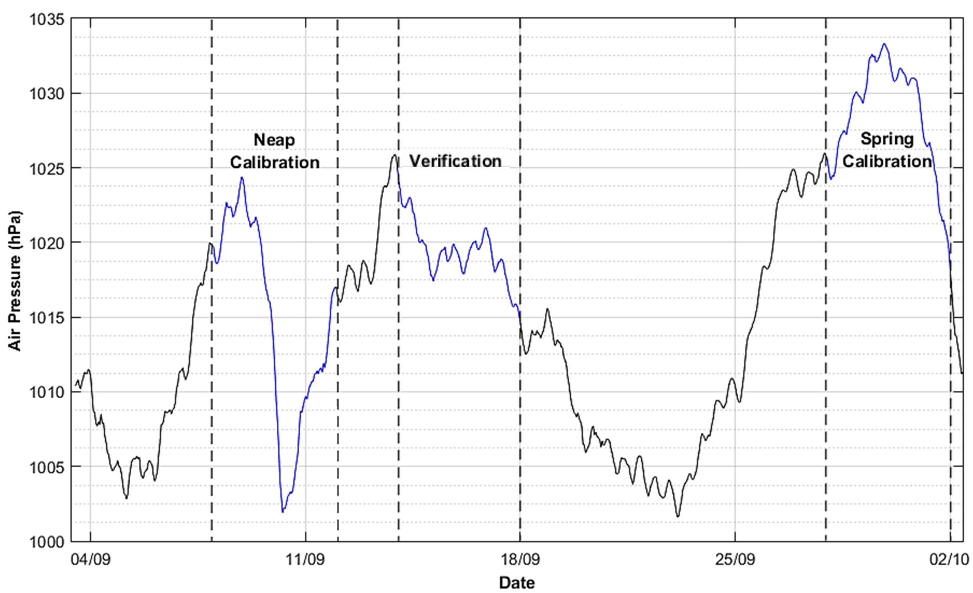

Figure 5.6: Difference in air pressure at MSL over the neap calibration, spring calibration and verification periods where 1015 hPa was the average air pressure over the field deployment period.

Variations in wind speed and direction over the field deployment period (Figure 4.15) could have also contributed to the fluctuations in tidal amplitude, seen in the measured field data. Wind direction in the upper harbour will either reduce or increase water levels by the creation or suppression of wind waves. Air pressure, wind and waves were not considered in the southern basin model as the inclusion would have greatly increased the computation time and have been found to have negligible effects on the overall accuracy of the predictions in previous models of Tauranga Harbour (McKenzie, 2014).

Instrument error will also factor into the model errors. Errors in measurements of current speeds and U and V velocities recorded by the S4 current meter can be seen at the end of the spring calibration period in Figure 5.4. Instrument errors like those in the above mentioned period were usually outliers in the datasets and taking the MAE rather than RMSE can reduce the effects of the instrument errors. Larger errors caused by instrument malfunction were recorded by the ADV at the Railway Bridge, where large variations in current speed and U and V velocities were measured during the spring calibration period in Figure 5.4. As noted previously, the likely cause of the errors was from seaweed or debris covering the probe head as the pressure measurements were not affected. As mentioned earlier, there may have also been impacts from the tsunami around the 17th and 18th of September.

CHAPTER SIX

HYDRODYNAMICS OF STELLA PASSAGE AND THE UPPER HARBOUR

6.1 Introduction

The southern basin model was used to simulate the hydrodynamic conditions within the study area, comparing spring and neap tides over the simulation period. As there are other extensive numerical models that simulate the hydrodynamics in the lower southern basin of Tauranga Harbour as summarised in Chapter Three, only a brief overview of the modelled hydrodynamics in the lower harbour is given. This chapter concentrates on describing and discussing the hydrodynamics within Stella Passage, Town Reach and the upper harbour. Residual velocity vectors and threshold velocities were used to identify the net flow and the potential sediment transport pathways within the model. Model predictions were later used as a baseline to assess any potential impacts from simulated alterations to the harbour.

6.2 Results

In this section an overview of the general hydrodynamics in the southern basin is given, followed by model predictions over the entire area of interest from Stella Passage to the upper harbour. Zoomed in plots are used to describe the model results in Stella Passage, Town Reach, and the upper harbour. Finally, plots of residual velocity vectors averaged over 29 days of the simulation are presented.

6.2.1 The Southern Basin

Water levels and current speeds over the entire model domain during a simulated neap and spring tide are displayed in Figure 6.1 to Figure 6.4. Peak ebb water levels (low tide) in the two hour plots were at 11:00:00 during the neap tide (Figure 6.1) and 03:00:00 during the spring tide (Figure 6.2). In plots of water levels, the grey areas are the inactive grid cells which were above MSL and represent the land and the exposed intertidal flats.

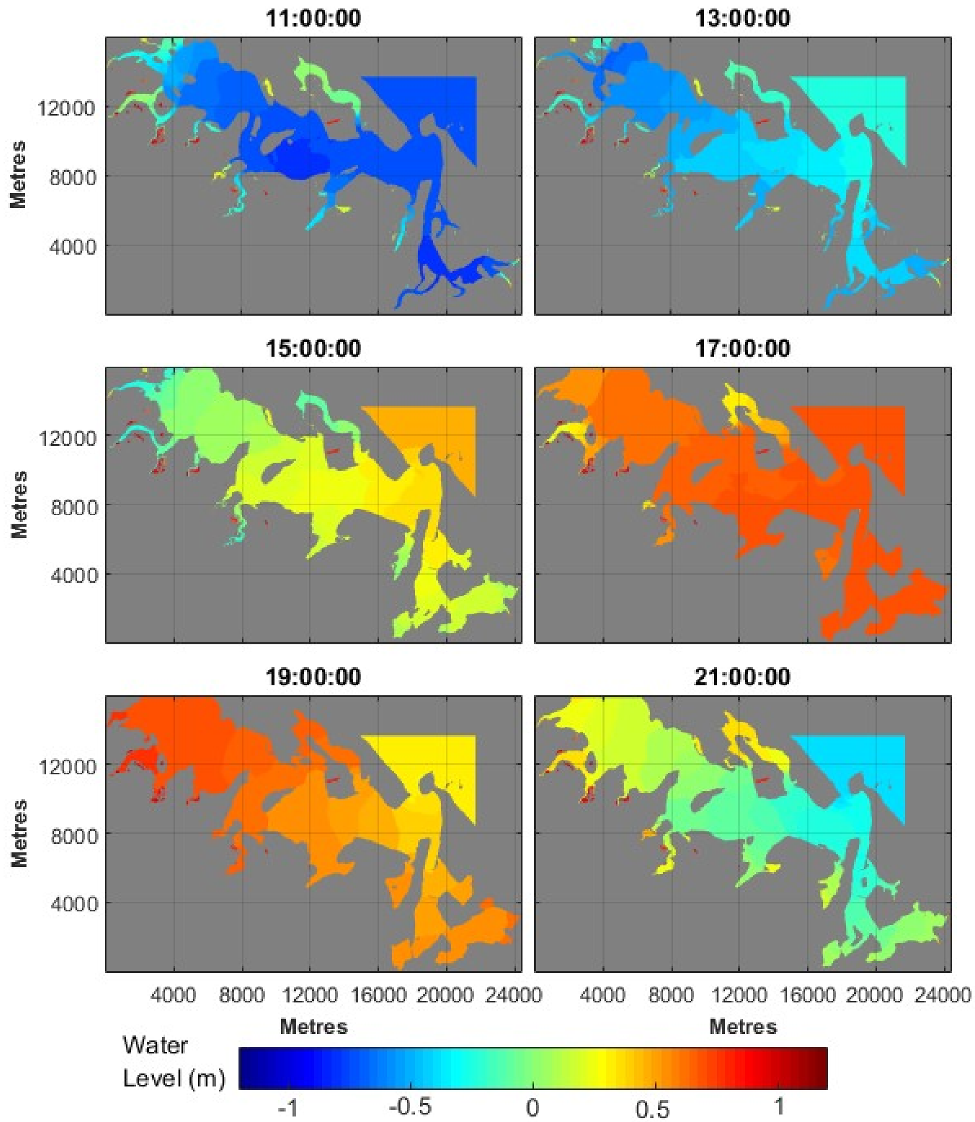

Figure 6.1: Instantaneous water levels at two hour intervals from simulations of a neap tide on the 10th September 2015 in the southern basin of Tauranga Harbour.

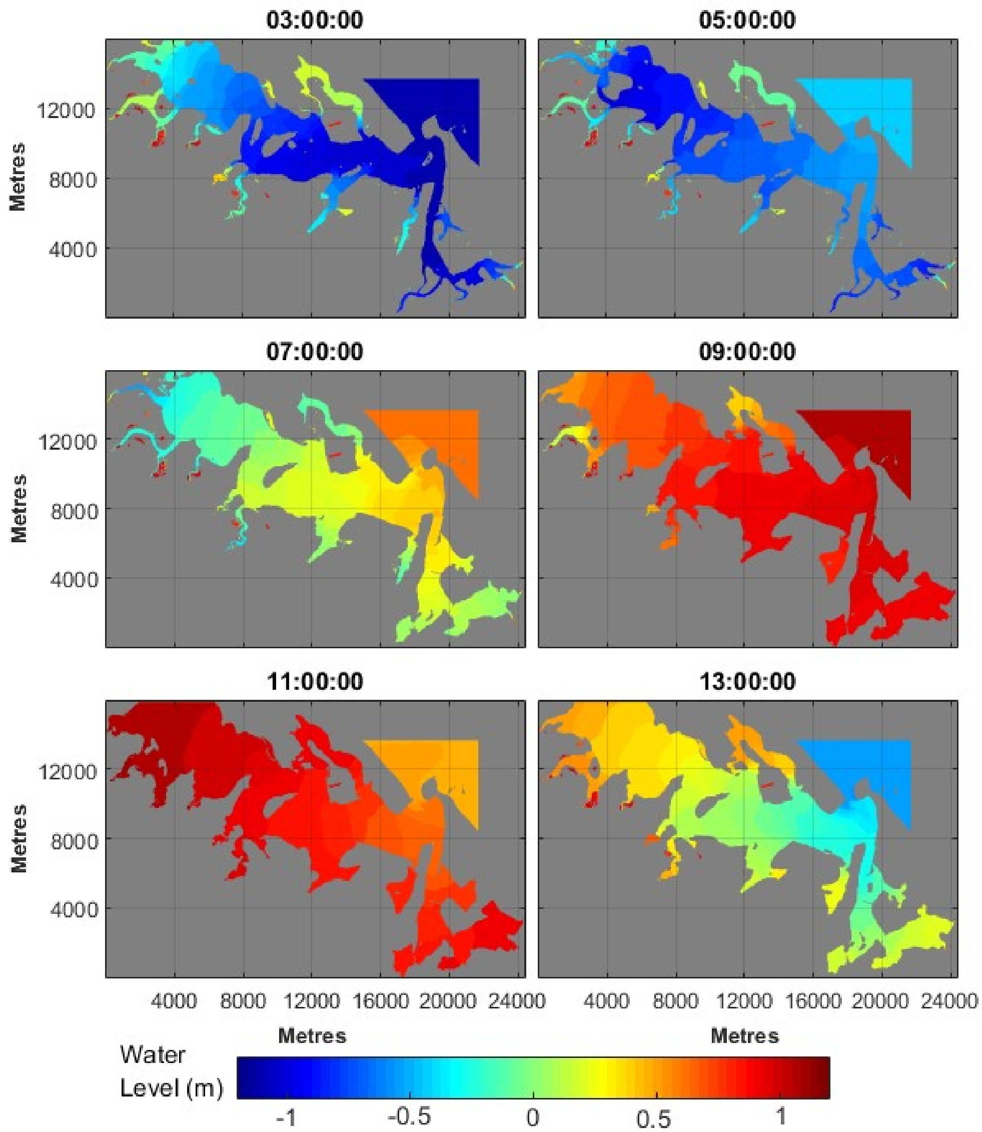

Figure 6.2: Instantaneous water levels at two hour intervals from simulations of a spring tide on the 1st October 2015 in the southern basin of Tauranga Harbour.

In both tidal simulations there was a phase lag in water levels from the Entrance Channel to the north-eastern reaches of the southern basin towards Omokoroa. The lowest water levels in the north-eastern region of the southern basin were two hours after the lowest water levels in the Entrance Channel. The largest differences in water levels over a short distance were through the constricted channel entrances such as the Entrance Channel and the entrance to Waikareao Estuary. In the southern basin model, apart from water levels increasing during a spring tide, there was little change to the overall patterns in water level over the tidal cycle. Maximum current speeds over a two hour period during a neap (Figure 6.3) and spring tide (Figure 6.4) occur in the main channels before high and low tides. Current speeds over the entire model domain were lowest when peak ebb and flood water levels were predicted (Figure 6.1 and Figure 6.2). During a neap tide, current speeds were above 1 $m.s^{-1}$ in the Entrance Channel and the Western Channel but below 1 $m.s^{-1}$ within Stella Passage and the upper harbour. Similar patterns in current speeds were simulated for a spring tide but there was an increase in magnitude. Current speeds reached above 1 $m.s^{-1}$ within Town Reach at peak ebb and flood tide on a spring tide, but were still below 0.5 $m.s^{-1}$ in the intertidal areas of the upper harbour.

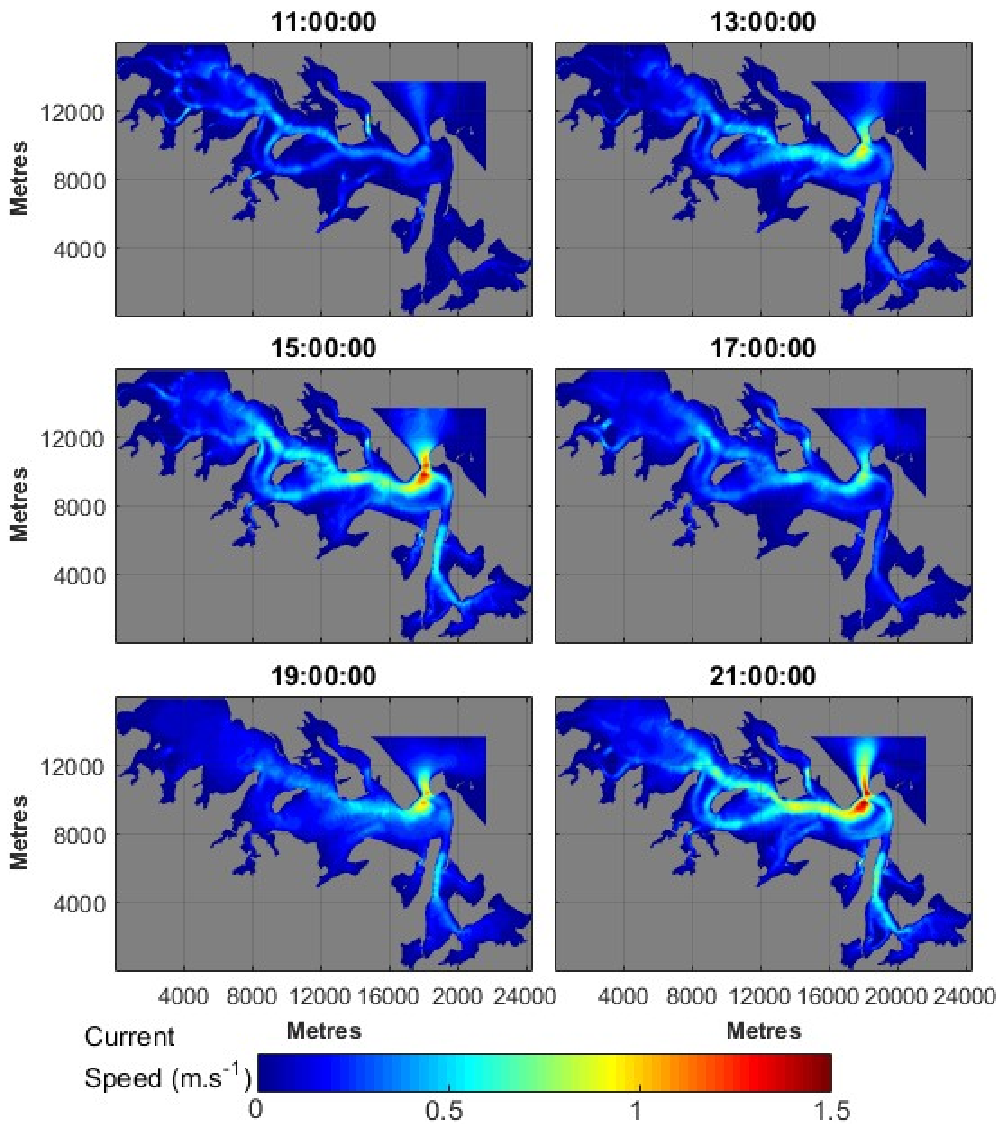

Figure 6.3: Instantaneous current speeds at two hour intervals from simulations of a neap tide on the 10th September 2015 in the southern basin of Tauranga Harbour.

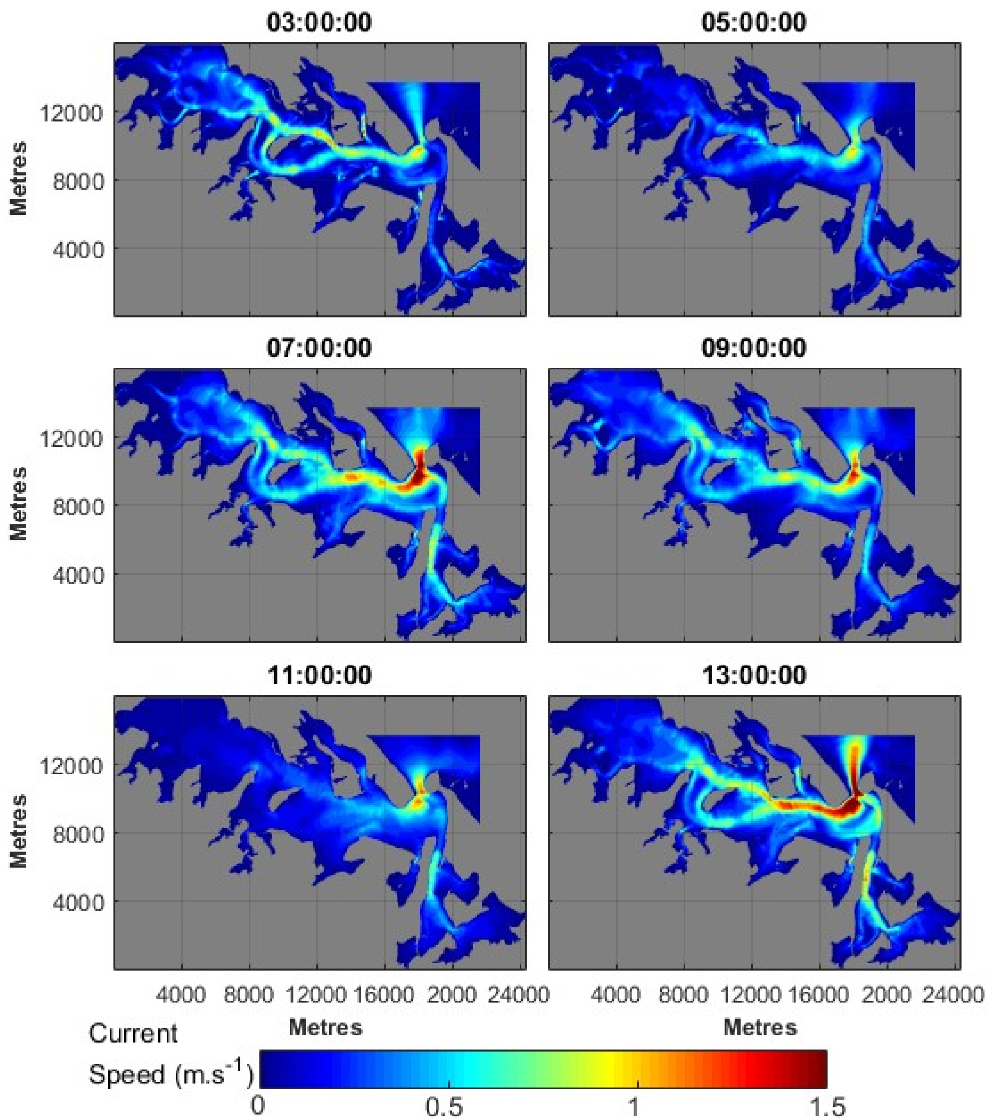

Figure 6.4: Instantaneous current speeds at two hour intervals from simulations of a spring tide on the 1st October 2015 in the southern basin of Tauranga Harbour.

6.2.2 Stella Passage and the Upper Harbour

Stella Passage and the upper harbour are part of the upper harbour system and in some studies have been described as separate to the tidal inlet system in the lower southern basin (de Lange, 2011). An overview of the hydrodynamics in this arm of the harbour were described over both a neap and spring tide. Water levels and current speeds at S4 Marker 21 in Stella Passage and the three ADV observation points in the upper harbour over a 14 day period are presented in Figure 6.5. During a spring tide, towards the end of the dataset, the water levels and current speeds increased at all locations.

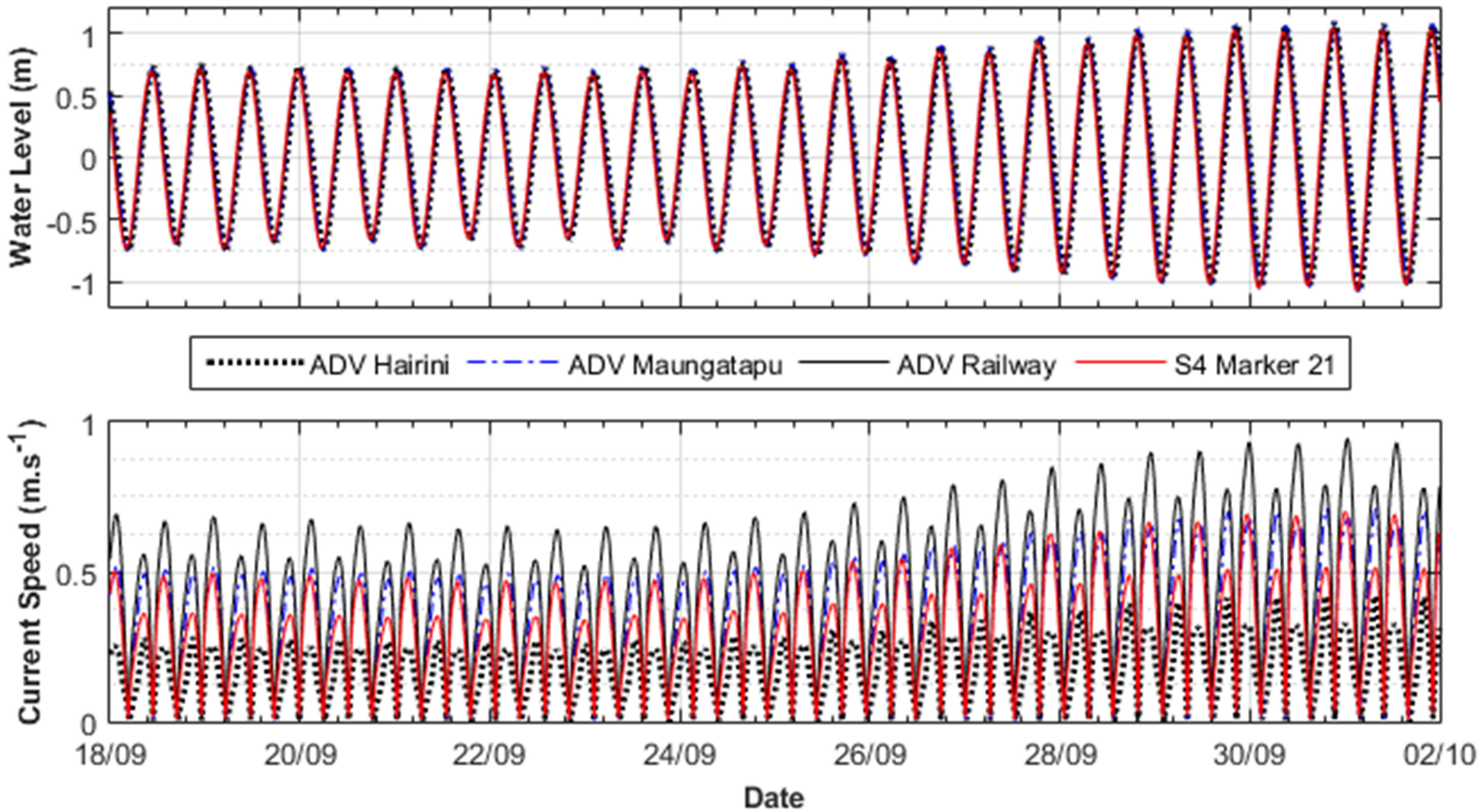

Figure 6.5: Water levels and current speeds over a 14 day period from simulations of a neap and spring tide from the 18th September to the 2nd October 2015 at ADV Hairini, ADV Maungatapu, ADV Railway and the S4 at Marker 21.

There was no significant change in tidal amplitude between locations over a neap tide in Figure 6.6. Over a spring tide in Figure 6.7 however, a small increase in tidal amplitude at both high and low tide was modelled with distance up the harbour. Changes in tidal phase between Stella Passage and ADV Hairini (the upper most observation point) were evident over both a neap and spring tide. During a spring tide there was an average lag in the timing of the tide between Stella Passage and the upper harbour of 42 minutes. High and low tide in Stella Passage were approximately 42 minutes before high and low tide at ADV Hairini.

Current speeds were the highest over both a neap and spring tide at ADV Railway, which was ebb dominant. Stella Passage was also ebb dominant but current speeds did not exceed 0.5 $m.s^{-1}$ during any stage of a neap tide, whereas on a spring ebb tide current speeds reached 0.7 $m.s^{-1}$. No tidal asymmetry was evident at ADV Maungatapu during a neap tide, but on a spring tide the location was flood dominant. ADV Hairini had the lowest modelled current speeds and was flood dominant, reaching 0.3 $m.s^{-1}$ and 0.4 $m.s^{-1}$ on a neap and spring flood tide respectively. Tidal asymmetry at all of the sites was more pronounced over a spring tide than on simulated neap tides. Current speeds dropped to less than 0.05 $m.s^{-1}$ at all of the observation points just after high and low tide which is known as slack water (de Lange, 2011). Peak ebb and peak flood current speeds were modelled just before high and low tide. At sites that were ebb dominant, the differences between ebb and flood current speeds were more pronounced than sites that showed slight flood dominance.

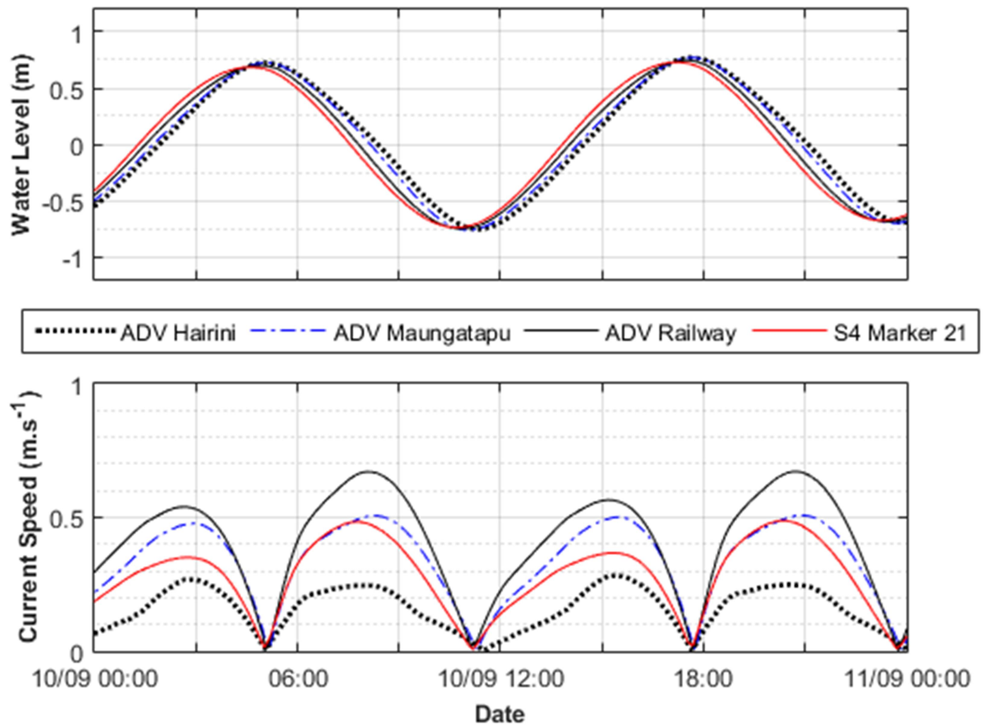

Figure 6.6: Water levels and current speeds from simulations of a neap tide from the 10th to the 11th September 2015 at ADV Hairini, ADV Maungatapu, ADV Railway and the S4 at Marker 21.

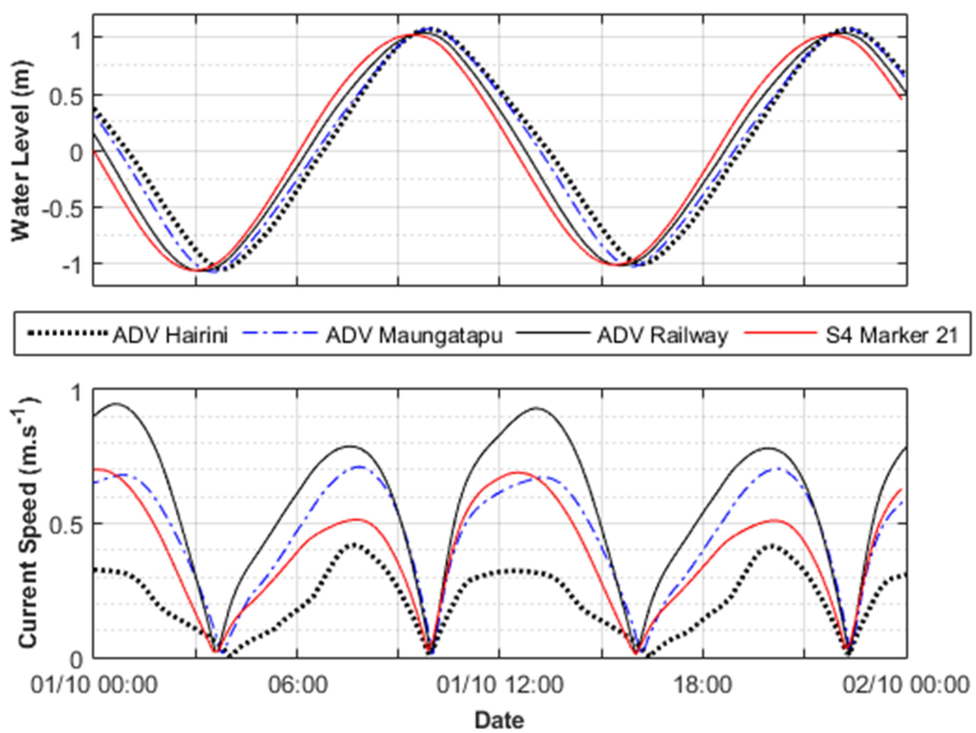

Figure 6.7: Water levels and current speeds from simulations of a spring tide from the 1st to the 2nd October 2015 at ADV Hairini, ADV Maungatapu, ADV Railway and the S4 at Marker 21.

Two hour instantaneous current speeds over a spring tidal cycle in Stella Passage and the upper harbour (Figure 6.8) shows that current speeds were highest in the main channel. The majority of the shallow intertidal areas had current speeds of below 0.1 $m.s^{-1}$ at all stages of the tidal cycle. The main channel within Town Reach and south towards the Railway Bridge had the largest current speeds for all time periods, except at 03:00:00 which was low tide. The lowest current speeds were just after low tide, and as there was a phase lag of the tide in the upper harbour, the timing of the slack tide in the upper harbour also lagged behind that in Stella Passage and Town Reach.

At peak ebb and flood tide over both a neap and spring tide (Figure 6.9 and Figure 6.10 respectively) the majority of the tidal volume in the upper harbour flowed through the eastern most channel of Waimapu Estuary and Rangataua Bay. The largest current speeds were within the upper Town Reach and Waimapu Estuary near the Railway Bridge and Harbour Bridge causeways. Current speeds were also higher under the Maungatapu Bridge and Hairini Bridge than in the channel approaches and surrounding intertidal areas. Neap current speeds were significantly less than those during a spring tide at both peak ebb and peak flood tide. Peak ebb tide current speeds were generally higher than peak flood tide current speeds. Current speeds over the extensive intertidal areas in Waipu Bay, Waimapu Estuary, Rangataua Bay and Welcome Bay were < 0.1 $m.s^{-1}$ during a neap tide and < 0.25 $m.s^{-1}$ on a spring tide as the tidal amplitude was larger.

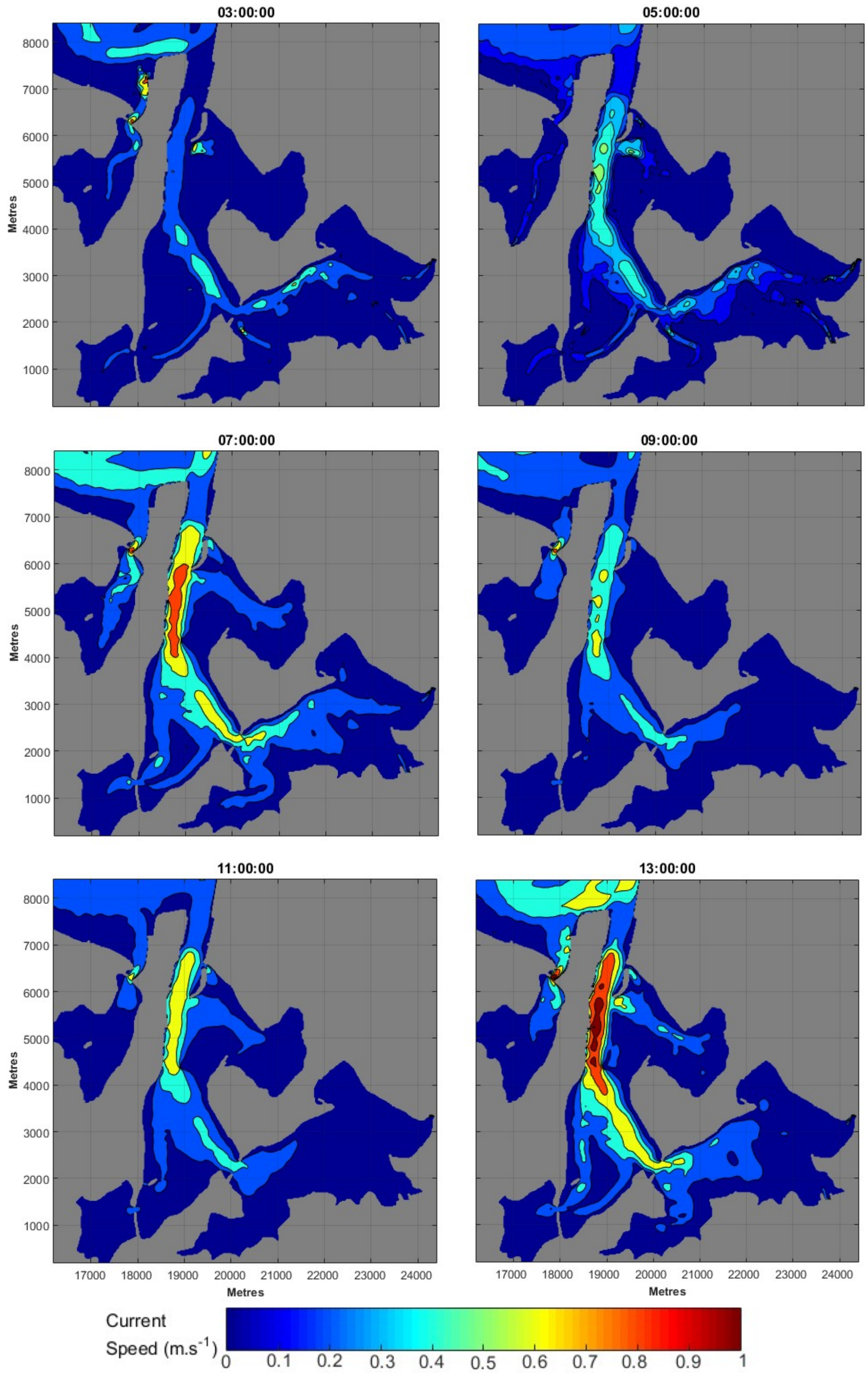

Figure 6.8: Instantaneous current speeds at two hour intervals in Stella Passage and the upper harbour from simulations of a spring tide on the 1st October 2015.

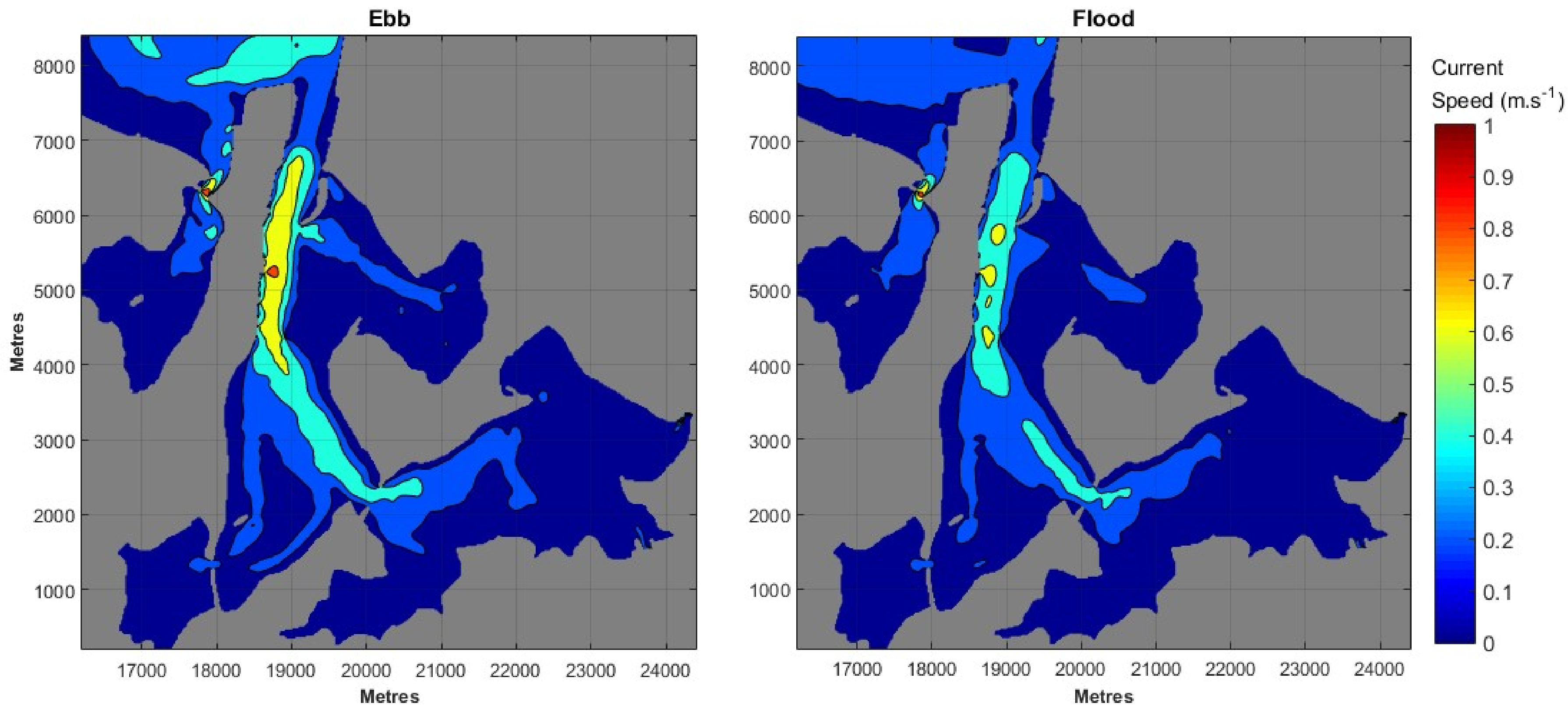

Figure 6.9: Current speeds at a peak ebb and peak flood tide in Stella Passage and the upper harbour from simulations of a neap tide at 8:00:00 (ebb) and 16:00:00 (flood) on the 10th September 2015.

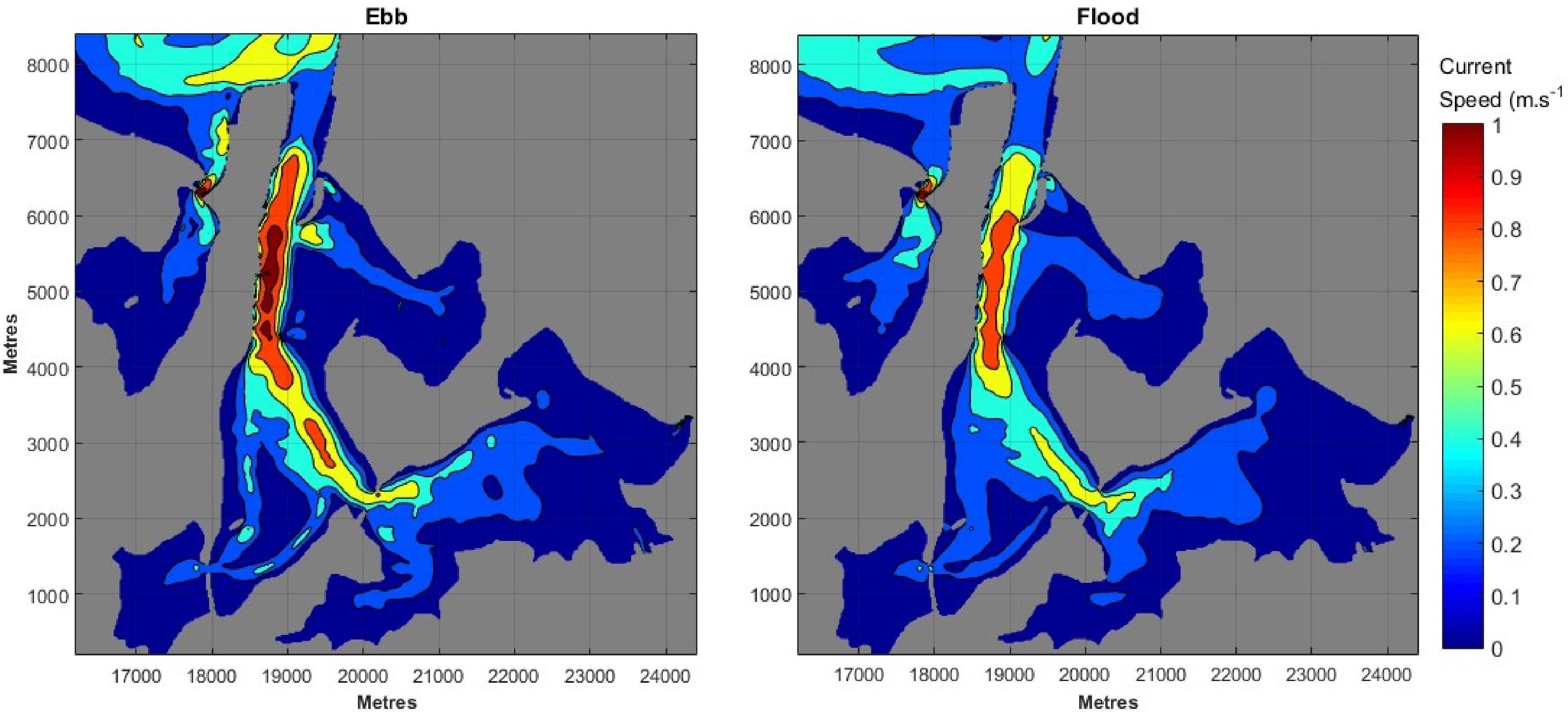

Figure 6.10: Current speeds at a peak ebb and peak flood tide in Stella Passage and the upper harbour from simulations of a spring tide at 01:00:00 (ebb) and 08:00:00 (flood) on the 1st October 2015.

6.2.3 Stella Passage and Town Reach

Plots of velocity vectors and current speeds within Stella Passage and Town Reach over a spring tidal cycle are displayed in Figure 6.11. Predicted current speeds within Stella Passage were below 0.4 m.s^{-1} during all stages of the tidal cycle. Peak ebb and peak flood tide velocities within Town Reach were just before low and high tide. During low tide from 03:00:00 to 05:00:00, maximum current speeds of approximately 0.5 m.s^{-1} flowed around the south-western tip and south of the causeway between Aerodrome Bridge and the Harbour Bridge. Apart from during low tide, the largest current speeds occurred within Town Reach. Current speeds were < 0.8 m.s^{-1} during most stages of the tidal cycle.

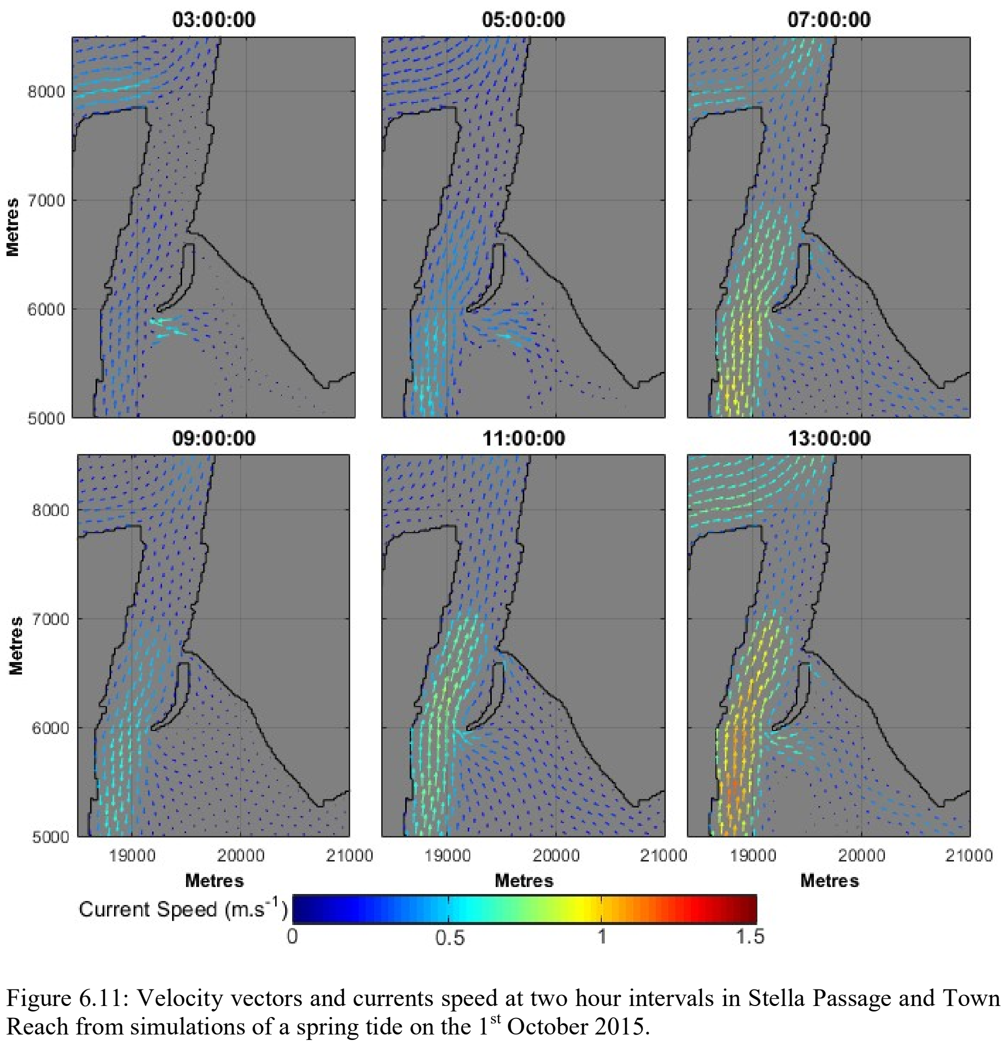

Figure 6.11: Velocity vectors and currents speed at two hour intervals in Stella Passage and Town Reach from simulations of a spring tide on the 1st October 2015.

Figure 6.12 and Figure 6.13 display the velocity vectors at peak ebb and peak flood tide. Maximum current speeds occurred within Town Reach during peak ebb tide. Town Reach and Marker 21 (Figure 6.7) were both ebb dominant. During both peak ebb and flood tide, current speeds were significantly reduced when flowing over the drop-off between Town Reach and the dredged Stella Passage. On an ebb tide, Waipu Bay predominantly drained out behind the causeway into Town Reach rather than under Aerodrome Bridge. As in previous studies, the majority of the tidal volume flows through Otumoetai Channel rather than into Stella Passage (Bell, 1991). The proposed breakwater to be constructed at the northern end of Tauranga Bridge Marina will further constrict the tidal flow in Town Reach (McKenzie, 2014).

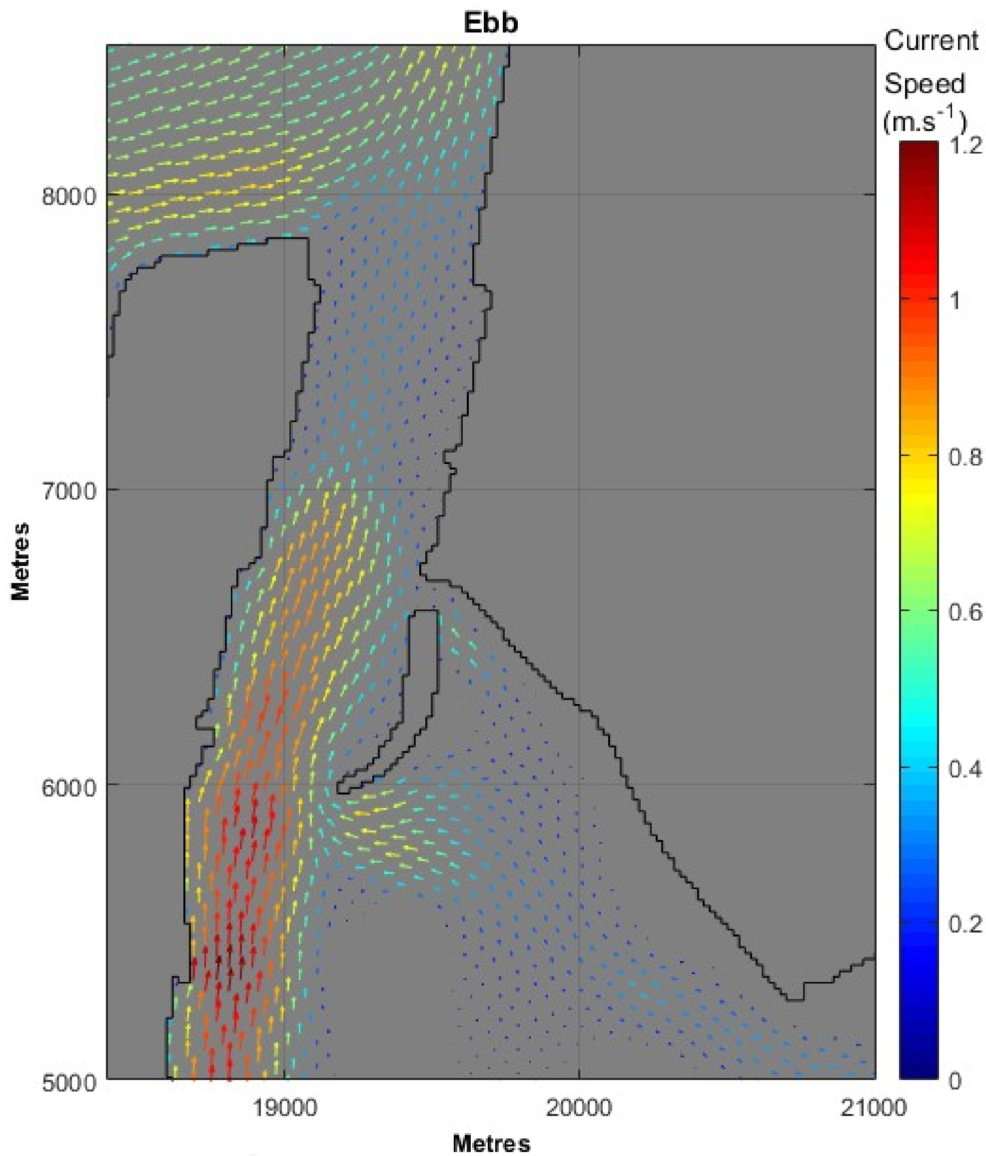

Figure 6.12: Velocity vectors and current speeds at a peak ebb tide in Stella Passage and Town Reach from simulations of a spring tide at 01:00:00 on the 1st October 2015.

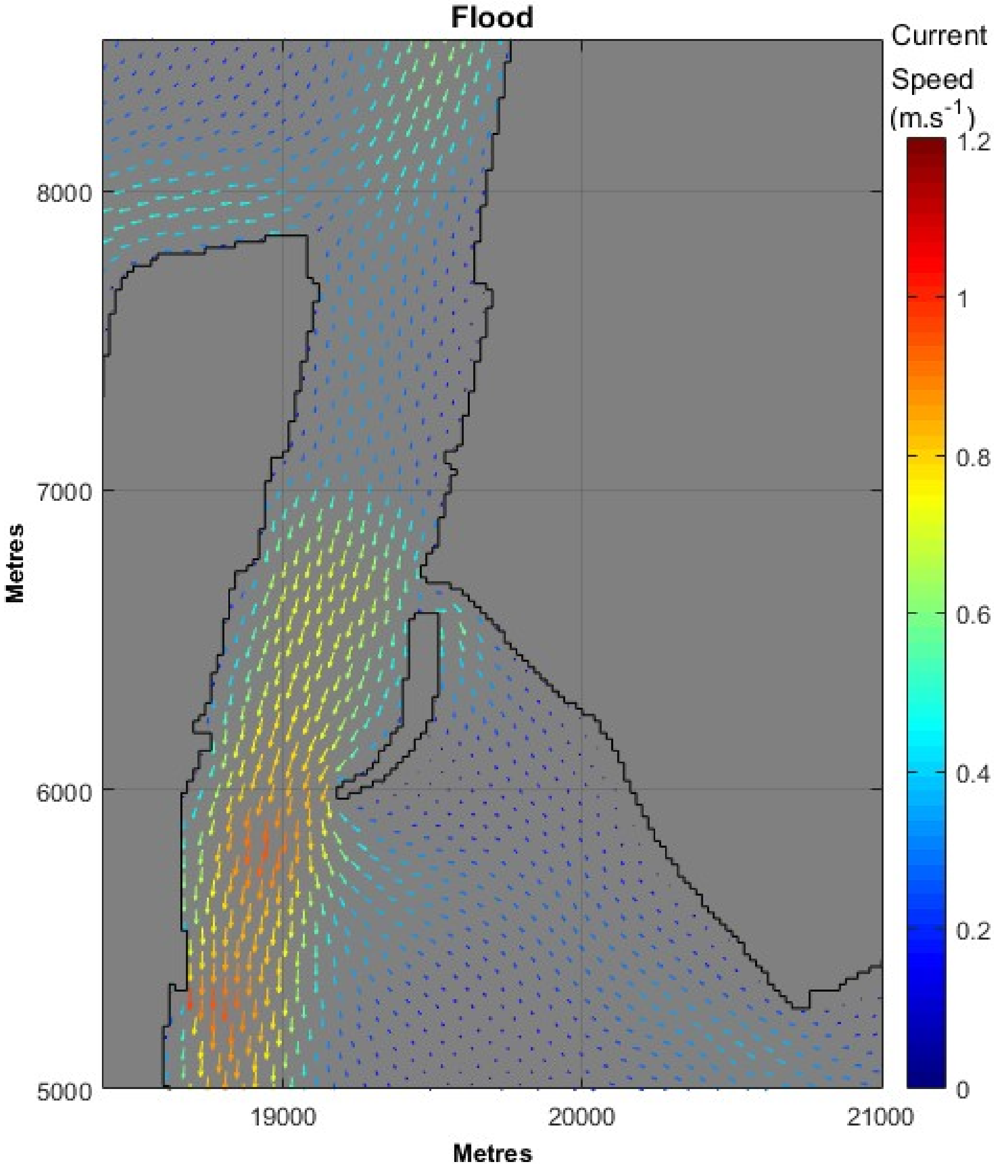

Figure 6.13: Velocity vectors and current speeds at a peak flood tide in Stella Passage and Town Reach from simulations of a spring tide at 08:00:00 on the 1st October 2015.

6.2.4 The Upper Harbour

Large intertidal areas within the upper harbour beyond Stella Passage can be seen during peak ebb tide in Figure 6.14, where areas containing no velocity vectors indicate the regions that were exposed at low tide. During a peak flood tide (Figure 6.15) most of the regions exposed at peak ebb tide had current speeds of < 0.3 m.s^{-1}. In Figure 6.7 ADV Maungatapu and ADV Hairini displayed a slight flood dominance during a spring tide, whereas ADV Railway was ebb dominant. As previously described, the largest current speeds were within the main channels and the majority of tidal currents flowed under Maungatapu Bridge into Rangataua Bay. Flood tidal currents on the eastern side of Maungatapu Bridge flowed relatively evenly into Rangataua Bay, whereas ebb tidal currents were concentrated through the north-eastern channel. The channel under Hairini Bridge had lower current speeds than the other estuary and bay entrances. The largest current speed were predicted at the Railway Bridge. The Railway Bridge causeway is displayed in Figure 4.17 and can be identified in the velocity vector plots by the area between Matapihi and Tauranga that contained no velocity vectors during all stages of the tide. A small eddy developed on the northern side of the Railway Bridge causeway on an ebb tide.

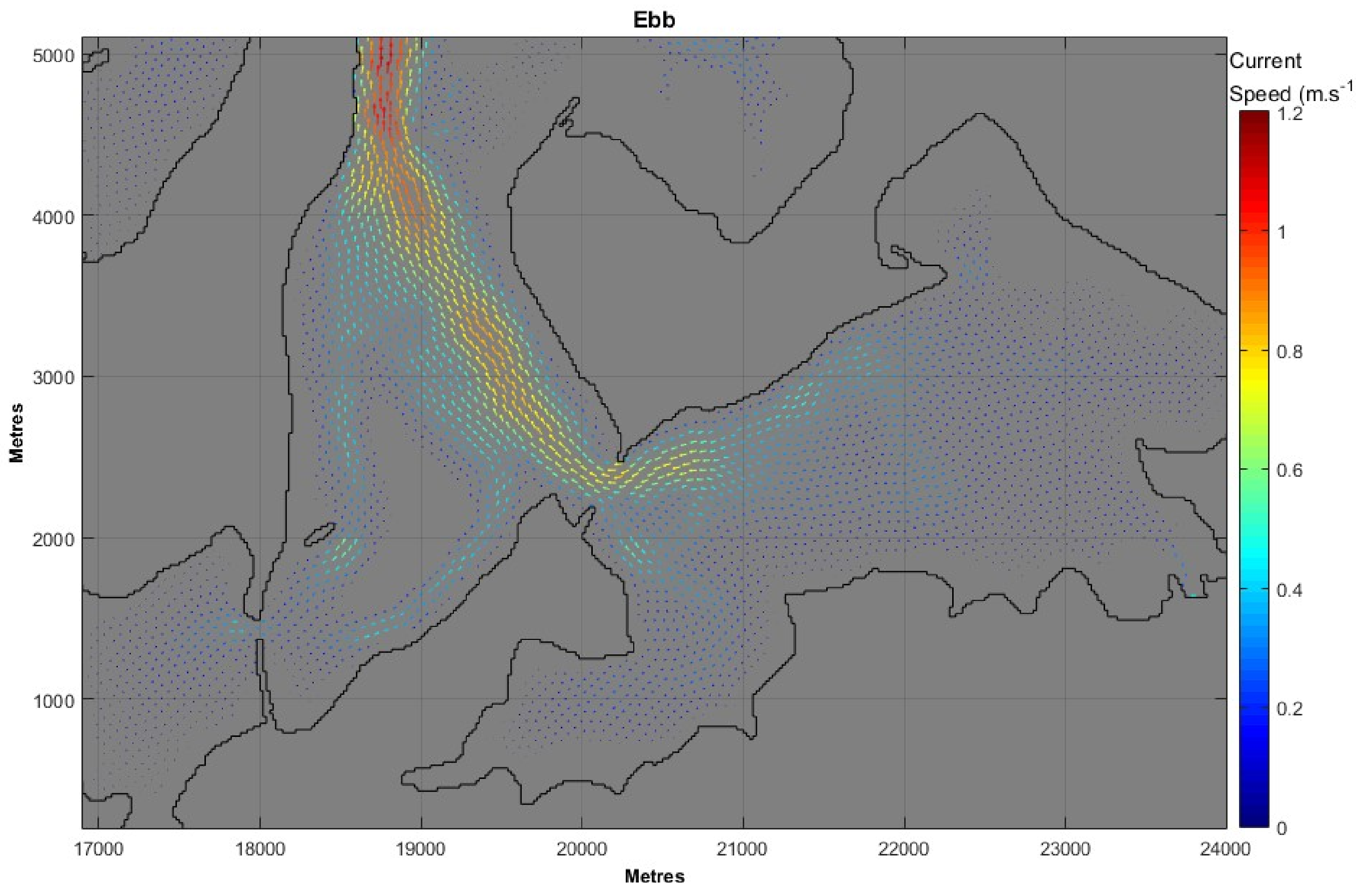

Figure 6.14: Velocity vectors and current speeds at a peak ebb tide in the upper harbour from simulations of a spring tide at 01:00:00 on the 1st October 2015.

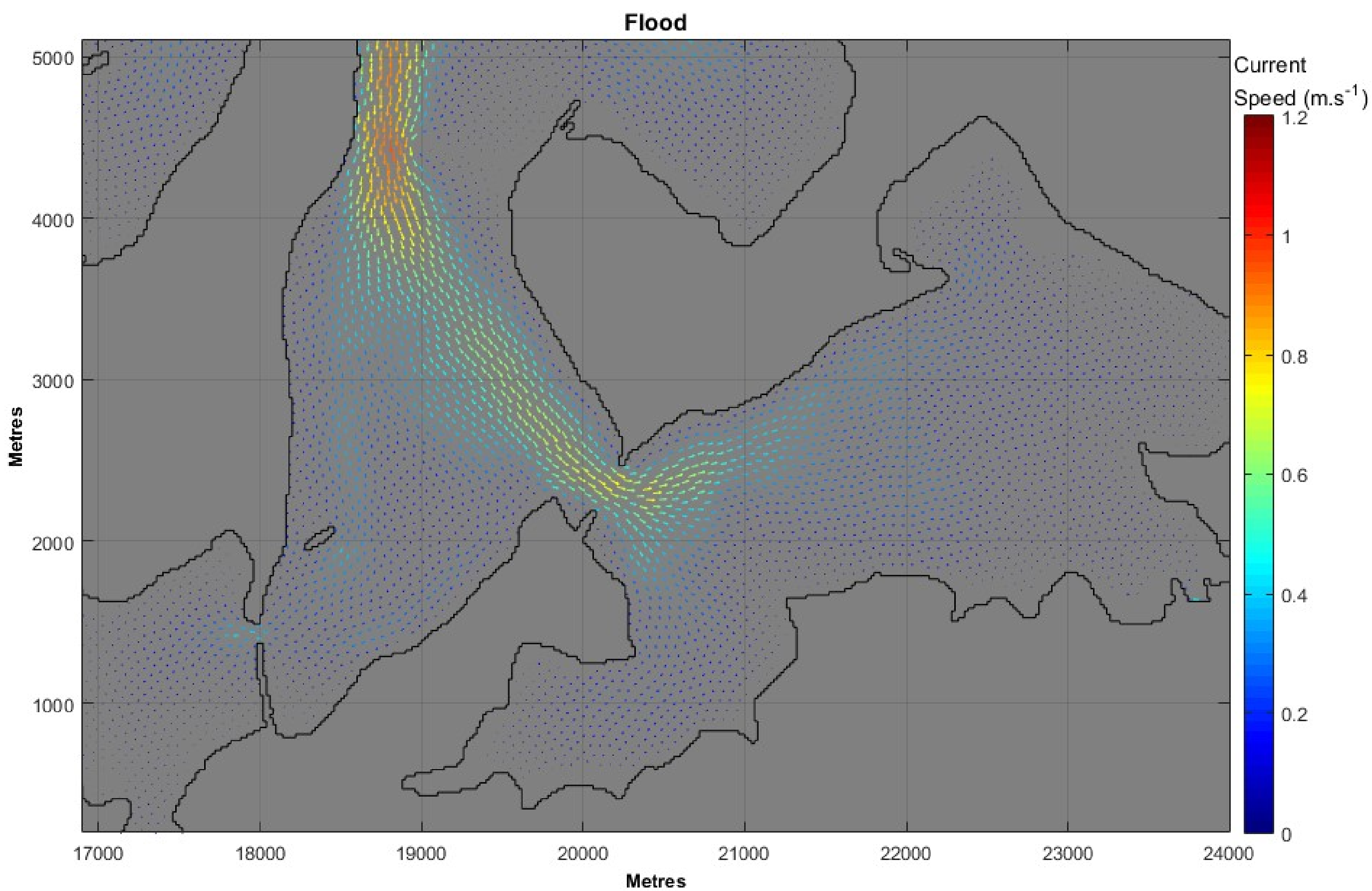

Figure 6.15: Velocity vectors and current speeds at a peak flood tide in the upper harbour from simulations of a spring tide at 08:00:00 on the 1st October 2015.

6.2.5 Residual Circulation

Residual velocities were calculated over 29 days of the model and contained both neap and spring tides (3rd September to the 2nd October 2015). Residual velocities display the net flow and tidal asymmetry by calculating the average current velocities over the tidal cycle (ASR, 2007). The magnitude of residual velocities in Stella Passage and the upper harbour are presented in Figure 6.16. Residual velocities were < 0.2 $m.s^{-1}$ in all areas except at the discharge points of Rocky Stream and Waitao Stream. Localised residual velocity vectors and current speeds are displayed within Stella Passage and Town Reach, and at Railway Bridge, Maungatapu Bridge and Hairini Bridge; the limits of four plotted areas are shown in Figure 6.16. Velocity vector arrows show the ebb or flood dominance and the magnitude of the net flow.

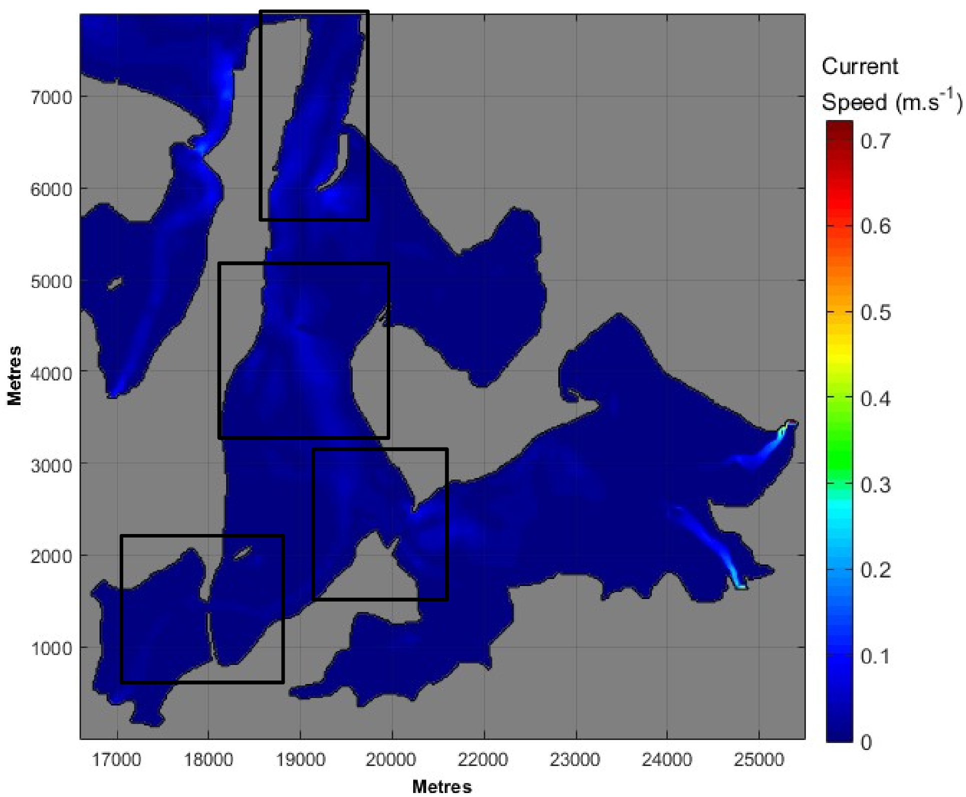

Figure 6.16: Residual velocities in Stella Passage and the upper harbour averaged over simulations of a neap and spring tide from the 3rd September to the 2nd October 2015. The black boxes indicate the plotted areas of the residual velocity vector plots at (from top to bottom) Stella Passage, Railway Bridge, Maungatapu Bridge and Hairini Bridge.

The maximum residual velocity in Stella Passage and Town Reach (Figure 6.17) was 0.1 $m.s^{-1}$. Western Town Reach was ebb dominant while eastern Town Reach was flood dominant. There were three residual eddies evident in Figure 6.17; a clockwise eddy on the eastern side of Stella Passage at the drop-off, a clockwise eddy at the location of Tauranga Bridge Marina in eastern Town Reach, and an anticlockwise eddy south of the Harbour Bridge causeway in-between Town Reach and Waipu Bay. Under the Harbour Bridge, residual velocities of 0.08 $m.s^{-1}$ were ebb directed on the east and flood directed on the west, but in the centre of the channel were < 0.03 $m.s^{-1}$. The largest residual velocities were southeast of the Harbour Bridge causeway and were ebb dominant. Residual velocities within the dredged area of Stella Passage were < 0.02 $m.s^{-1}$ and were neutral directly in front of the Sulphur Point and Maunganui wharves. Under Aerodrome Bridge the residual velocity was ebb and flood directed on the west and east respectively, but small in magnitude.

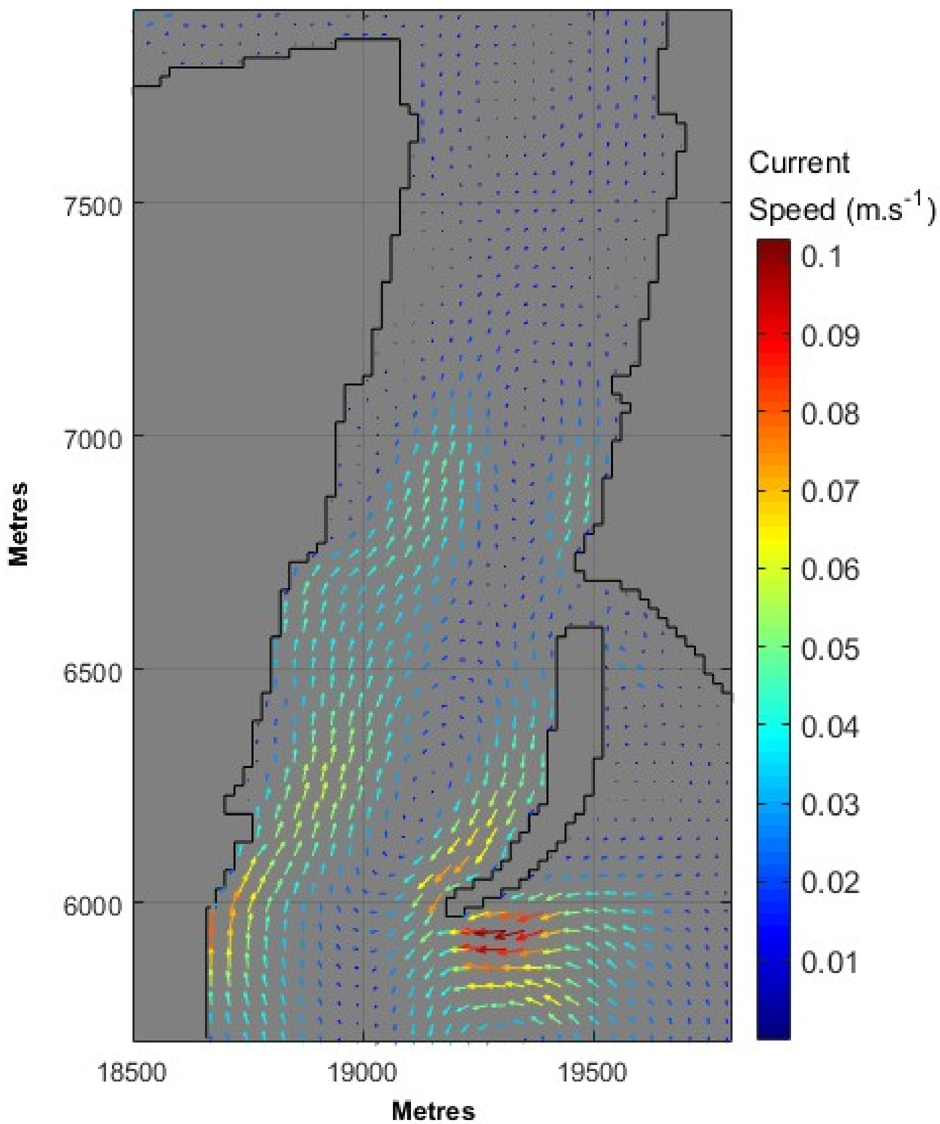

Figure 6.17: Residual velocity vectors and current speeds in Stella Passage and Town Reach averaged over 29 days of the simulation.

Figure 6.18 shows the residual velocities at Railway Bridge in the upper harbour. North of the Railway Bridge causeway there was a large clockwise eddy of residual velocity which was flood directed on the eastern side of the main channel until reaching the Railway Bridge causeway where the current was diverted to the western side of the main channel. On the northern side of the causeway there was no residual velocity to the east. Residual velocities in Waipu Bay were negligible. South of the Railway Bridge causeway, residual velocities were ebb dominant through the main channel within Waimapu Estuary. The maximum residual velocities of around 0.07 m.s^{-1} were flood directed and flowed from the main channel around the south-western tip of the causeway. On the main sandbank directly south of the Railway Bridge, a weak clockwise eddy was evident involving the blind channel to the west.

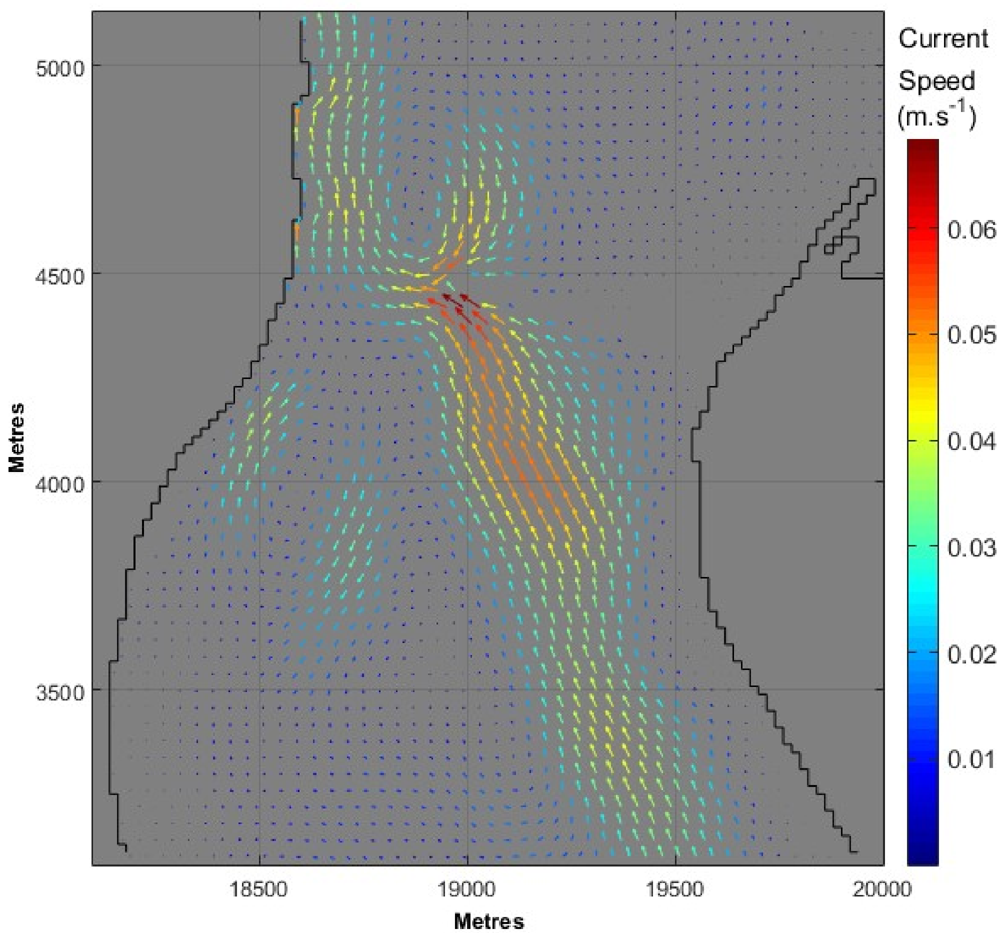

Figure 6.18: Residual velocity vectors and current speeds at the Railway Bridge averaged over 29 days of the simulation.

At Maungatapu Bridge (Figure 6.19), the patterns in residual velocity were dominated by an anticlockwise eddy in the entrance of Rangataua Bay east of the bridge. The eddy was stronger on its northern side which was ebb directed, and residual velocities reached 0.07 $m.s^{-1}$ alongside the eastern bridge approach. There was small ebb directed residual velocity in the main channel out of Welcome Bay. North of Maungatapu Bridge there were a number of small residual eddies present, the largest one being a clockwise eddy directly north of the bridge. Maximum residual velocities of just under 0.09 $m.s^{-1}$ in Figure 6.19 flowed southwest, directly underneath the Maungatapu Bridge on the south-eastern side of the channel. The residual velocities were at the intersection point of two opposing eddies.

The final residual velocity plot is of the Hairini Bridge area in Figure 6.20. The magnitude of the residual velocities were significantly smaller in the area around Hairini compared to the other residual plots. The maximum residual velocities were just over 0.03 $m.s^{-1}$ and only occurred in the channel east of Motuopuhi Island in Waimapu Estuary where they contributed to the ebb directed residuals off the western shoreline. The next largest residual currents were between 0.015 $m.s^{-1}$ and 0.02 $m.s^{-1}$ and were ebb directed under Hairini Bridge and through the main channel east towards Maungatapu Bridge. A small clockwise residual eddy was evident east of Hairini Bridge slightly north of the main channel. Overall the residual velocity in the Hairini Bridge area was ebb directed.

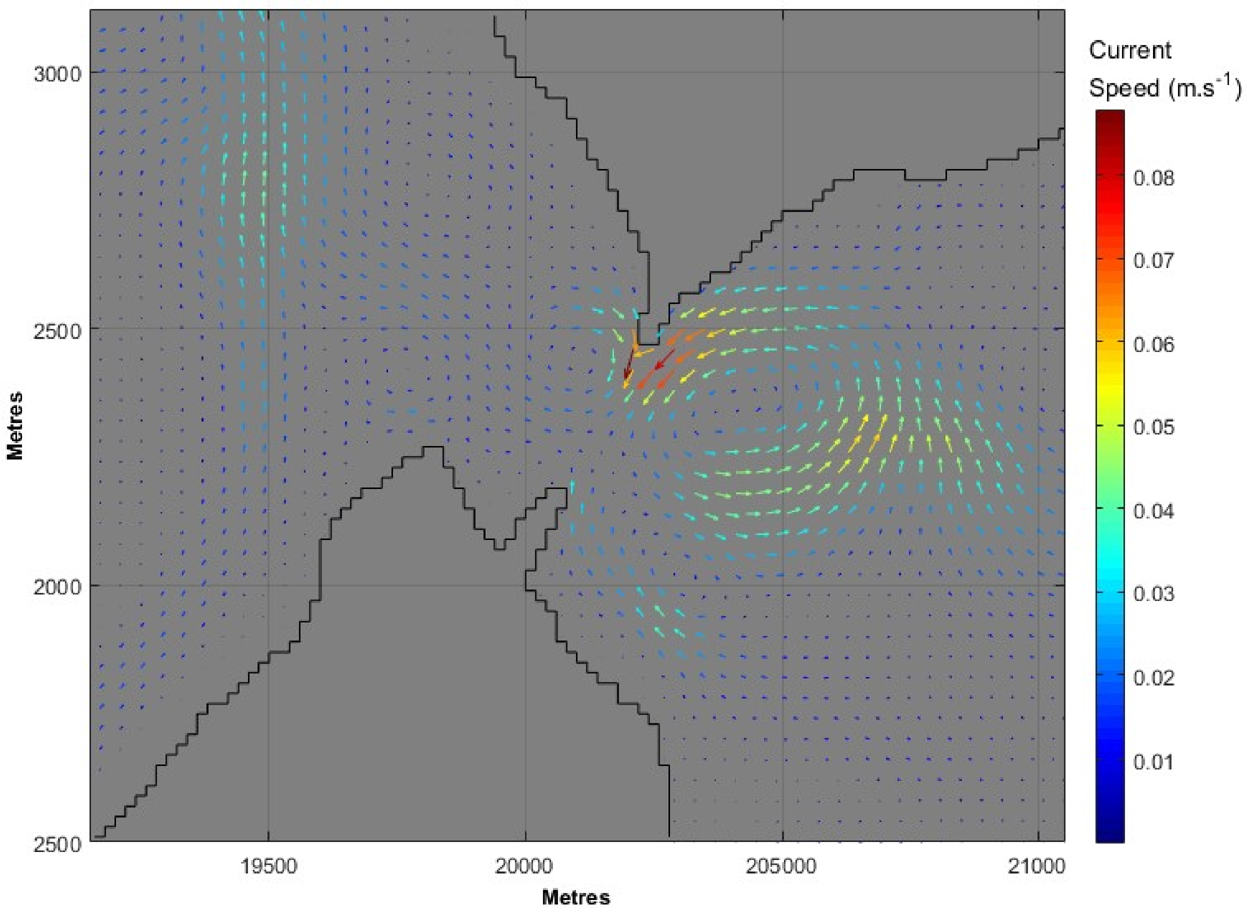

Figure 6.19: Residual velocity vectors and current speeds at Maungatapu Bridge averaged over 29 days of the simulation.

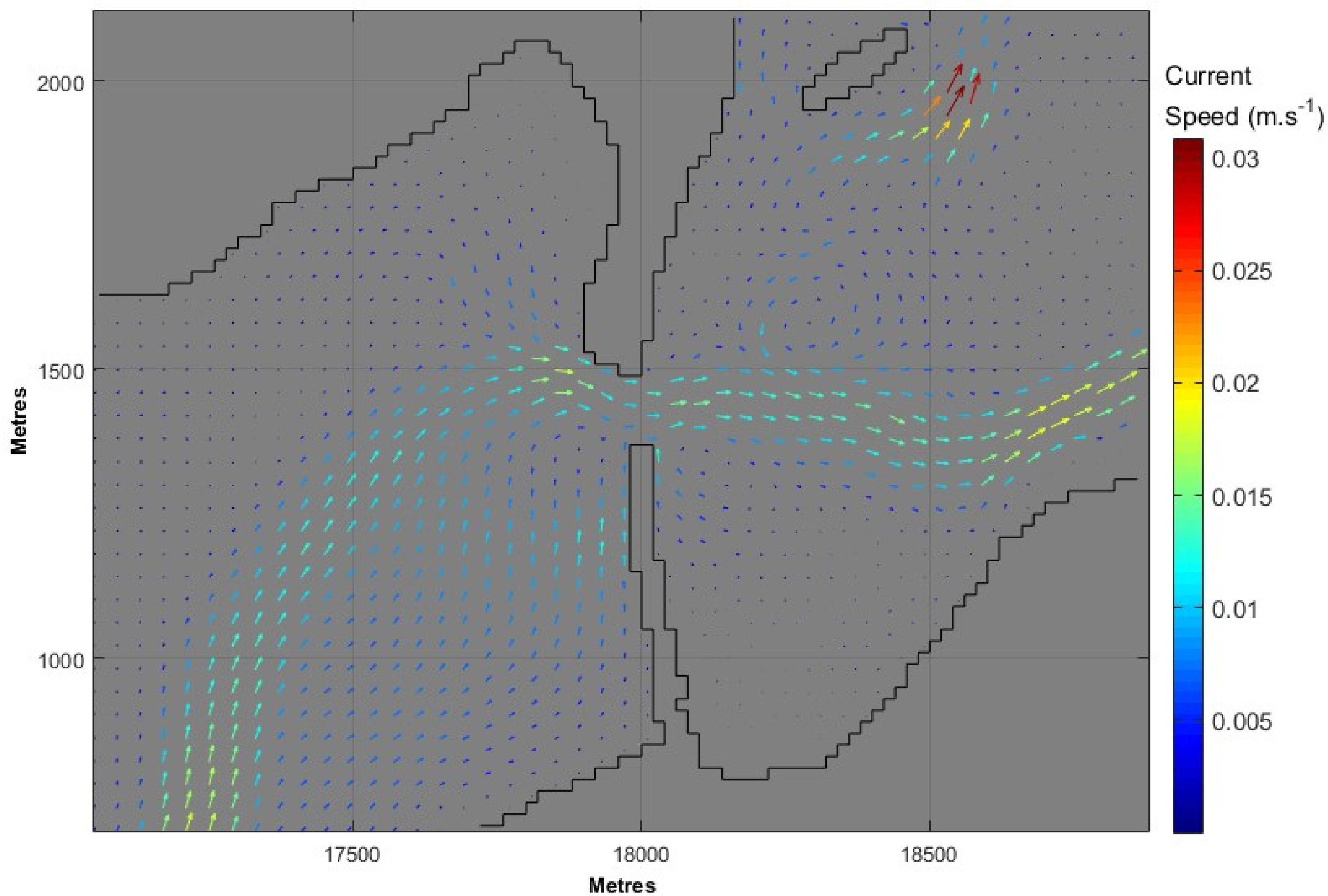

Figure 6.20: Residual velocity vectors and current speeds at Hairini Bridge averaged over 29 days of the simulation.

6.3 Discussion

Simulations of the hydrodynamics over the entire southern basin were similar to those described in previous numerical modelling studies (Bell, 1991, 1994; Tay et al., 2013; McKenzie, 2014). Hydrodynamics within the southern basin were controlled by the size and shape of the bays and estuaries (McKenzie, 2014). Constricted morphology caused attenuation of the tidal wave and increased current speeds by way of pressure gradients (Tay et al., 2013; McKenzie, 2014). As morphology narrowed, water built up and pressure gradients were created between the high and low surface elevations either side of the constricted channels (McKenzie, 2014). Flow from high to low pressure forced currents to accelerate through the constricted channels to conserve mass (McKenzie, 2014). The sea gradient created by the lag between the open water and inside the harbour was also what pushed and pulled the currents into and out of the upper harbour (ASR, 2007).

In the southern basin, large attenuation of the tidal wave was evident though the Entrance Channel and into Waikareao Estuary. The tidal wave slowed down which resulted in a phase lag in the upper reaches of the harbour and into the estuaries and bays (Tay et al., 2013). The change in tidal amplitude from the entrance to Omokoroa was also modelled by Tay et al. (2013) who predicted a 12 cm increase at high tide and a 2 cm decrease at low tide. Further into the southern basin, the hydrodynamic conditions were also controlled by the size and shape of the intertidal areas, especially the tidal asymmetry.

In plots of the larger scale hydrodynamic conditions in Stella Passage and the upper harbour, the largest influence on current speeds were the causeways. The highest current speeds were within upper Town Reach and Waimapu Estuary which were both directly influenced by the Harbour Bridge and Railway Bridge causeways. The causeways created constricted morphology which increased current speeds through the channels to conserve mass; similar to the tidal constriction described through the Entrance Channel and Waikareao Estuary. Within Stella Passage and the upper harbour peak ebb tide current speeds were generally higher than at peak flood tide, which was in keeping with the patterns in tidal asymmetry seen at the four observation points in Figure 6.6 and Figure 6.7.

The small residual velocities in Figure 6.16 indicate that the upper harbour beyond Stella Passage was generally in dynamic equilibrium, where the layout of the sand bars and channels may migrate slightly but the overall hydrodynamics and morphology remained the same (ASR, 2007).

6.3.1 Stella Passage and Town Reach

Velocity vector plots showed that the majority of Town Reach was ebb dominant, whereas no obvious tidal asymmetry was seen within the deeper Stella Passage as the current speeds were below 0.4 $m.s^{-1}$. Ebb dominance within Town Reach was due to the large area of exposed intertidal flats in Waipu Bay at low tide. Flow at low tide was restricted to Town Reach and current speeds increased within the channels. During the flood tide some of the tidal volume flows into Waipu Bay, increasing the cross-sectional area and reducing current speeds in the main channels. The reduction in current speeds over the drop-off into Stella Passage was evident on both a flood and ebb tide and was due to the change in depth from past dredging works. On an ebb tide, mass conservation reduced the ebb tidal currents from Town Reach into Stella Passage as the depth and cross-sectional area increased. On a flood tide, currents increased as the flow was restricted over the drop-off into Town Reach to conserve mass as the depth and cross-sectional area reduced.

During low tide, current speeds were highest around the south-western tip and south of the Harbour Bridge causeway as flow was restricted to the intertidal channels and the majority of Waipu Bay was exposed. As found in the investigations into the currents under Aerodrome Bridge by Healy (1994), current speeds were strongest on the ebb tide but the majority of the tidal volume flowed out into Town Reach rather than under Aerodrome Bridge (Healy, 1994). The clockwise eddy development on an ebb tide in Stella Passage that was simulated in both the McKenzie (2014) and Bell (1994) models was not evident in Stella Passage in Figure 6.11.

In the plots of residual velocity, central and the eastern side of Stella Passage and Town Reach were ebb dominant and the west of Town Reach and was flood dominant. Within Waipu Bay and south of the Harbour Bridge causeway residual velocities were ebb dominant, with some areas of neutral residual velocity in

Waipu Bay. McKenzie (2014) reported the same general patterns in residuals and tidal asymmetry within Stella Passage and Town Reach. At the drop-off the ebb directed residual currents accelerated and were diverted towards the northeast. The deflection of the ebb dominant flow was also modelled by McKenzie (2014) who attributed and the change in current direction to the Sulphur Point wharves acting as a barrier and redirecting flow.

As well as giving insight into the net direction of flow, residual velocity vectors indicate the potential sediment pathways (Black, 1984). A threshold velocity can be applied to the residual velocity vectors to isolate the residual currents that have the potential to transport sediment; the residual velocities over the threshold are known as the sediment residuals (ASR, 2007; de Lange, 2011). In previous studies of the southern basin, a threshold velocity of > 0.3 $m.s^{-1}$ was applied; which was the velocity needed to transport medium sands typically found in the southern basin (ASR, 2007; de Lange, 2011). The higher the residual velocity, the greater the potential for sediment transport (Black, 1984). Accelerating or diverging residual velocities indicate areas where erosion was likely to occur, and decelerating or converging vectors and areas of zero residual velocity indicate areas of potential sedimentation (Black, 1984). Areas with neutral residual velocity are where bedforms typically develop (Black, 1984; ASR, 2007).

With the threshold velocity limit of 0.3 $m.s^{-1}$, the largest feature was the recirculating clockwise sediment loop in Town Reach, also identified in the Tauranga Harbour Study by Black (1984). Areas where erosion was likely to occur were on the western side of Town Reach and over the drop-off, on the eastern side of Town Reach in the area of Tauranga Bridge Marina, and south of the Harbour Bridge causeway. Areas of potential sedimentation were central Town Reach, southern Stella Passage, areas of Waipu Bay, and directly in front of the existing Sulphur Point and Maunganui wharves. Boulay (2012) identified that areas of shell lag were the dominant within Town Reach between the Harbour Bridge and the drop-off, apart from eastern Town Reach under the Tauranga Bridge Marina which was an area of fine sands. Erosion from the accelerating residual velocities in Town Reach would be reduced due to the shell lag facies armouring the seabed (ASR, 2007; Boulay, 2012). Overall the ebb directed residuals were stronger and covered a larger area and within Town Reach and there was a greater potential for sediment transport than within the dredged Stella Passage.

6.3.2 The Upper Harbour

The extensive intertidal areas in Waipu Bay, Waimapu Estuary, Rangataua Bay and Welcome Bay controlled the tidal asymmetry in the upper harbour. Ebb dominance at ADV Railway was due to the reduced area at low tide limiting the tidal volume to the main channels and increasing current speeds on an ebb tide. Although constricted by a causeway, current speeds at Hairini Bridge were lower than at other locations within the upper harbour that were also constricted. The small current speeds may be attributed to the limited storage area, and hence tidal discharge, in the Waimapu Estuary beyond Hairini Bridge. The causeways within the upper harbour constricted the tidal flow through the channels and increased current speeds. The Railway Bridge causeway which extends out across over half of the original channel, had the most significant impact on current speeds and velocity vectors. McKenzie (2014) predicted the acceleration of current speeds from bridge causeways constricting the flow, and predicted current speeds of 1.0 $m.s^{-1}$ and 1.1 $m.s^{-1}$ to occur under the Railway Bridge and Harbour Bridge respectively.

On an ebb tide, a small eddy developed on the northern (lee) side of the Railway Bridge causeway in Figure 6.14. The model developed by ASR (2007) for the Southern Pipeline also showed large gradients in current speed on the lee side of the Railway Bridge causeway. The gradients were created by low current speeds in shadow zones to the north and south of the causeway on the ebb and flood tides respectively (ASR, 2007). Evidence of the gradients in current speed at the Railway Bridge can be seen in the residual velocity vector plot (Figure 6.18) where currents were flood dominant to the north and ebb dominant to the south of the causeway. The accelerating velocity vectors at the western tip of the causeway indicate an area of erosion, however the speeds were < 0.07 $m.s^{-1}$ which were below the threshold velocity needed to transport sediment. The low potential for sediment transport modelled at the Railway Bridge was in keeping with the Southern Pipeline study which predicted net sediment transport rates of a maximum 20,000 m^3 per year; small in comparison to the 1 million m^3 annual net sediment transport rate through the Entrance Channel stated by Black (1984).

ASR (2007) deemed the harbour bed at the Railway Bridge to be in dynamic equilibrium .

At Maungatapu Bridge the main controlling aspect on the patterns in residual velocity was the orientation of Rangataua Bay and the location of the main intertidal channels within the bay. Currents flowed directly into the bay on the flood tide, but were concentrated into the main channel on the ebb tide which flowed from Oruamatua to the east. The drainage of Rangataua Bay through the main channel resulted in an anticlockwise sediment transport loop east of Maungatapu Bridge. Residual velocities reached a maximum speed of just under 0.09 $m.s^{-1}$, also below the threshold velocity for sediment transport; although the velocities were still capable of transporting buoyant material and dissolved or suspended contaminants. Hairini Bridge had the lowest potential for sediment transport. The maximum residual velocity in the area was only 0.03 $m.s^{-1}$, and 0.02 $m.s^{-1}$ under Hairini Bridge. Overall the residual velocity in the area was ebb dominant which was due to the discharge from Waimapu River being stronger than the tidal volume that flows into the area on a flood tide.

CHAPTER SEVEN

HYDRODYNAMIC IMPACTS OF PROPOSED DREDGING AND WHARF EXTENSIONS

7.1 Introduction

Numerical modelling scenarios can be used to predict potential impacts to an area brought about by changes to the system such as dredging and the addition of man-made structures (de Lange, 2011). Such changes could alter the hydrodynamic conditions and dynamic equilibrium of an area (Boulay, 2012). In this chapter, four modelling scenarios are used to simulate the hydrodynamic conditions before any harbour works, after the 2015-2016 capital dredging, wharf extension dredging into Town Reach, and the wharf extensions and associated reclamation. Model predictions were compared between the simulations to determine the impacts at each stage of the harbour works over both a spring and neap tide. As well as determining the larger localised impacts in Stella Passage and Town Reach, any impacts on the upper harbour are also discussed.

7.2 Modelling Scenarios

To simulate the hydrodynamic impacts of the wharf extensions planned by the Port of Tauranga, comparisons were made between four modelling scenarios. The calibrated southern basin model simulated the conditions in 2015 and provided the baseline for comparisons; while the three other models simulated the stages of dredging and wharf extensions. The four models that were utilised are listed below:

- Pre-Works model — The calibrated southern basin model with no modifications to the bathymetry or model grid.
- Dredging model — The bathymetry was lowered to the design depths after the 2015-2016 capital dredging works, as specified in Figure 7.1.
- Wharf Dredging model — The dredging boundary was extended into Town Reach as part of the wharf extension works. The depths and dredged area are specified in Figure 7.2.

- Wharf Extension model — The wharf extensions and associated reclamation were added to the Wharf Dredging model to simulate all of the works associated with the wharf extensions. Figure 7.3 and Figure 7.4 outline the wharf structures and reclamation area.

Extending the dredged limits into Town Reach and adding the wharf extensions and reclamation will occur after the 2015-2016 dredging works are completed. Updating the bathymetry to the 2016 post dredging depths in the Dredging model before modelling any wharf extension works was essential to determine at which stage of construction any hydrodynamic impacts occur; identifying if the wharf extension works were the cause of any impacts or rather the completed 2015-2016 dredging. The bathymetries used in the four of the modelling scenarios are shown in Figure 7.5. Spatially varying bottom roughness maps were developed for each of the altered bathymetries. The wharf extensions and reclamation were simulated in the final modelling scenario and were represented as thin dams in the model grid; the placement of the thin dams is shown in Figure 7.6. Inserting thin dams around a grid cell blocks the flow into the cell. The use of thin dams to represent not only the reclamation but the wharf structures blocked all flow under the wharves, simulating the largest potential impact the wharves would have on the hydrodynamics. All of the models ran over the same simulation period as the calibrated southern basin model.

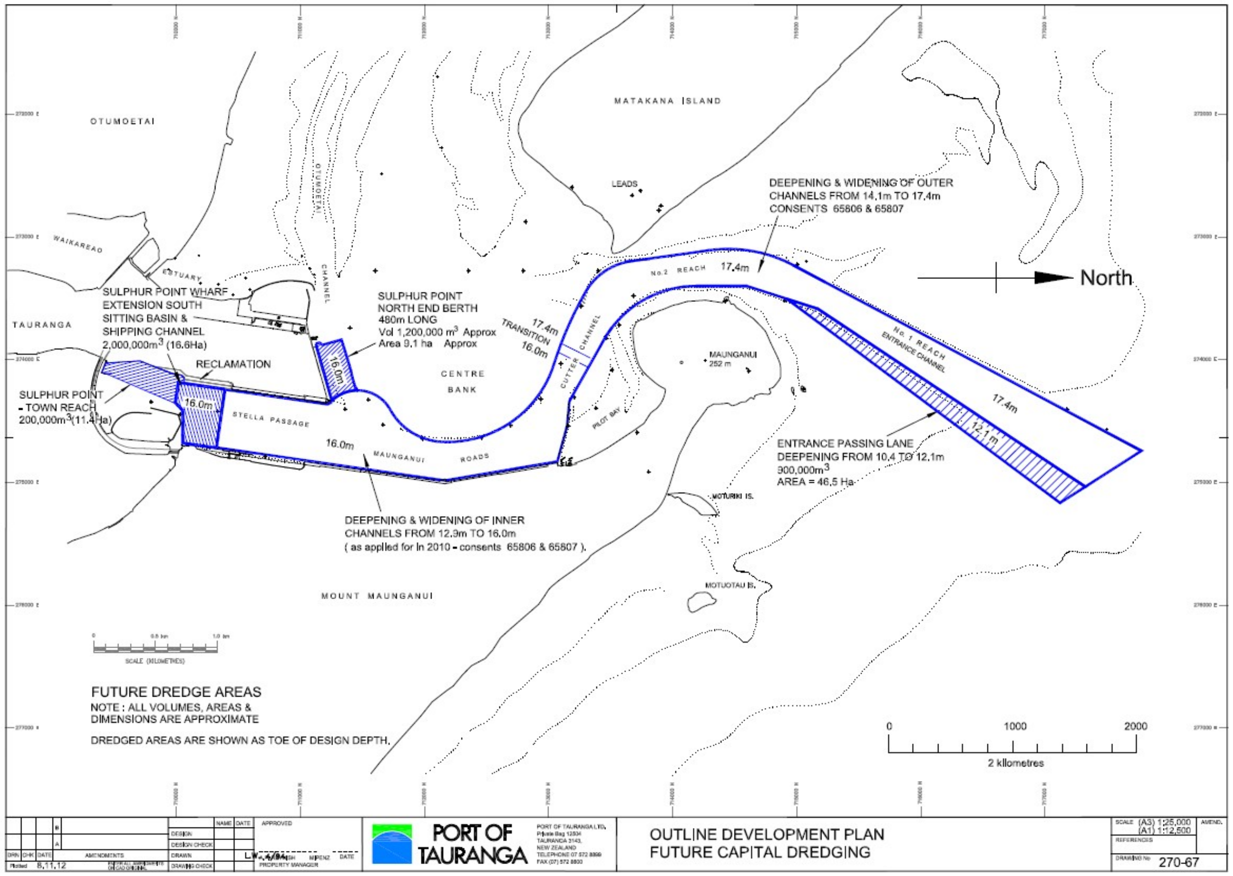

Figure 7.1: Development plan of 2015-2016 capital dredging works and future dredging (blue filled in areas) to be carried out in Tauranga Harbour and approach. Source: The Port of Tauranga (2015). Personal Communication (email).

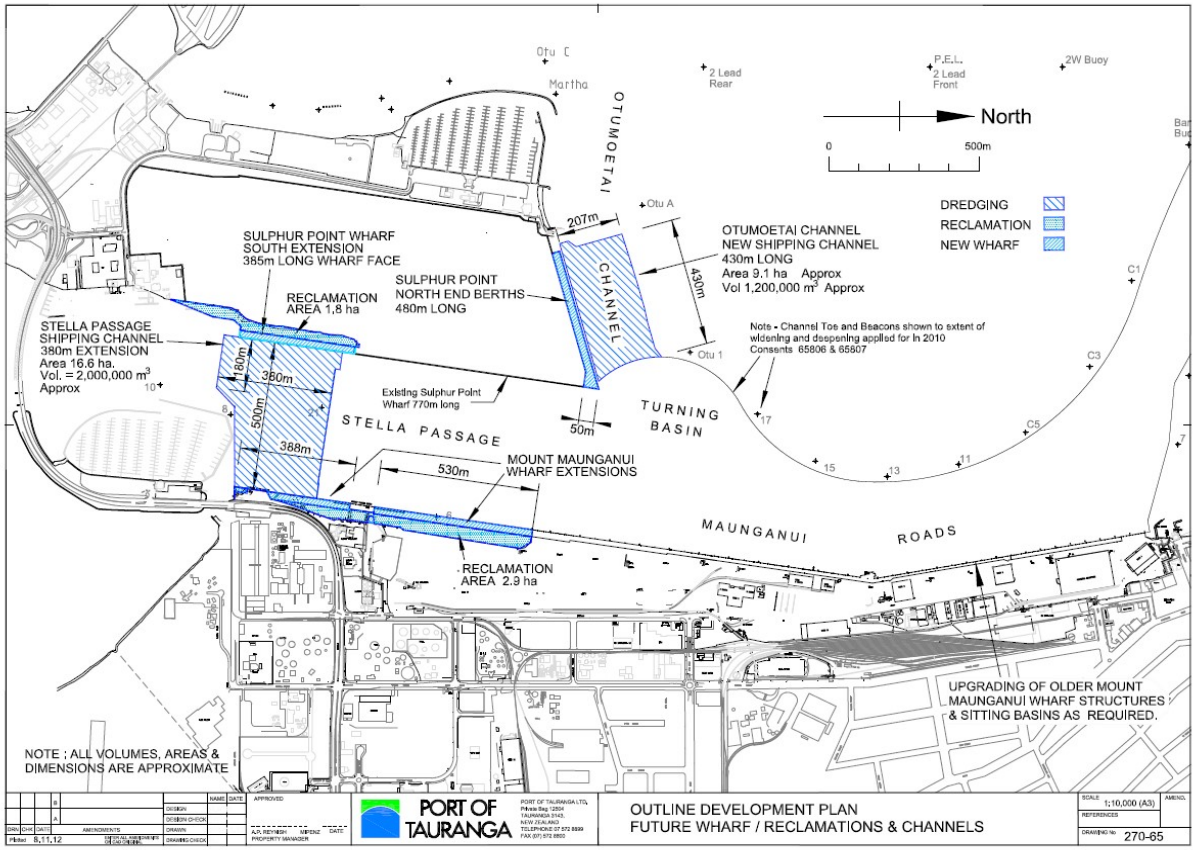

Figure 7.2: Development plan for the future wharf extensions and associated dredging and reclamation works at the Port of Tauranga. Note that the Sulphur Point North End berth is no longer included in the extension plans. Source: The Port of Tauranga (2015). Personal Communication (email).

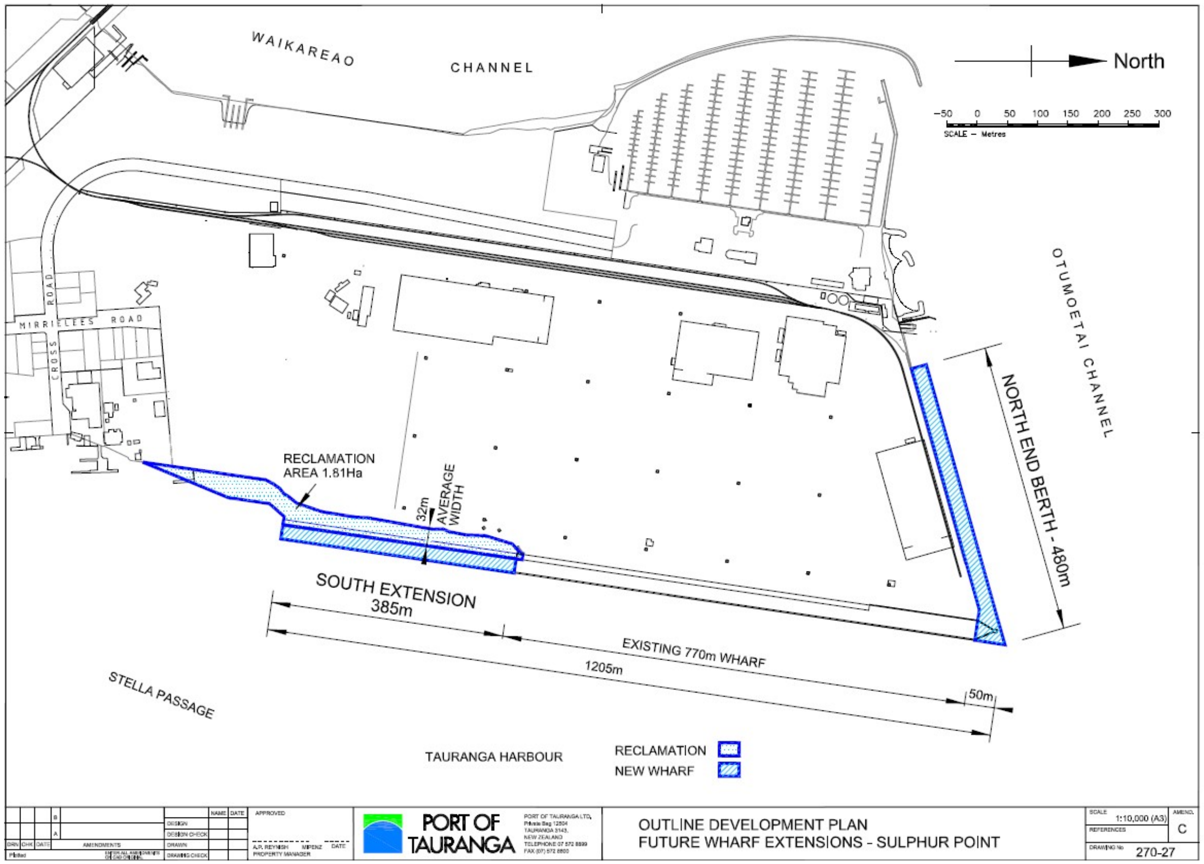

Figure 7.3: Wharf development plan for the future wharf extension at Sulphur Point at the Port of Tauranga. Note that the Sulphur Point North End berth is no longer included in the extension plans. Source: The Port of Tauranga (2015). Personal Communication (email).

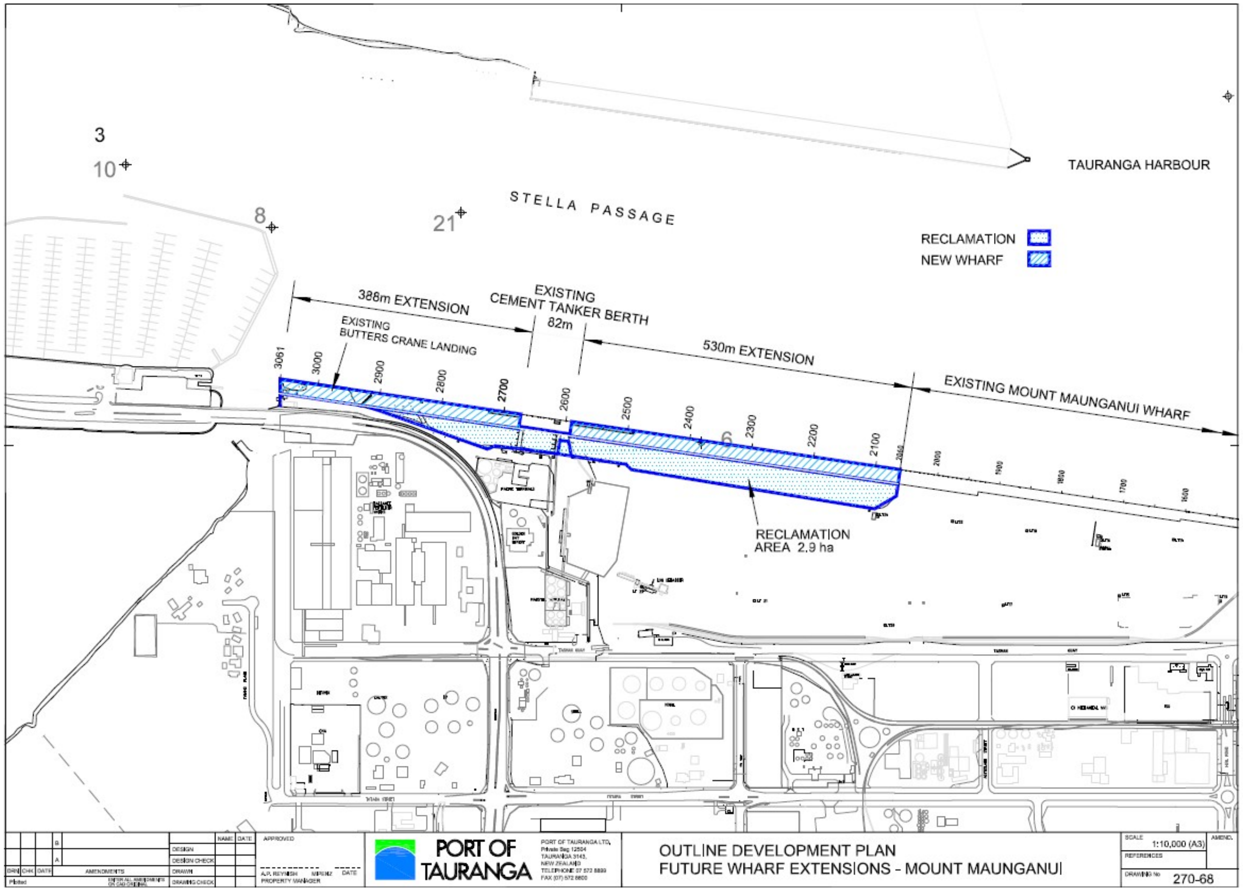

Figure 7.4: Wharf development plan for the future wharf extension at Maunganui wharves at the Port of Tauranga. Source: The Port of Tauranga (2015). Personal Communication (email).

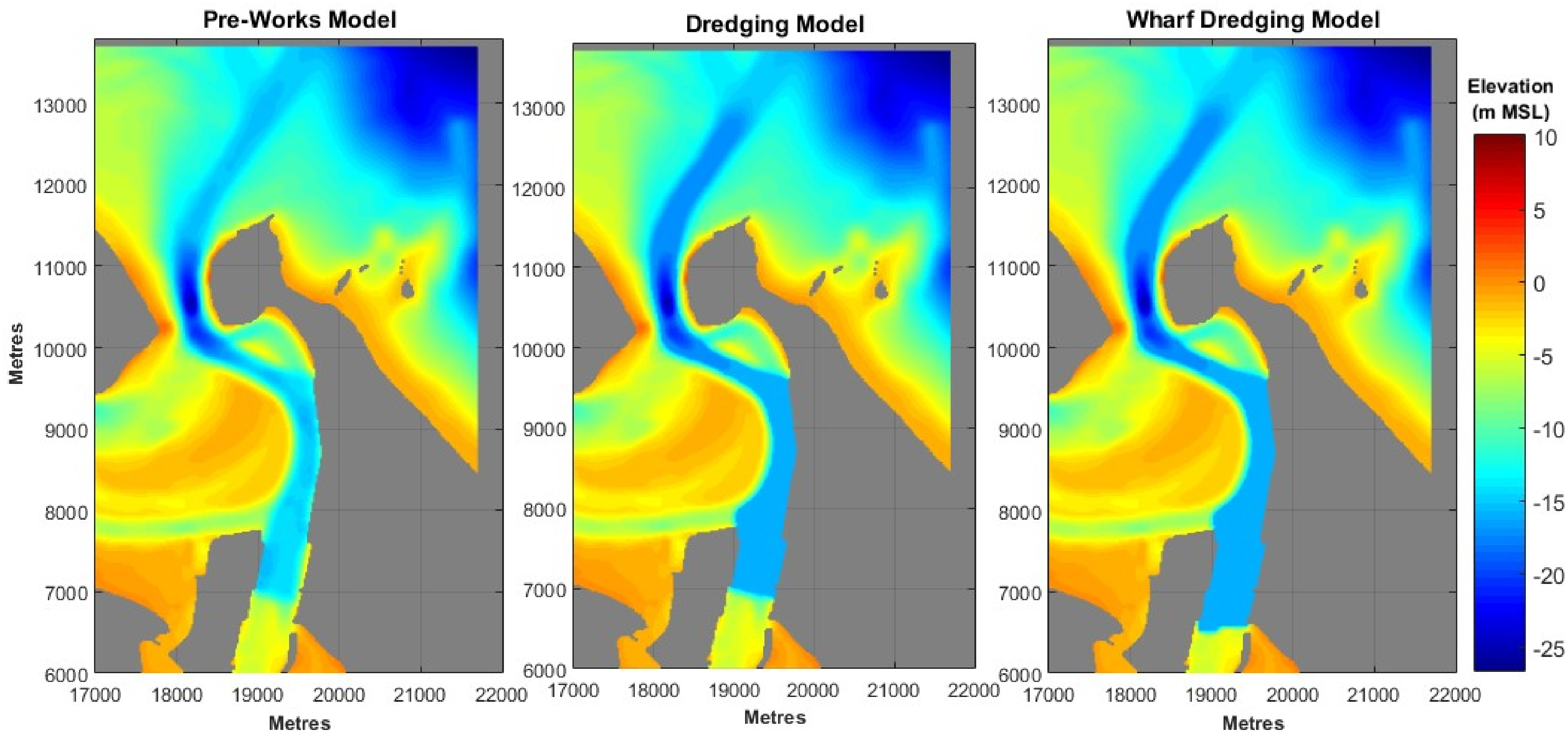

Figure 7.5: Bathymetry used in the existing southern basin model (Pre-Works model), the Dredging model and the Wharf Dredging model (also used in the Wharf Extension model). Note a negative elevation is below MSL.

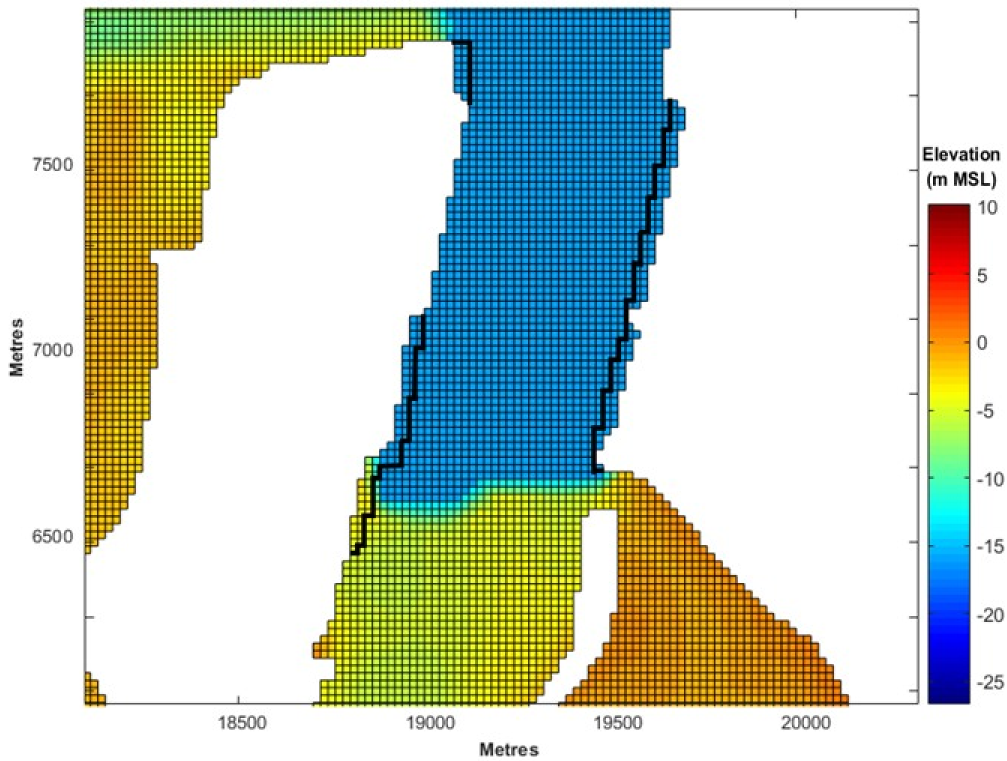

Figure 7.6: Placement of thin dams (bold black lines) in the Wharf Extension model to simulate the wharf extensions and reclamation in Stella Passage where each grid cell is 20 x 20 m. The northern-most thin dams at Sulphur Point represent the 2014 Sulphur Point wharf extension No. 2 and was included in all of the models. Note a negative elevation is below MSL.

7.3 Results

The four modelling scenarios were compared to determine the impacts of the dredging and wharf extensions on the hydrodynamics during both a neap and spring tide. The water levels and current speeds predicted over a 14 day period and over 24 hours of a neap and spring tide are presented for the Dredging, Wharf Dredging and Wharf Extension models in Figures AII.1 to AII.9 in Appendix II. Difference plots are presented where the water levels and current speeds in the Dredging, Wharf Dredging and Wharf Extension models were compared to those in the Pre-Works model. Plots of Stella Passage and the upper harbour show the large scale impacts to the hydrodynamics between modelling scenarios, while smaller scale plots within Stella Passage and Town Reach show the localised impacts on current patterns. Differences in water levels and current speeds over the entire southern basin are displayed in Figures AII.10 to AII.15 in Appendix II.

7.3.1 Water Levels

During a spring tide (Figure 7.7), the difference between modelled water levels at ADV Hairini in the upper harbour was less than 0.01 m. From visual comparisons of the entire tidal signal, there was no significant change in the phase of the tidal wave at ADV Hairini. Smaller scale plots of water levels during a high and low tide, inset in Figure 7.7, show a maximum increase in water levels of 0.006 m. The Dredging and Wharf Dredging models slightly increased the tidal amplitude at high and low tide whereas there was no significant change between the Pre-Works and Wharf Extension models. At low tide the slight increase in tidal amplitude at ADV Hairini suggested that the intertidal areas in the upper harbour may be exposed for a longer period of time (approximately 12 minutes) after both dredging works due to the slight increase in tidal amplitude; however the impact would be minor as the difference in elevation was less than 1 cm, which corresponds to the effect associated with a 1 hPa change in atmospheric pressure. After the wharves were constructed there was no significant change in exposure time at low tide. The phase of the tidal wave also speeds up in the Dredging and Wharf Dredging models. Peak high and low tide were approximately 5 minutes earlier than in the Pre-Works and Wharf Extension models.

As the changes in water levels between the modelling scenarios were small, difference plots were used to show the slight changes to water levels within Stella Passage and the upper harbour. Figure 7.8 displays the differences in water levels between low and high tide during a neap tide, and during a spring tide in Figure 7.9. At low tide (ebb) a negative difference in water level indicates a drop in water levels and an increase in tidal amplitude, and when tidal amplitude decreases there was a positive difference in water levels. Whereas at high tide (flood), a positive difference indicates an increase in tidal amplitude and water levels, and a negative difference a decrease. Comparing the Pre-Works to the three other modelling scenarios, the impacts of the various harbour works were larger during a spring tide than a neap tide. During a neap tide, the differences in tidal amplitude for all three of the altered modelling scenarios were only 0.005 m.

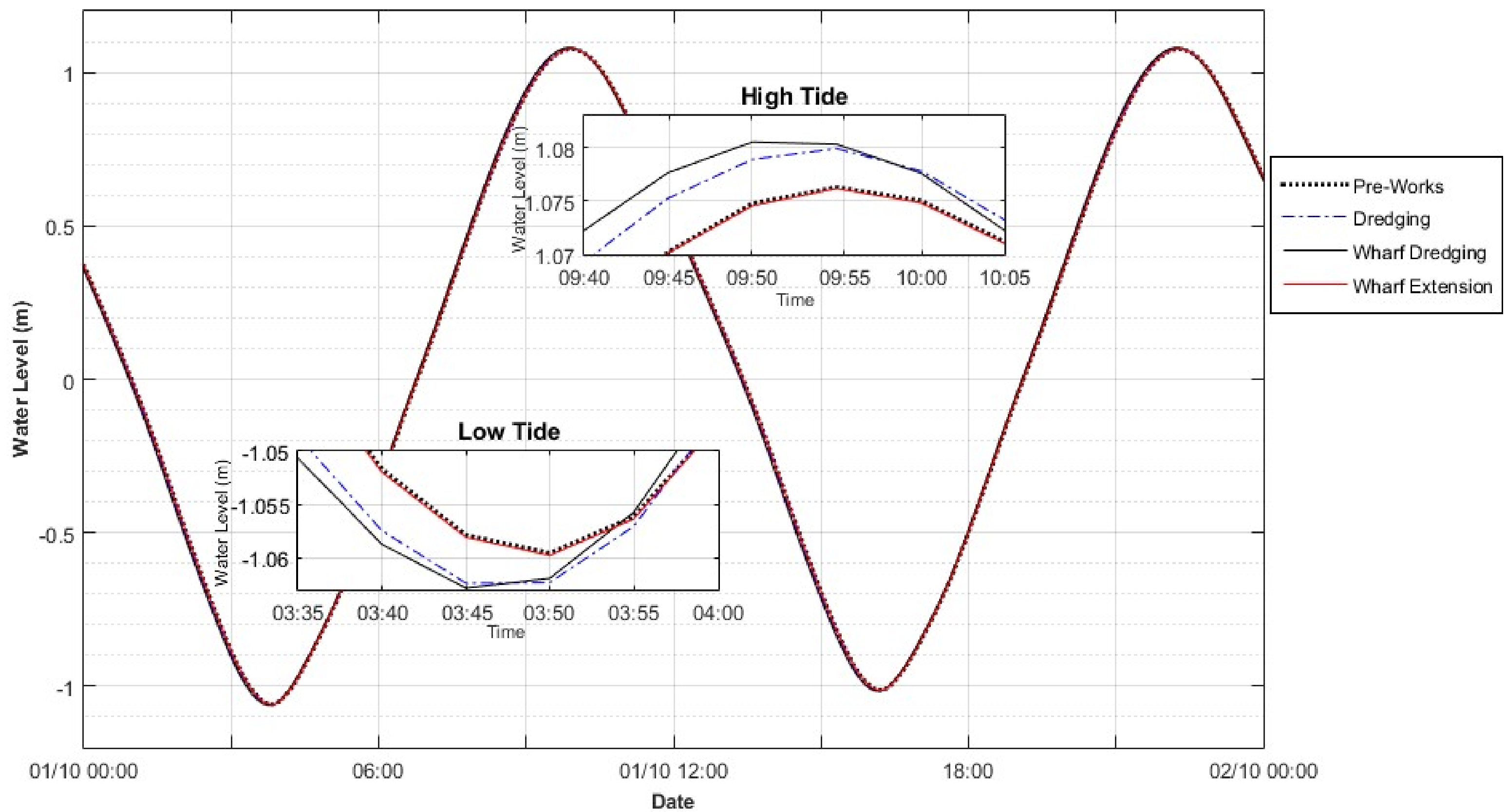

Figure 7.7: Difference in water levels at ADV Hairini at a low (ebb) and high (flood) tide between the four modelling scenarios from simulations of a spring tide.

Differences in water levels between the Pre-Works and altered modelling scenarios during a spring tide were larger in magnitude and affected more areas than those on a neap tide. As the tidal amplitudes were larger during a spring tide, so too were the impacts to the water levels from alterations to the bathymetry and harbour channels. From Pre-Works water levels, the tidal amplitude increased at low tide in all three of the altered modelling scenarios. At low tide in the Dredged model, tidal amplitude increased in almost all of the upper harbour beyond the Railway Bridge (the grey areas were the areas that were exposed at low tide and therefore had no water level). Tidal amplitude in the upper harbour increased again with the extension of the dredged area into Town Reach in the Wharf Dredging model. Water levels in Waipu Bay increased by 0.005 m, and Rangataua Bay, Welcome Bay and upstream and the approach to Hairini Bridge increased to have a difference of 0.015-0.025 m.

The addition of the wharves and associated reclamation in the Wharf Extension model decreased the impacts of the dredging on tidal amplitude in the upper harbour; the differences in water levels reduced between the Wharf Dredging and Wharf Extension models. At high tide, tidal amplitude increased by only 0.005 m over the entire upper harbour, apart from within Stella Passage where there was no difference. After the dredging was extended into Town Reach, there was no predicted differences in water levels in Waipu Bay.

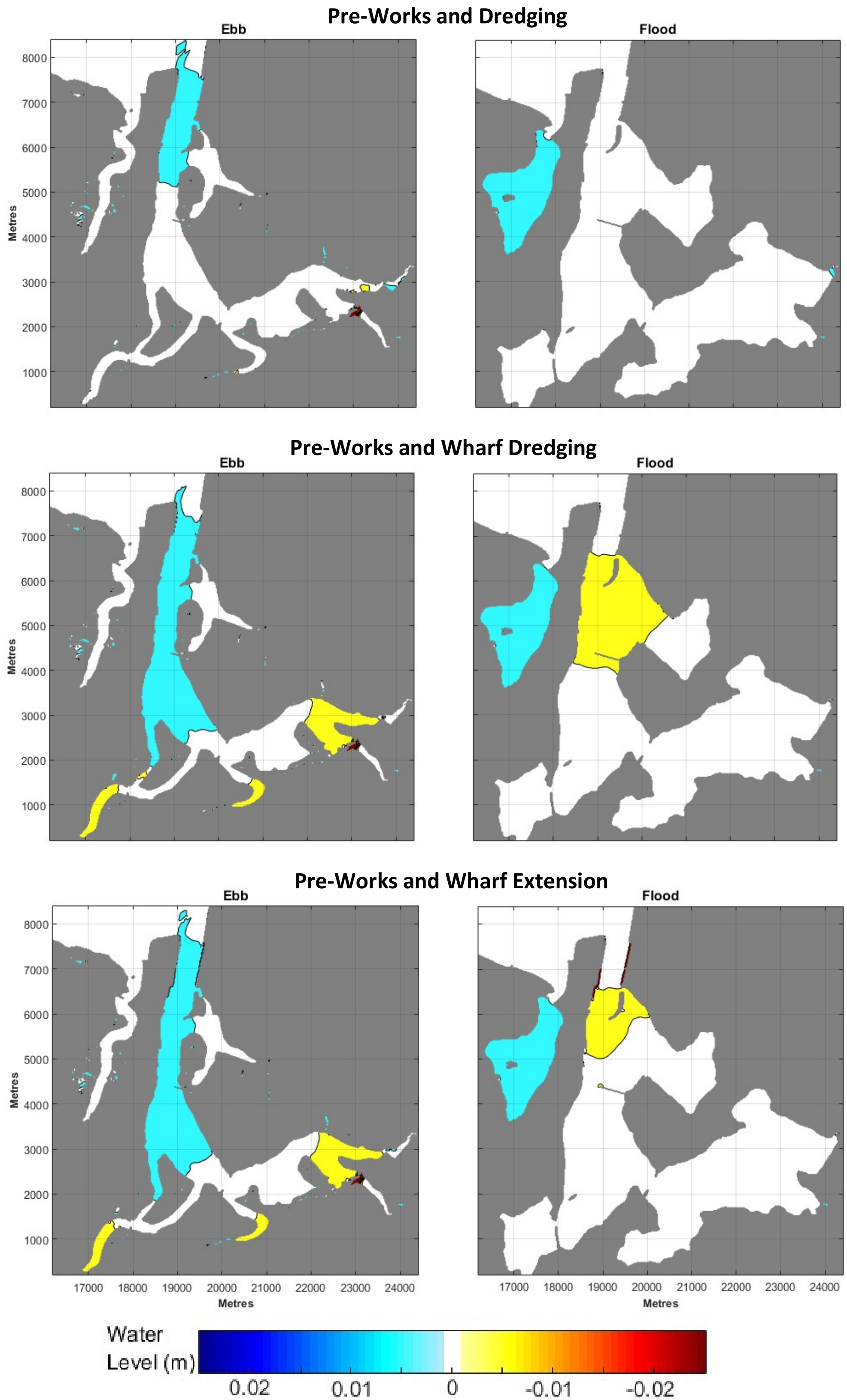

Figure 7.8: Difference in water levels between the Pre-Works and Dredging models, Pre-Works and Wharf Dredging models, and Pre-Works and Wharf Extension models at a low (ebb) and high (flood) tide from simulations of a neap tide in Stella Passage and the upper harbour.

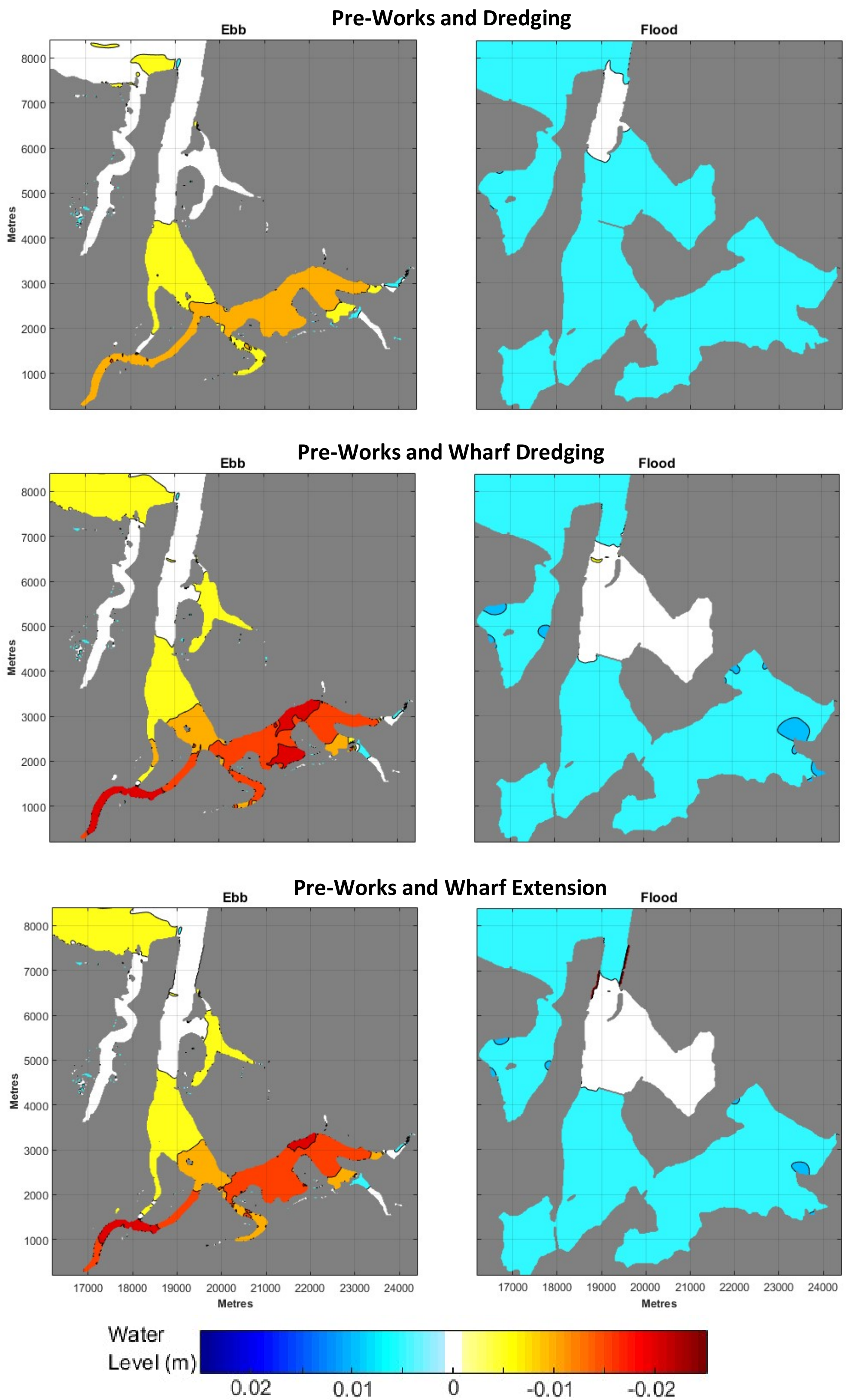

Figure 7.9: Difference in water levels between the Pre-Works and Dredging models, Pre-Works and Wharf Dredging models, and Pre-Works and Wharf Extension models at a low (ebb) and high (flood) tide from simulations of a spring tide in Stella Passage and the upper harbour.

7.3.2 Current Speeds

Maximum velocities at the four main observation points during an ebb and flood tide over both a neap and spring tide are presented for the four modelling scenarios in Table 7.1. Current speeds at the observation points were from model predictions at 5 minute intervals. Maximum spring ebb and flood velocities were larger than the maximums on a neap tide for all of the modelling scenarios; except on a flood tide at ADV Hairini which was 0.3 $m.s^{-1}$ during both a spring and neap tide in all of the models. Apart from a slight change to flood dominance at Marker 21 on a spring tide in the Dredging and Wharf Dredging models, the ebb or flood dominance at each observation point did not change between the modelling scenarios.

The Wharf Dredging model was the only modelling scenario to predict a change in maximum velocities at the three observation points in the upper harbour. Maximum velocities decreased by about 3.6 % at ADV Hairini on a spring ebb tide, increased by 2 % at ADV Maungatapu on a neap flood tide, and increased by 1.5 % at ADV Railway on a spring flood tide. The largest maximum velocities were predicted at ADV Railway in all four modelling scenarios. The smallest maximum velocities were at ADV Hairini in all models except the Wharf Dredging model which predicted smaller velocities at Marker 21. At Marker 21 in Stella Passage, there were small changes in maximum velocities at all stages of the tide in the Dredging model, with the largest difference being a decrease of 5.4 % at spring ebb tide. In the Wharf Dredging model the maximum velocities at Marker 21 decreased further by 50 % on both a neap and spring ebb tide, and decreased by 44 % and 48 % on a neap and spring flood tide respectively; reflecting the large increase in depth and cross-sectional area at Marker 21 in the Wharf Dredging model. In both the Wharf Dredging and Wharf Extension models, depths at Marker 21 increased as the dredged area extended into Town Reach. In the Wharf Extension model, the maximum velocities were similar to those in the Pre-Works model as the wharf extensions and reclamation reduced the channel width and partially compensated for the increase in depth. The smaller scale differences in Stella Passage between the Pre-works and Wharf Extension models, compared to the region around Marker 21, can be seen in the difference plots of current speeds and velocity vectors.

Table 7.1: Maximum velocities ($m.s^{-1}$) predicted at the four main observation points at a peak ebb and peak flood tide during a neap and a spring tide in the four modelling scenarios. The underlined values are the velocities that were different to the Pre-Works velocities. Note the neap and spring tidal periods were the same as those used in calibration.

	Pre-Works				**Dredging**				**Wharf Dredging**				**Wharf Extension**			
	Neap		**Spring**		**Neap**		**Spring**		**Neap**		**Spring**		**Neap**		**Spring**	
Observation Point	Ebb	Flood	Ebb	Flood	Ebb	Flood	Ebb	Flood	Ebb	Flood	Ebb	Flood	Ebb	Flood	Ebb	Flood
ADV Hairini	0.26	0.30	0.28	0.30	0.26	0.30	0.28	0.30	0.26	0.30	0.27	0.30	0.26	0.30	0.28	0.30
ADV Maungatapu	0.54	0.52	0.62	0.57	0.54	0.52	0.62	0.57	0.54	0.53	0.62	0.57	0.54	0.52	0.62	0.57
ADV Railway	0.72	0.59	0.83	0.70	0.72	0.59	0.83	0.70	0.72	0.59	0.83	0.71	0.72	0.59	0.83	0.70
S4 Marker 21	0.52	0.39	0.56	0.56	0.50	0.38	0.53	0.54	0.26	0.22	0.28	0.29	0.52	0.39	0.56	0.56

In Figure 7.8, the differences in peak ebb and flood current speeds during a neap tide in Stella Passage and the upper harbour were mostly localised around the dredging and wharf extensions. In all of the models, there was a slight increase in current speed of less than 0.03 $m.s^{-1}$ at peak ebb tide in the upper harbour; during flood tide there was also an increase but over a smaller area in the upper harbour. Current speeds decreased in Stella Passage in all three of the modelling scenarios; decreases were smaller at peak flood tide than peak ebb tide. The Dredging model predicted the smallest decrease in current speeds in Stella Passage, and the Wharf Dredging model predicted the largest decrease.

Differences in current speeds between modelling scenarios were largest during a spring tide. Figure 7.11, Figure 7.12 and Figure 7.13 show the differences between the Pre-Works model and the Dredging, Wharf Dredging and Wharf Extension models during a spring tide. Current speeds in the upper harbour increased on a spring tide and there was a slight decrease of less than 0.03 $m.s^{-1}$ in Waipu Bay on an ebb tide after the wharf extension dredging. Current speeds decreased in all of the dredged channels in the Dredging model.

In the Wharf Dredging and Wharf Extension models, current speeds decreased in the extended dredged area, but increased slightly on the eastern and western sides of Stella Passage on an ebb tide. The increases in current speeds at the sides of Stella Passage decreased in area slightly between the Wharf Dredging and Wharf Extension models. Decreases to current speeds extended into western Town Reach beyond the wharf extension dredging limits in the Wharf Dredging model, and to a lesser extent in the Wharf Extension model. In western Town Reach beyond the dredging limits, current speeds increased by approximately 0.3 $m.s^{-1}$ after the wharf extension dredging; the increase was larger on an ebb tide.

In the Wharf Dredging model, there was a small area in the middle of Stella Passage where current speeds decreased by approximately 0.27 $m.s^{-1}$; the same area as the S4 Marker 21 observation point. On a flood tide, current speeds increased under Aerodrome Bridge by less than 0.1 $m.s^{-1}$ in the Wharf Dredging model, and less than 0.3 $m.s^{-1}$ in the Wharf Extension model. In all three of the modelling scenarios, current speeds to the north of Sulphur Point in Otumoetai Channel increased.

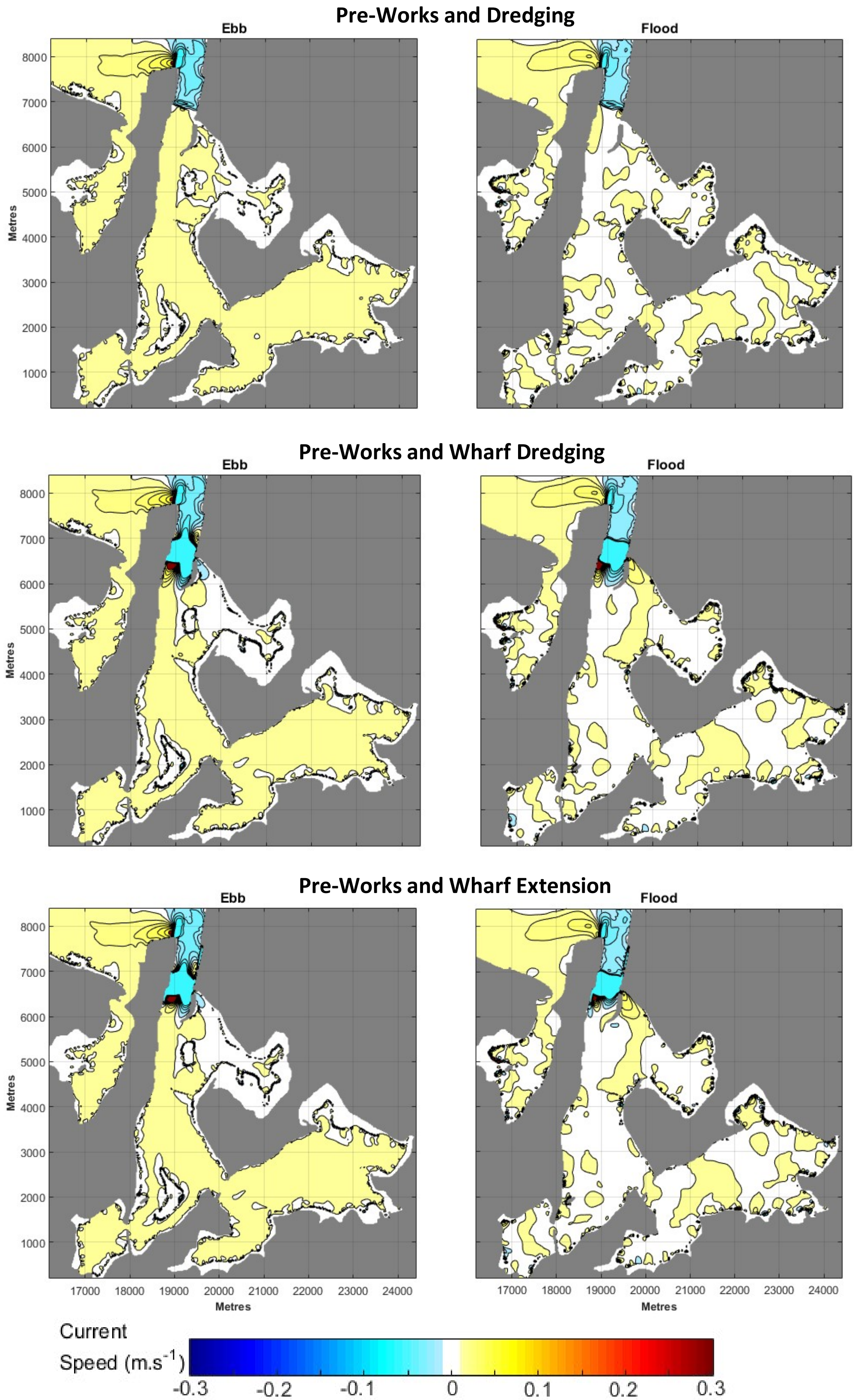

Figure 7.10: Difference in current speeds between the Pre-Works and Dredging models, Pre-Works and Wharf Dredging models, and Pre-Works and Wharf Extension models at peak ebb and peak flood tides from simulations of a neap tide in Stella Passage and the upper harbour.

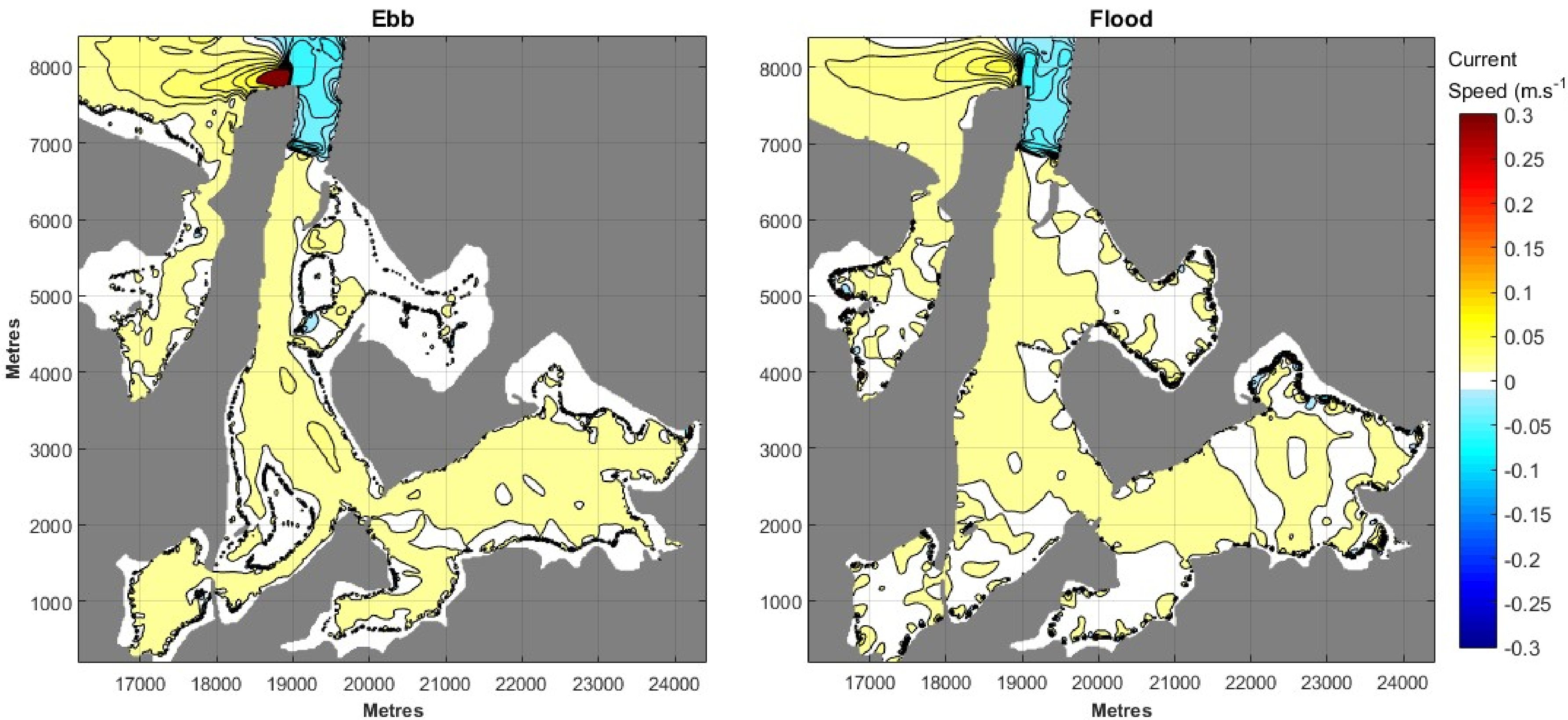

Figure 7.11: Difference in current speeds between the Pre-Works and Dredging models at peak ebb and peak flood tides from simulations of a spring tide in Stella Passage and the upper harbour.

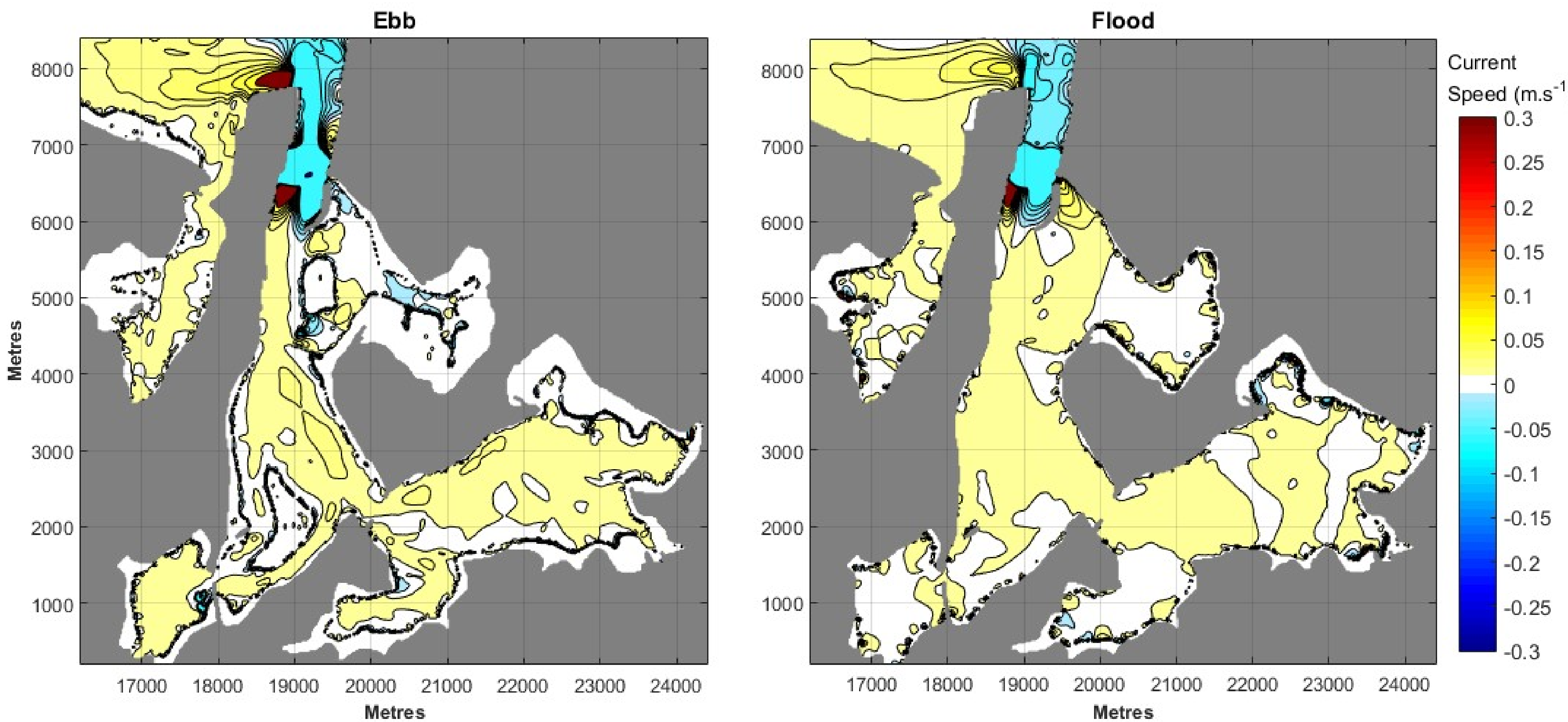

Figure 7.12: Difference in current speeds between the Pre-Works and Wharf Dredging models at peak ebb and peak flood tides from simulations of a spring tide in Stella Passage and the upper harbour.

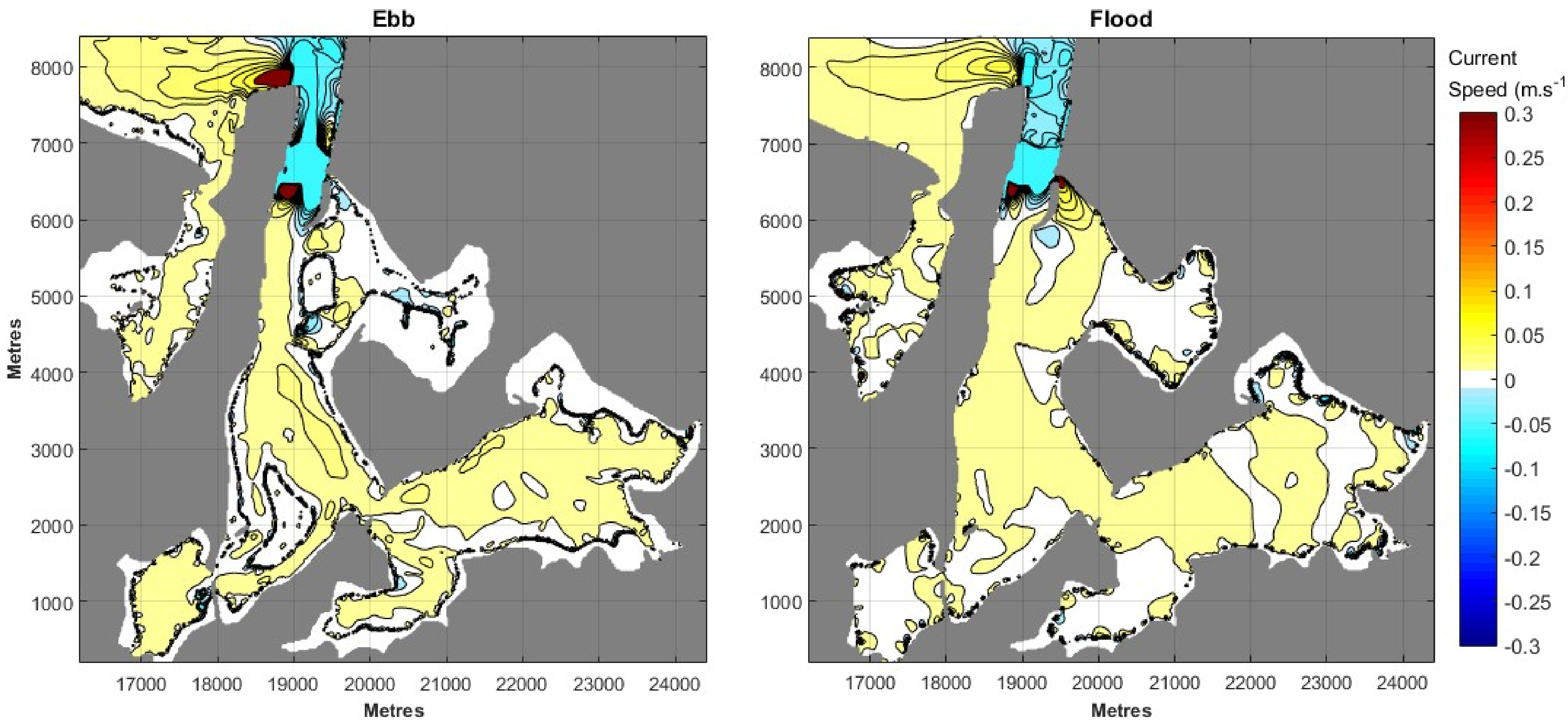

Figure 7.13: Difference in current speeds between the Pre-Works and Wharf Extension models at peak ebb and peak flood tides from simulations of a spring tide in Stella Passage and the upper harbour.

7.3.3 Localised Current Patterns

Localised impacts of the dredging and wharf extensions on the current patterns in Stella Passage and Town Reach are shown at peak ebb tide in Figure 7.14 and peak flood tide in Figure 7.15. Velocity vectors on an ebb tide were similar in the Pre-Works and Dredging models. Both had the largest current speeds through Town Reach under the Harbour Bridge with the greatest current speeds in the middle of the channel which decreased into the dredged Stella Passage. In the Wharf Dredging model, current speeds increased through Town Reach up to the new dredging drop-off and decreased in the newly dredged area. Current speeds decreased in the area and north of Tauranga Bridge Marina. There were only slight differences visible between the velocity vectors in the Wharf Dredging and Wharf Extension models where the wharves and reclamation were added; there were no velocity vectors in areas of the wharves and reclamation as thin dams blocked the flow. On an ebb tide, no significant change in the velocity vectors under Aerodrome Bridge and to the south of the Harbour Bridge causeway could be seen between the four modelling scenarios.

The velocity vectors on a flood tide were smaller in magnitude to those on an ebb tide. On a flood tide, the largest current speeds in all four modelling scenarios were in Town Reach south of the Harbour Bridge. The velocity vectors were similar in the Pre-Works and Dredging models but current speeds did increase slightly at the drop-off. After the dredging was extended, current speeds decreased in the dredged area and further south into Town Reach. In the Wharf Extension model the current speeds still decreased in the dredged area but did not decrease as far south into Town Reach. As on the ebb tide, current speeds reduced in the area and north of Tauranga Bridge Marina after the wharf extension dredging in Town Reach. Current speeds under Aerodrome Bridge were highest in the Wharf Extension model.

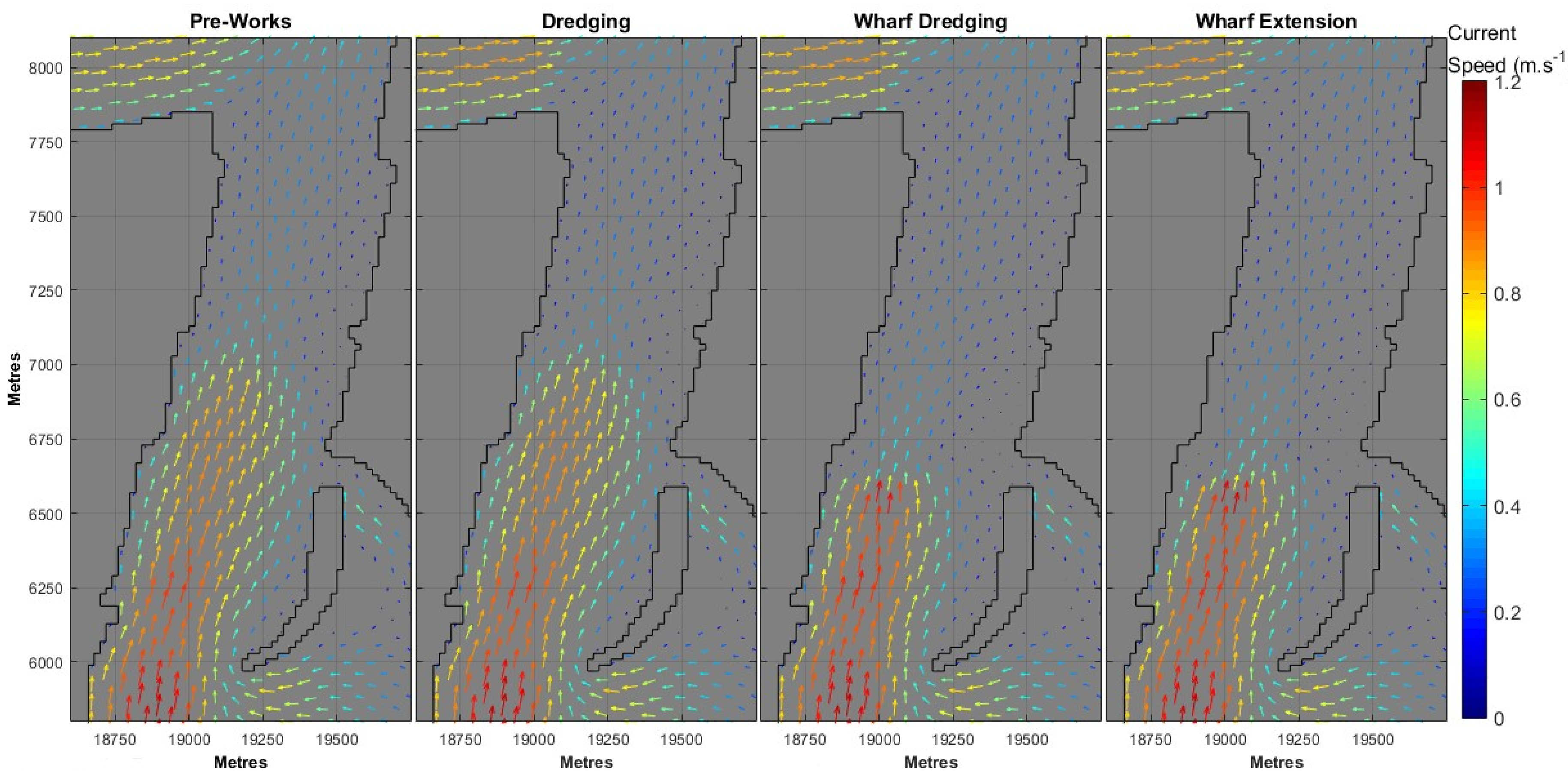

Figure 7.14: Velocity vectors and current speeds at a peak ebb tide in Stella Passage and Town Reach from simulations of a spring tide in the four modelling scenarios.

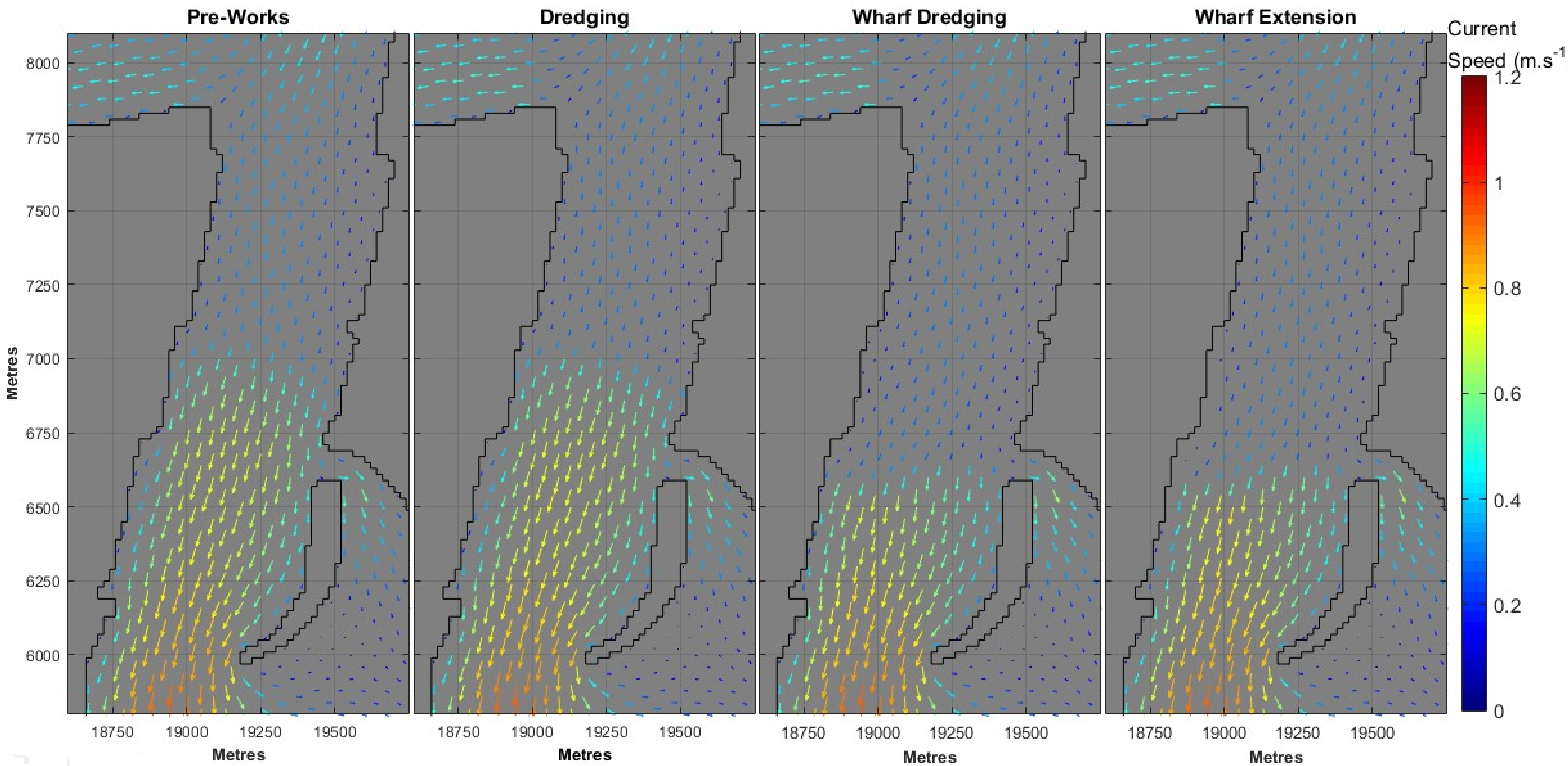

Figure 7.15: Velocity vectors and current speeds at a peak flood tide in Stella Passage and Town Reach from simulations of a spring tide in the four modelling scenarios.

7.4 Discussion

7.4.1 Impacts on the Upper Harbour

The small changes in the hydrodynamic conditions in the upper harbour that were predicted between the models were due solely to the harbour works modelled in each scenario. Within the upper harbour, differences in tidal amplitude and phase after the 2015-2016 capital dredging and the wharf extension dredging into Town Reach were due to the increase in tidal discharge. Dredging increased the cross-sectional area which increased the tidal discharge and sped up the tidal waves propagation into the upper harbour (Healy et al., 2009). The wharf extensions then decreased the cross-sectional area which increased the phase lag of the tidal wave (reducing the rate of propagation), bringing the water levels in the upper harbour back to the timing in simulated pre-works conditions. Tidal asymmetry at the four main observation points was unchanged throughout the modelling scenarios. Therefore, it is more likely that there would be no significant change in exposure time of the intertidal areas in the upper harbour.

From previous models it was determined that erosion and sedimentation in the upper harbour were most likely due to local processes rather than any changes in the dredged area (de Lange, 2011). Even the Southern Pipeline works which were within the upper harbour were only predicted to have localised effects, with impacts only extending a maximum of 50 m either side of the Railway Bridge (ASR, 2007). The small predicted impacts were consistent with those expected in a tidally dominated system, where the theory of equilibrium morphodynamics of systems such as the southern basin states that the influences of the tidal inlet system lessens with distance into the harbour (de Lange, 2011). Consequently, any changes to the tidal inlet system (such as dredging or wharf extensions) will also have lessening impacts with distance into the harbour (de Lange, 2011).

Changes to the hydrodynamics in the upper harbour were greatest during a spring ebb tide in the main channels, however the maximum differences in water levels and current speeds were still < 0.025 m and < 0.05 $m.s^{-1}$ respectively. Differences in water levels and current speeds in the upper harbour were smaller than the errors within the model, and significantly less than the natural fluctuations in environmental conditions. Changes in air pressure, wind speed and direction, wave height and rainfall will all cause larger changes to water levels and current speeds in the upper harbour than the predicted differences between the models.

7.4.2 Impacts on Stella Passage and Town Reach

The largest impacts on the hydrodynamics were localised around the dredging and wharf extension works. Current speeds and velocity vectors in Stella Passage and Town Reach changed with each harbour works modelled.

7.4.2.1 2015-2016 Capital Dredging

Overall, dredging has been found to reduce current speeds in dredged channels, increase current speeds in unaltered channels and reduce flow over shallow intertidal areas (de Lange, 2011). The 2015-2016 capital dredging increased the cross-sectional area of Stella Passage, reducing current speeds in Stella Passage and increasing current speeds in Town Reach. Increases in current speed in Town Reach were larger on an ebb tide as the increased depth of Stella Passage caused the ebb tidal flow to be pulled into the deeper channel (Healy et al., 2009). In previous numerical models of the 2015-2016 dredging works, changes to the hydrodynamics during a spring tide in Stella Passage were an advancement of the tidal phase by 5 minutes, an increase in high tide water levels of 0.02 m, and a decrease in current speeds of 40 % on an ebb tide and 12.5 % on a flood tide (de Lange, 2011). Impacts predicted in the Dredging model were less than those previously modelled by McKenzie (2014), with only a 5.4 % decrease in current speeds modelled at spring ebb tide at Marker 21.

The limited changes to current patterns between the Pre-Works and Dredging models in Figure 7.14 and Figure 7.15 support the conclusions of previous studies that the dredging will likely reinforce the existing sedimentation patterns of deposition at the southern end of Stella Passage (Healy et al., 2009). In the AEE for the dredging works, the report stated that an increase in deposition of fine sediments and organic seston would likely occur at the southern end of Stella Passage. The AEE also predicted the scour and eventual deposition of sediments at the north-western corner of Stella Passage at the end of Sulphur Point to be enhanced after the dredging works (Healy et al., 2009).

In investigations into previous dredging works, Kruger & Healy (2006) also found a decrease in velocity in the dredged channels throughout the harbour, which was attributed to not only the vertical stretching of the water column but to an increase in bottom friction. Dredging increased the variation in bathymetry, increasing the bottom friction in the main channels and decreasing the velocity. An increase in bottom friction increases the velocity shear and in turn promotes the formation of eddies and complex currents (Krüger & Healy, 2006). In this study however, bottom roughness was based on depth, and a minimum frictional value was given for the dredged area of Stella Passage in both the Pre-Works and Dredging models. Specifying the same frictional value in the modified area had the effect of reducing the influence of bottom friction within the main channels as a consequence of dredging.

7.4.2.2 Wharf Dredging and Extensions

The extension of the dredged area south into Town Reach in the Wharf Dredging model had the greatest impact on the local hydrodynamics. Current speeds decreased significantly within and slightly south of the dredged area due to the increased depth enlarging the cross-sectional area. The area to be dredged (Figure 7.2) extended further south on the western side of the channel as the Tauranga Bridge Marina restricted the area available to be dredged on the eastern side. The asymmetrical shape of the dredging extension channelled flow and increased current speeds on the western side of Town Reach, while decreasing the currents at Tauranga Bridge Marina. Over the drop-off there was vertical compression of the flow, accelerating currents over the drop-off on an ebb tide and decelerating currents on a flood tide (McKenzie, 2014). The wharf extension dredging moved the dredged boundary and thus changed the location of where the currents accelerate. The moving of the drop-off combined with the channelling of the flow to the west increased the current speeds in western Town Reach. The addition of the wharf extension dredging to the model also caused an increase in current speeds on both the eastern and western sides of Stella Passage directly in front of the original Sulphur Point and Maunganui wharves on an ebb tide.

The 44 % to 50 % decrease in maximum velocities at Marker 21 in Table 7.1 was larger than in the decreases shown in the difference plots of current speeds. The difference plots may not have shown as great a decrease, as model prediction over the entire grid were assessed every hour, whereas results at observation points were predicted every 5 minutes. It is unlikely that the maximum velocities would fall on the hour. Previous studies have also noted that errors may arise when comparing the water levels and current speeds between models at the same timestep as the modifications to the model may have altered the phase of the tide (de Lange, 2011). Therefore comparisons at the same timestep may not necessarily be showing the changes at the same part of the tidal curve. When comparing between observation points a phase adjusted predictions can be used to compare the true peak water levels and current speeds (de Lange, 2011). The maximum current speeds in Table 7.1 however do represent the maximum difference between the models for corresponding locations and times.

The wharf extensions and reclamation modelled in the Wharf Extension model reduced the impacts of the wharf extension dredging. The area where current speeds decreased receded back slightly into Stella Passage. Increased current speeds in western Stella Passage and Town Reach receded north. The increases in current speeds in front of the Sulphur Point and Maunganui wharves also lessened. Hydrodynamic impacts reduced as the dredging into Town Reach increased the cross-sectional area, whereas the wharf extensions decreased the cross-sectional area by narrowing the channel. Between the Wharf Dredging and Wharf Extension models, current speeds increased under Aerodrome Bridge by 0.2 $m.s^{-1}$ on a flood tide. Wharf extensions to the Maunganui wharves narrowed the channel approach under Aerodrome Bridge, constricting the flow and increasing current speeds.

The Sulphur Point wharf extension and dredging were modelled by Bell (1994) and McKenzie (2014). The dredging modelled by Bell (1994) was the same area as the proposed wharf extension dredging but only to a depth of 12.9 m. A more accurate prediction of the impacts of the wharf dredging and Sulphur Point wharf extension was modelled by McKenzie (2014) for the purpose of determining the combined impacts of the wharf extension and the future breakwater construction at Tauranga Bridge Marina. Bell (1994) stated that the largest changes to currents and potential sediment pathways were caused by the dredging of the ebb tidal shoal (Town Reach) rather than the wharf extensions and reclamation themselves. The dredging did not alter the larger current patterns, but did impact the localised current patterns within Stella Passage (Bell, 1994).

McKenzie (2014) and Bell (1994) both predicted an increase in current speed in western Stella Passage and an increase in peak ebb current speeds in front of the Sulphur Point wharves. The ebb tide no longer deflected to the eastern side of Stella Passage after the dredging was extended which caused current speeds to increase on the western side and a decrease in currents to the east. The increase was greatest in McKenzie's (2014) model where an increase of 0.3 $m.s^{-1}$ was predicted in front of the Sulphur Point wharves; which was larger than predictions in the Wharf Extension model. The increase in current speeds in front of Maunganui wharves was not predicted so may be directly caused by the Maunganui wharf extension which was not included in the previous models. In the Wharf Extension model the increases in current speeds in front of the Maunganui wharves were larger than the increases in front of the Sulphur Point wharves. The 0.3 $m.s^{-1}$ decrease in current speed north and in the location of the Tauranga Bridge Marina modelled by McKenzie (2014) were similar to the differences predicted in the Wharf Extension model. McKenzie (2014) predicted that the wharf extension and dredging would minimize the impact of the breakwater by reducing the increase in current speeds on the western side of Stella Passage and decreasing current speeds north of Tauranga Bridge Marina.

While the residual velocity and sedimentation patterns after the 2015-2016 dredging were predicted to be reinforced, alterations to the harbour morphology were greater for the wharf extension works. The large clockwise recirculating sediment transport loop covering Stella Passage and Town Reach was interrupted by the wharf dredging, which would change the sediment transport and dynamic equilibrium in the area. The ebb directed side of the clockwise residual velocity loop would be enhanced by the increased velocities along western Town Reach as ebb flows were drawn into Stella Passage. Consequently, the potential for erosion in western Town Reach increased. McKenzie (2014) also predicted that the increase in peak ebb currents from channelling of the flow through western Town Reach would increase the potential for erosion of the western side. Reduction in velocity in the dredged areas of Town Reach decreased the sediment transport potential and the low currents increased the potential for sedimentation of fine particles. The wharf extensions and reclamation would lessen the potential for sediment transport caused by the wharf extension dredging in Town Reach.

Changes to residual velocity patterns has been found to result in changes to the sediment transport pathways and morphology, but the actual impact will depend on the seabed facies and sediment sources (de Lange, 2011). Differences in current speeds change the sediment grain size and fluxes in an area (ASR, 2007). The change in sediment composition can balance out the effects of the changing hydrodynamics by creating a new dynamic equilibrium (ASR, 2007). In the southern basin it has been found that armouring of the sea floor from shell lag areas may prevent erosion despite the fact that the potential for sediment transport may have increased (de Lange, 2011). Shellfish are abundant in New Zealand estuaries, and it is common for shell lags to develop in high velocity areas where the faster currents remove the fine sands leaving shells (which have a higher threshold velocity) to form an armoured surface, protecting the seabed from erosion (ASR, 2007).

Armouring of sea beds is associated with high velocities within the southern basin (de Lange, 2011). Historically there has been an extension of the shell lag areas where currents and scour have increased, and a reduction in areas of decreased velocity; examples are the ebb and flood tidal deltas of the southern basin respectively (Healy et al., 2009). Investigations into the construction of the Railway Bridge found that the increased velocities around the bridge piers resulted in scour holes of 2.15 m in depth (ASR, 2007). However the increased velocities lead to the development of shell lags which stabilised the areas around the piers. If the shell lag did not develop the scour holes were predicted to have continued eroding (ASR, 2007).

Boulay (2012) identified the sediment facies and features within Stella Passage and Town Reach. Figure 3.9 to Figure 3.11 showed that shell lag facies dominated in Town Reach, with a smaller area to the west being comprised of very shelly medium sand. Boulay (2012) hypothesised that the Harbour Bridge construction, which increased current speeds through Town Reach after its construction, may have increased the grain size and shell density which lead to the shell lag surface and armouring of the flat shelf. Some of the shell lag surface is in the area to be removed in the wharf extension dredging. Current speeds in western Town Reach in the vicinity of the shelly medium sand area were predicted to increase, along with the sediment transport potential. However, erosion of western Town Reach may be prevented by the development of shell lag facies from increased current speeds removing the finer sediments. Once the seabed is armoured, erosion of western Town Reach may be minor. With the limited erosion, the predicted increase in sedimentation in the dredged area may reduce due to the lack of sediment availability. The development of shell lags will not occur immediately after the works and the sediments will be redistributed for a period before the full geomorphic impacts can be determined (de Lange, 2011).

It has been suggested that a staged approach to the harbour works may have less of an impact and allow the shell lags to develop between construction phases. Studies have found that for dredging works, the overall impacts of the works would be the same after a staged or non-staged dredging (de Lange, 2011). Staged works may reduce impacts within Town Reach if the western side is allowed to develop a shell lag surface before the next stage of construction. However impacts were also reduced by the decreases in current speeds after the construction of the wharves and reclamation in the Wharf Extension model. The variations in impacts between a staged works and completing the works in a short period may be minor.

CHAPTER EIGHT

CONCLUSION

8.1 Overview

The primary aim of this thesis was to predict the potential impacts of the wharf extensions on the hydrodynamics in Stella Passage and the upper harbour. The proposed wharf extensions included extending the existing Sulphur Point and Maunganui wharves, as well as the dredged channel south into Town Reach. The dredged sediments were to be used in reclamation behind the wharves and along the shoreline. Previous impact assessments have been carried out on sections of the wharf extension works but the full impacts had not been modelled. To achieve the primary aim, three thesis objectives were created. In this chapter a summary of how the thesis objectives were achieved and the key results and findings are given. Finally, recommendations are given for areas of further research and study.

8.2 Summary of Thesis Objectives

All of the thesis objectives listed in Chapter One were successfully completed. For the three thesis objectives, a summary of the key aspects and findings are presented below:

1) *Develop a hydrodynamic model of the southern basin of Tauranga harbour. Calibrate and verify the model with field data recorded by oceanographic instruments deployed over a spring and neap tide.*

A 2D hydrodynamic model of the southern basin was developed on the Delft3D FLOW modelling software. A 20 x 20 m rectangular grid was used and the bathymetry was compiled from a number of sources. The southern basin model simulated the hydrodynamics for 32 days from the 1st of September 2015. Sensitivity analysis was carried out to identify the key model parameters that influenced the model outcomes. The model parameters that were identified were bottom roughness, eddy viscosity and the drying and flooding threshold. During sensitivity analysis multiple simulation runs were carried out with four separate values of each model parameter specified in a total of 12 simulation runs. It was found that the bottom roughness value specified significantly influenced the model outcomes. As the preferred bottom roughness value varied over the model domain, a spatially varying bottom roughness map was developed based on depth.

Three ADVs and an S4 current meter were deployed from 3rd of September to the 2nd of October 2015, and the instruments recorded measurements of pressure and velocity within Stella Passage and the upper harbour. Additional data were obtained from existing tide gauges within the harbour. The southern basin model was calibrated and verified against the measured field data. Two four day periods over a neap and a spring tide were selected for calibration, while model outcomes were verified over an average tide. Visual comparisons were made between the model predictions and the measured water levels, current speeds and U and V velocities. Statistical analysis was also carried out to calculate the bias, accuracy and skill of the modelled water levels during calibration and verification. Bias was calculated using the mean while the accuracy was measured using the MAE and RMSE. The BBS was used as a measure of skill as it is commonly used in the evaluation of hydrodynamic models (Sutherland et al., 2004).

From visual comparisons the largest errors were in predicted current speeds. In all of the calibration and verification periods the patterns in errors for modelled current speeds were similar, but the magnitude of the error differed. The largest errors were during the spring calibration period. Overall, the timing and magnitude of the current speeds at ADV Hairini and S4 Marker 21 in Stella Passage were well predicted but the model failed to predict the larger ebb current speeds at S4 Marker 21. The ebb tidal dominance at ADV Maungatapu was not predicted by the model, and on the flood tide, current speeds were over-predicted by approximately 0.2 $m.s^{-1}$. Measured flood tidal dominance at ADV Railway was not replicated in the model as the current speeds on an ebb tide were over-predicted.

During all of the calibration and verification periods an 'excellent' skill score was obtained for water levels at every observation point within the model. For the neap calibration period, MAE was < 0.1 m at all sites except at ADV Hairini where it was 0.13 m. During the spring calibration period the majority of the observation sites had larger bias, MAE and RMSE than for the neap calibration period. The largest MAE of 0.16 m was at ADV Hairini, which tended to under-predict water levels; all other sites had a tendency to over-predict water levels. During the verification of an average tide, calculations of MAE were all

< 0.1 m. Errors in modelled water levels were determined to be predominantly due to errors in the phase. The error in phase increased with distance up the harbour which was attributed to the approximation of bathymetry by the model grid as the depths from conservative LINZ charts needed to be modified to better represent the area.

2) *Simulate and discuss the existing hydrodynamic conditions and inferred sediment transport pathways within Stella Passage and the upper harbour.*

The calibrated southern basin model was used to simulate the existing hydrodynamic conditions over a spring and neap period. Plots of water levels, current speeds, velocity vectors and residual velocities within Stella Passage and Town Reach displayed similar findings to previous studies of the area (Bell, 1994; Tay et al., 2013; McKenzie, 2014). The major features modelled within Stella Passage and Town Reach were:

- The acceleration of current speeds over the drop-off from the deeper dredged Stella Passage into the shallower Town Reach were caused by the change in cross-sectional area and depth.
- Constriction of the tidal flow in main channels enclosed by causeways increased current speeds, especially on an ebb tide.
- The ebb flow from Town Reach into Stella Passage accelerated over the drop-off and to form a jet that was deflected northeast by the Sulphur Point wharves which acted as a barrier to flow.
- The stronger ebb directed residuals and the recirculating clockwise loop of residual velocities in Town Reach indicated the potential for erosion in western Town Reach.

The largest influence on the hydrodynamics within the upper harbour beyond Stella Passage were the causeways which constricted the tidal flow, and the size and shape of the large estuaries and bays in the upper harbour. Attenuation of the tidal wave as it travelled through the harbour, resulted in a change in the timing of the high and low tides, or phase lag, between the lower and the upper harbour. Current speeds were higher in the main channels and lowest over the extensive intertidal areas. In the vicinity of the Railway Bridge, the greatest influence on the hydrodynamics was the Railway Bridge causeway. The causeway constricted the tidal flow and increased current speeds under the Railway Bridge. Eddies were evident in the residual velocities, and developed on the lee side of the causeway on both an ebb and flood tide as shadow zone areas of low current speeds created velocity gradients. Studies carried out as part of the Southern Pipeline investigation estimated a net sediment transport rate of < 20,000 m^3 per year (ASR, 2007).

Maungatapu Bridge causeway also constricted the tidal flow, but the shape and orientation of Rangataua Bay beyond the bridge was the main controlling aspect on the hydrodynamics in the area. An ebb dominant anticlockwise eddy developed east of Maungatapu Bridge, which was due to the drainage of the ebb tide through the main channel of Rangataua Bay. The lowest current speeds and residual velocities in the upper harbour were predicted at Hairini Bridge, even though the channel was constricted by a causeway. Hairini was ebb dominant as the influence of the freshwater discharge from Waimapu River was stronger than the tidal volume flowing into the area. Overall, the small residual velocities and small net sediment transport rates indicated that the general hydrodynamic conditions and morphology in the upper harbour were in dynamic equilibrium.

3) *Predict the impacts of the Port of Tauranga's 2015-2016 capital dredging and the proposed wharf extension works on the existing hydrodynamic conditions and the inferred sediment transport pathways within Stella Passage and the upper harbour.*

Hydrodynamic modelling of the 2015-2016 capital dredging and the proposed wharf extension works were carried out by altering the calibrated southern basin model within Delft3D to determine the potential impacts on the hydrodynamics resulting from the simulated changes. The wharf extension works were modelled in two stages, the first stage modelled the dredging extension into Town Reach while the second stage modelled the wharf extensions and reclamation. The four modelling scenarios were the Pre-works model (the southern basin model), the Dredging model, the Wharf Dredging model and the Wharf Extension model.

Predicted changes to the hydrodynamics from the dredging and wharf extensions were separated into the impacts on the upper harbour and the localised impacts within Stella Passage and Town Reach. Impacts on the upper harbour were greatest during a spring tide reflecting a larger asymmetry of the tide, but the changes to water levels and current speeds were < 0.025 m and < 0.05 $m.s^{-1}$ respectively. The predicted differences were significantly less than the error within the model and the impacts on hydrodynamic conditions due to changes in air pressure, waves, wind and other environmental conditions. Overall, it was predicted that the dredging and wharf extension works would have no significant impact on the hydrodynamics and sediment transport pathways within the upper harbour.

Previous studies have indicated that the largest impacts from changes to the harbour system were localised around the modified area (Bell, 1994; ASR, 2007; McKenzie, 2014). Bell (1994) and McKenzie (2014) predicted that larger current patterns would not be altered but the localised current patterns within Stella Passage and Town Reach were impacted. In the Dredging model the 2015-2016 dredging increased the cross-sectional area, which was predicted to reduce current speeds in the dredged Stella Passage and increase current speeds in the unaltered Town Reach. The largest difference was an increased current speed in Town Reach on an ebb tide. Predicted impacts of the 2015-2016 dredging were less than those previously modelled by McKenzie (2014). Existing patterns in sediment transport would be reinforced by the 2015-2016 capital dredging and the deposition of fine sediments at the southern end of Stella Passage would increase; depending on the availability of fine sediment (Healy et al., 2009).

The largest potential impact to the localised hydrodynamics was caused by the wharf extension dredging into Town Reach. In the dredged area, current speeds reduced significantly as the cross-sectional area increased. Current speeds increased within western Town Reach due to a combined effect of the asymmetrical shape of the dredging extension channelling flow and the southward movement of the dredged boundary drop-off. A decrease in current speeds in eastern Town Reach in the area of the Tauranga Bridge Marina, and a slight increase in current speeds directly in front of the original Sulphur Point and Maunganui wharves was also predicted. The addition of the thin dams simulating the construction of the wharf extensions and reclamation reduced the impacts of the wharf extension dredging. Changes to current speeds reduced in both magnitude and area as the wharves narrowed the channel, decreasing the cross-sectional area. Bell (1994) also determined that the largest changes to the hydrodynamics and sediment pathways would be caused by dredging in Town Reach rather than the wharf extensions and reclamation.

Localised patterns in sediment transport will be altered by the wharf extension dredging as the existing recirculating transport loop within Town Reach would be disrupted. Increased current speeds along western Town Reach may enhance the ebb directed western side of the residual velocity loop and increase the potential for sediment transport and erosion. Sedimentation would likely occur in the dredged area of Town Reach. Although the increase in current speeds in western Town Reach indicated that erosion may occur, the actual impacts on the sediment transport depends on the seabed facies (de Lange, 2011). Boulay (2011) identified that historically within Town Reach, increasing current speeds have led to the development of shell lag areas which then armoured the seabed. Shell lag areas may develop in Town Reach and protect against erosion. Therefore staged works may reduce the impacts on sediment transport by allowing time for the shell lag to develop.

8.3 Recommendations for Future Studies

The approximation of the bathymetry within the numerical grid was found to significantly affect the modelled current speeds. Improvements to the simulated hydrodynamics in the upper harbour, especially in the vicinity of Hairini Bridge, would require an extensive survey by LiDAR for the intertidal flats and hydrographic surveys of the channels to provide more accurate bathymetric datasets. As the upper harbour was found to be in dynamic equilibrium, continued surveying of the area beyond the Railway Bridge would not be needed once an accurate bathymetry dataset was available. Continued surveying is recommended for Stella Passage and Town Reach during and upon completion of the wharf extension works to monitor any changes to the system. The field data collected in this study by the three ADVs is the most extensive hydrodynamic dataset available for the upper harbour. To improve the confidence in the predicted flow patterns, it is recommended that additional field datasets be recorded within the upper harbour.

Deltares now offer a numerical modelling software with flexible mesh, the Delft3D Flexible Mesh Suite 2016 (Delft3D FM) (Deltares Systems, 2016).

Delft3D FM is the successor to the Delft3D FLOW software used to develop the southern basin model in this thesis. The new software allows the modeller to generate unstructured curvilinear grids that increase the resolution in specific areas of interest which increases the complexity and accuracy of the simulated hydrodynamics (Deltares Systems, 2016). It is recommended that any further numerical models simulating the potential impacts of the wharf extensions be developed on the Delft3D FM suite. A higher resolution can be applied over Stella Passage and Town Reach to model the larger localised impacts while still modelling any minor impacts in the upper harbour. Increasing the resolution by reducing the grid size in the Delft3D FLOW rectangular grid would have significantly increased computation times which were already around three days for the 32 day simulation.

Delft3D FM also offers the module D-Real Time Control which allows real-time control of hydrodynamic structures, ideal for modelling staged works in harbours (Deltares Systems, 2016). To fully assess the benefits of staged construction, a sediment transport model would need to be developed as this thesis identified that the advantages of staged construction were dependent on patterns in sediment transport and the behaviour of the surficial sediments. Future studies into the development of shell lag areas and scour may be key to mitigating the impacts of the continued harbour works at the Port of Tauranga. A 3D model within Stella Passage and Town Reach may also be beneficial if the need arises for complex modelling of flow under the wharves and scour around the piles.

The Port of Tauranga may benefit from the development of a complex hydrodynamic model. Constant modelling of future harbour developments would give accurate predictions of changes to current patterns and water levels, potentially saving time and resources on the management, construction and alterations to the harbour system. The forecasting of any potential changes to the harbour system would be an advantage in mitigating any impacts on the environment and aid the resource consent application process. The modelled currents would also aid with ship handling simulations.

REFERENCES

ASR. (2007). *Southern Pipeline: Estuarine and hydrodynamic physical process assessment.* Final Report 72. Report prepared for URS New Zealand Limited and Tauranga City Council. ASR Marine Consulting and Research, Tauranga, New Zealand. 282p.

Barnett, A. G. (1985). *Tauranga Harbour study: Part I overview and part III hydrodynamics.* Report prepared for the Bay of Plenty Harbour Board. Tauranga, New Zealand.

Bell, R. G. (1991). *Port of Tauranga model study: Deepened shipping channel proposal.* Consultancy report No. 6127/1. Report prepared for the Port of Tauranga Ltd. Water Quality Centre, Hamilton, New Zealand. 76p.

Bell, R. G. (1994). *Port of Tauranga model study: Sulphur Point wharf extension.* NIWA Consultancy report No. POT 002/1. Report prepared for the Port of Tauranga Ltd. National Institute of Water and Atmosphere (NIWA), Hamilton, New Zealand. 85p.

Black, K. P. (1984). *Tauranga Harbour study: part IV sediment transport.* Report prepared for the Bay of Plenty Harbour Board. Tauranga, New Zealand.

Boulay, S. O. C. (2012). *Analysis of multibeam sonar data for benthic habitat characterization of the Port of Tauranga, New Zealand.* MSc thesis, University of Waikato, Hamilton, New Zealand.

Cea, L., & French, J. R. (2012). Bathymetric error estimation for the calibration and validation of estuarine hydrodynamic models. *Estuarine, Coastal and Shelf Science, 100*, 124-132.

CliFlo. (2016). *National Climate Database*. Retrieved from http://cliflo.niwa.co.nz/

Davies-Colley, R. J. (1976). *Sediment dynamics of Tauranga Harbour and the Tauranga Inlet.* MSc thesis, University of Waikato, Hamilton, New Zealand.

Davies-Colley, R. J., & Healy, T. R. (1978). Sediment and hydrodynamics of the Tauranga entrance to Tauranga Harbour. *New Zealand Journal of Marine and Freshwater Research, 12*(3), 225-236.

de Lange, W. P., & Healy, T. R. (1990). Wave spectra for a shallow meso-tidal estuarine lagoon: Bay of Plenty, New Zealand. *Journal of Coastal Research, 6*(1), 189-199.

de Lange, W. P. (2011). Statement of evidence of Willem Pieter de Lange. In *Te Runanga o Ngai te Rangi Iwi Trust & others v Bay of Plenty Regional Council & others, ENV-2010-AKL-000185*.

de Lange, W. P., Moon, V. G., & Johnstone, R. (2015) Evolution of the Tauranga Harbour Entrance: Influences of tsunami, geology and dredging. *Proceedings of the Australasian Coasts & Ports Conference 2015* (pp. 7). Wellington, New Zealand.

Deltares Systems. (2013). *Delft3D-FLOW: Simulation of multi-dimensional hydrodynamic flows and transport phenomena, including sediments*. [User Manual: Hydro-morphodynamics]. Rotterdamseweg, The Netherlands: Deltares.

Deltares Systems. (2016). *Delft3D Flexible Mesh Suite*. [Brochure]. Rotterdamseweg, The Netherlands: Deltares.

Fletcher Construction. (1985). *Tauranga Harbour crossing: Design report.* Report prepared for Tauranga Harbour Bridge Committee. The Fletcher Construction Company Ltd, Tauranga, New Zealand. 33p.

Fletcher Construction. (1986). *Tauranga Harbour crossing: Schedule 1 & 2.* Report prepared for the Tauranga City Council and Tauranga Harbour Bridge Committee. The Fletcher Construction Company Ltd, Wellington, New Zealand. 33p & 22p.

Hancock, N., Hume, T., & Swales, A. (2009). *Tauranga Harbour sediment study: Harbour bed sediments.* NIWA client report HAM2008-123. NIWA project BOP09216. Report prepared for Environment Bay of Plenty. National Institute of Water and Atmosphere (NIWA), Hamilton, New Zealand. 65p.

Hansen, N. G. (1997). *History of Tauranga Harbour & Port*. Tauranga, New Zealand: Author.

Healy, T. R. (1985). *Tauranga Harbour study: Part II field data collection and V morpholgical study.* Report prepared for the Bay of Plenty Harbour Board. Tauranga, New Zealand.

Healy, T. R. (1994). *Harbour shoreline erosion fronting Whareroa Marae: Causes and possible remedies.* Report prepared for the Tauranga District Council. University of Waikato, Hamilton, New Zealand. 30p.

Healy, T. R. (1996). *Review of the capital dredging impacts for the Port of Tauranga Ltd 1992 major channel deepening and widening programme.* Report prepared for the Port of Tauranga Ltd. Hamilton, New Zealand.

Healy, T. R., Cole, R., & de Lange, W. P. (1996). Estuarine shores: Evolution, environments and human alterations. In K. F. Nordstrom & C. T. Roman (Eds.), *Geomorphology and ecology of New Zealand shallow estuaries and shorelines* (pp. 115-154). London: Wiley & Sons.

Healy, T. R., Thompson, G., Grace, R. V., & Spiers, K. (2009). *Assessment of Environmental Effects for Port of Tauranga channel deepening and widening.* Report prepared for the Port of Tauranga Ltd. University of Waikato, the Port of Tauranga Ltd, & Marine Biological Consultants, Tauranga, New Zealand 220p.

Hume, T. M., Bell, R. G., de Lange, W. P., Healy, T. R., Hicks, D. M., & Kirk, R. M. (1992). Coastal oceanography and sedimentology in New Zealand, 1967-91. *New Zealand Journal of Marine and Freshwater Research, 26*, 1-36.

Hume, T. M., Snelder, T., Weatherhead, M., & Liefting, R. (2007). A controlling factor approach to estuary classification. *Ocean and Coastal Management, 50*(11-12), 905-929.

Hydraulics Research Station. (1968). *Tauranga Harbour investigation: Report on second stage.* Consultancy report No. ex 395. Report prepared for the Port of Tauranga Ltd. Hydraulics Research Station, Wallingford, Berkshire, England.

InterOcean Systems. (2016). *InterOcean Systems Inc*. S4 current meter family. Retrieved April, 2016, from http://www.interoceansystems.com/s4main.htm.

Krüger, J. C., & Healy, T. R. (2006). Mapping the morphology of a dredged ebb tidal delta, Tauranga Harbour, New Zealand. *Journal of Coastal Research*, 720-727.

LINZ. (2015). *Standard port tidal levels*. Retrieved from http://ww.linz.govt.nz/hydro/tidal-info/tide-tables/tidal-levels

McKenzie, J. S. (2014). *Predicted hydrodynamic and sediment transport impacts of breakwater construction in Tauranga Harbour, New Zealand.* MSc thesis, University of Waikato, Hamilton, New Zealand.

NIWA. (2016). *NIWA tide forecaster* Retrieved from https://www.niwa.co.nz/services/online-services/tide-forecaster

Pawlowicz, R., Beardsley, B., & Lentz, S. (2002). Classical tidal harmonic analysis including error estimates in MATLAB using T-TIDE. *Computers and Geosciences, 28*(8), 929-937.

Port of Tauranga Ltd. (1988). *Sulphur Point wharves: Environmental Impact Assessment.* Report prepared for the Port of Tauranga Ltd. Tauranga, New Zealand. 19p.

Port of Tauranga Ltd. (1990). *Tauranga wharves - extension No.1: Environmental Impact Assessment.* Report No. 327-0-18. Report prepared for the Port of Tauranga Ltd. Tauranga, New Zealand. 24p.

Port of Tauranga Ltd. (1994). *Environmental Impact Assessment: Sulphur Point wharf extension No.2 -north (1994).* Report prepared for the Port of Tauranga Ltd. Tauranga, New Zealand. 48p.

Resource Management Act. (1991). Wellington, New Zealand. Retrieved from http://www.legislation.govt.nz/act/public/1991/0069/latest/whole.html#DLM230265.

Schwartz, M. L. (2005). *Encyclopedia of coastal science* Encyclopedia of earth sciences series. Dordrecht, The Netherlands: Springer.

SonTek. (2011). *Triton-ADV*. [Brochure]. San Diego, CA: SonTek/YSI.

Spiers, K. C., Healy, T. R., & Winter, C. (2009). Ebb-jet dynamics and transient eddy formation at Tauranga Harbour: Implications for entrance channel shoaling. *Journal of Coastal Research, 25*(1), 234-247.

Sutherland, J., Peet, A. H., & Soulsby, R. L. (2004). Evaluating the performance of morphological models. *Coastal Engineering, 51*(8–9), 917-939.

Tay, H. W., Bryan, K. R., de Lange, W. P., & Pilditch, C. A. (2013). The hydrodynamics of the southern basin of Tauranga Harbour. *New Zealand Journal of Marine and Freshwater Research, 47*(2), 249-274.

Thompson, G. S. (2001). *Assessment of Environmental Effects: Sulphur Point wharf extension No.2 - north (2001).* Report prepared for the Port of Tauranga Ltd. Tauranga, New Zealand. 62p.

Winthrop, M. (2014). Stretching the point. *Engineering Insight, 14*(2), 16-19.

APPENDIX I

CALIBRATION AND VERIFICATION PLOTS

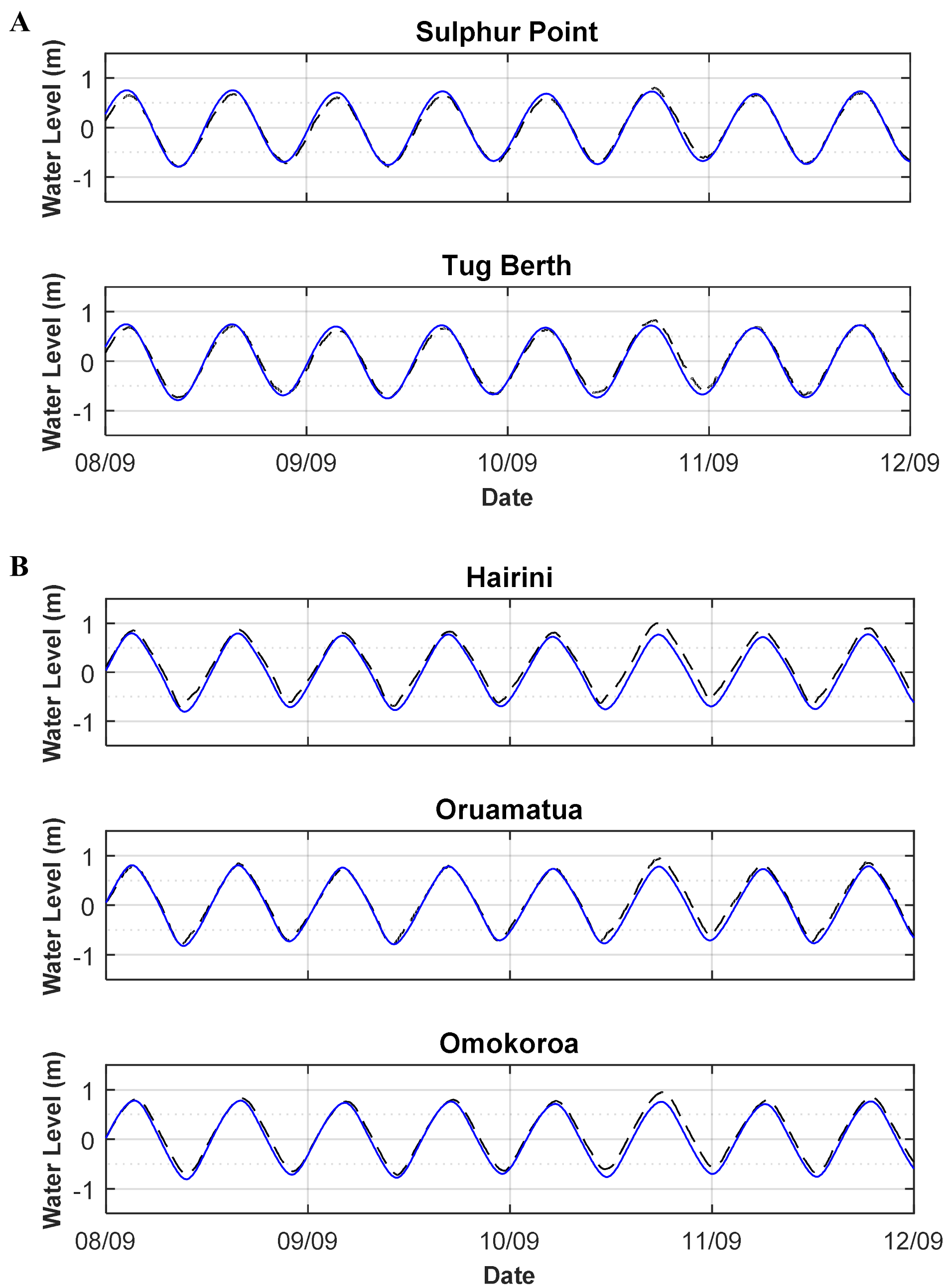

Figure AI.1: Neap calibration plots of measured (black dashed line) and modelled (solid blue line) water levels from the 8th to the 12th September 2015 at the Port of Tauranga (A) and BOPRC (B) tide gauges.

A

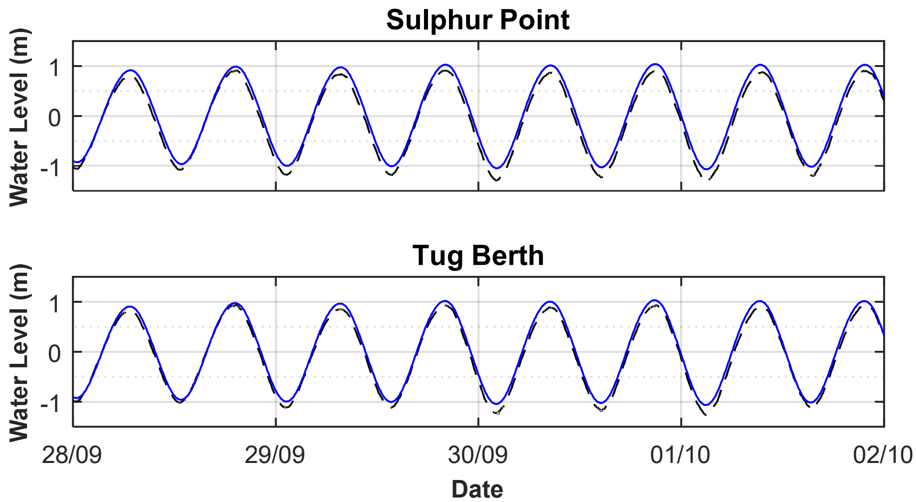

B

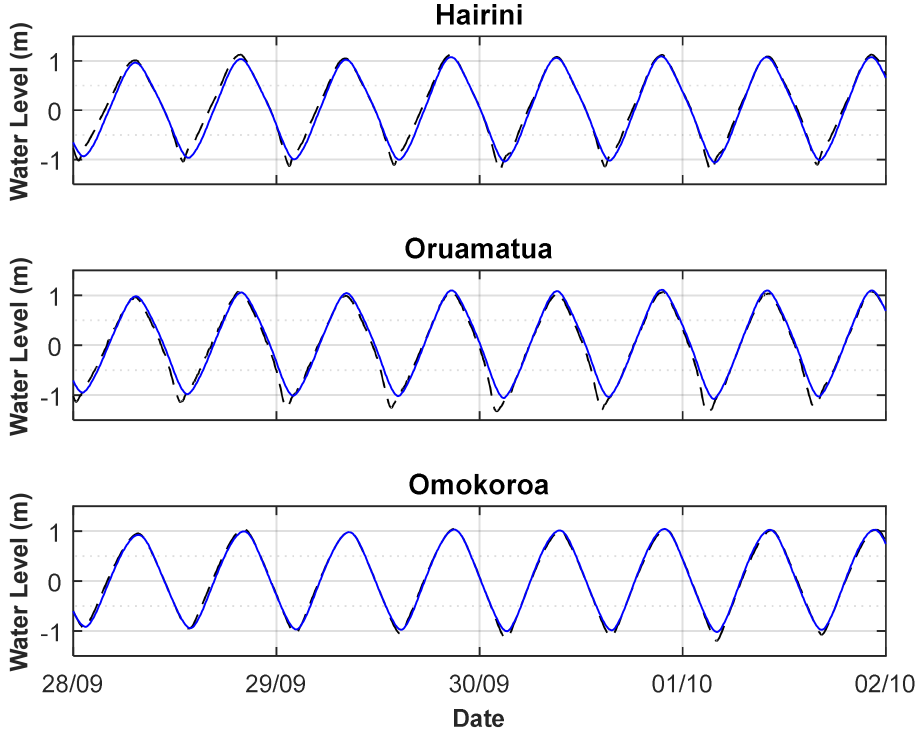

Figure AI.2: Spring calibration plots of measured (black dashed line) and modelled (solid blue line) water levels from the 28th September to the 2nd October 2015 at the Port of Tauranga (A) and BOPRC (B) tide gauges.

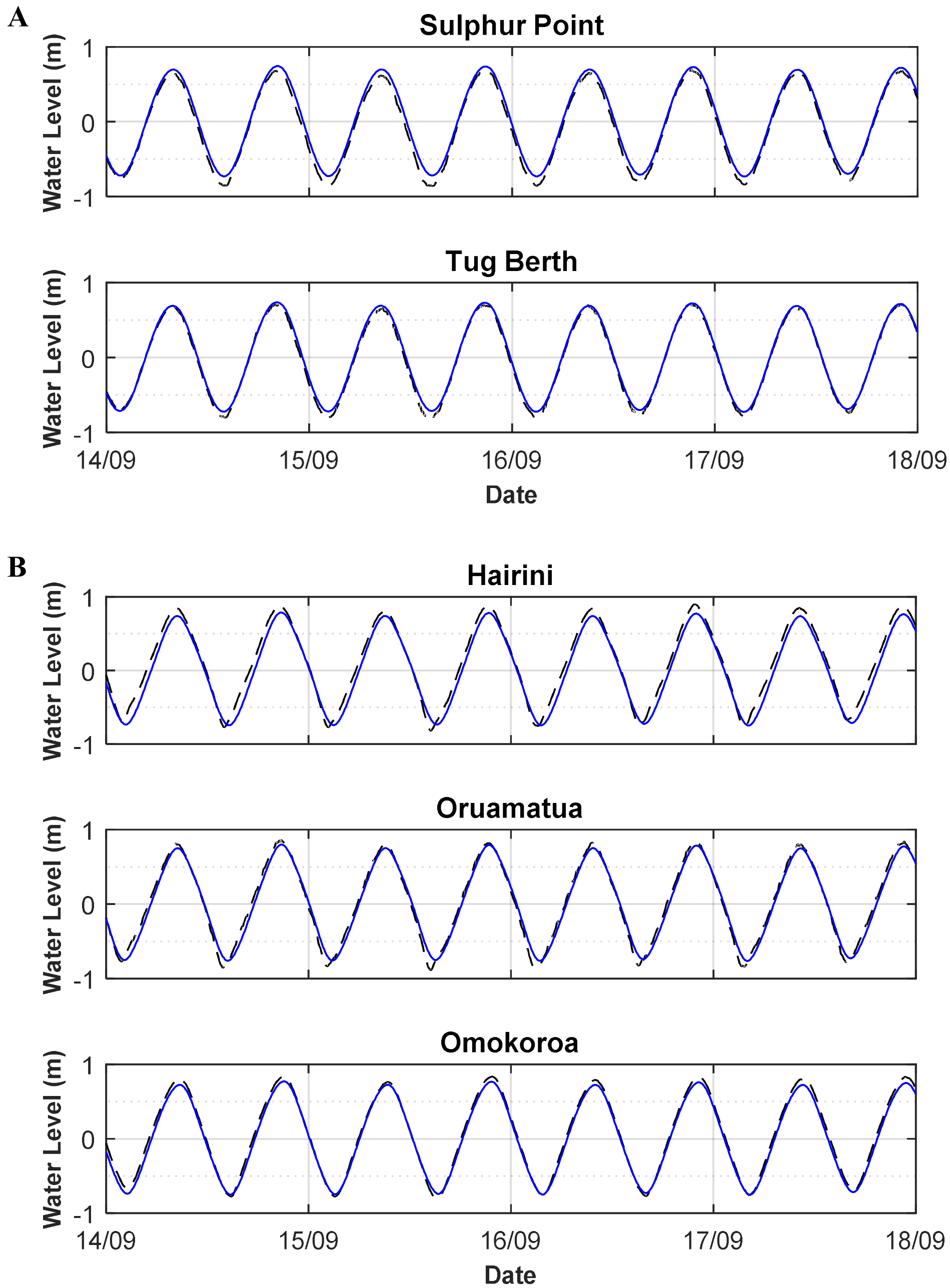

Figure AI.3: Verification plots of measured (black dashed line) and modelled (solid blue line) water levels from the 14th to the 18th September 2015 at the Port of Tauranga (A) and BOPRC (B) tide gauges.

APPENDIX II
HYDRODYNAMIC IMPACTS ANALYSIS

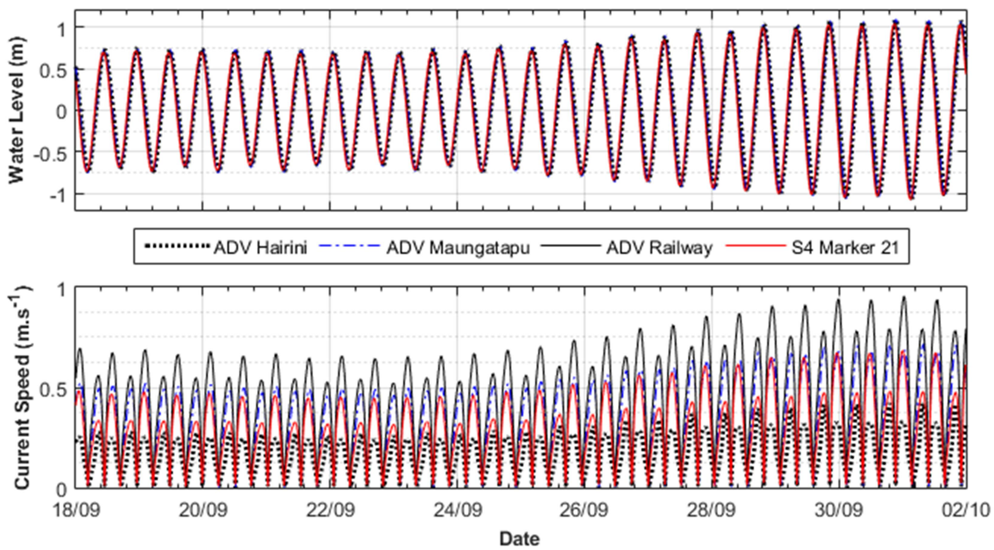

Figure AII.1: Water levels and current speeds over a 14 day period from simulations of a neap and spring tide in the Dredging model from the 18th September to the 2nd October 2015 at ADV Hairini, ADV Maungatapu, ADV Railway and the S4 at Marker 21.

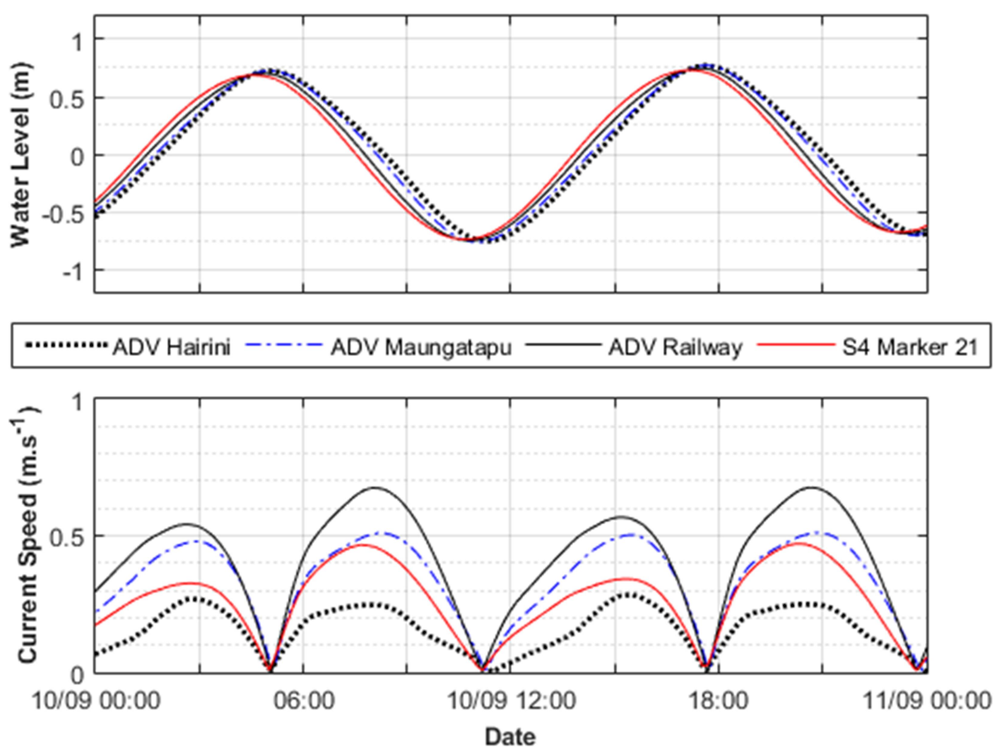

Figure AII.2: Water levels and current speeds from simulations of a neap tide in the Dredging model from the 10th to the 11th September 2015 at ADV Hairini, ADV Maungatapu, ADV Railway and the S4 at Marker 21.

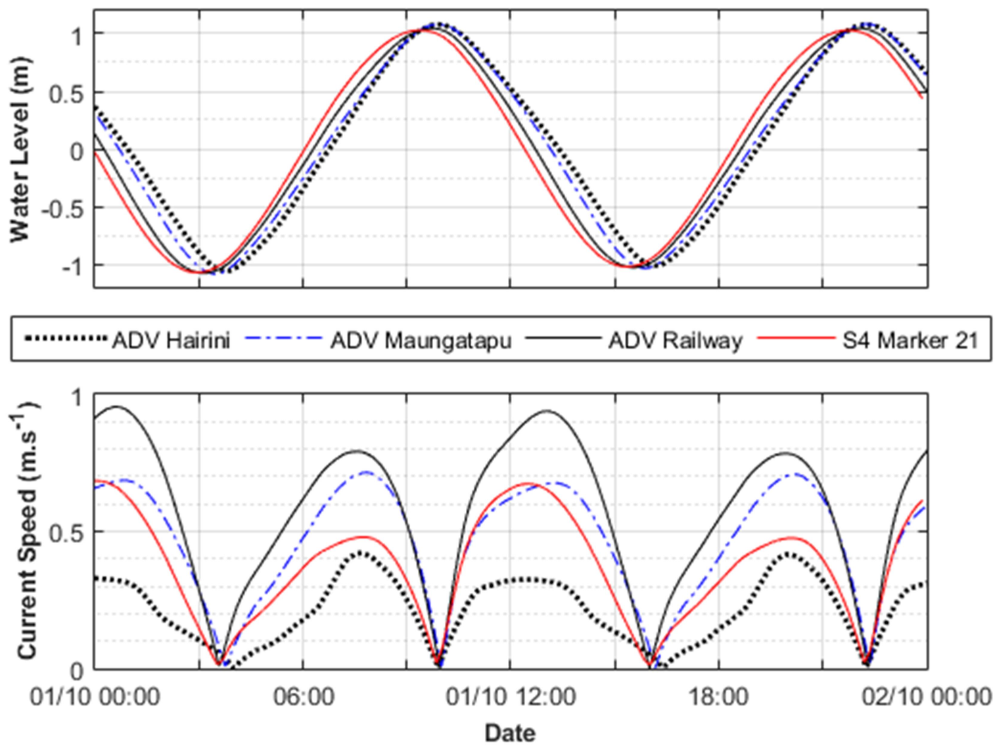

Figure AII.3: Modelled water levels and current speeds from simulations of a spring tide in the Dredging model from the 1st to the 2nd October 2015 at ADV Hairini, ADV Maungatapu, ADV Railway and the S4 at Marker 21.

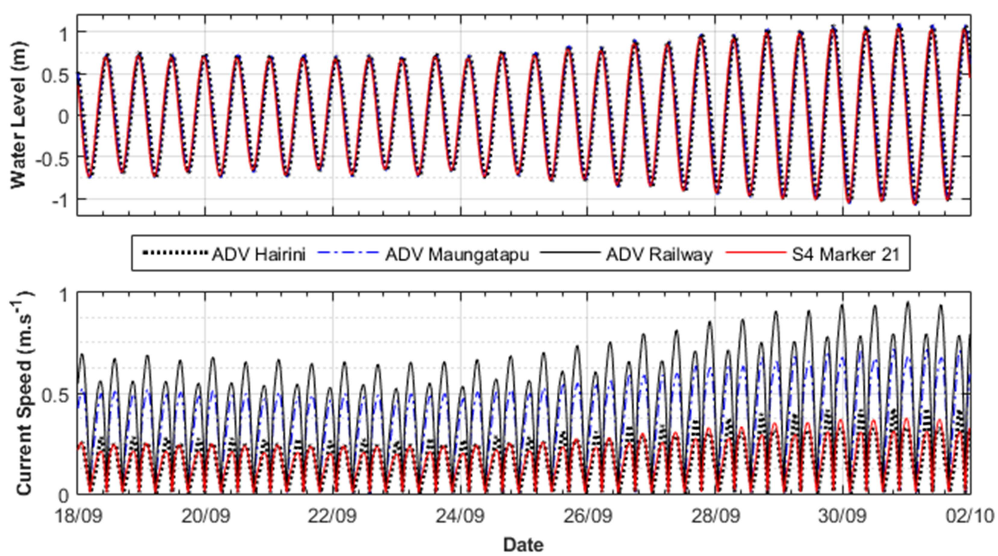

Figure AII.4: Water levels and current speeds over a 14 day period from simulations of a neap and spring tide in the Wharf Dredging model from the 18th September to the 2nd October 2015 at ADV Hairini, ADV Maungatapu, ADV Railway and the S4 at Marker 21.

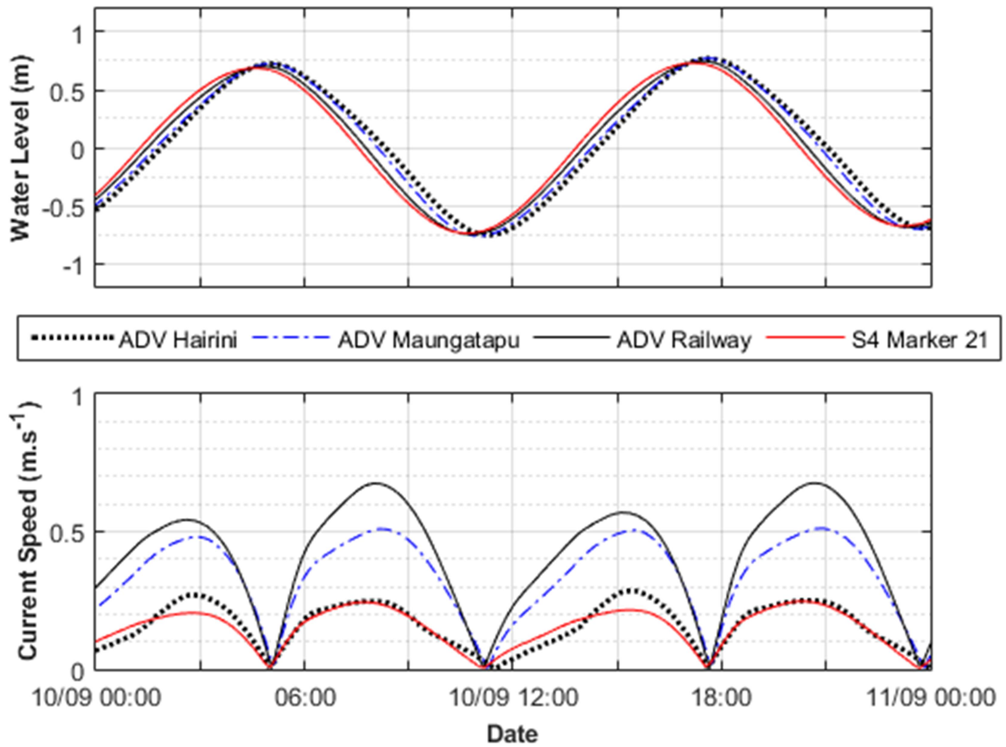

Figure AII.5: Water levels and current speeds from simulations of a neap tide in the Wharf Dredging model from the 10th to the 11th September 2015 at ADV Hairini, ADV Maungatapu, ADV Railway and the S4 at Marker 21.

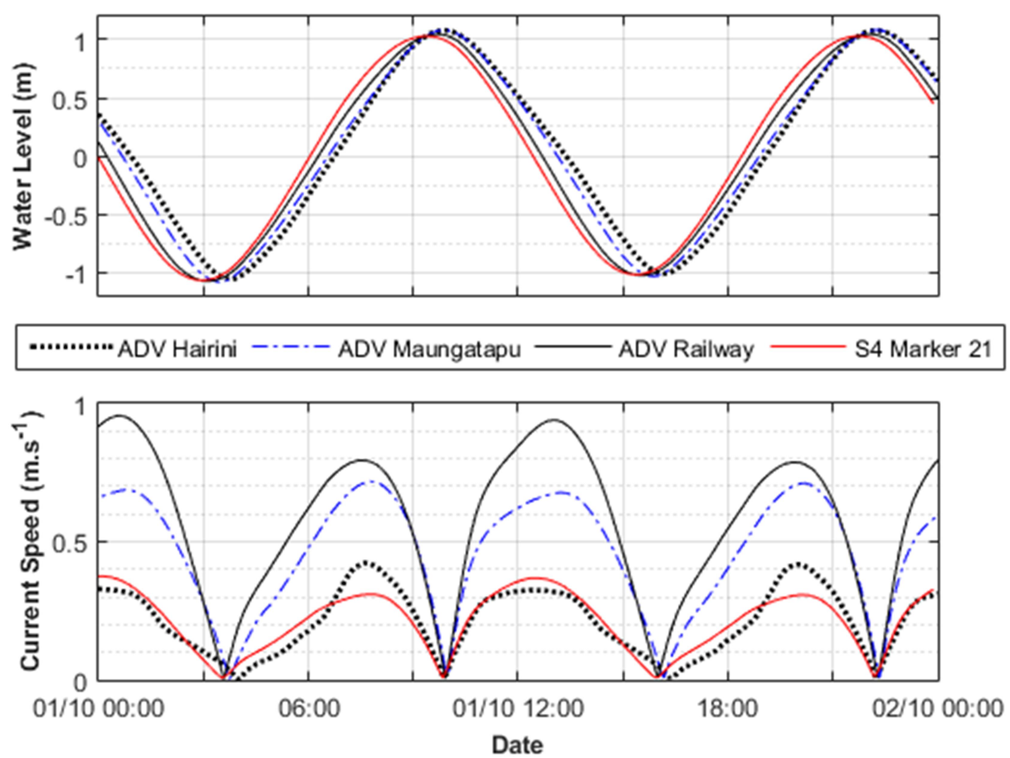

Figure AII.6: Modelled water levels and current speeds from simulations of a spring tide in the Wharf Dredging model from the 1st to the 2nd October 2015 at ADV Hairini, ADV Maungatapu, ADV Railway and the S4 at Marker 21.

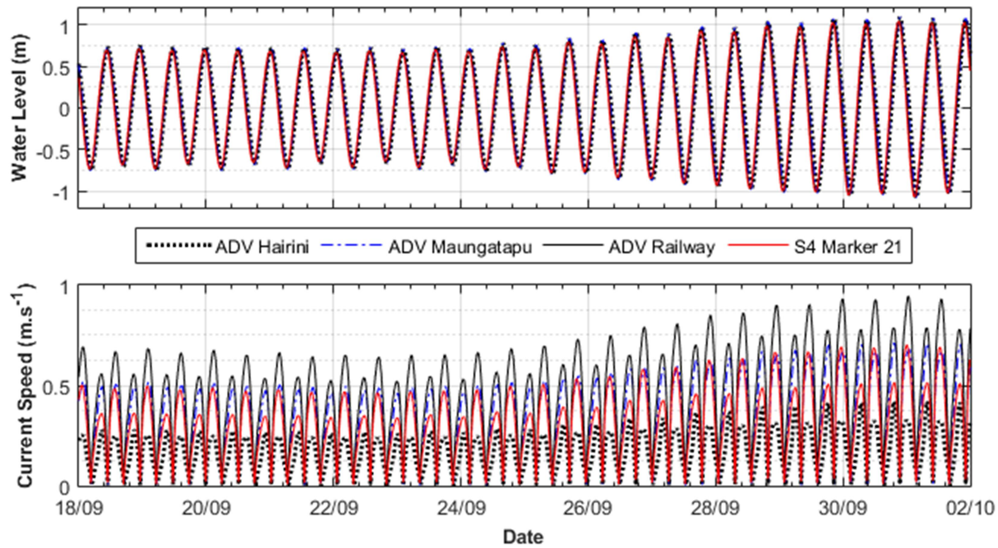

Figure AII.7: Water levels and current speeds over a 14 day period from simulations of a neap and spring tide in the Wharf Extension model from the 18th September to the 2nd October 2015 at ADV Hairini, ADV Maungatapu, ADV Railway and the S4 at Marker 21.

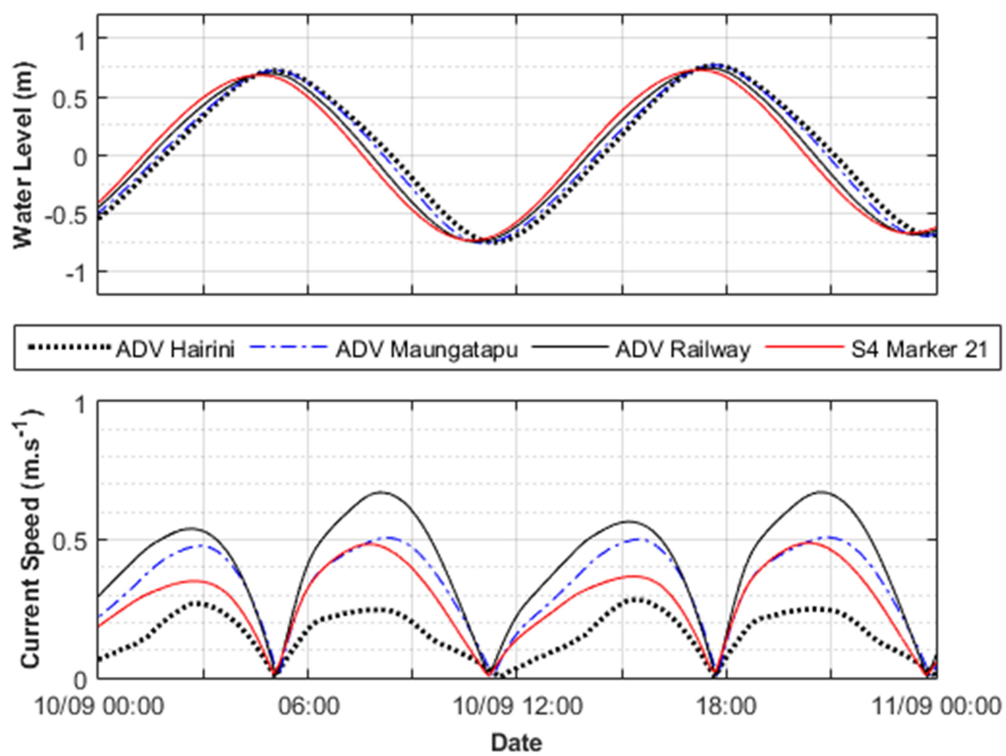

Figure AII.8: Water levels and current speeds from simulations of a neap tide in the Wharf Extension model from the 10th to the 11th September 2015 at ADV Hairini, ADV Maungatapu, ADV Railway and the S4 at Marker 21.

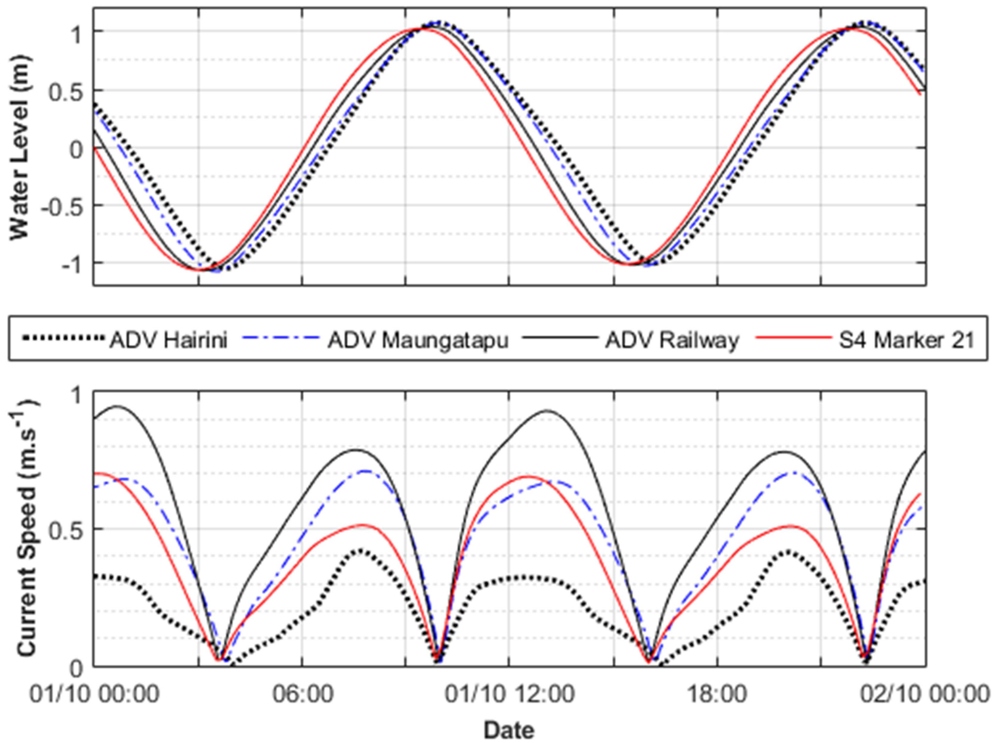

Figure AII.9: Modelled water levels and current speeds from simulations of a spring tide in the Wharf Extension model from the 1st to the 2nd October 2015 at ADV Hairini, ADV Maungatapu, ADV Railway and the S4 at Marker 21.

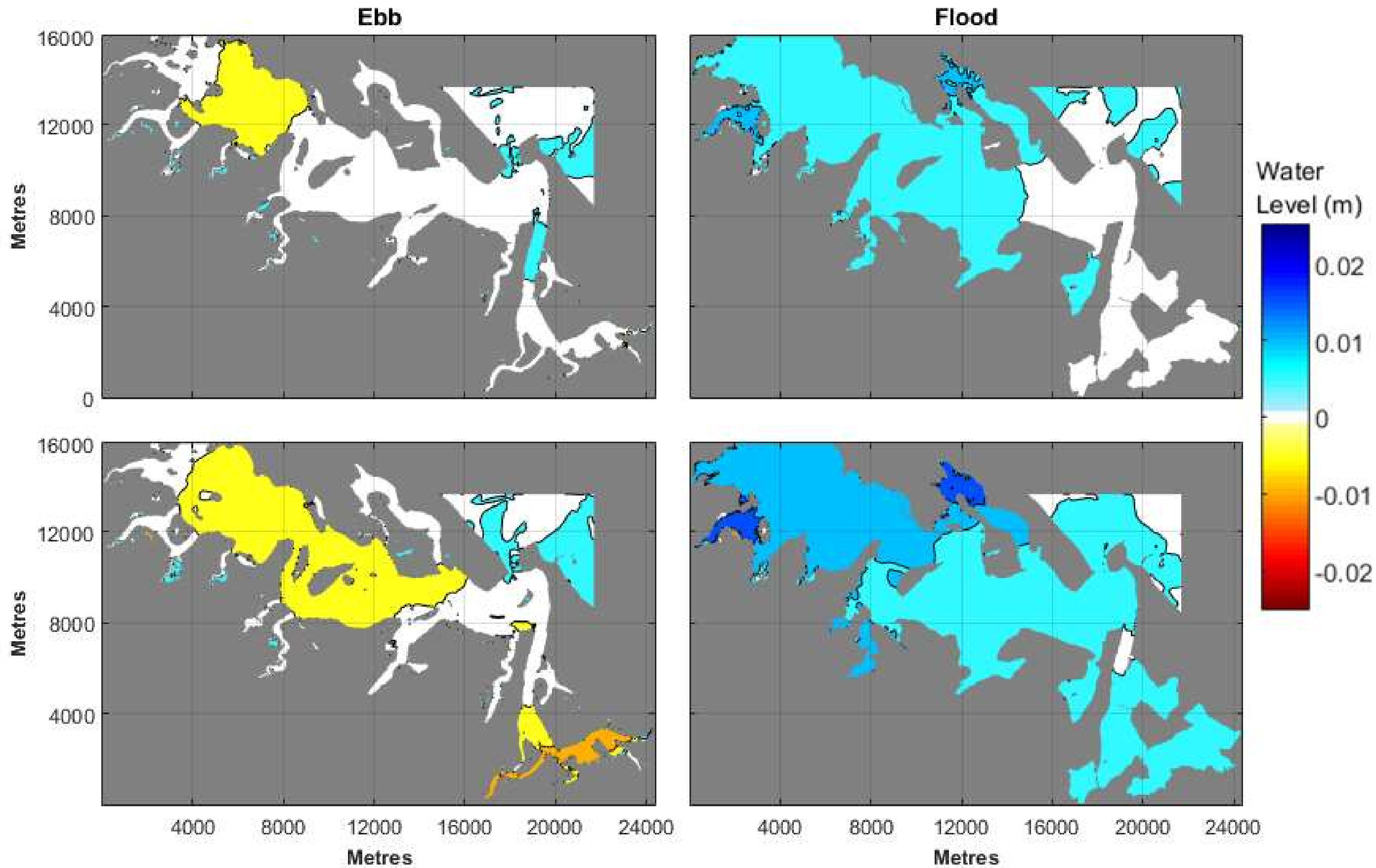

Figure AII.10: Difference in water levels between the Pre-Works and Dredging models at a low (ebb) and high (flood) tide from simulations of a neap (top) and spring tide (bottom) in the southern basin of Tauranga Harbour.

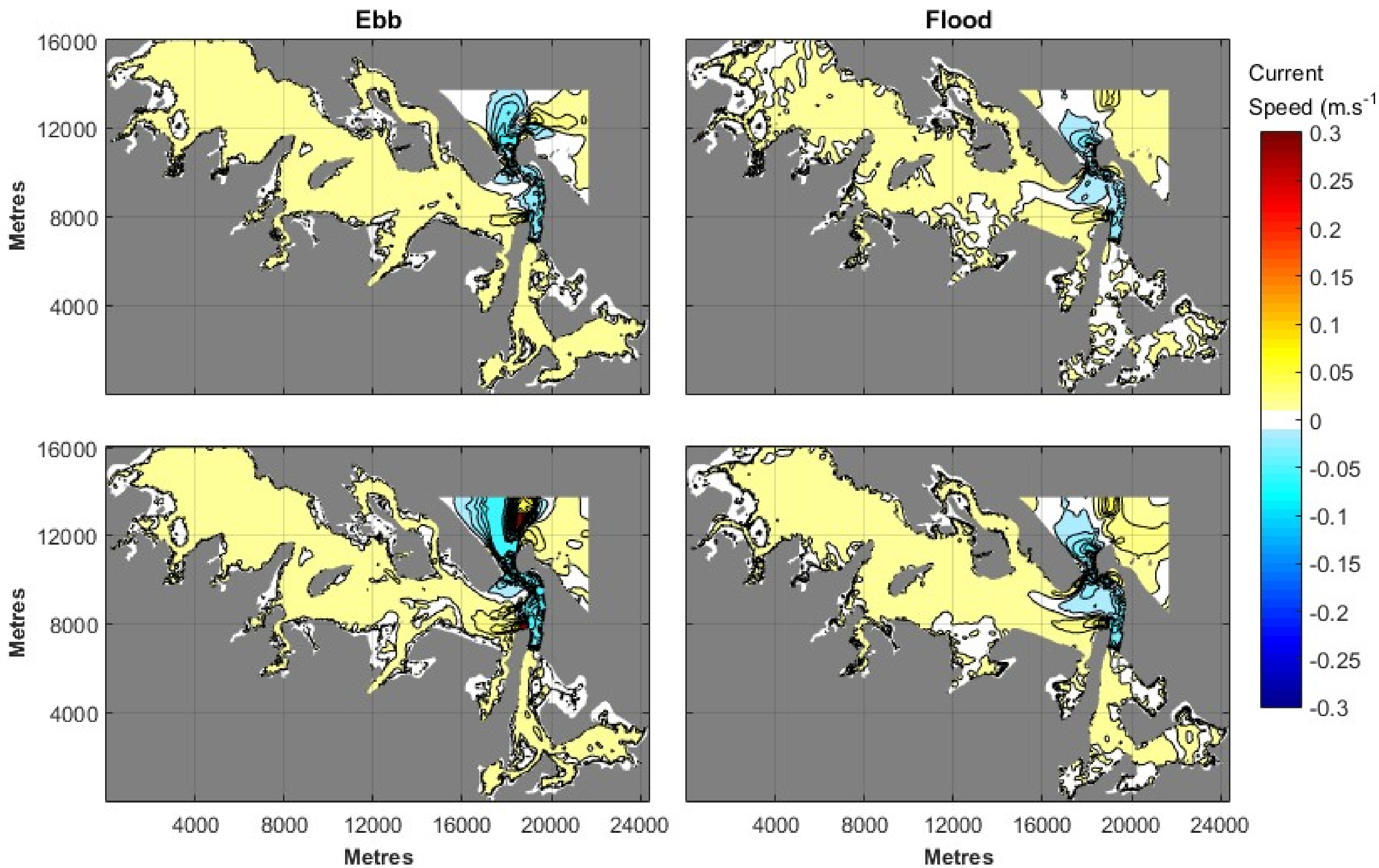

Figure AII.11: Difference in current speeds between the Pre-Works and Dredging models at peak ebb and peak flood tides from simulations of a neap (top) and spring tide (bottom) in the southern basin of Tauranga Harbour.

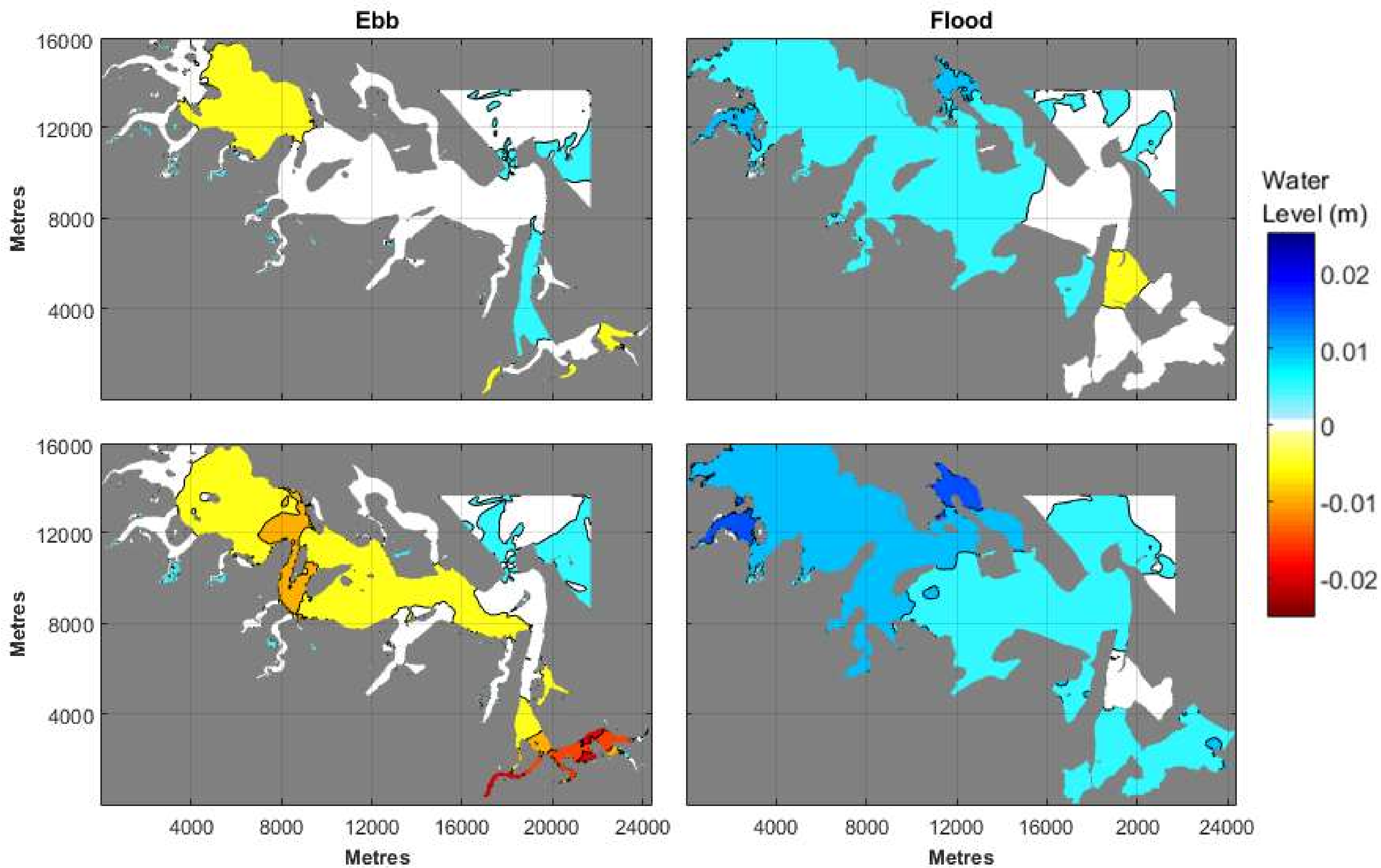

Figure AII.12: Difference in water levels between the Pre-Works and Wharf Dredging models at a low (ebb) and high (flood) tide from simulations of a neap (top) and spring tide (bottom) in the southern basin of Tauranga Harbour.

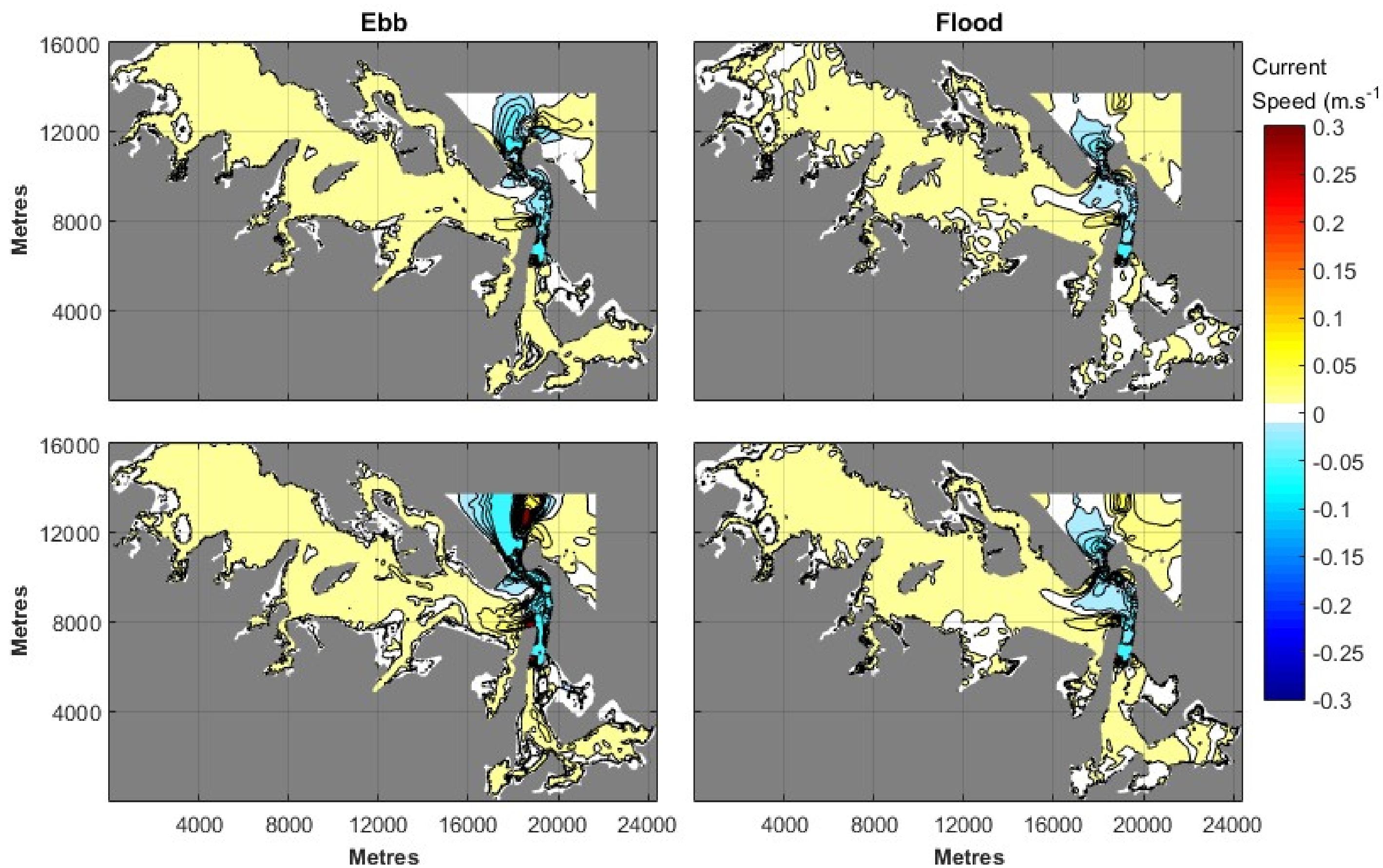

Figure AII.13: Difference in current speeds between the Pre-Works and Wharf Dredging models at peak ebb and peak flood tides from simulations of a neap (top) and spring tide (bottom) in the southern basin of Tauranga Harbour.

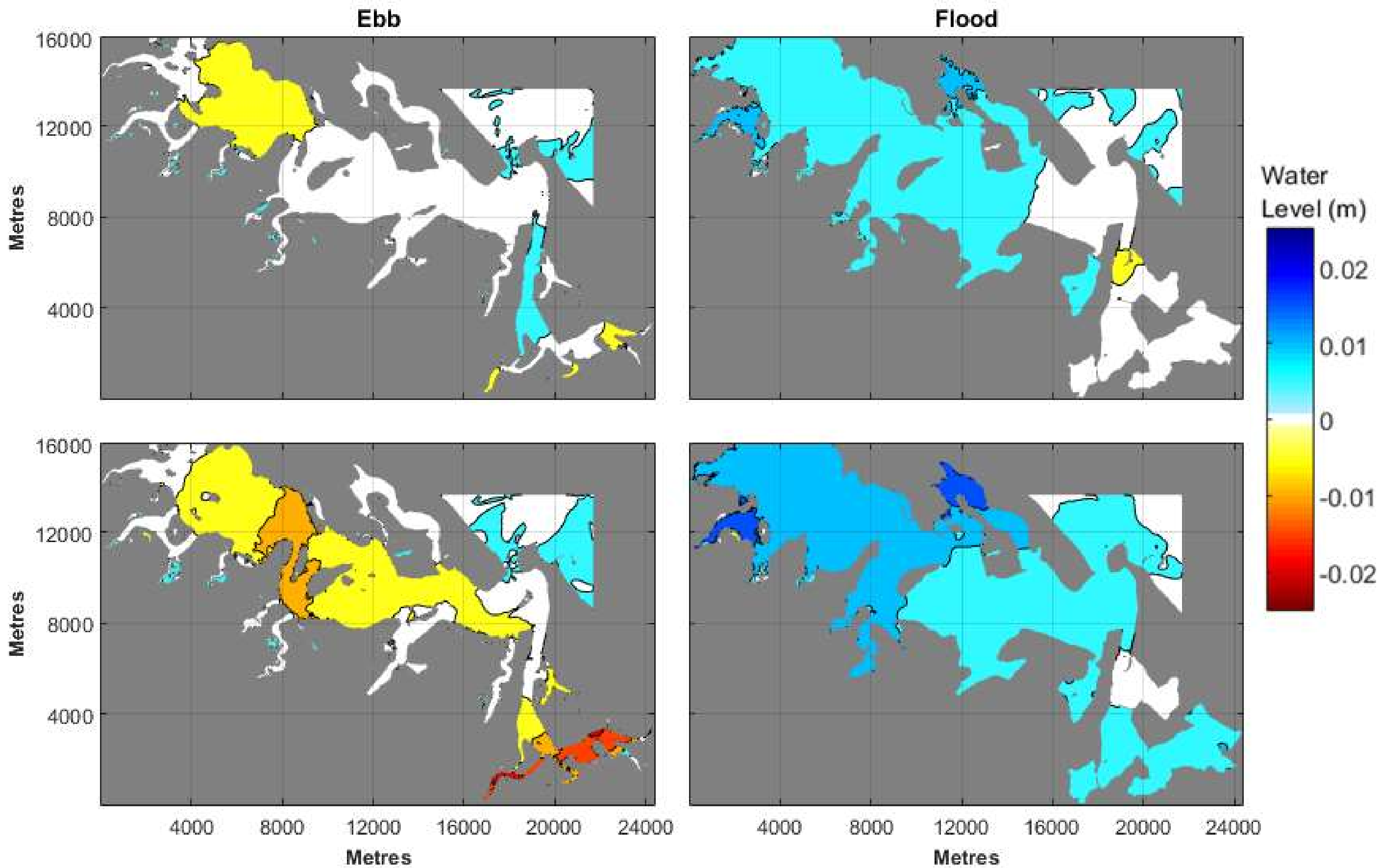

Figure AII.14: Difference in water levels between the Pre-Works and Wharf Extension models at a low (ebb) and high (flood) tide from simulations of a neap (top) and spring tide (bottom) in the southern basin of Tauranga Harbour.

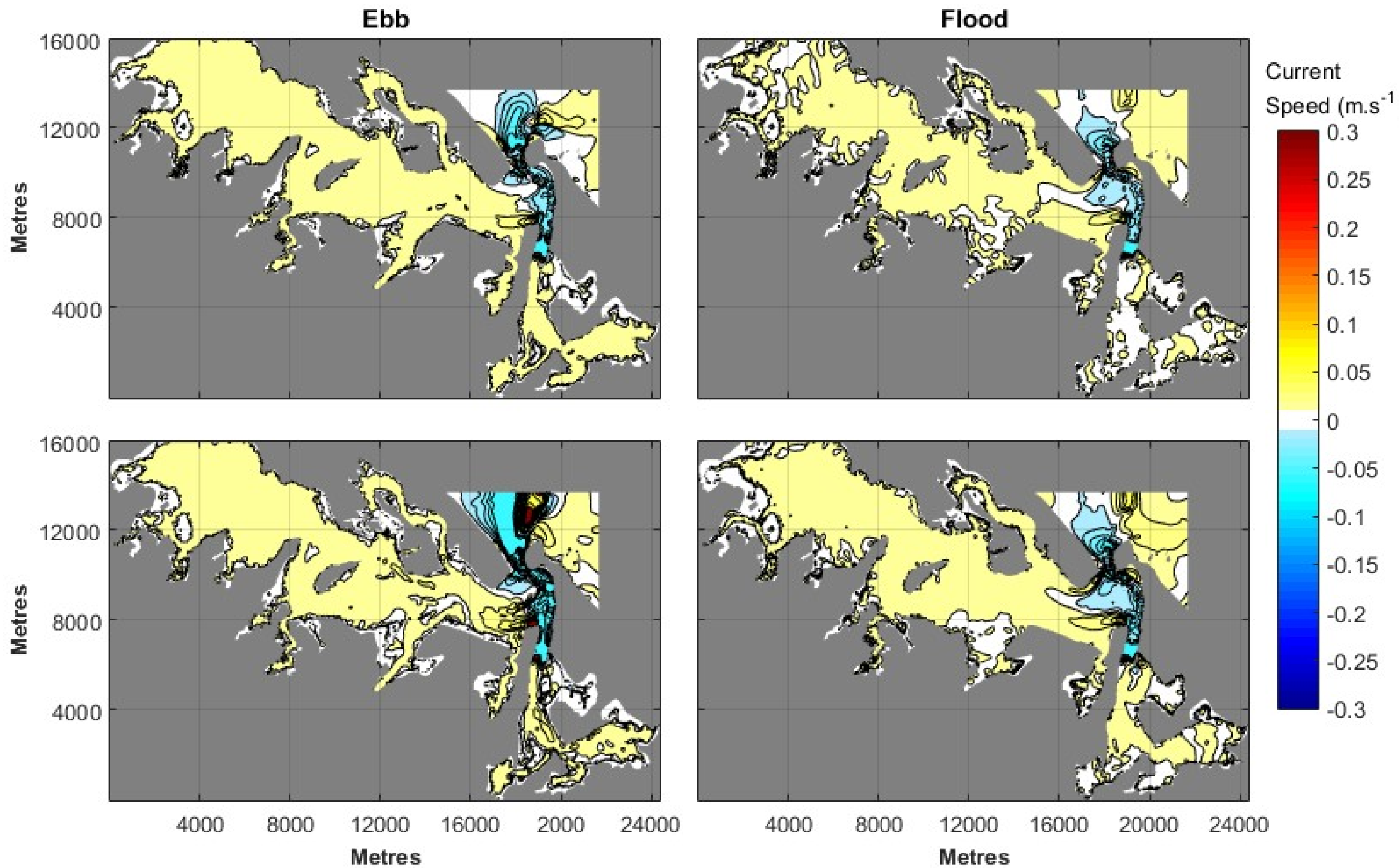

Figure AII.15: Difference in current speeds between the Pre-Works and Wharf Extension models at peak ebb and peak flood tides from simulations of a neap (top) and spring tide (bottom) in the southern basin of Tauranga Harbour.